DEVELOPING NOVEL SUPERSENSITIVE FLUID BIOMARKER ASSAYS FOR NEURODEGENERATIVE DISEASES

A thesis submitted for the degree of Doctor of Philosophy

Deborah Oluwadamilola Alawode

UK Dementia Research Institute
UCL Institute of Neurology/Division of Medicine

Primary Supervisor:	Professor Henrik Zetterberg
Secondary Supervisor:	Dr. Amanda Heslegrave
Tertiary Supervisor:	Professor Nick Fox

Declaration

I, Deborah Oluwadamilola Alawode, confirm that the work presented in this thesis is my own. Where information has been derived from other sources, I confirm that this has been indicated in the thesis.

Abstract

Alzheimer's disease (AD) is the most common form of neurodegenerative dementia worldwide. In recent years, there has been a shift in the diagnostic methodology used from a purely symptoms-based to a more holistic criteria, which incorporates both neuroimaging and fluid biomarkers. Whilst previously, cerebrospinal fluid (CSF) biomarkers dominated the AD fluid biomarker territory, the recent update to the 'ATXN' diagnostic criteria has seen the addition of blood-based biomarkers. Whilst for AD biomarkers like phosphorylated tau, plasma measurements have shown a similarly strong diagnostic accuracy to their CSF counterparts, the same cannot be said for the main measure of amyloid-β (Aβ) pathology, the $A\beta_{42}/A\beta_{40}$ ratio ($A\beta_{42/40}$), with several studies observing extensive overlap between diagnostic groups in plasma, most likely due to the peripheral production of Aβ. As such, there is a need for more robust Aβ biomarkers which better distinguish between diagnostic groups. Two such biomarkers worth investigating are pyroglutamate-modified Aβ ($A\beta_{pE}$), which is a plaque-specific form of Aβ, and $A\beta_{43}$. Although in the past, plasma biomarker measurements were limited by the analytical sensitivity of instruments available, recent advances in technology, particularly the development of Single molecule array (Simoa), have mitigated this limitation. Yet, there is evidently still a sensitivity issue plaguing the scientific world and the fluid biomarker space, given that $A\beta_{43}$ has yet to be measured in blood, and $A\beta_{pE}$ has not successfully been measured in either CSF or blood.

In this thesis, we independently assess the performance of AD CSF and plasma biomarkers, particularly focusing on the diagnostic performance of $A\beta_{42/40}$. Alongside this, we validate the increased sensitivity of a protype upgrade to the standard Simoa instrument, termed the 'SRx Pro'. On the basis of these results, we describe the process of developing novel Simoa assays for the detection of $A\beta_{43}$ and $A\beta_{pE}$.

Impact statement

This thesis is the first of its kind, not only validating the performance of novel Single molecule array (Simoa) technology that is not yet commercially available, but also developing novel assays for isoforms of amyloid-β (Aβ) which, to date, have not been measured in either cerebrospinal fluid (CSF), blood, or both biofluids. The presented research contributes to the rapidly changing Alzheimer's disease (AD) fluid biomarker field in three main ways.

Firstly, it provides further evidence of the poor diagnostic accuracy of the plasma $A\beta_{42}/A\beta_{40}$ ratio ($A\beta_{42/40}$) for AD, particularly in comparison to the robust performance of CSF $A\beta_{42/40}$. Alongside this, we observe that plasma phosphorylated tau-217 (p-tau_{217}) performs equally as well as its CSF counterpart, and arguably better than p-tau_{181} in both CSF and plasma, which until recently was the only p-tau biomarker measured in relation to AD. Given the recent update to the 'ATXN' diagnostic criteria for AD to include $A\beta_{42/40}$ as the only plasma biomarker for Aβ neuropathology, our findings emphasise the need for additional, more robust, Aβ biomarkers. This is particularly important for patients as we will begin to see an increased number of individuals diagnosed with AD using blood biomarkers in the first instance, particularly in countries with more limited clinical resources. Therefore, it is imperative that the field has full confidence in the diagnostic tests used, which as of now cannot be said of the plasma $A\beta_{42/40}$.

Secondly, our research is the first to independently validate the increased analytical sensitivity provided by the upgraded Simoa instrument, termed the 'SRx Pro', in comparison to standard Simoa technology. With the commercial roll out of this technology due to occur in the coming months, our validation of its performance verifies the role the SRx Pro will undoubtedly play in enabling the quantification of previously undetectable analytes, particularly in blood. In addition, we observe no significant difference in interleukin

17A concentrations between AD and control samples in either CSF or serum – a surprising finding given the known neuroinflammatory nature of AD, but nonetheless a key finding to help steer the field towards the most plausible initiating mechanism behind the disease.

Finally, the presented research describes the development of novel Simoa assays detecting $A\beta_{43}$ and pyroglutamate-modified Aβ ($A\beta_{pE}$), both of which we propose may function as alternative direct biomarkers of Aβ pathology, in replacement of $A\beta_{42/40}$. We show the quantification of $A\beta_{pE}$ in CSF for the first time, further emphasising the need for the additional sensitivity provided by the SRx Pro. However, the dawn of anti-Aβ immunotherapy agents, particularly Donanemab, mean that our novel $A\beta_{pE}$ assay may prove beneficial in enabling the direct monitoring of Aβ plaque pathology in individuals treated with these drugs using biofluids, and without the need for repeated neuroimaging.

Ultimately, this research provides unique insight into the challenges faced within the AD fluid biomarker field in relation to analytical sensitivity, and it provides potential solutions by way of detecting alternative Aβ isoforms using novel technology.

Research paper declaration form 1

1. **For a research manuscript that has already been published** (if not yet published, please skip to section 2)

   a) **What is the title of the manuscript?**

   Transitioning from cerebrospinal fluid to blood tests to facilitate diagnosis and disease monitoring in Alzheimer's disease

   b) **Please include a link to or doi for the work**

   https://doi.org/10.1111/joim.13332

   c) **Where was the work published?**

   Journal of Internal medicine

   d) **Who published the work?** (e.g. OUP)

   John Wiley & Sons Ltd

   e) **When was the work published?**

   22nd May 2021

   f) **List the manuscript's authors in the order they appear on the publication**

   Deborah O.T. Alawode, Amanda J. Heslegrave, Nicholas J. Ashton, Thomas K. Karikari, Joel Simrén, Laia Montoliu-Gaya, Josef Pannee, Antoinette O´Connor, Philip S. J. Weston, Juan Lantero-Rodriguez, Ashvini Keshavan, Anniina Snellman, Johan Gobom, Ross W. Paterson, Jonathan M. Schott, Kaj Blennow, Nick C. Fox, Henrik Zetterberg

   g) **Was the work peer reviewed?**

   Yes

   h) **Have you retained the copyright?**

   Yes

   i) **Was an earlier form of the manuscript uploaded to a preprint server?** (e.g. medRxiv). If 'Yes', please give a link or doi)

   No

   If 'No', please seek permission from the relevant publisher and check the box next to the below statement:

   ☒

   *I acknowledge permission of the publisher named under **1d** to include in this thesis portions of the publication named as included in **1c**.*

2. **For multi-authored work, please give a statement of contribution covering all authors** (if single-author, please skip to section 4)

   Deborah O. Alawode wrote, reviewed and edited the full manuscript. All other authors played a supporting role, providing comments and suggestions.

3. **In which chapter(s) of your thesis can this material be found?**

   Chapter 1: Introduction

4. e-Signatures confirming that the information above is accurate
(this form should be co-signed by the supervisor/ senior author unless this is not appropriate, e.g. if the paper was a single-author work)

Candidate

Deborah Alawode

Date:

19/03/2024

Supervisor/ Senior Author (where appropriate)

Prof. Henrik Zetterberg

Date

19/03/2024

Research paper declaration form 2

1. **For a research manuscript that has already been published** (if not yet published, please skip to section 2)

   a) **What is the title of the manuscript?**

   Alzheimer's Disease Biomarkers Revisited From the Amyloid Cascade Hypothesis Standpoint

   b) **Please include a link to or doi for the work**

   https://doi.org/10.3389/fnins.2022.837390

   c) **Where was the work published?**

   Frontiers in Neuroscience

   d) **Who published the work?** (e.g. OUP)

   Frontiers in Neuroscience

   e) **When was the work published?**

   27th April 2022

   f) **List the manuscript's authors in the order they appear on the publication**

   Deborah O.T. Alawode, Nick C. Fox, Henrik Zetterberg, Amanda J. Heslegrave

   g) **Was the work peer reviewed?**

   Yes

   h) **Have you retained the copyright?**

   Yes

   i) **Was an earlier form of the manuscript uploaded to a preprint server?** (e.g. medRxiv). If 'Yes', please give a link or doi)

   No

   If 'No', please seek permission from the relevant publisher and check the box next to the below statement:

   ☒

   *I acknowledge permission of the publisher named under **1d** to include in this thesis portions of the publication named as included in **1c**.*

2. **For multi-authored work, please give a statement of contribution covering all authors** (if single-author, please skip to section 4)

   Deborah O. Alawode wrote, reviewed and edited the full manuscript. All other authors played a supporting role, providing comments and suggestions.

3. **In which chapter(s) of your thesis can this material be found?**

   Chapter 1: Introduction

4. **e-Signatures confirming that the information above is accurate** (this form should be co-signed by the supervisor/ senior author unless this is not appropriate, e.g. if the paper was a single-author work)

Candidate

Deborah Alawode

Date:

19/03/2024

Supervisor/ Senior Author (where appropriate)

Dr. Amanda Heslegrave

Date

19/03/2024

Research paper declaration form 3

1. **For a research manuscript that has already been published** (if not yet published, please skip to section 2)

   a) **What is the title of the manuscript?**

   Donanemab removes Alzheimer's plaques: what is special about its target?

   b) **Please include a link to or doi for the work**

   https://doi.org/10.1016/s2666-7568(21)00144-6

   c) **Where was the work published?**

   The Lancet: Healthy Longevity

   d) **Who published the work?** (e.g. OUP)

   Elsevier Ltd

   e) **When was the work published?**

   July 2021

   f) **List the manuscript's authors in the order they appear on the publication**

   Deborah O.T. Alawode, Amanda J. Heslegrave, Nick C. Fox, Henrik Zetterberg

   g) **Was the work peer reviewed?**

   Yes

   h) **Have you retained the copyright?**

   Yes

   i) **Was an earlier form of the manuscript uploaded to a preprint server?** (e.g. medRxiv). If 'Yes', please give a link or doi)

   No

   If 'No', please seek permission from the relevant publisher and check the box next to the below statement:

   ☒

   *I acknowledge permission of the publisher named under **1d** to include in this thesis portions of the publication named as included in **1c**.*

2. **For multi-authored work, please give a statement of contribution covering all authors** (if single-author, please skip to section 4)

   Deborah O. Alawode wrote, reviewed and edited the full manuscript. All other authors played a supporting role, providing comments and suggestions.

3. **In which chapter(s) of your thesis can this material be found?**

   Chapter 1: Introduction

4. **e-Signatures confirming that the information above is accurate** (this form should be co-signed by the supervisor/ senior author unless this is not appropriate, e.g. if the paper was a single-author work)

   Candidate

Deborah Alawode

Date:

19/03/2024

Supervisor/ Senior Author (where appropriate)

Prof. Henrik Zetterberg

Date

19/03/2024

Acknowledgements

Throughout the duration of this PhD, I have achieved more than I imagined, from publishing 3 first-author papers to representing England at the Birmingham 2022 Commonwealth Games, where I placed 4th. I could not have achieved any of this, and more, without the support of several key figures in my life.

First and foremost, I would like to give all glory to God for seeing me through this season. I would not be where I am today without His love, faithfulness and guidance. I have experienced His goodness firsthand and can't imagine trying to navigate any of this without Him. If I had had my way back in 2015/16 when I was applying for Medical School, I would not even have been at UCL, let alone be completing a PhD. As such, the biggest thing I have learned throughout my time at university so far, but even more so during this PhD, is to trust wholeheartedly in His plans and purposes for my life, even if they do not yet make sense to me at the time, knowing that His plans for me are better than any I could have for myself.

To my close friends and flatmates past and present – Dr. Oluwaseyitan Adeleye, Dr. Nisha Thapa, Dr. Eleanor Harding, Debra Kelsall, Syntiche Dedji and Paige Reeves – thank you for being there during Medical School and in the early and latter stages of my PhD, whether that be navigating COVID-19 lockdown life, or being there to pray with me and for me, and keeping me accountable after I began putting pen to paper. Having you all in my corner has meant more than you will ever realise, and I thank God constantly for blessing me with such an incredible support network. I look forward to spending the next few years disturbing you (Seyi, Nisha and Eleanor) for help with Medical School now that you've all graduated without me!

To Sarah Lawrence, Deborah Bell, Lamar Henry, Luke Bevis, Paul Paine and everyone else in my Bible Study Group and at King's Cross Church. Thank you for all the prayers and your constant

support. I have valued our regular debriefs about how things were going during my PhD, and could not have asked for more loving people to call my Church family.

To Henrik and Amanda, words can't describe how grateful I am to have had supervisors like you. You are the kindest and most supportive supervisors I could have dreamed of having, despite being as world renowned in the Fluid Biomarker field as you both are. Yet, you welcomed me into your lab (and your home in Sweden, in Henrik's case!) with open arms and offered me your expert guidance. For that, I am eternally grateful. When the time comes for me to return to Medical School this coming August after completing my post-doctoral role at the lab, I will miss the weekly lab meetings and our regular chats. But I will definitely be back to visit!

To Rhiannon Laban, Elena Veleva and everyone else in the UK DRI Fluid Biomarker Lab, thank you for making the office such a friendly and safe environment to work in. I can only apologise that I spent most of my lunch times watching EastEnders, but I'm glad that we were all still able to build good friendships. I will miss the 'word of the day' giving us a tiny insight into what goes on in Owen's mind and life, but I hope it continues long after I am gone!

To Lindsey Marsh, Syrena Fernandes and everyone at Quanterix Corporation, thank you for your help and support with tackling homebrew assay development right to navigating the SRx Pro. My knowledge and experience in these topics can largely be attributed to discussions with you both, whether via email or during meetings, and for that I am extremely grateful.

To my weightlifting coach, Kristian McPhee, and all my teammates at London Strength weightlifting club, I cannot thank you enough for providing such a banterous yet supportive environment to train in. I have yet to have a training session where I have not left laughing or smiling, regardless of how my session has gone. I realise it is a

unique blessing to be a member of a club that fosters such an environment. Weightlifting may be an individual sport, but a huge part of any success I have had on the competition platform has come from having a team I love being a member of walking with me every step of the way; a team where we are more than just teammates, but actual friends. In my 9 years and 8 months of weightlifting, I have only had two coaches and been a member of two clubs, so I couldn't have asked for a better club to call my second weightlifting home.

To my thesis committee – Dr. Ross Paterson and Dr. Frances Wiseman – thank you for your support throughout the past few years, from helping me think critically about my research to giving invaluable advice. Likewise, thank you to the MBPhD programme – Prof. Aine Burns, Prof. Reza Motallebzadeh and Carolyn Cohen – for believing in me and giving me the opportunity to conduct this PhD during Medical School.

On a more practical note, I'd like to thank Emily Abel, Dr. Miguel Rosa Grilo, and Prof. Nick Fox for helping me gain access to the DRC cognitive clinic samples, Owen Swann for conducting the CSF p-tau$_{217}$ measurements using Simoa on these samples, and Danielle Eastwick from the UCLH neuroimmunology laboratory for conducting the CSF Aβ_{42}, Aβ_{40} and p-tau$_{181}$ measurements on these same samples using the Lumipulse instrument. A huge thank you to Prof. Henrik Zetterberg and Celia Hök Fröhlander for sending the samples from Gothenburg on which I conducted the IL17A analysis as well as the pilot experiments on our novel assays, and finally to Syrena Fernandes for conducting the SRx Pro IL17A measurements at Quanterix Corporation Research and Development department in Billerica, USA.

Last, but by no means least, I would like to thank my parents – Thomas and Julianah – my brothers and sister-in-law – Isaac, Daniel and Rebekah – and the rest of my extended family for their continued support throughout my many many years of studying. I'm grateful to

be part of a family who know and love God, and who support me in all He has called me to, regardless of how crazy it may seem! I hope I have made you proud with this piece of work. I promise I will complete the degree I originally went to university for, but you know I wouldn't be me if I didn't add in a few extra stops along the way!

Apologies if there is anyone I have forgotten to mention. I am blessed to have so many people pouring into my life and supporting me in unique ways. This chapter of my life may be coming to a close, but I will always look back on this time fondly. With that, I hope anyone who has set themselves the task of reading this thesis enjoys it as much as I did conducting the work.

Table of Contents

Table of Figures

Table of Tables

Abbreviations

α-synSAA	α-synuclein seed amplification assays
Aβ	amyloid-beta
AD	Alzheimer's disease
ADLs	activities of daily living
AEB	average number of enzyme complexes per bead
ANOVA	analysis of variance
APOE	apolipoprotein E gene
ApoE	apolipoprotein E protein
APP	amyloid-beta precursor protein
ARIA	amyloid-related imaging abnormalities
ARIA-E	amyloid-related imaging abnormalities with oedema and effusions
AUC	area under the receiver operator characteristic curve
BBB	blood-brain barrier
BCB	bead conjugation buffer
BSA	bovine serum albumin
BWB	bead wash buffer
CAA	cerebral amyloid angiopathy
CNS	central nervous system
CP	custom peptide
CTRL	control
CV	coefficient of variation
DLB	dementia with Lewy bodies
DRC	Dementia Research Centre
DS	Down syndrome
ECL	electrochemiluminescence
EDC	1-ethyl-3-(3-dimethylaminopropyl)carbodiimide hydrochloride
EDTA	ethylenediaminetetraacetic acid
FAD	familial Alzheimer's disease
FDA	Food and Drug Administration

FDG-PET	[^{18}F]-fluorodeoxyglucose-positron emission tomography
FL	full-length
f_{on}	fraction of on beads
FTLD	frontotemporal lobe dementia
γ-secretase	gamma-secretase
GC	gas chromatography
GFAP	glial fibrillary acidic protein
HB	homebrew
I_{bead}	mean fluorescence intensity of active beads in an array
Ig	immunoglobulin
IL17A	interleukin 17A
IP	immunoprecipitation
I_{single}	mean fluorescence intensity of a single enzyme immunocomplex on a bead
K_D	equilibrium dissociation constant
LC	liquid chromatography
LLOQ	lower limit of quantification
LOD	limit of detection
MMS	magnetic-meniscus sweeping
MOSAIC	Molecular On-bead Signal Amplification for Individual Counting
MP	mixed phenotype
MS	mass spectrometry
MSD	Meso Scale Discovery
m/z	mass-to-charge ratio
N4PE	neurology 4-plex E
NAD	non-Alzheimer's disease
NfL	neurofilament light chain
NFT	neurofibrillary tangle
NIA-AA	National Institute on Aging and the Alzheimer's Association
NSAID	non-steroidal anti-inflammatory drug
PBS	1x phosphate buffer saline

PBST	1x phosphate buffer saline + 0.1% tween-20
PD	Parkinson’s disease
PET	positron emission tomography
PSEN1	presenilin 1
PSEN2	presenilin 2
p-tau	phosphorylated tau
RGP	resorufin β-D-Galactopyranoside
RnD	Research and Development
ROC	receiver operator characteristic
SAD	sporadic Alzheimer’s disease
SβG	streptavidin–β-galactosidase
Simoa	single molecule array
S/N	signal:background noise ratio
S-NHS	sulfo-N-hydroxysulfosuccinimide
SST	serum separator tube
SUVR	standard uptake value ratio
TREM2	triggering receptor expressed on myeloid cells 2
t-tau	total tau
VaD	vascular dementia

CHAPTER 1: INTRODUCTION

Dementia is an umbrella term used to describe any disorder characterised by decreased cognitive function that is severe enough to interfere with day-to-day functions. It is considered a syndrome as any single symptom can be caused by a variety of diseases, rather than only by one specific disease (1). However, the symptoms displayed depend on which region of the brain is affected. Dementia can be divided into two broad categories: 1) neurodegenerative, including Alzheimer's disease (AD), dementia with Lewy bodies (DLB) and frontotemporal lobe dementia (FTLD); and 2) non-neurodegenerative, including depression, normal pressure hydrocephalus, metabolic causes (*e.g.* hypothyroidism, vitamin B12 deficiency, chronic uraemia) and infection (1). The neurodegenerative dementias are all characterised by progressive neurodegeneration, including neuronal dysfunction and neuronal loss, eventually culminating in brain atrophy. However, many individuals may have multiple dementias at once, and it is this comorbid picture that makes clinical diagnosis particularly challenging.

1.1 Alzheimer's disease – a general overview

AD is the most common form of neurodegenerative dementia worldwide, with cases estimated to double in Europe and triple worldwide by 2050 (2). Described by Dr. Alois Alzheimer using a case study in 1906, individuals with AD often display a wide range of symptoms, including changes to their episodic memory, thinking and behaviour. It should be noted, though, that these symptoms are not unique to AD, and can be seen in several other neurodegenerative and non-neurodegenerative disorders. Alongside these symptoms, AD can be further characterised neuropathologically by three key hallmarks: 1) the presence of amyloid beta (Aβ) plaques in the brain parenchyma, and commonly also within cerebral blood vessels (cerebral amyloid angiopathy [CAA]); 2) intraneuronal neurofibrillary

tangles (NFTs), composed of hyperphosphorylated tau; and 3) neurodegeneration (3-5). The accumulation of misfolded proteins, in the form of Aβ plaques and NFTs, has led to AD being termed a proteinopathy (6). However, of particular interest is the role Aβ plays in AD pathogenesis.

1.1.1 Alzheimer's disease genetics

AD can be divided into two groups based on whether it is inherited along a family line, termed familial AD (FAD), or whether it has been acquired with no consistent inheritance pattern, termed sporadic AD (SAD). FAD, which represents <1% of AD cases, typically presents before the age of 60, and is caused by autosomal dominant inheritance of mutations in the Aβ precursor protein (*APP*), presenilin 1 (*PSEN1*) and presenilin 2 (*PSEN2*) genes (7). Mutations in the *APP* gene, located on chromosome 21, were the first identified cause of FAD, and can result in several differing effects on APP processing. These effects include increased production of total Aβ, and selective increase in production of longer Aβ peptides, which also increases aggregation propensity as well as increasing the $A\beta_{42}/A\beta_{40}$ ratio ($A\beta_{42/40}$) (8, 9). Trisomy 21, more commonly known as Down syndrome (DS), is the leading genetic cause of AD (10), with all individuals developing AD neuropathology by age 30-40 (11, 12), and 67% developing AD-like dementia by age 72 (13-16). Individuals with DS have three copies of chromosome 21, and it is likely these additional copies of the *APP* gene that contribute to these individuals developing AD pathology. Mutations in the *PSEN1* gene on chromosome 14 and *PSEN2* gene on chromosome 1 cause similar downstream effects on Aβ as *APP* mutations, namely an increase in the $A\beta_{42/40}$ (9). These genes encode the PSEN1 and PSEN2 proteins, respectively, which are essential for the proteolytic activity of gamma (γ)-secretase, one of the key enzymes responsible for producing pathogenic Aβ peptides of varying lengths (see Figure 1.2) (17). Consequently, mutations in these genes cause an increase in the ratio of longer and stickier Aβ isoforms, such as $A\beta_{42}$, to shorter, more hydrophilic isoforms, such as $A\beta_{40}$, resulting in an increased

$A\beta_{42/40}$. Interestingly, individuals with *PSEN1* gene mutations typically have a younger age of onset than those with *APP* gene mutations, whereas individuals with *PSEN2* gene mutations typically present later (18, 19).

Whilst SAD has no known specific causative gene mutations, studies have revealed two key genes with several risk loci implicated in the development of AD. First identified by Strittmatter and colleagues (20) and Pourier and colleagues (21), polymorphisms in the apolipoprotein E gene (*APOE*), located on chromosome 19 and encoding apolipoprotein E (ApoE), are the strongest genetic risk factor for the development of SAD (22). ApoE, mainly secreted by astrocytes, is the only cholesterol transporter in the brain (23), and is a key component for synapse formation and maintenance, and immune regulation within the brain (24). Of the three polymorphic alleles of *APOE*, the ε4 allele is associated with both an increased risk as well as a lower age of onset, with the ε2 allele being protective (25, 26). Similarly, mutations in the triggering receptor expressed on myeloid cells 2 gene (*TREM2*), located on chromosome 6, have been associated with an increased risk of SAD (27, 28). TREM2 is an innate immune transmembrane receptor which is upregulated in microglia to mediate their phagocytic function, particularly of Aβ (29, 30).

1.1.2 Alzheimer's disease as a continuum

In recent years, it has become clear that AD is not merely a binary condition whereby individuals either have it and display symptoms, or do not. Rather, evidence has shown that AD exists on a continuum, whereby AD neuropathology begins up to 20 years before symptom-onset in both FAD and SAD (31-34), and spans from cognitively normal/asymptomatic to mild cognitive impairment to mild/moderate/severe dementia, depending on the severity of symptoms (2) (see Figure 1.1). Evidence has shown that AD biomarkers become abnormal prior to symptom onset (35). As such, there has been a move away from a solely symptoms-based

diagnosis of AD, to a multidisciplinary approach, involving a combined review of patient history and neurocognitive assessments, alongside clinical biomarkers (36). The biomarker-based diagnostic criteria for AD will be covered in more depth in section 1.4.

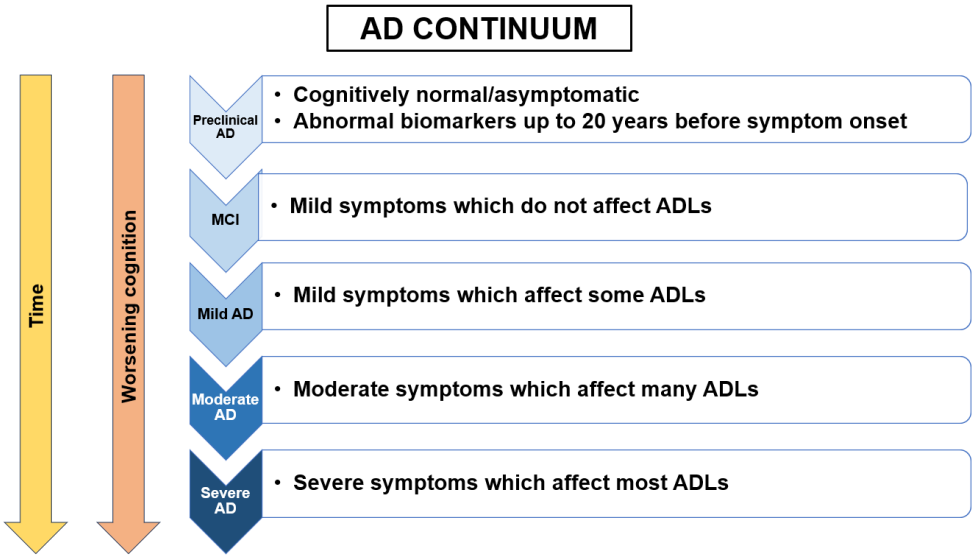

Figure 1.1 - AD continuum

Five key stages of Alzheimer's disease (AD) continuum. Stage 1: Preclinical AD can occur up to 20 years before symptom onset. Abnormal biomarkers are present. Stage 2: mild cognitive impairment (MCI) presents with mild symptoms which do not affect activities of daily living (ADLs). Stage 3: mild AD presents with symptoms which do affect ADLs. Stage 4: moderate AD presents with worsening of symptoms seen in stage 3, and an increased number of ADLs disrupted. Stage 5: severe AD presents with further worsening of symptoms seen in stage 4, and most ADLs disrupted. As individuals progress through the disease stages, cognition worsens.

1.2 Amyloid-β plaque formation, isoforms, and pathogenicity

Aβ is a peptide that is naturally present within the healthy human brain, where it is produced intracellularly and at the cell membrane, and subsequently released into the extracellular space (37). Its physiological roles include antimicrobial properties, tumour suppression, sealing leaks in the blood-brain barrier (BBB), promoting neural recovery post-injury and regulating synaptic function (38). However, pathogenic Aβ is produced when APP, a transmembrane protein, is sequentially cleaved along its amyloidogenic pathway by β- and γ-secretases (39). The site of γ-secretase cleavage determines the length of the resultant Aβ peptide (40), ranging from 37 to 49 amino acids in length (41). This is illustrated in Figure 1.2. The most abundant isoforms of Aβ in cerebrospinal fluid (CSF) are $Aβ_{38}$, $Aβ_{40}$ and $Aβ_{42}$ (42), with the 40 and 42 amino acid length isoforms being the two most widely researched in relation to AD. This is predominantly due to the important role that the $Aβ_{42}/Aβ_{40}$ ratio ($Aβ_{42/40}$) plays in supporting a diagnosis of AD, as highlighted by the recently updated National Institute on Aging and the Alzheimer's Association (NIA-AA) diagnostic guidelines for AD[1] (43, 44). Whilst the CSF concentration of $Aβ_{40}$ remains unchanged in AD, the $Aβ_{42}$ concentration decreases, which is thought to reflect aggregation and deposition within the brain (45). Therefore, looking at the two in combination, as a ratio, provides a more accurate marker of plaque pathology in comparison to the overall Aβ production in that individual, and combats issues of inter-individual baseline concentration differences posed by looking at CSF $Aβ_{42}$ concentration in isolation (46). The $Aβ_{40}$ and $Aβ_{42}$ peptide chains can be seen graphically in Figure 1.3A&B.

In line with the secondary structure of proteins, monomeric Aβ exists in both an α-helical and β-pleated sheet conformation, and is

[1] https://alz.org/media/Documents/scientific-conferences/Clinical-Criteria-for-Staging-and-Diagnosis-for-Public-Comment-Draft-2.pdf?_gl=1*1ugortz*_ga*NzAyNzAzODMuMTcwOTIyNjA1Mw..*_ga_QSFTKCEH7C*MTcwOTIyNjA1My4xLjAuMTcwOTIyNjA3NS4zOC4wLjA.*_ga_9JTEWVX24V*MTcwOTIyNjA1My4xLjAuMTcwOTIyNjA3NS4zOC4wLjA

amphiphatic in nature, exhibiting hydrophilicity at the N-terminal amino acids, and hydrophobicity at the C-terminus (37). These monomeric isoforms can subsequently aggregate to form: 1) soluble oligomers, which are heterogeneous in size and can spread throughout the brain; 2) protofibrils, which are larger soluble oligomers; or 3) insoluble fibrils, which can further aggregate to form Aβ plaques (41, 47). All of these aggregated forms of Aβ are known to be neurotoxic (47-50). However, studies have observed soluble oligomers to be more neurotoxic than fibrils or monomers (51-53). Fibril formation is now widely considered to occur by nucleation-dependent polymerisation (54, 55). This process involves the initial formation of nuclei, followed by an elongation phase, resulting in fibril formation (37, 54). Furthermore, this process is concentration dependent. However, $A\beta_{42}$ is much more prone to aggregation than $A\beta_{40}$, requiring a five-fold lower minimum concentration to aggregate into fibrils, highlighting why $A\beta_{42}$ is much more abundant in plaques than $A\beta_{40}$ (37). But interestingly, longer-length Aβ peptides, such as $A\beta_{43}$, have been observed more frequently than $A\beta_{40}$ within plaque cores in FAD, SAD and DS brains (56-58). Indeed, post-mortem analysis of AD brains has revealed a positive correlation between Aβ peptide length and plaque load ($A\beta_{43} > A\beta_{42} > A\beta_{40}$) (59), and *in vivo* studies in mouse models of FAD have revealed that $A\beta_{43}$ is more neurotoxic, and has a greater propensity to aggregate, than $A\beta_{42}$ (60). Furthermore, CSF concentrations of $A\beta_{43}$ are significantly reduced in FAD mutation carriers (40), mimicking the reduction in $A\beta_{42}$ seen in AD, and highlighting a potential role of $A\beta_{43}$ in the disease. The $A\beta_{43}$ peptide chain can be seen graphically in Figure 1.3C.

As alluded to above, variability in the C-terminus of Aβ is a well-known phenomenon. However, there is similar heterogeneity at the N-terminus of the peptide (61, 62). In fact, investigations have revealed that only a small proportion of the Aβ ending at amino acids 40 and 42 within cerebral blood vessels and parenchymal plaques, respectively, is made up by $A\beta_{1\text{-}40}$ and $A\beta_{1\text{-}42}$ (63), highlighting the

overriding presence of truncated or modified Aβ in AD brains. One such truncated species, pyroglutamate-modified Aβ ($Aβ_{pE}$), is one of the dominant forms of Aβ in the hippocampi and cortices of AD patients (64), and compared to full-length Aβ, irrespective of the C-terminus, $Aβ_{pE}$ that has been truncated and modified at the third amino acid ($Aβ_{pE3}$) has shown an increased rate of aggregation of up to 250-fold (65).

Pyroglutamate, or pyrrolidone carboxylate, is a cyclic amino acid typically found at the N-terminus of some proteins and peptides (66). It is formed by the cyclisation of either glutamine or glutamate (67). Non-enzymatic cyclisation to form pyroglutamate has been well known for many years (68, 69). However, this process tends to occur relatively scarcely, and it can be particularly slow (70). In contrast, enzymatic pyroglutamate formation is less well understood. Twardzik and Peterkofsky (69) demonstrated that N-terminal pyroglutamate can be produced from glutamate without prior conversion to glutamine, but concluded that it must occur enzymatically. This view was challenged by Chelius and colleagues (67), who demonstrated the non-enzymatic formation of pyroglutamate from glutamate *in vitro*. Whilst it is possible that both spontaneous and enzymatic glutamate cyclisation can occur, further investigation has revealed a key role of the enzyme glutaminyl cyclase in catalysing the conversion of glutamate at amino acid positions 3 or 11 of Aβ, following truncation by N-terminal proteases, into $Aβ_{pE}$ (71-74).

The increased propensity of $Aβ_{pE}$ to aggregation is most likely due to the increased hydrophobicity caused by the pyroglutamate ring (75), which is resistant to degradation by peptidases thus increasing peptide stability (76-78). $Aβ_{pE}$ has been found in a range of brain regions in greater concentrations than full-length Aβ, suggesting that it is deposited earlier in the disease process (77, 79, 80). This is also supported by $Aβ_{pE3}$ being found in diffuse plaques in DS (75, 81). Finally, *in vivo* studies looking at transgenic mouse models overexpressing $Aβ_{pE}$ revealed that $Aβ_{pE}$ induces neurodegeneration

and exacerbates behavioural deficits in these mice (82, 83), supporting Güntert and colleagues, who found a correlation between the presence of $A\beta_{pE3}$ and disease severity (84). Finally, $A\beta_{pE}$ is the only identified form of Aβ that is solely found within plaques, and is not produced by neurones (74), making it a plaque-specific form of Aβ and a promising immunotherapy target. The $A\beta_{pE3-40}$ peptide chain can be seen graphically in Figure 1.3D.

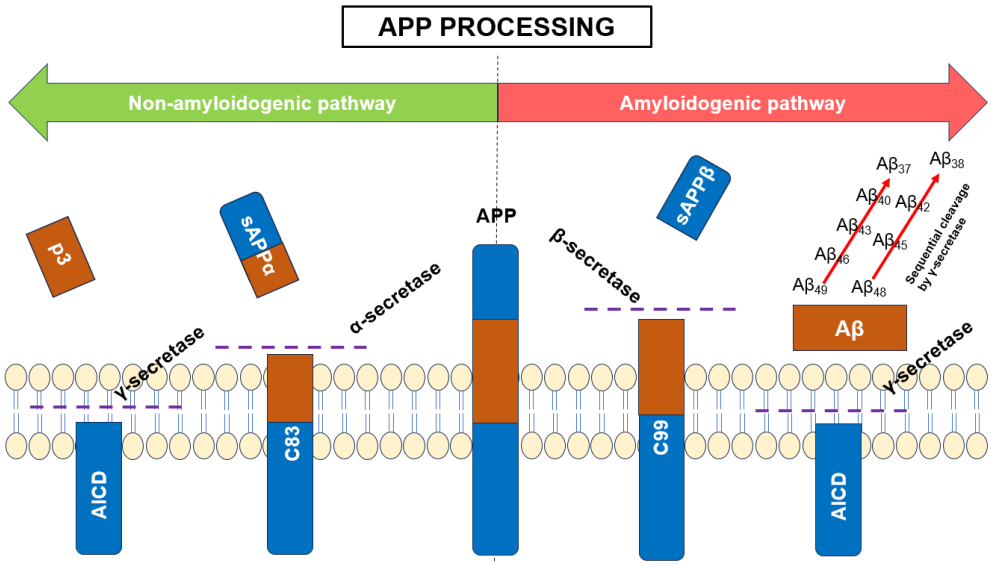

Figure 1.2 - APP processing

Amyloid precursor protein (APP) processing along the non-amyloidogenic pathway occurs first by cleavage with α-secretase, producing secreted APP alpha (sAPPα) and an 83-amino acid C-terminal fragment (C83). Subsequent cleavage by γ-secretase produces p3 peptide and the APP intracellular domain (AICD). In contrast, APP processing along the amyloidogenic pathway occurs first by cleavage with β-secretase, producing sAPPβ and a 99-amino acid C-terminal fragment (C99). Subsequent cleavage by γ-secretase produces AICD, along with the amyloid-β (Aβ) peptide characteristic of Alzheimer's diseases. The amino acid chain length of the Aβ peptide produced is dependent on where the final cleavage by γ-secretase occurs. Sequential cleavage of $A\beta_{49}$ by γ-secretase produces $A\beta_{46}$, $A\beta_{43}$, $A\beta_{40}$ and $A\beta_{37}$. Whereas sequential cleavage of $A\beta_{48}$ by γ-secretase produces $A\beta_{45}$, $A\beta_{42}$ and $A\beta_{38}$.

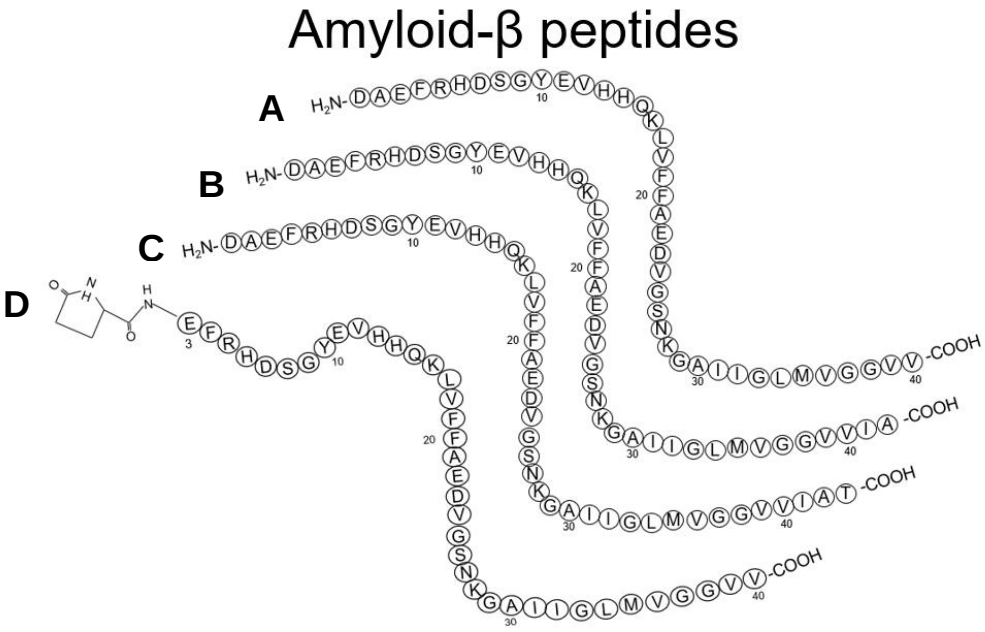

Figure 1.3 – Aβ amino acid structure

*Amino acid structures of the two most widely researched amyloid-β (Aβ) isoforms in relation to Alzheimer's disease – $Aβ_{42}$ (**A**) and $Aβ_{40}$ (**B**) – along with two alternative Aβ isoforms – $Aβ_{43}$ (**C**) and pyroglutamate modified $Aβ_{3-40}$ (**D**)*

1.3 The amyloid cascade hypothesis and alternative hypotheses

1.3.1 The amyloid cascade hypothesis

The amyloid cascade hypothesis, first described by Hardy and Higgins (85) in 1992 but which traces back to 1984 (86), introduced the idea of Aβ misfolding and deposition as being the primary precipitant of AD, with the other neuropathological hallmarks, including NFT formation and neuronal loss, occurring as a direct consequence of the misfolded Aβ. This pathophysiological process, along with the key AD-related biomarkers described in the ATXN criteria (see section 1.4.1 The ATXN criteria), is summarised in Figure 1.4. Along with Aβ misfolding, Hardy and Selkoe (87) also described an imbalance between Aβ production and clearance, resulting in an increased presence of cerebral Aβ in its various forms, including monomers, oligomers, insoluble fibrils and plaques (88). Genetic evidence in favour of this hypothesis can be seen in DS, already discussed in section 1.1.1 Alzheimer's disease genetics, as well as in the Swedish and Icelandic *APP* gene mutations. The K595N/M595L double point mutation in *APP*, known as the Swedish mutation, causes enhanced cleavage of APP by β-secretase, increasing the production and secretion of Aβ (89). This is in contrast to the A673T point mutation in *APP*, frequently termed the Icelandic mutation, which is the first *APP* gene mutation known to be protective against Aβ deposition and AD (90). This mutation has the opposite effect to the Swedish mutation, whereby it reduces cleavage of APP by β-secretase along its amyloidogenic pathway, and produces Aβ that is less prone to aggregation (91). This genetic evidence in favour of the amyloid cascade hypothesis is further supported by CSF $A\beta_{40}$, $A\beta_{42}$ and $A\beta_{42/40}$ being the first biomarkers to significantly change in AD, prior to other CSF biomarkers and amyloid positron emission tomography (PET) positivity (92). However, it is important to acknowledge that controversies do exist regarding the plausibility of the amyloid cascade hypothesis (93).

In recent years, there have been several criticisms posed against the amyloid cascade hypothesis, many of which have been summarised

in a recent review by Kepp and colleagues (86). One such criticism lies with the vast number of anti-Aβ clinical trials which have failed to show any significant clinical benefit, with phase III clinical trials on crenezumab, bapineuzumab and solanezumab all showing no improvement in cognitive or Aβ pathology outcomes (94-99). Given the centrality of Aβ to the amyloid cascade hypothesis, an antibody specifically targeting Aβ should not only reduce the extent of Aβ pathology seen on amyloid PET imaging, but it should at the least halt further deteriorations in cognition, if not improve cognitive decline. However, in recent years, it has become clear that the isoform of Aβ targeted by the immunotherapy agent plays a huge role in whether such an antibody successfully reduces Aβ plaque burden and improves cognition. In addition to reducing Aβ pathology, research has shown that the reduction must happen relatively quickly to gain time for the brain to recover in a clinically meaningful manner (100). This is highlighted in the recent successes in clinical trials, discussed in more detail in section 1.6, which emphasise the need for specificity in Aβ-targeting immunotherapy agents (101, 102). Indeed, the clinical benefits of plaque removal and the slowing of cognitive decline seen with the third generation of anti-Aβ immunotherapy agents can largely be attributed to their selectivity for targeting aggregated forms of Aβ. This is in contrast to their predecessors, the first and second generations of anti-Aβ immunotherapy agents, which were either non-selective or selective for monomeric forms of Aβ, and displayed poor outcomes in clinical trials.

Another criticism lies with the presence of pathological Aβ in the brains of cognitively unimpaired individuals (103, 104), or conversely the diagnosis of some individuals with AD but in whom no evidence of Aβ pathology is found (98). Whilst the latter could be attributed to an incorrect diagnosis, the former suggests that Aβ may not be the primary driving factor for the development of AD (105, 106). Plausible explanations exist as to why this would be case. As already highlighted in section 1.2, certain Aβ isoforms exhibit greater

neurotoxicity than others. Therefore, it is possible that the increased presence of these more neurotoxic isoforms, alongside the location of Aβ burden, have a greater propensity to drive symptom-onset in otherwise cognitively unimpaired individuals. Furthermore, the extent of cognitive reserve within each individual may also play a role in neuroprotection against symptom-onset, thus resulting in cognitively unimpaired individuals exhibiting ample pathological Aβ (107). In fact, biomarker studies suggest these individuals would have been at an extremely high risk of developing dementia, had they lived on (108). Regardless, the amyloid cascade hypothesis remains central to our understanding of AD, although alternative hypotheses do exist.

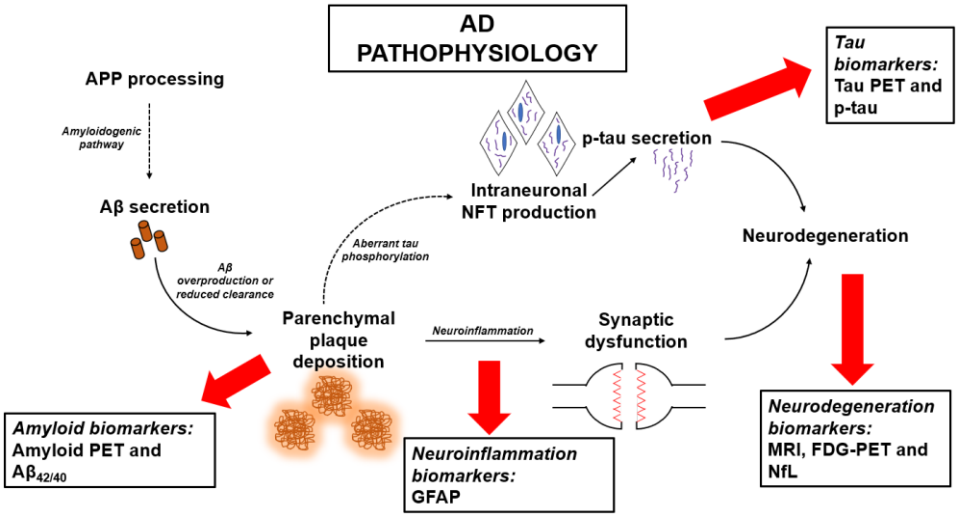

Figure 1.4 – AD pathophysiology

The pathological sequence of Alzheimer's disease (AD), as described by the amyloid cascade hypothesis, pinpoints amyloid-β (Aβ) misfolding and deposition as being the primary precipitant of AD. Following the processing of the amyloid precursor protein (APP) along its amyloidogenic pathway, Aβ is secreted from neurones. Overproduction, or reduced clearance, of this peptide results in the deposition of Aβ plaques within the brain parenchyma and the consequent activation of the neuroinflammatory cells of the brain. This neuroinflammatory process results in synaptic dysfunction and neurodegeneration. However, alongside neuroinflammation, the presence of Aβ causes hyperphosphorylation of tau, producing neurofibrillary tangles intraneuronally and the secretion of phosphorylated tau (p-tau). This, too, contributes to neurodegeneration. Key biomarkers of this pathological process, as indicated by the ATXN criteria include the biomarkers of: amyloid pathology – amyloid positron emission tomography (PET) and $A\beta_{42}/A\beta_{40}$ ratio ($A\beta_{42/40}$); neuroinflammation – glial fibrillary acidic protein (GFAP); neurodegeneration – magnetic resonance imaging (MRI), fluorodeoxyglucose (FDG)-PET and neurofilament light chain (NfL); and tau pathology – tau PET and p-tau.

1.3.2 Alternative hypotheses

Given the multi-factorial nature of AD, there are several alternative hypotheses that exist regarding the initiating mechanisms behind the disease. Indeed, it is possible that the accumulation of by-products of Aβ production, such as the 99 amino acid C-terminal fragment of APP, or even the neuroprotective nature of shorter Aβ peptide fragments, may play a large role in AD pathogenesis (109, 110). Furthermore, there is growing evidence in favour of alternative hypotheses which place other proteins or processes, such as tau and neuroinflammation, as the central initiating mechanisms of AD pathogenesis (111-114). Addressing all such hypotheses is beyond the scope of this thesis. Therefore, this section will focus on three alternative hypotheses – the PSEN hypothesis, the tau hypothesis, and the neuroinflammatory hypothesis.

1.3.2.1 The presenilin hypothesis

The PSEN hypothesis places the pathogenic emphasis of AD on PSEN, proposing that loss-of-function mutations in the *PSEN1* and *PSEN2* genes directly lead to AD, bypassing the need for Aβ-induced neuropathology (115). PSEN1 and PSEN2 play an essential role in learning and memory, synaptic function and neuronal survival (116). As such, it is not surprising that *in vivo* investigations on *PSEN* knockout mice revealed that these mice developed AD-like pathology, including neurodegeneration and tau hyperphosphorylation, in the absence of Aβ pathology (117). Whilst PSEN1 and PSEN2 have a clear role in Aβ production through their role in γ-secretase function, Shioi and colleagues (118) argue that they also promote neurodegeneration separate to their effect on Aβ, an argument strongly supported by Xia and colleagues (119). Recent *in vitro* investigations have shown *PSEN1* gene mutations decrease γ-secretase activity (120), suggesting *PSEN* mutations operate via a loss-of-function mechanism. However, further analysis revealed that this decreased activity increases the $A\beta_{42/40}$ ratio. Interestingly, *in vivo* investigations by Veugelen and colleagues (121) observed that *PSEN* gene mutations cause an increased production of $A\beta_{42}$ and $A\beta_{43}$. However, this evidence was quickly disputed by Xia and

colleagues (119), who observed the opposite and challenged the robustness of the study conducted by Veugelen and colleagues (121). Whilst it is possible that PSEN may cause neurodegeneration independently of Aβ, the presence of Aβ pathology remains an important neuropathological feature required for a diagnosis of AD. This is further emphasised by the recently updated NIA-AA diagnostic guidelines for AD[1] (discussed further in section 1.4.1 The ATXN criteria), where Aβ biomarkers remain core biomarkers for confirmation of AD. Consequently, it remains difficult to accept the PSEN hypothesis as being the primary causative mechanism behind AD, given the centrality of Aβ to AD neuropathology, and the recent clinical trial successes of anti-Aβ immunotherapy agents (see section 1.6).

1.3.2.2 The tau hypothesis

Whereas the amyloid cascade hypothesis states that NFT production occurs as a consequence of Aβ, the tau hypothesis states that hyperphosphorylation or excessive phosphorylation of tau causes the production of NFTs, resulting in neurodegeneration and worsening cognition independently of Aβ (122). Tau, a microtubule-associated protein, is a natural component of mature neurones that regulates the stability of microtubules within the neurone by protecting against depolymerisation (123-126). Some healthy individuals may have a small percentage of phosphorylated tau (p-tau), as phosphorylation appears to be important in enabling the normal function of tau in the neuronal microtubule (127). However, tau is 3-4-fold more phosphorylated in AD, and it is this hyperphosphorylation that promotes the intraneuronal aggregation of tau into NFTs (128-130). This hyperphosphorylation disrupts the neuronal cytoskeleton, and similar to Aβ, contributes to synapse loss and cognitive decline (131, 132). The recent update to the NIA-AA guidelines for AD diagnosis highlights the centrality of tau in AD, with both tau PET and p-tau being included as core AD biomarkers[1]. This is in contrast to the 2018 update to the NIA-AA criteria, where tau pathology in the

absence of Aβ was thought to indicate a non-AD (NAD) pathological change (44).

The Braak and Braak staging for AD is centred around NFTs, and shows a strong correlation between tau burden and an increased severity of cognitive and clinical symptoms (133). In fact, despite changes in Aβ fluid biomarkers occurring prior to changes in tau fluid biomarkers (92), concrete evidence has shown tau pathology appears decades before Aβ plaque deposition (134). Indeed, Arnsten and colleagues (135) propose that p-tau enhances APP cleavage and hence Aβ generation, thus resulting in AD.

Additional arguments in favour of the tau hypothesis have largely been centred around the previous failures of immunotherapy agents targeting Aβ pathology. Indeed, Kametani and Hasegawa (123) argue that it is in fact impairments in APP metabolism, rather than Aβ production and Aβ plaque formation, that triggers AD, and that the disease progresses through tau pathology. Furthermore, *in vitro* and *in vivo* studies looking at the effects of tau suppression or deletion have shown a neuroprotective effect on neurodegeneration and the associated cognitive deficits, even in the presence of Aβ pathology (136-138). However, a study conducted by Shipton and colleagues (139) emphasises the complexity of the relationship between Aβ and tau. Their mouse study revealed that whilst tau is required to induce cognitive impairment in the presence of Aβ pathology, Aβ pathology is required to induce excessive tau phosphorylation, indicating a synergistic relationship between the two proteins. Indeed, current evidence supports this finding by Shipton and colleagues (139), proposing that tau phosphorylation is most likely a neuronal response to Aβ, rather than a stand-alone pathological event that can lead to AD directly (140). This suggests that tau phosphorylation, and the subsequent tau pathology, seen in AD is Aβ-induced – a view further highlighted by increases in CSF p-tau being unique to AD, not being observed in other tauopathies (140-142).

Whilst plasma p-tau was found to increase prior to any significant changes in the plasma $A\beta_{42/40}$, plasma $A\beta_{42}$ does significantly decrease prior to any changes in plasma p-tau concentrations (92). It is clear that the relationship between Aβ and tau is complex, such that the role of one cannot be separated from that of the other in the context of AD neuropathology and initiating mechanisms. However, it is not clear whether the complexities of this relationship warrant the acceptance of the tau hypothesis.

1.3.2.3 The neuroinflammatory hypothesis – Alzheimer's disease as a neuroinflammatory condition

Neuroinflammation refers to the inflammatory processes occurring within the central nervous system (CNS), triggered by an inflammatory challenge such as an infection or trauma. It is mediated by the innate immune cells of the CNS – glial cells – becoming activated in response to the assault. As such, the neuroinflammatory hypothesis proposes that it is the uncontrolled and prolonged activation of these glial cells, due to increasing Aβ and NFT burden, that drives disease progression in AD through the promotion of chronic inflammation and the loss of synapses around plaques (143, 144).

Increasing amounts of evidence are emerging to show that neuroinflammation and the activation of glial cells, particularly microglia, play a central role in AD pathogenesis and neuropathology (29, 145). As the primary immunosurveillance cells of the CNS, microglia are the first cells to be activated in response to foreign material within the brain. In contrast to microglia, astrocytes function predominantly as a neurosupportive cell type, contributing largely to synaptogenesis, and maintaining synapse and BBB integrity (145, 146). Evidence has shown that both Aβ and tau induce microglial activation (147, 148). Upon activation, microglia secrete pro-inflammatory cytokines, and act as the macrophages of the brain to clear the abnormal debris (149, 150). Furthermore, *in vivo*

investigations have revealed the presence of dystrophic neurites in close proximity to Aβ plaques, which both microglia and astrocytes respond to in an attempt to repair the damage (151). Should inflammation truly be the driver of AD, it would be expected that targeting this inflammation should halt disease progression. However, studies looking at the effects of anti-inflammatory drug use in AD have shown mixed results, with some finding that non-steroidal anti-inflammatory drugs (NSAIDs), but not corticosteroids, reduces risk of AD (152), whilst others show no effect (153). Although *in vitro* and *in vivo* investigations have observed an anti-amyloidogenic effect of NSAID treatment (154, 155), the few clinical trials conducted in humans have observed little to no effect of NSAIDs in preventing AD progression (156). Of the observational studies conducted, most required long-term treatment of over two years to produce any protective effect, which poses safety concerns associated with long-term NSAID use.

Interestingly, the role of neuroinflammation in AD pathogenesis remains highly debated. Some papers argue that neuroinflammation is neuroprotective, designed to clear Aβ plaques, whilst others argue that it is neurotoxic by promoting AD progression through cytokine release, phagocytosis of synapses, neurodegeneration, and the inhibition of neurogenesis (157-162). Further still, a review paper by Edwards (163) proposed an alternative unifying hypothesis for AD pathogenesis, whereby they suggest the primary driver for AD progression following Aβ plaque deposition and Aβ-induced synaptic damage is an inadequate microglial response. The author introduces the idea that the magnitude with which microglia respond correlates with disease progression, proposing that microglia are responsible for removing damaged synapses and hence play a neuroprotective role in AD. Consequently, this protective role of microglia prevents damage from propagating down the axon, thus breaking the cycle of Aβ-induced synaptic dystrophy. This hypothesis provides an alternative explanation for why some elderly patients exhibit an equivalent burden of plaques and tangles as advanced AD patients

following post-mortem, without displaying any noticeable cognitive deficits during examination prior to death (164). In essence, the plaque load an individual can tolerate prior to neurodegeneration occurring is dependent on the genetic characteristics of their microglia, which determines the rate at which damaged synapses are phagocytosed (163). Whilst this argument seems compelling, evidence has shown that in the presence of AD neuropathology, both microglia and astrocytes adopt a reactive phenotype, termed reactive gliosis, which has both neuroprotective and neurotoxic effects within AD brains (145). Therefore, it is possible that the role of innate immunity in AD is a mixture of the two, whereby it is neuroprotective during the pre-symptomatic stage, but later becomes neurotoxic during the symptomatic stages of the disease (165, 166).

In recent years, the neuroinflammatory hypothesis has moulded into a potentially more plausible argument termed the amyloid cascade-inflammatory hypothesis, whereby neuroinflammation is thought to link Aβ plaques and tau phosphorylation, acting as an extension to the amyloid cascade hypothesis (156). Given the multifactorial nature of AD, it is clear that neuroinflammation plays a role, albeit not fully understood.

1.4 Biomarkers, existing cerebrospinal fluid and plasma amyloid-β tests, and the need for novel biomarkers

Histopathological analysis of the brain at autopsy remains the gold standard for definitively diagnosing AD. However, given that the neuropathological processes underlying AD begin several years before symptom-onset, molecular biomarkers have been developed to increase the accuracy of diagnosing AD clinically (167). A biomarker is a naturally occurring, detectable indicator that can be measured to assess a physiological or pathological state (168, 169). The importance of biomarkers is highlighted in the recent update to the NIA-AA research framework[1], in which a clinical diagnosis of AD is supported by biomarker evidence of a disease-specific pathophysiological signature, rather than by clinical symptoms alone (44). A key reason for this is the inaccuracy of a diagnosis based solely on symptoms, with one multi-centre study observing the sensitivity and specificity of clinically probable AD to detect Braak stages V/VI to be 76.6% and 59.5%, respectively (170, 171). Additionally, AD can present differently in younger patients, and its symptoms overlap with several other neurodegenerative disorders, including vascular dementia (VaD), and mood disturbances such as depression (172). A correct diagnosis is important to ensure patients receive the correct management (of AD, or of alternative conditions), and to provide prognostic information, advice, and support. In light of the recent advances in disease-modifying treatments, delaying diagnosis until symptoms are displayed would not be in the best interests of the patient.

1.4.1 The ATXN criteria

There are two main types of biomarkers for molecular AD cerebral changes – neuroimaging biomarkers and fluid biomarkers (173). The ATXN criteria for AD diagnosis, previously called the AT(N) criteria, divides both neuroimaging and fluid AD biomarkers into groups, based on the pathophysiological characteristic of AD that they measure. Fluid biomarkers offer the advantage of being able to detect the presence of multiple molecular pathologies in one bio-

sample, as well as being of lower cost in comparison to neuroimaging. However, they do not provide anatomical information on the location and extent of pathologies, which can be gained from neuroimaging. This therefore highlights the benefit of using both types of biomarkers in combination with one another to gain the clearest picture of pathology within an individual.

The ATXN criteria is summarised in Table 1.1, and is depicted graphically in Figure 1.4. “A” refers to Aβ pathology, as depicted by increased amyloid PET uptake, or decreased CSF or plasma $A\beta_{42/40}$. “T” refers to tau pathology, as depicted by positive tau PET tracer uptake or increased CSF or plasma p-tau_{181} or p-tau_{217}. “A” and “T” biomarkers are the ‘core AD biomarkers’, meaning that their sole presence is sufficient to warrant an AD diagnosis. “N” refers to neurodegeneration or neuronal injury, as depicted by decreased signal on [^{18}F]-fluorodeoxyglucose (FDG)–PET, grey matter atrophy on anatomic magnetic resonance imaging (MRI) or increased CSF or plasma neurofilament light chain (NfL). “I” refers to neuroinflammation, but specifically astrocytic activation, as depicted by increased CSF or plasma glial fibrillary acidic protein (GFAP). “N” and “I” biomarkers are the non-specific biomarkers of tissue reactions involved in AD pathophysiology. “V” refers to vascular brain injury for patients with concurrent cerebrovascular disease, as depicted by anatomic infarction, white matter hyperintensities and abundant dilated perivascular spaces seen on MRI. Finally, “S” refers to α-synuclein pathology for patients with concurrent neuronal synuclein diseases (Parkinson’s disease [PD)] and DLB), as depicted by CSF or plasma α-synuclein seed amplification assays (α-synSAA). “V” and “S” biomarkers are the biomarkers of common NAD co-pathologies.

As an extension to the AT(N) criteria detailed in the 2018 edition of the NIA-AA research framework, the category “X” in the ATXN criteria details three additional categories for inflammatory/immune biomarkers (“I”), and biomarkers of common NAD pathologies that often co-exist with AD (“V” and “S”) (174). The N is no longer in

brackets as additional biomarker categories that are not specific to AD are featured within the criteria. A comparison of the ATXN criteria with the AT(N) criteria can be seen in Table 1.2. Whereas the AT(N) criteria recognised CSF as the only source of fluid biomarkers, this recent update to the NIA-AA research framework for AD diagnosis has incorporated blood-based biomarkers, in line with advances in the fluid biomarker field. Although CSF has the advantage of being in direct contact with the cerebral extracellular space, blood is less invasive to collect. Consequently, it is more suitable for obtaining repeated measurements from patients, and is more easily accessible in low-resource and non-specialist settings worldwide (175-177). However, whilst blood-based biomarkers have the potential to function as an initial diagnostic screening tool in a primary care setting, prior to more in-depth investigations in specialist centres (175, 178), measuring biomarkers of brain diseases in the blood is not without its challenges, namely: 1) analyte concentrations are 10-100-fold lower in blood compared with CSF as a direct consequence of the BBB (179); 2) some AD biomarkers are expressed by extra-cerebral tissues; 3) proteases in the blood may break down analytes of interest prior to their measurement (180). This puts extra demand on the pre-analytical and analytical processes of relevance to blood biomarker measurements for CNS diseases, and emphasises the need for increased sensitivity in the instruments used to measure such analytes in blood.

Alongside the incorporation of blood-based biomarkers into the framework, the ATXN criteria has also seen the addition of tau biomarkers as core AD biomarkers. Previously, for an individual to be characterised as being on the AD continuum, they must have displayed an A+ profile, indicating the presence of abnormal Aβ biomarkers. Individuals displaying only tau pathology would be categorised as having NAD pathological changes (44). It is well known that p-tau is a biomarker unique to AD, and is not increased in individuals with other tauopathies or neurological conditions (130, 181, 182). In fact, both CSF and plasma/serum p-tau are significantly

increased in AD compared to control (CTRL) and other neurodegenerative diseases, regardless of which epitope is measured (128, 129, 183-189). However, building on this, increasing evidence is suggesting that p-tau is secreted in response to Aβ pathology, and hence may function as a measure of Aβ-induced tau phosphorylation (140-142). Indeed, in their cross-sectional study looking at biomarker trajectories with increasing Aβ burden, Palmqvist and colleagues (92) showed that plasma p-tau changes significantly before CSF and plasma $A\beta_{42/40}$, and CSF p-tau, and it continues to increase with worsening Aβ burden. This suggests plasma p-tau may be one of the earliest biomarkers to change in AD, and it continues to reflect Aβ pathology whilst also giving additional information on the progression of tau pathology up to 10 years before tau PET positivity is detected (33). One benefit of tau PET compared to biofluid measurements of p-tau is that it allows the localisation of tau pathology as well as the monitoring of tau accumulation over time, rather than only providing a snapshot of the pathological state in the individual at the time of measuring (44). Indeed, Mattsson and colleagues (190) found that whilst tau PET and CSF p-tau showed identical diagnostic performance in earlier stages of AD, tau PET showed a superior diagnostic performance in more advanced disease stages. However, one key drawback of tau PET is that increased signals are not unique to AD, and can be seen in other NAD dementias and tauopathies (191, 192). As such, this change to the ATXN criteria to allow AD diagnoses based solely on the presence of tau pathology, including tau pathology identified by tau PET alone, may be seen as controversial. However, given that clinicians diagnose patients based off a holistic picture of the individual, and additionally, the localisation of tau PET tracer uptake will help inform a correct diagnosis of an AD or NAD cause of pathology, a change to include “T” as one of the core AD biomarkers is understandable and clearly evidence-based.

Finally, another key alteration seen in the ATXN criteria is the removal of $A\beta_{42}$ measurements in isolation as an “A” biomarker,

along with the removal of total tau (t-tau) as an “N” biomarker, leaving $A\beta_{42/40}$ and NfL as the only “A” and “N” fluid biomarkers, respectively. Whilst it is well-known that biofluid concentrations of $A\beta_{42}$ reduce in AD, as mentioned in section 1.2, looking at $A\beta_{42}$ in combination with $A\beta_{40}$, as part of the $A\beta_{42/40}$, is of far greater benefit than looking at either isoform of Aβ in isolation, as it combats the issues of inter-individual differences in Aβ production which may result in misinterpretation of their individual Aβ concentrations (193, 194). Furthermore, evidence has shown that $A\beta_{42/40}$ has an increased diagnostic accuracy compared with looking at $A\beta_{42}$ alone (42, 45, 195, 196), and CSF $A\beta_{42/40}$ shows a higher concordance with amyloid PET than $A\beta_{42}$ alone (197). With regards to t-tau, whilst CSF t-tau was previously featured in the 2018 NIA-AA framework for AD diagnosis, it was included as a general biomarker of neurodegeneration (44). Although increased CSF t-tau is not only observed consistently in AD (198), but is also seen in other cases of neuronal injury (199), recent studies have suggested that the t-tau measured in the context of AD is secreted alongside p-tau, and reflects Aβ-induced tau secretion from living neurones (200). Although these neurones will eventually degenerate and die, the t-tau being measured in AD is not thought to be a direct marker of this neuronal injury and death (201). In contrast, the high CSF t-tau with normal CSF p-tau, measured in the context of NAD neurodegeneration is a direct result of massive neuronal death, and in these cases, t-tau is a marker of neuronal injury (201). Therefore, in combination with raised p-tau, increased CSF t-tau is thought to reflect AD pathology, rather than simply being a non-specific effect of neuronal damage (46). However, studies looking at blood t-tau measurements have found conflicting results. Whilst most studies agree that plasma t-tau increases in AD (202-205), some observe a strong correlation between plasma and CSF t-tau (204), whilst others observe a weak (205) or even absent (203) correlation. Furthermore, several studies have observed a significant overlap in plasma t-tau between AD and NAD groups (202, 203, 205), highlighting that plasma t-tau may not be a useful diagnostic blood biomarker for AD.

Given that this most recent update to the NIA-AA criteria for AD diagnosis[1] centres on the addition of blood-based biomarkers to the criteria, the removal of t-tau due to its limited usefulness in blood is understandable.

Criteria Aspect	Pathology	Neuroimaging Biomarkers	CSF Biomarkers	Blood biomarkers
A	Aβ	↑Amyloid PET	↓$Aβ_{42/40}$	↓$Aβ_{42/40}$
T	Tau	↑Tau PET	↑$p\text{-}tau_{181}$ or $p\text{-}tau_{217}$	↑$p\text{-}tau_{181}$ or $p\text{-}tau_{217}$
X (V)	Vascular brain injury	MRI		
X (S)	α-synuclein		α-synSAA	α-synSAA
X (I)	Neuroinflammation (astrocyte activation)		↑GFAP	↑GFAP
N	Neurodegeneration	MRI or ↓FDG-PET	↑NfL	↑NfL

Table 1.1 - ATXN criteria for AD diagnosis

Summary of ATXN criteria for Alzheimer's disease (AD) diagnosis. "A" refers to amyloid-β (Aβ) pathology, as depicted by increased amyloid positron emission tomography (PET) uptake, or decreased cerebrospinal fluid (CSF) or plasma $Aβ_{42}/Aβ_{40}$ ratio ($Aβ_{42/40}$). "T" refers to tau pathology, as depicted by increased tau PET tracer uptake or increased CSF or plasma $p\text{-}tau_{181}$ or $p\text{-}tau_{217}$. "A" and "T" biomarkers are the 'core AD biomarkers', indicated by the yellow highlighting. "V" refers to vascular brain injury for patients with concurrent cerebrovascular disease, as depicted on magnetic resonance imaging (MRI). "S" refers to α-synuclein pathology for patients with concurrent neuronal synuclein diseases, as depicted by CSF or plasma α-synuclein seed amplification assays (α-synSAA). "V" and "S" biomarkers are the biomarkers of common non-AD co-pathologies, indicated by the red highlighting. "N" refers to neurodegeneration or neuronal injury, as depicted by decreased signal on [^{18}F]-fluorodeoxyglucose (FDG)–PET, grey matter atrophy on MRI or increased CSF or plasma neurofilament light chain (NfL). "I" refers to neuroinflammation, but specifically astrocytic activation, as depicted by increased CSF or plasma glial fibrillary acidic protein (GFAP). "N" and "I" biomarkers are the non-specific biomarkers of tissue reactions involved in AD pathophysiology, indicated by the blue highlighting.

AT(N) CRITERIA (2018)	ATXN CRITERIA (2023)
3 categories – A, T, (N)	4 categories – A, T, X, N – with X containing 3 subcategories
CSF recognised as only source of fluid biomarkers	CSF and blood recognised as sources of fluid biomarkers
Abnormal “A” biomarkers necessary for AD diagnosis	AD can be diagnosed with abnormal “A” biomarkers and/or “T” biomarkers
$A\beta_{42}$ included in “A” fluid biomarkers alongside $A\beta_{42/40}$	$A\beta_{42}$ removed from “A” fluid biomarkers, leaving only $A\beta_{42/40}$
P-tau_{181} as the only “T” fluid biomarker	P-tau_{217} added alongside p-tau_{181} as the “T” fluid biomarkers
T-tau included in “(N)” fluid biomarkers	T-tau removed from “N” fluid biomarkers

Table 1.2 - Comparison of AT(N) criteria with ATXN criteria for AD diagnosis

Summary of key differences between the AT(N) criteria and ATXN criteria for Alzheimer’s disease (AD) diagnosis. Namely: the addition of the “X” category, containing 3 subcategories of biomarkers; the addition of blood-based biomarkers; the addition of “T” biomarkers as core AD biomarkers, indicating that AD can be diagnosed solely by the presence of abnormal tau pathology; the addition of phosphorylated tau 217 (p-tau_{217}) alongside p-tau_{181} as “T” biomarkers; and finally, the removal of amyloid-β 1-42 ($A\beta_{42}$) and total-tau (t-tau) from the “A” and “T” categories, respectively.

1.4.2 Existing cerebrospinal fluid and plasma biomarkers for Alzheimer’s Disease

In this section, we will delve deeper into the fluid biomarkers for AD pathology detailed in the ATXN criteria, namely $A\beta_{42/40}$, p-tau, GFAP and NfL.

1.4.2.1 Amyloid-β biomarkers

The formation and pathogenicity of Aβ has been reviewed in section 1.2. Furthermore, the fluid biomarkers for Aβ pathology recognised by the ATXN criteria are decreased CSF or plasma $A\beta_{42/40}$. Whilst CSF $A\beta_{42/40}$ measurement is extremely robust and has been for several years, showing a clear distinction between AD and NAD diagnostic groups (206), plasma $A\beta_{42/40}$ remains less so. Early investigations into the use of plasma $A\beta_{42}$ and $A\beta_{42/40}$ as predictors of future AD development showed inconsistent results, with some

reporting that high plasma $A\beta_{42}$ concentrations or a high $A\beta_{42/40}$ are risk factors for AD development, whilst others reported the opposite, and still others reported no significant differences in plasma $A\beta_{40}$ and $A\beta_{42}$ between AD and CTRL cases (207-211). The potential reasons for this include: the limited analytical sensitivity of the enzyme-linked immunosorbent assay (ELISA)-based techniques in use at the time; sub-optimal or variable sample handling protocols; and, in many cases, the use of clinical criteria for diagnosis rather than evidence for Aβ pathology. Recent advances in immunoassay technology to detect and quantify single protein measurements have increased their analytical sensitivity and have made it possible to quantify protein biomarkers at subfemtomolar (10^{-15} M) concentration levels. There have been three main developments that have allowed for this. One has been to replace the enzyme label of the detection antibody with a molecule that emits light upon an electrochemical reaction, so called electrochemiluminescence (ECL) (212). The second is a refinement of the basic ELISA technology, so called Single molecule array (Simoa), compartmentalising the detection reaction within femtolitre-sized wells using magnetic beads onto which the immunocomplexes are captured, and digitalising protein detection (213-215). The final advancement has been the development of sensitive mass spectrometry (MS)-based assays to quantify plasma Aβ peptides (216). These technological advances have led to breakthroughs in efforts to detect and quantify Aβ present in peripheral blood.

Following these advances, several studies have observed a significant decrease in plasma $A\beta_{42/40}$ compared to CTRLs and patients with either mild cognitive impairment (MCI) or subjective cognitive decline (178, 217-220). Some have also observed a correlation between CSF and plasma $A\beta_{42/40}$ (92, 206, 221), albeit with less pronounced changes seen in plasma compared to those seen in CSF. The subtle changes observed in plasma $A\beta_{40}$ and $A\beta_{42}$, and hence the $A\beta_{42/40}$, are due to continuous contributions from extra-cerebral tissues, resulting in less dynamic changes in these

analytes in the blood (92, 222). This is further highlighted in the AlzBiomarker database[2], which reveals that in contrast to the 8.7% decrease in CSF $A\beta_{40}$ concentration (p=<0.0001) and 44.8% decrease in CSF $A\beta_{42}$ concentration (p=<0.0001), which is expected as this reflects Aβ aggregation into plaques, plasma $A\beta_{40}$ increases by 4.4% (p=0.151), and plasma $A\beta_{42}$ increases by 4.9% (p=0.0300). The marginal increases in these biomarkers in plasma, particularly considering that $A\beta_{42}$ concentrations should decrease in the presence of plaque pathology, as well as the lower overall degree of change observed, is most likely a consequence of the peripheral production of Aβ, which is unaffected by pathology. Furthermore, a clear overlap in plasma $A\beta_{42/40}$, measured using MS, but not CSF $A\beta_{42/40}$, measured using Elecsys (ECL-based) was seen in amyloid PET-negative compared to PET-positive individuals in a study conducted by Schindler and colleagues (206). Whilst the authors argue that this overlap highlights amyloid PET-negative individuals at greatest risk of conversion to amyloid PET-positivity, this was only true for 8 (10.8%) of the amyloid PET-negative individuals who were followed up longitudinally in the study, with the remaining 66 amyloid PET-negative individuals remaining as so. Although plasma $A\beta_{42/40}$ has been included in the most recent update to the NIA-AA diagnostic criteria for AD[1], there remains less than a 20% difference in plasma $A\beta_{42/40}$ of individuals with AD compared to NAD (221, 223, 224). A 2022 review by myself and colleagues (225) proposed plasma GFAP or p-tau as indirect blood biomarkers of Aβ pathology. Whilst GFAP has since been added to the NIA-AA diagnostic criteria for AD diagnosis[1], it has been included as a marker of neuroinflammation, rather than of Aβ pathology. Taken together, the evidence presented highlights the need to develop and measure biomarkers of Aβ pathology which can better distinguish between AD and NAD individuals, particularly in blood, but which also better reflect the pathology occurring within the brains of AD patients, whether that be through developing more sensitive technology to

[2] https://www.alzforum.org/alzbiomarker/ad-vs-ctrl - accessed 13th August 2023

measure these biomarkers, or by developing assays for novel Aβ biomarkers.

1.4.2.2 Phosphorylated tau biomarkers

Similar to Aβ, and as already addressed briefly in section 1.3.2.2 The tau hypothesis, tau is a natural component of mature neurones, with some healthy individuals also having a small percentage of p-tau, as phosphorylation appears to be important in enabling the normal function of tau within neurones (127). However, in AD, tau is 3-4-fold more phosphorylated, and it is this hyperphosphorylation that promotes the intraneuronal aggregation of tau into NFTs (128-130). However, alongside intraneuronal aggregation, p-tau is secreted from neurones, and can subsequently be measured in CSF and blood. In fact, it is possible that CSF changes in p-tau occur prior to NFT formation (127). There are up to 85 sites at which tau can be phosphorylated (226), with the three most widely investigated sites in relation to AD being tau phosphorylated at threonine 181 (p-tau$_{181}$), threonine 217 (p-tau$_{217}$) and threonine 231 (p-tau$_{231}$). In contrast to t-tau – which was previously included in the AT(N) criteria for AD diagnosis as a general marker of neurodegeneration and neuronal injury (44), but has since been removed from the ATXN criteria[1] (see section 1.4.1 The ATXN criteria) – there is no change in CSF p-tau concentrations in other tauopathies and neurological conditions (130, 181, 182). Rather, CSF p-tau is significantly increased in AD compared to CTRLs and other neurodegenerative diseases, regardless of which epitope is measured (128, 129, 183-185). In light of this, several studies have shown a clear correlation between CSF p-tau and Aβ pathology measures (33, 127, 227), with changes in CSF p-tau also being observed several years prior to symptom onset, and when only subtle changes in Aβ pathology measures are detected. Furthermore, CSF p-tau has been shown to correlate more strongly with cognitive impairment than Aβ biomarkers (44, 131, 228). Given that increases in CSF p-tau are unique to AD, and are not observed in other tauopathies, it is hypothesised that p-tau may be a measure of Aβ-induced tau phosphorylation (140-142).

Furthermore, CSF p-tau$_{181}$, p-tau$_{217}$ and p-tau$_{231}$ exhibit remarkably high increases of 87%, 999% and 489%, respectively, in AD compared to CTRLs[2]. Comparing and contrasting p-tau$_{181}$, p-tau$_{217}$ and p-tau$_{231}$ is beyond the scope of this thesis. However, the analytical and clinical performance of assays detecting all three of these tau epitopes has recently been assessed by Bayoumy and colleagues (229). Given the overwhelming evidence showing CSF p-tau to be a robust biomarker for AD, the question lies with whether plasma p-tau correlates as strongly with Aβ pathology, and whether there is scope for plasma p-tau to function as a biomarker of Aβ pathology better than Aβ biomarkers.

Attempts to quantify plasma p-tau began in 2016 and have proven largely successful. Similar to CSF p-tau, plasma p-tau has been found to increase in AD compared to MCI, NAD dementias and cognitively unimpaired CTRLs (186-189). In particular, Mielke and colleagues (230) showed that plasma p-tau is strongly associated with Aβ PET imaging, and is highly sensitive and specific to increased cerebral Aβ burden, whilst Karikari and colleagues (231) showed that plasma p-tau increases markedly in amyloid PET-negative individuals who also have decreased CSF Aβ concentrations. Furthermore, in their cross-sectional study looking at biomarker trajectories with increasing Aβ burden, Palmqvist and colleagues (92) showed that in AD plasma p-tau changes significantly before CSF and plasma Aβ$_{42/40}$, and CSF p-tau, all of which exhibit changes before amyloid PET positivity is detected. In addition, they showed that plasma p-tau continues to increase as Aβ burden increases (92). This highlights that plasma p-tau may be one of the earliest biomarkers to change in AD, and it continues to reflect Aβ pathology whilst also giving additional information on the progression of tau pathology up to 10 years before tau PET positivity is detected (33). This is further highlighted by increases in plasma p-tau$_{181}$ and p-tau$_{217}$ of 80% and 288%, respectively, in AD compared to CTRLs[2].

1.4.2.3 Glial fibrillary acidic protein

GFAP is a well-known marker of astrocytosis in the CNS. Early *in vivo* studies observed Aβ-containing astrocytes in the brains of AD patients (232, 233). A subsequent *in vitro* investigation revealed that astrocytes can phagocytose Aβ (234), which is the most likely cause of the intracellular Aβ observed in the two aforementioned *in vivo* studies. Whilst the exact role of astrocytosis in AD remains unclear, it is apparent that reactive astrocytes follow the same spatial distribution as plaques in post-mortem analyses of AD brains (235, 236). Furthermore, investigations have revealed that reactive astrocytes are involved in Aβ production and toxicity (237, 238). It was previously thought that the number of astrocytes surrounding plaques increases as the disease progresses (239, 240). However, more recent studies using a combination of PET tracers have revealed that astrocytosis (depicted by the ^{11}C-deuterenium-L-deprenyl tracer), is an early phenomenon in AD (depicted by the ^{11}C-Pittsburgh compound-B tracer for Aβ plaques), and this astrocytosis decreases as plaque load increases (241-243).

Studies have shown that CSF GFAP concentrations in AD are significantly increased compared to healthy CTRLs (244, 245), and are significantly increased in the cognitively unimpaired Aβ-positive, tau-positive preclinical stage of AD (246). However, cross-disease comparisons between AD, FTLD and DLB reveal that CSF GFAP concentrations are significantly increased in all three diseases compared to CTRLs, with FTLD concentrations being significantly greater compared to AD and DLB (245). This highlights that elevated CSF GFAP is not specific to AD, and hence has little diagnostic value in distinguishing AD from other neurodegenerative diseases.

Interest in GFAP as a plasma biomarker for AD came about due to the possibility of more sensitive assays making it possible to measure within blood. Similar to CSF GFAP, elevated plasma GFAP concentrations have been observed in a variety of neurodegenerative and non-neurodegenerative neurological conditions, including AD

(247-250). However, further investigations have revealed that plasma GFAP concentrations correlate strongly with cerebral Aβ pathology, as measured by PET (251), as well as with decreasing white matter volume and worsening cognitive function (251-254), and hence it is relatively AD- and Aβ-specific. In fact, simultaneous comparisons in two independent cohorts between plasma GFAP and NfL, a sensitive biomarker of neuronal injury independent of Aβ pathology, revealed that plasma GFAP may be more sensitive to cortical and cognitive changes than plasma NfL (252). Plasma GFAP is higher in Aβ-positive cognitively unimpaired individuals at risk of developing AD (255), and longitudinal investigations have observed that plasma GFAP can predict subsequent conversion of MCI patients to AD with an AUC of 0.84 (95% CI 0.77-0.91) (256). Furthermore, individuals with a positive CSF $A\beta_{42/40}$, but with amyloid PET levels below the cut off for being deemed amyloid PET-positive (i.e. individuals in the earliest preclinical stage of AD), were observed to have significantly higher plasma GFAP concentrations than Aβ-negative individuals, despite there being no significant difference in CSF GFAP concentrations between the two groups (257). One possible reason for this is that GFAP may be released more directly into the bloodstream by astrocytic end feet, thus making plasma changes in GFAP concentrations more pronounced than changes in CSF GFAP concentrations (258). This is further supported by a plethora of evidence highlighting that the integrity of the BBB is abnormal in AD, resulting in microvascular leakage of proteins into the blood (259). Another reason for significant increases in plasma GFAP, but not CSF GFAP, in AD patients may be due to GFAP being extremely stable in blood, whereas CSF GFAP is much more sensitive to freeze-thaw cycles over time (260, 261). However, further work must be undertaken to better understand the reason for this discrepancy between plasma and CSF GFAP. Nonetheless, together these studies highlight that astrocytosis begins in the prodromal stage of AD, and elevated plasma GFAP is associated with neuronal injury, worsening cognition, and markers of cerebral Aβ pathology, giving a much broader picture of the state of the individual. Furthermore, CSF

GFAP increases by 50.2% (p=0.0555) in AD vs CTRLs, compared to an increase of 92.8% (p<0.0001) in plasma[2], highlighting why both CSF and plasma GFAP have been added to the recent update of the NIA-AA diagnostic criteria for AD[1] as non-specific biomarkers of tissue reactions involved in AD pathophysiology (see section 1.4.1 The ATXN criteria).

1.4.2.4 Neurofilament light chain

Along with microtubules and microfilaments, neurofilaments form the neuronal cytoskeleton (262). However, one particular subunit, NfL, is expressed predominantly in large-calibre myelinated axons (263). Following neuronal damage and degeneration, NfL is released into the extracellular space, and is detectable both in CSF and in blood (264). Therefore, by proxy, biofluid changes in NfL are not specific to AD, but reflect general neuronal death and axonal loss. Nonetheless, CSF NfL is significantly increased in AD compared to CTRLs, and predicts progression from MCI to AD (198, 264-268). Of particular interest to us is whether CSF NfL correlates with Aβ pathology. A study by Zetterberg and colleagues (266) observed that whilst there were correlations between increased CSF NfL and decreased CSF $A\beta_{42}$, there was no significant difference in CSF NfL concentrations between the Aβ-positive and Aβ-negative groups. This has been further corroborated by several studies (269-271). Interestingly, Dhiman and colleagues (271) observed that a combination of CSF NfL and a ratio between NfL and $A\beta_{42}$ (NfL/$A\beta_{42}$) predicted Aβ burden, brain atrophy and altered cognition. Nonetheless, these studies highlight that changes in CSF NfL occur independently of Aβ pathology, and correlate better with tau biomarkers and other measures of neurodegeneration (198, 266, 271).

Overwhelming evidence has shown that not only does plasma NfL significantly increase in AD compared to CTRLs, but it also correlates with CSF NfL and with tau biomarkers (272-274). Mattsson and colleagues (272) and Lewczuk and colleagues (273) both observed a correlation between increased plasma NfL and decreased CSF $A\beta_{42}$.

However, when this correlation was investigated further, Lewczuk and colleagues (273) found it to no longer be significant when the diagnosis of each individual was taken into consideration – a finding supported by Sanchez-Valle and colleagues (275). Although increases in plasma NfL are not unique to AD, and can be seen in several other neurodegenerative and non-neurodegenerative conditions (276-279), a recent longitudinal study revealed that plasma NfL is increased up to 22 years prior to expected AD symptom onset (280), which is consistent with earlier studies of serum NfL in FAD (281, 282). With very little difference between plasma and CSF NfL increases in AD compared to CTRLs (98% in CSF vs 85% in plasma[2]) it is clear that plasma NfL may be a more useful biomarker in AD than CSF NfL.

1.5 Immunoassays, mass spectrometry and the need for increased sensitivity

Following the development of ELISA in 1971 (283, 284), which harnessed the immunofluorescence technology first developed in 1941 (285), ELISA became the gold standard method for protein detection throughout the scientific field. This is particularly due to the improved sensitivity of ELISA compared to other techniques such as western blotting and protein microarrays (213). However, over time, it has become clear that more sensitive methods for protein detection are needed, particularly for neurodegenerative diseases. Advancements in the immunoassay and MS domains in recent years have made the greatest contributions to increasing the analytical sensitivity at which protein biomarkers can be measured. The first direct comparison between ECL and conventional ELISA measurements of plasma Aβ were conducted by Oh and colleagues (286). In their study, they observed a vastly improved dynamic range of plasma $A\beta_{40}$ and $A\beta_{42}$ measurements by using ECL, with a range of 29.3 to 213 pg/mL for ELISA $A\beta_{40}$ compared with 74.9 to 5344.4 pg/mL in ECL, and a range of 9.5 to 219 pg/mL for ELISA $A\beta_{42}$ compared with 10 to 3000 pg/mL in ECL. However, alongside ECL, arguably of greatest significance has been the development of digital ELISA, known as Simoa, and MS, all three of which have enabled the detection of proteins down to subfemtomolar (10^{-15} M) concentrations (215, 287), compared to ELISA detecting proteins down to picomolar (10^{-12} M) concentrations only. This is particularly important as the serum concentration of proteins involved in AD are thought to range from 10^{-16} to 10^{-12} M (288, 289).

1.5.1 Simoa overview

Simoa technology, developed by Quanterix Corporation (Billerica, USA), measures the fluorescence from single enzyme-labelled protein molecules conjugated onto superparamagnetic beads which are trapped within femtolitre-sized wells (215). These wells are designed to fit only one bead immunocomplex and are sealed with oil so that when the enzyme is exposed to its substrate, the resultant

fluorescence remains confined, allowing more accurate measurement of the intensity of the signal produced. The digital reading quantifies the fraction of enzyme-associated ("on") beads (f_{on}) compared with the fraction of beads with no immunocomplexes bound ("off" beads), and it is this digital quantification that greatly increases its sensitivity in comparison to ELISA (215). The mean fluorescence intensity of all active beads within the array (I_{bead}) is used alongside the mean fluorescence intensity of a single enzyme immunocomplex on a bead (I_{single}) and f_{on} to calculate the average number of enzyme complexes per bead (AEB). From the calculated AEBs of a standard calibration curve of known concentrations, the concentration of the analyte within the tested sample can be extrapolated. The Simoa workflow is summarised in Figure 1.5.

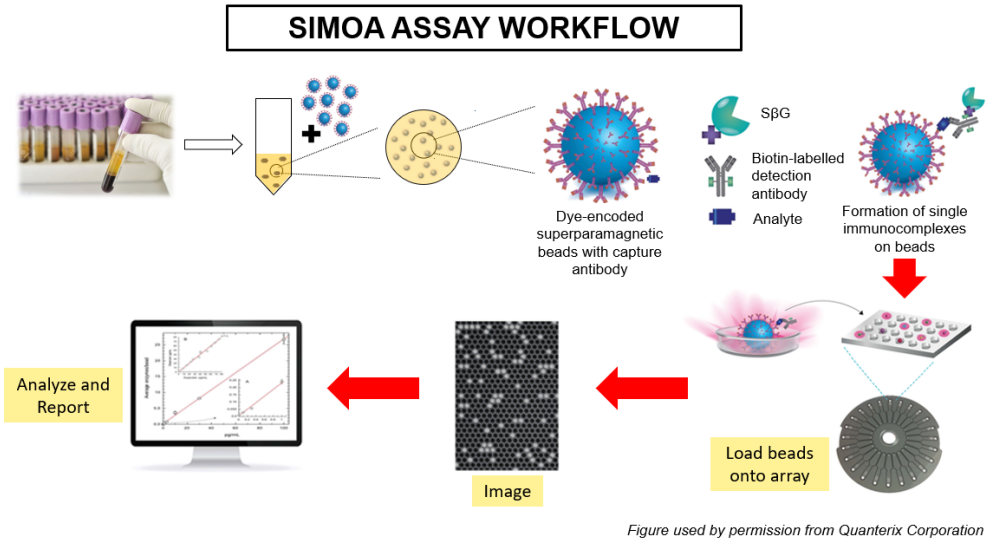

Figure 1.5 – Simoa assay workflow

Simoa assay workflow. Cerebrospinal fluid or blood is extracted from patient and processed as per centre guidelines. Sample is incubated with dye-encoded superparamagnetic beads, biotin-labelled detection antibody and streptavidin-β-galactosidase (SβG) in a series of incubations, forming single enzyme immunocomplexes on the beads. Beads are loaded onto an array disc, re-solubilised using resorufin-β-D-galactopyranoside, and imaged using the Simoa reader, which digitally analyses and reports the fluorescence.

1.5.2 Mass spectrometry overview

In contrast to Simoa, MS is an analytical technique for measuring analyte ions (or gas-phase-produced fragments) at their specific mass-to-charge ratio (*m/z*), and assessing the ion/fragment abundance at that specific *m/z* (290). This antibody-independent

method of protein detection and quantification naturally gives MS a higher specificity and selectivity compared to immunoassays. This can be important where there are no suitable antibodies for detection purposes, although antibodies can be utilised to enrich samples by immunoprecipitation (IP) prior to the MS step, so called IP-MS (291). Furthermore, because samples analysed by MS are typically handled under denaturing conditions, in aqueous-organic solvents, results are less influenced by matrix effects (i.e. the effect of other substances in the sample matrix on the ability to detect the analyte of interest) (292-294). Standard MS workflow involves an initial separation step of the analyte prior to analysis and detection within the mass spectrometer. In addition to IP, two common separation techniques coupled to MS include liquid chromatography (LC), so called LC-MS, and gas chromatography (GC), so called GC-MS (295, 296).

1.5.3 Comparisons of amyloid-β measurements using immunoassays vs mass spectrometry

Several comparisons between immunoassay- and MS-based measurements of Aβ have been conducted. A direct (same-sample) comparison of MS with Simoa-based quantification of $A\beta_{40}$ and $A\beta_{42}$ in a preclinical AD cohort, conducted by Keshavan and colleagues (297), observed that at this stage of disease, MS measurements showed a higher correlation with brain Aβ pathology than Simoa measurements. Further comparisons between MS and other immunoassay techniques have shown similar results. A head-to-head comparison of eight plasma $A\beta_{42/40}$ assays, including four MS and four immunoassays, two of which were Simoa-based assays, revealed that MS methods for plasma $A\beta_{42/40}$ measurement provide greater discriminative accuracy between Aβ-positive and Aβ-negative individuals, as measured by amyloid PET (298). Furthermore, MS correlates better with CSF $A\beta_{42/40}$ measurements, than immunoassay methods in the two independent disease cohorts assessed (298). In particular, an IP-MS workflow developed by Randall Bateman at Washington University was observed as the most superior in all aspects assessed.

More recently, a literature review conducted by Brand and colleagues (287) assessed the performance of MS and immunoassay measurements of plasma Aβ, alongside their clinical utilities for identifying Aβ plaques. The review compared twenty-one publications between 2014 and 2022 – ten MS-based (mostly IP-MS), three ECL-based, three Simoa-based, one ELISA-based, and four assessing multiple techniques (including Keshavan and colleagues (297) and Janelidze and colleagues (298)). Whist statistical analyses could not be performed to compare all the studies due to the differences in the cohorts used, comparisons of the area under the receiver operator characteristic curve (AUC) revealed that the MS assays consistently outperformed the immunoassays, not only when comparing studies with different cohorts but also when comparing studies using the same disease cohort. Overall, they observed weighted average AUCs when using a PET standard were 0.834 for IP-MS across twenty-one cohorts (0.846 for the Washington University-developed IP-MS alone across fourteen cohorts), 0.742 for IP-free LC-MS across five cohorts, 0.818 for ECL across six cohorts, 0.690 for Simoa across ten cohorts, and 0.734 for ELISA across three cohorts. When using a CSF standard, these weighted average AUCs were 0.866 for IP-MS across four cohorts, 0.803 for ECL across four cohorts and 0.726 for Simoa across two cohorts (287). To put these AUCs into perspective, an AUC between 0.8 and 0.9 is often described as optimal for disease diagnosis (299, 300), although in practice this depends on the disease being considered (*e.g.* prevalence, severity, treatability), and the diagnostic tools available.

Taken together, the promising results seen with MS, specifically IP-MS, in comparison to immunoassays opens questions as to whether MS may be the future of Aβ measurements. Indeed, one key advantage of MS is its simultaneous quantification of $A\beta_{40}$ and $A\beta_{42}$ with an internal standard, thus reducing the variance introduced by measuring them separately with external standards, as is the case for immunoassays. Furthermore, immunoassays are more impacted

by matrix effects than MS (292-294). However, it is important to consider the space, cost and sample preparation time required for a mass spectrometer, and whether the differences between MS and immunoassays are significant enough to warrant a complete change to purely MS-based analyses of these proteins.

In addition, the review by Brand and colleagues (287) opens questions as to whether Simoa truly is as remarkable a modality as expected for Aβ quantification, particularly given that its diagnostic accuracy is outperformed by all other modalities analysed when using either a PET standard or a CSF standard, and its AUC remains far from the 0.8-0.9 optimal range for disease diagnosis. It is possible that differences in pre-analytical handling may account for the relatively poor diagnostic performance of Simoa. However, if the standardised guideline for pre-analytical variables in AD blood-based biomarker research, developed in 2015 by O'Bryant and colleagues (301), is being applied correctly, this should not be the case. Alternatively, the diagnostic accuracy of Simoa may be impacted by the number of beads lost through the steps involved prior to bead analysis, many of which likely contain immunocomplexes of the analyte of interest bound. Whilst this bead loss has been addressed to some extent with the upgraded Simoa instrument prototype, discussed in more detail in section 1.5.4 The need for increased sensitivity, upgraded Simoa, and MOSAIC technology, addressing this bead loss issue with the standard Simoa instruments could be extremely beneficial in improving the diagnostic accuracy of the instrument.

1.5.4 The need for increased sensitivity, upgraded Simoa, and MOSAIC technology

As we move into the era of disease-modifying therapies for AD which target Aβ pathology, there is a need for more sensitive and robust techniques to measure changes in these proteins in trial participants. Indeed, despite the success seen in blood Aβ measurements in recent years, particularly using IP-MS, a more sensitive detection

method provides the possibility of further diluting samples prior to analysis, thereby reducing matrix effects experienced with immunoassays without compromising the detectability of proteins of interest (302). $A\beta_{42}$ concentration in blood is approximately 20 pg/mL (297). Upon dilution of samples, $A\beta_{42}$ concentrations sit in the femtomolar range, which can be measured with the currently available instruments. However, other isoforms of Aβ that are becoming of interest, such as $A\beta_{pE}$ and $A\beta_{43}$, are expected to sit significantly below this order of magnitude, and hence would be unmeasurable with the current instruments at our disposal.

There are two possible solutions to this ongoing issue of sensitivity, both of which involve changes to Simoa technology that allow protein detection down to sub-attomolar (10^{-18} M) concentrations. The first is the development of upgraded Simoa technology by Quanterix themselves (214). This increased sensitivity to sub-attomolar concentrations has been achieved primarily by: 1) increasing the molecule:bead ratio through the use of fewer beads (5000 beads compared to 500 000 beads in conventional Simoa); 2) reducing bead loss during assay steps by removing liquids via a centrifugal pump rather than needle aspiration; 3) using magnetic-meniscus sweeping (MMS) to increase the proportion of beads loaded into the microwells; 4) increasing the field of view of the camera used to image the microwells; and 5) relaxing the classification threshold of beads from 10% with conventional Simoa to 0% due to the analysis of only a single bead type, rather than multiplex analysis (214). These changes to the operating system resulted in a cumulative bead-reading efficiency of 48.5% (2688 beads) with this Simoa upgrade, compared to 4.9% (24 325 beads) with conventional Simoa, and a measured bead-reading efficiency of 47.2% (2614 beads) with upgraded Simoa, compared to 4.8% (23 823) with conventional Simoa (214). Alongside these changes to the bead washing and reading protocols, changes to the user-conducted assay protocol, such as incubation times, were also made, which are described in further detail in section 4.3.3.5 2-step and 3-step assay protocol –

SRx Pro and Table 4.3. Although this upgrade is not yet commercially available, preliminary investigations have revealed an increase in sensitivity of up to 189-fold provided by this technique compared to conventional Simoa (214).

The second upgrade to Simoa technology has been developed outside of Quanterix, and has been termed the Molecular On-bead Signal Amplification for Individual Counting (MOSAIC) platform (303). The MOSAIC digital ELISA platform utilises flow cytometry alongside the 'dropcast' Simoa and droplet digital ELISA previously developed by the same group (304-306). Whilst immunoassay platforms already exist which use flow cytometry, such as the Luminex platform, the advantage posed by MOSAIC is the measurement of particles individually using sheath flow to enable single-file analysis, rather than the bulk signal read out produced by Luminex, which only detects down to picomolar (10^{-12} M) concentrations. Furthermore, the on-bead signal amplification combined with the flow cytometry, alongside the reduction in bead numbers, enables detection of high-intensity signals at the single-molecule level (303). Unlike the upgraded Simoa platform previously discussed, this platform has shown only up to a 12-fold improvement in sensitivity using 20 000 beads compared to conventional Simoa. This contrasts with the 189-fold improvement in the upgraded Simoa using 5000 beads. However, it is important to note that the maximum improvements in sensitivity on these two platforms were assessed on different established conventional Simoa assays. Had they been tested on the same assay, it would be easier to compare improvements in sensitivity between the two platforms. Nonetheless, one advantage of the MOSAIC platform compared to the Simoa upgrade is that it can already be used in multiplex analyses, which has yet to be demonstrated with the upgraded Simoa, and has shown some improvements in saliva measurements of analytes. Furthermore, the use of flow cytometry requires less than one-minute to read each sample, compared with three to four minutes per sample on the upgraded Simoa due to the more thorough MMS bead-loading

technique implemented. Finally, MOSAIC displayed a bead-reading efficiency of 50-60% of the total initial assay beads, a 10-fold improvement on conventional Simoa (4.8%), but only a small improvement compared to upgraded Simoa (47.2%). Given that both of these novel platforms have improved sensitivity down to sub-attomolar concentrations, it is difficult to ascertain at this stage which of the two is the better technique. However, it is clear that both instruments have the potential to greatly advance biomarker detection within the scientific field, particularly with regards to AD biomarkers.

1.6 Monoclonal antibody treatments for Alzheimer's disease

For nearly 20 years, the drugs approved to treat AD have only been aimed at managing disease symptoms. These drugs include acetylcholinesterase inhibitors, such as donepezil, and N-methyl-D-aspartate receptor antagonists, such as memantine (307). This period of time has not been devoid of clinical trials. In fact, there has been a significant shift towards investigating disease-modifying therapies specifically targeting underlying mechanisms of AD pathogenesis, rather than focussing on reducing symptom-severity. A large proportion of these trials have targeted various forms of Aβ, based on the premise that in light of the amyloid cascade hypothesis, clearance of Aβ should improve cognition and slow, or perhaps even halt, cognitive decline (308). However, until recently, most anti-Aβ trials have failed to show any significant clinical benefit. One possible reason for the poor results in clinical trials thus far has been due to the inclusion of symptomatic patients who have progressed too far along the disease process, and in whom significant irreversible neuronal loss has already occurred (202). Conversely, it may be due to some participants having a false AD diagnosis. This is particularly true of the solanezumab trial, where some recruited participants were later found to be amyloid PET-negative, hence were unlikely to have had AD (98). Furthermore, the lack of success in recent clinical trials may be due to too short trial duration and is further complicated by some participants displaying AD mixed with other disease pathologies, rather than being pure AD cases. Identifying individuals with AD pathology years prior to symptom onset will enable recruitment into clinical trials at a much earlier, and potentially more tractable, disease stage, and hence may prove more effective at identifying treatments to slow, or perhaps even halt, the disease process. Moreover, as participants in such trials would not be displaying cognitive symptoms, conventional cognitive/symptomatic endpoints are unlikely to be effective for identifying response to treatment, and so dynamic biomarkers which are sensitive to progression in pre-symptomatic disease will be important.

1.6.1 First, second and third generation anti-amyloid-β immunotherapy agents

Following the AN1792 clinical trial investigating the active immunisation against Aβ (309), there have been three generations of immunotherapy drugs targeting Aβ pathology (310). The first-generation comprises one antibody, bapineuzumab, which binds to the N-terminus of Aβ monomers (94). The second-generation antibodies comprise: 1) crenezumab, which binds to monomeric, fibrillar and oligomeric Aβ to varying degrees (311); 2) gantenerumab, which binds fibrillar and monomeric Aβ (311, 312); and 3) solanezumab, which is directed against the mid-domain of the Aβ monomer (98). In essence, these first- and second-generation antibodies are largely either non-selective, or selective for monomeric forms of Aβ. Phase III clinical trials conducted on the first- and second-generation antibodies lacked promise, with crenezumab and bapineuzumab not improving cognitive or Aβ pathology outcomes, although bapineuzumab did decrease CSF p-tau$_{181}$ (94-96). Likewise, solanezumab failed to improve cognitive outcomes (97-99). Furthermore, the recently published results of the DIAN-TU trial, which started in 2013 and involved patients being randomly assigned to receive either gantenerumab, solanezumab or placebo for 4-7 years, revealed that neither drug improved cognition (99). Although, gantenerumab did improve all AT(N) biomarkers.

In contrast, the third-generation antibodies, comprising aducanumab, lecanemab and donanemab, all of which will be discussed in further detail in the subsequent sections (1.6.2 Aducanumab, 1.6.3 Lecanemab and 1.6.4 Donanemab, respectively), are much more selective for aggregated forms of Aβ (313-315), and have consistently been observed to remove plaques (316-319). The lack of success in the first- and second-generation antibodies, combined with the promising results observed with third-generation antibodies, highlights the need for specificity of Aβ-targeting immunotherapy agents to aggregated forms.

1.6.2 Aducanumab

Aducanumab, commercially known as Aduhelm, is a human immunoglobulin (Ig) G1 monoclonal antibody that selectively targets aggregated Aβ, including soluble oligomers and insoluble fibrils (318). Furthermore, due to its accelerated approval by the Food and Drug Administration (FDA) on 7th June 2021, it became the first drug treatment to be approved for AD in 18 years, as well as the first approved immunotherapy treatment for AD. The first-in-human, double-blinded trial in patients with mild-to-moderate AD by Ferrero and colleagues (320), and further reported by Sevigny and colleagues (318), observed that after 54 weeks of treatment, aducanumab reduced brain Aβ plaques in a dose- and time-dependent manner, as measured by florbetapir PET. The participants who received the 3, 6 and 10mg kg^{-1} doses all had statistically significant reductions in the standard uptake value ratio (SUVR) composite score compared with baseline florbetapir PET uptake measurements, with those receiving 10mg kg^{-1} observing the largest fold changes. Furthermore, the trial showed a correlation between Aβ removal and slowing of cognitive decline, although the study did not directly assess clinical changes. However, the approval by the FDA, which was made on the basis of the reduction in Aβ plaques observed in patients treated with aducanumab, sparked uproar in the scientific community. This was primarily due to: 1) safety concerns; 2) contradictory results reported in the two phase III trials, including the EMERGE trial displaying a slowing of cognitive decline and meeting both its primary and secondary endpoints but the identical ENGAGE trial showing no cognitive benefit and meeting neither its primary or secondary endpoints (321); and 3) the extremely high cost of the drug ($56 000 per person per year) (322-324). Nonetheless, the approval of aducanumab is a large step forward for disease-modifying therapies in AD, particularly for those targeting Aβ pathology. Furthermore, its continued approval is contingent upon confirmation of its clinical benefits in further trials, hence time will tell whether the correct decision was made by the FDA.

1.6.3 Lecanemab

Lecanemab, commercially known as Leqembi, is a humanised IgG1 monoclonal antibody that specifically targets soluble forms of aggregated Aβ (oligomers and protofibrils) (319). Similar to aducanumab, lecanemab was approved by the FDA under accelerated approval on 6th January 2023. The phase II trial conducted by Swanson and colleagues (319) involved treating patients with either lecanemab or placebo over the course of 5 years. Results showed a failure to reach the primary cognitive endpoint at 12 months. However, further analysis at 18 months revealed that the highest prescribed dose of 10mg kg^{-1} bi-weekly had significantly lowered Aβ burden, as measured by amyloid PET, by 0.306 SUVR units, compared to an increase in the placebo group by 0.004 SUVR units. Furthermore, the drug did indeed slow cognitive decline by 47% on the Alzheimer's Disease Assessment Scale – Cognitive Subscale (325) at 18 months, and improved CSF $Aβ_{42}$ and p-tau concentrations at both 12 and 18 months (319). This fed into the Clarity AD phase III trial on lecanemab (326), which met both their primary and secondary endpoints, and contributed to its traditional approval by the FDA on 7th July 2023.

1.6.4 Donanemab

Donanemab is a humanised IgG1 monoclonal antibody that specifically targets N-terminally truncated $Aβ_{pE}$ (317). Its phase II clinical trial found a dramatic reduction in cerebral Aβ plaque load, as measured by amyloid PET, in the intervention group compared with the placebo group (317). At the end of the 76-week trial period, donanemab reduced amyloid PET binding by 84.13 centiloids, compared with an increase of 0.93 centiloids in the placebo group. In fact, by week 76, approximately two-thirds of the participants treated with donanemab were re-classified as being amyloid PET-negative. Furthermore, the recently published phase III trial showed similarly impressive results, with a 35.1% slowing of cognitive decline, and a reduction in amyloid PET binding by 87.0 centiloids, compared with a small decrease of 0.67 centiloids in the placebo group (327). This is

in comparison to lecanemab reducing amyloid PET binding by 59.12 centiloids compared with an increase of 3.64 in the placebo group (326). What is most significant about donanemab is that it does not target merely any aggregated form of Aβ found within the brain, which many of the previously investigated anti-Aβ immunotherapies do, sometimes resulting in off-target effects. Rather, it targets $A\beta_{pE}$, a pathology-specific form of Aβ that is not produced by neurones, but instead is formed within plaques (74). Targeting this particular form with an antibody like donanemab should not affect normal Aβ, which may reduce the risk of amyloid related imaging abnormalities (ARIA). In particular, ARIA with oedema and effusions (ARIA-E) is a prominent side effect associated with amyloid-modifying therapies, especially immunotherapies (328, 329). Indeed, in the phase III study of donanemab, ARIA-E had a greater rate of occurrence among participants in the donanemab group (24%) compared to the placebo group (2.1%) (327). However, symptomatic ARIA-E only occurred in 6.1% of the donanemab group, compared to 2.8% of those receiving lecanemab (326) and as high as 29% of those on high dose aducanumab (although it was not made clear whether this figure only encompasses symptomatic ARIA-E) (321). Interestingly, there were 3 reported deaths due to ARIA in the donanemab group. This is compared to 0 reported deaths due to ARIA in either of the phase III aducanumab trials (321), nor in the phase III lecanemab trial (326). This could potentially be attributed to the extent of Aβ clearance seen with donanemab in comparison to lecanemab and aducanumab. However, it would be interesting to see whether this impacts donanemab's approval by the FDA. Regardless, the effect of donanemab is clearly comparable to that of aducanumab and lecanemab, so it may only be a matter of time until a third anti-Aβ immunotherapy agent is approved for the treatment of AD. Were this to happen, it would be beneficial to be able to quantify whether the drug is truly decreasing concentrations of $A\beta_{pE}$ within treated individuals as it claims to do. Whilst an ELISA assay which quantifies $A\beta_{pE}$ does exist, to our knowledge, attempts to measure $A\beta_{pE}$ in CSF and/or blood have yet to prove successful. Whilst Wu and colleagues

(330) argue that the lack of detectability of this analyte in biofluids suggests that it may be concentrated in the brain parenchyma, we hypothesise that its detection is largely limited by the sensitivity of the protein detection methods available at present.

1.7 PhD aims, hypotheses and objectives

As we move into the era of blood biomarkers for AD, robust blood measurements for Aβ are needed now more than ever. The above presented evidence has highlighted that whilst CSF biomarkers for Aβ are well established and are robust at differentiating between diagnostic groups, CSF is invasive to collect, hence there has been a shift to measuring blood-based biomarkers for AD diagnosis. However, the plasma $Aβ_{42/40}$ has repeatedly exhibited significant overlap between AD and NAD individuals. Although alternative biomarkers exist which could be used as surrogate biomarkers of Aβ pathology in blood, namely plasma GFAP and p-tau (although plasma p-tau is presently being used a marker of tau pathology), the plasma $Aβ_{42/40}$ has still been included as the only blood biomarker for Aβ pathology in the recent update of the NIA-AA diagnostic criteria for AD[1], with GFAP being included in its own category. However, whilst indirect measures of Aβ exist, the direct measure of Aβ in blood would provide the most conclusive information about the extent of Aβ pathology within individuals on the AD continuum. As such, this PhD aims to examine the performance of the currently available blood biomarkers for AD diagnostics, and on the basis of those results, develop novel Simoa Aβ assays for $Aβ_{43}$ and $Aβ_{pE3-40}$ for use in both CSF and blood. This is based on the following hypotheses: 1) that an $Aβ_{43/40}$ ratio will decrease more than and/or earlier than the $Aβ_{42/40}$, and hence would be a more beneficial biomarker to differentiate between diagnostic groups in blood biomarker measurements of AD; and 2) $Aβ_{pE}$ is secreted in small quantities in the presence of established Aβ plaque pathology from within the plaque into the CSF, and hence would serve as a definitive diagnostic biomarker for AD. Current Simoa technology is unlikely to be sensitive enough to detect either $Aβ_{43}$ or $Aβ_{pE3-40}$, hence these assays will predominantly be developed for use on the upgraded Simoa platform – the SRx Pro.

To achieve these aims, the objectives that must be met are:

1) Independently assess the need for additional Aβ biomarkers, particularly in blood
2) Independently validate the increased sensitivity of the SRx Pro, particularly in relation to standard Simoa instruments
3) Develop novel assays on standard Simoa instruments and the SRx Pro, followed by testing on clinical samples

As such, these three objectives will form the main structure of this thesis.

CHAPTER 2: EXISTING PLASMA BIOMARKERS FOR ALZHEIMER'S DISEASE

2.1 Introduction and rationale

Following the success of CSF biomarkers for AD diagnosis, plasma biomarkers are becoming of increasing interest due to their ease of access in comparison to CSF, particularly in low-resource and non-specialist settings worldwide (175-177). The CSF and plasma biomarkers recognised by the ATXN criteria for AD diagnosis are $A\beta_{42/40}$, p-tau_{181}, p-tau_{217}, GFAP and NfL, all of which have been reviewed extensively in section 1.4.2 Existing cerebrospinal fluid and plasma biomarkers for Alzheimer's Disease. Whilst advancements in the analytical sensitivity of instruments used to measure proteins in biofluids has enabled the quantification of AD biomarkers in blood, some of these biomarkers do not perform as well as their CSF counterparts in differentiating between diagnostic groups. This is particularly true of $A\beta_{42/40}$, which thus far has consistently shown significant overlap between diagnostic groups (331). Given that we have proposed a possible need for additional fluid biomarkers for Aβ pathology in AD, it is important to independently validate whether these biomarkers are truly needed, or whether the plasma $A\beta_{42/40}$ performs sufficiently for diagnostic purposes. As such, the aim of this project is to independently examine the performance of blood biomarkers for AD diagnostics, looking specifically at $A\beta_{42/40}$, p-tau_{181}, p-tau_{217}, GFAP and NfL on the Quanterix Simoa HDx instrument. Where available, we will compare and assess the correlation between both plasma and CSF measurements. However, we will be focussing more in-depth on the ability of $A\beta_{42/40}$ to differentiate between AD and NAD diagnostic groups. We hypothesise that, in line with previously published data, the plasma $A\beta_{42/40}$ will show significant overlap between diagnostics groups, and thus highlight the need for alternative biomarkers for Aβ pathology in plasma.

2.2 Materials and methods

2.2.1 Cohort and diagnostic criteria

A total of 115 plasma samples collected from individuals between the years of 2013 and 2023 were obtained from the UCL Dementia Research Centre (DRC) cognitive clinic. Of these samples, 49 were classified as AD (23 male and 26 female) and 66 were classified as NAD (43 male and 23 female) based on the criteria described below. Samples were organised into 4-year age brackets ranging from age 55-79. 111 of these samples (47 AD and 64 NAD) had matched CSF available. Diagnoses of NAD participants are detailed in Table 2.1, and include other dementias (*e.g.* VaD, FTLD, DLB) and non-neurodegenerative disorders (*e.g.* chronic fatigue syndrome, mood-related, normal pressure hydrocephalus, meningioma). Cognitively normal samples were not available, given the specialised nature of referrals to the DRC, nor did we deem it essential to obtain such samples for this study.

Samples collected before 17th December 2020 were diagnosed using criteria which used a combination of CSF t-tau/Aβ_{42} ratio >1 and a CSF Aβ_{42} <450 pg/mL to distinguish AD from FTLD with a sensitivity and specificity of 87.4% and 77.3%, respectively. Samples collected on or after this date were diagnosed using a new criteria, which uses a CSF A$\beta_{42/40}$ <0.065 with a sensitivity and specificity of 85% and 95%, respectively, to detect abnormal Aβ deposition as measured by amyloid PET. This is combined with CSF p-tau$_{181}$ >57 pg/mL with a sensitivity and specificity of 77% and 88%, respectively, compared with amyloid PET, as well as CSF t-tau between 146-595 pg/mL and CSF NfL outside the normal range for that age group (Table 2.3), values of which are taken from Yilmaz and colleagues (332). The previous and new diagnostic criteria are summarised in Table 2.2.

NAD diagnosis	Number of individuals
FTLD and subtypes (FTLD:PNFA:bvFTLD:PPA)	18 (6:7:4:1)
Subjective	12
Semantic dementia	6
Non-degenerative	5
Vascular dementia	5
Mood-related	3
PD and atypical parkinsonism (PD:CBS:PSP)	3 (1:1:1)
Psychiatric (anxiety:bipolar:depression)	3 (1:1:1)
Functional neurological disorder	2
NAD MCI (e.g. DLB-related)	2
Unclear diagnosis	2
Autoimmune	1
Chronic fatigue syndrome	1
DLB	1
Meningioma	1
Normal pressure hydrocephalus	1

Table 2.1 – NAD diagnoses

Non-Alzheimer's disease (NAD) diagnoses of UCL Dementia Research Centre cognitive clinic samples. 'FTLD' indicates frontotemporal lobe dementia; 'PNFA', progressive non-fluent aphasia; 'bvFTLD', behavioural variant FTLD; 'PPA', primary progressive aphasia; 'PD', Parkinson's disease; 'CBS', corticobasilar syndrome; 'PSP', progressive supranuclear palsy; 'MCI', mild cognitive impairment; 'DLB', dementia with Lewy bodies

CSF biomarker	Criteria 1 (used before 17th December 2020)	Criteria 2 (used after 17th December 2020)
T-tau/Aβ$_{42}$ ratio	Value > 1	N/A
Aβ$_{42}$	<450 pg/mL (Se: 87.4%; Sp: 77.3%)	N/A
Aβ$_{42/40}$	N/A	<0.065 (Se: 85%; Sp: 95%)
P-tau$_{181}$	N/A	>57 pg/mL (Se: 77%; Sp: 88%)
T-tau	N/A	146-595 pg/mL
NfL	N/A	*See* Table 2.3

Table 2.2 – AD diagnostic criteria used at UCL Dementia Research Centre cognitive clinic

Cerebrospinal fluid (CSF) Alzheimer's disease (AD) diagnostic criteria used before and after 17th December 2020. 'T-tau' indicates total tau; 'Aβ', amyloid-β; 'p-tau', phosphorylated tau; 'NfL', neurofilament light chai; 'Se', sensitivity; 'Sp', specificity

Age group	Normal CSF NfL concentration range (pg/mL)
0-20	<387
21-30	<525
31-40	<713
41-50	<967
51-60	<1313
61-70	<1781
71-80	<2417

Table 2.3 - Normal NfL concentrations by age groups

Normal cerebrospinal fluid (CSF) neurofilament light chain (NfL) concentration cut off values by age group, taken from Yilmaz and colleagues (317)

2.2.2 Sample collection, processing and storage

Samples were processed as soon as possible after collection. Samples were centrifuged for 5 minutes – CSF at 1750xg and 4°C, blood at 1800xg and room temperature – and were subsequently aliquoted into 1mL aliquots before storage at -70 to -80°C. Both blood and CSF samples were left to stand for 10 minutes after centrifugation before aliquoting. Serum, ethylenediaminetetraacetic

acid (EDTA) plasma and heparin plasma were aliquoted and stored separately.

2.2.3 Simoa measurements

Plasma and CSF measurements of p-tau$_{217}$, and plasma measurements of Aβ_{40}, Aβ_{42}, GFAP, NfL and p-tau$_{181}$ were conducted on the Quanterix Simoa HDx instrument in duplicate measurments using the Quanterix Corporation neurology 4-plex E (N4PE) and p-tau$_{181}$ kits, and ALZpath p-tau$_{217}$ kits (purchased from Quanterix), all of which were used according to manufacturer's instructions.

In brief, all three assays were run simultaneously on three different HDx instruments to ensure each analyte was measured under the same sample conditions. Sample diluent, calibrator diluent, calibrators/calibrator concentrate stock and samples were left to equilibrate to room temperature, allowing minimum 30 minutes for refrigerated reagents and minimum 1 hour for frozen reagents. All other reagents for the assay (beads, detector, and streptavidin–β-galactosidase [SβG]) remained refrigerated until sample plate had been prepared. Appropriate number of resorufin β-D-galactopyranoside (RGP) vials were shaken in orbital shaker (Quanterix Corporation) at 30°C and 800rpm for minimum 30 minutes and maximum 4 hours. Calibration curve and CTRLs were made using calibrator stock to concentrations detailed on assay instructions for p-tau$_{217}$. For all other analytes measured, calibrators were provided in pre-prepared vials. Samples were diluted, then 250µL of sample, CTRLs and calibrators were pipetted onto a conical 96-well plate. Plate was sealed with Simoa perforated plate seal. Reagents were subsequently loaded onto Simoa HDx instrument, vortexing beads for minimum 30 seconds, and run was performed.

2.2.4 Lumipulse measurements

CSF Aβ_{40}, Aβ_{42} and p-tau$_{181}$ measurements were conducted in singlicates on a Lumipulse G600-II (Fujirebio, Japan) instrument.

Measurements were conducted as per manufacturer's instructions. In brief, samples, calibrators and other reagents were left to equilibrate to room temperature. Samples, calibrators and other reagents were subsequently loaded onto the Lumipulse, and target analytes were measured.

2.2.5 Statistical analysis

Frequency distribution analyses revealed the samples were not normally distributed. Therefore to compare results between AD and NAD groups, non-parametric analyses were performed throughout. All statistical analysis was performed using GraphPad Prism 9.3.1. Mann Whitney U-test was used to compare the means between the AD and NAD groups for each biomarker. Spearman correlation analysis revealed the extent of correlation between both plasma and CSF measurements. Plasma samples without corresponding CSF sample values were removed from Spearman correlation analysis, but included in all other analyses. Receiver operator characteristic (ROC) curves and AUCs were assessed to consider the diagnostic accuracy of each analyte. 95% confidence intervals (CI) were reported, and a p-value <0.05 was considered statistically significant. All numerical values are displayed to three significant figures, or to the nearest whole number where more appropriate.

2.3 Results

2.3.1 Amyloid-β results

2.3.1.1 Amyloid-$\beta_{42/40}$ is significantly decreased in cerebrospinal fluid but not plasma Alzheimer's disease samples

$A\beta_{40}$ and $A\beta_{42}$ were measured separately in both plasma and CSF in order to establish the $A\beta_{42/40}$ for each individual in both biofluids. Plasma $A\beta_{40}$ was significantly reduced in AD (Figure 2.1A) with a mean concentration of 92.6 pg/mL (95% CI 81.3-104 pg/mL; p-value 0.0001***) compared with NAD which had a mean concentration of 118 pg/mL (95% CI 110-126 pg/mL), although a large overlap between AD and NAD cases was visible. However, no significant difference in CSF $A\beta_{40}$ was seen (Figure 2.1B), with a mean concentration of 12 391 pg/mL (95% CI 11 457-13 326 pg/mL; p-value 0.0719) in AD compared with 11 303 pg/mL (95% CI 10 264-12 342 pg/mL) in NAD individuals.

In contrast, $A\beta_{42}$ was significantly decreased in AD individuals in both biofluids, with far less overlap seen between AD and NAD individuals (Figure 2.1C&D). Plasma $A\beta_{42}$ had a mean concentration of 6.34 pg/mL (95% CI 5.74-6.94 pg/mL; p-value <0.0001) in AD compared with 8.36 pg/mL (95% CI 7.72-9.00 pg/mL) in NAD individuals, whilst CSF $A\beta_{42}$ had a mean concentration of 581 pg/mL (95% CI 538-624 pg/mL; p-value <0.0001) in AD compared with 1133 pg/mL (95% CI 1012-1255 pg/mL) in NAD.

However, of most interest is the $A\beta_{42/40}$, which was significantly decreased in CSF AD individuals (Figure 2.1F), but not in plasma AD individuals (Figure 2.1E). In CSF, the mean AD $A\beta_{42/40}$ was 0.0478 (95% CI 0.0451-0.0505; p-value <0.0001) whilst the mean NAD $A\beta_{42/40}$ was 0.0993 (95% CI 0.0949-0.104). Whereas in plasma, the mean AD $A\beta_{42/40}$ was 0.0817 (95% CI 0.0696-0.0938; p-value 0.975) compared with 0.0749 (95% CI 0.0683-0.0815) in NAD.

2.3.1.2 Plasma amyloid-$\beta_{42/40}$ does not correlate with CSF measurements

Spearman correlation analysis revealed poor correlation between CSF and plasma $A\beta_{40}$ concentrations (r-value -0.0648 [95% CI -0.253-0.129]; p-value 0.500; Figure 2.2A), and a weakly positive but statistically significant correlation between CSF and plasma $A\beta_{42}$ concentrations (r-value 0.371 [95% CI 0.193-0.525]; p-value <0.0001; Figure 2.2B). However, when combined in the $A\beta_{42/40}$, there was poor correlation between CSF and plasma concentrations (r-value 0.149 [95% CI -0.0446-0.331]; p-value 0.120; Figure 2.2C). This is summarised in Figure 2.2, the legend of which also details individual r-values and statistical significance for AD and NAD with each Aβ parameter measured.

2.3.1.3 Plasma amyloid-$\beta_{42/40}$ shows poor diagnostic accuracy for Alzheimer's disease

ROC curves and AUCs were assessed to consider the diagnostic accuracy of each Aβ biomarker. CSF $A\beta_{42/40}$ showed the highest diagnostic accuracy, with an AUC of 0.988 (95% CI 0.975-1.00; Figure 2.3C), closely followed by CSF $A\beta_{42}$, which had an AUC of 0.869 (95% CI 0.800-0.937; Figure 2.3B). Interestingly, plasma $A\beta_{42/40}$ had the worst diagnostic accuracy within this cohort, with an AUC of 0.502 (95% CI 0.388-0.616; Figure 2.3C). This is compared with plasma $A\beta_{40}$, CSF $A\beta_{40}$ and plasma $A\beta_{42}$, which had AUCs of 0.706 (95% CI 0.610-0.802), 0.600 (95% CI 0.496-0.705) and 0.738 (95% CI 0.646-0.830), respectively (Figure 2.3).

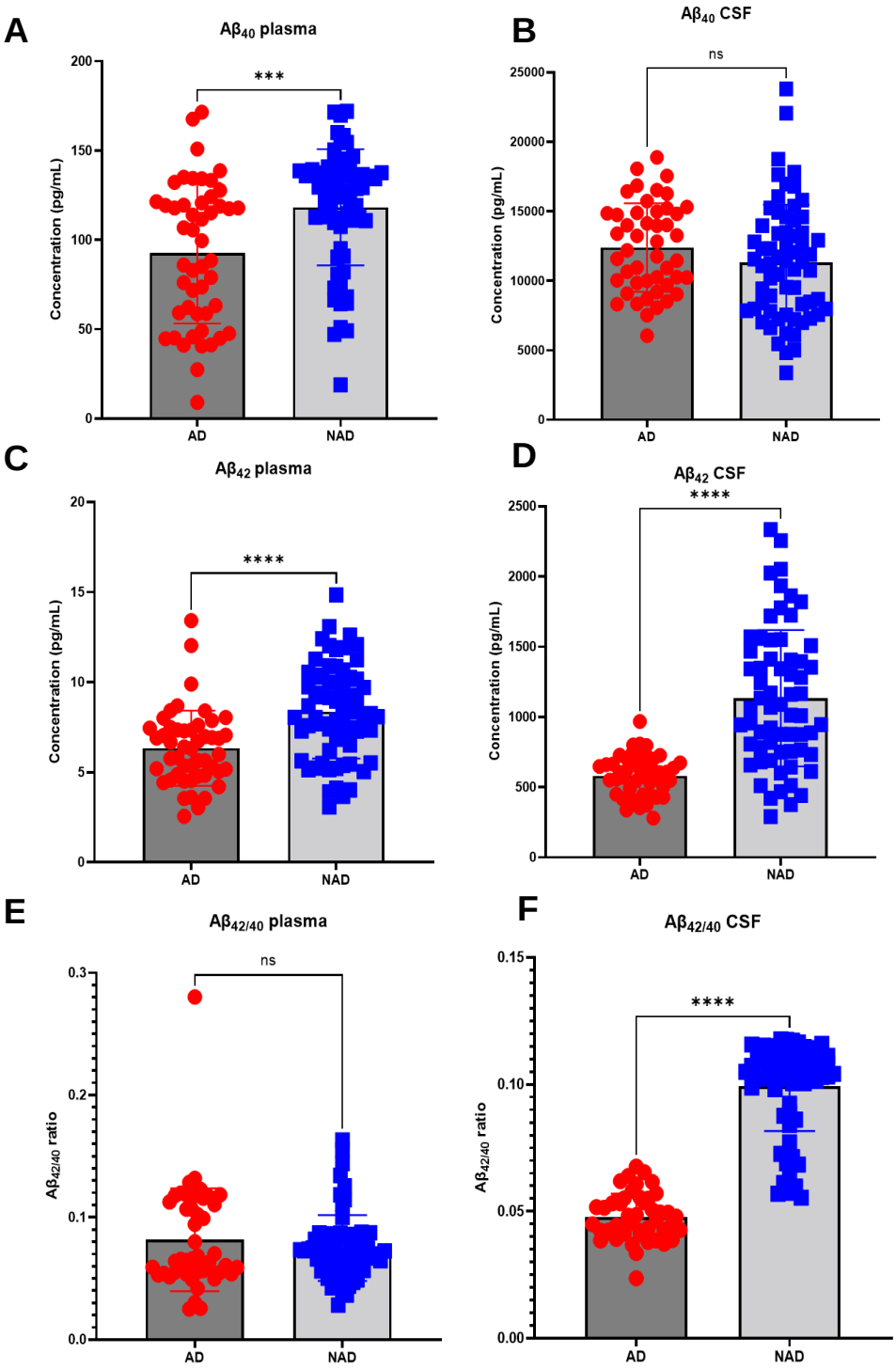

Figure 2.1 – Plasma and CSF Aβ concentrations

A&B**: Amyloid-β (Aβ)$_{40}$ is significantly reduced in plasma (p = 0.0001) but not cerebrospinal fluid (CSF; p = 0.0719) Alzheimer's disease (AD) compared to non-AD (NAD) individuals. **C&D:** Aβ$_{42}$ is significantly reduced in both plasma (p = <0.0001****) and CSF (p = <0.0001****) AD compared to NAD. **E&F:** Aβ$_{42/40}$ is significantly reduced in CSF (p = <0.0001****) but not plasma (p = 0.975) AD compared to NAD. 'ns' indicates non-significant findings (p>0.05).*

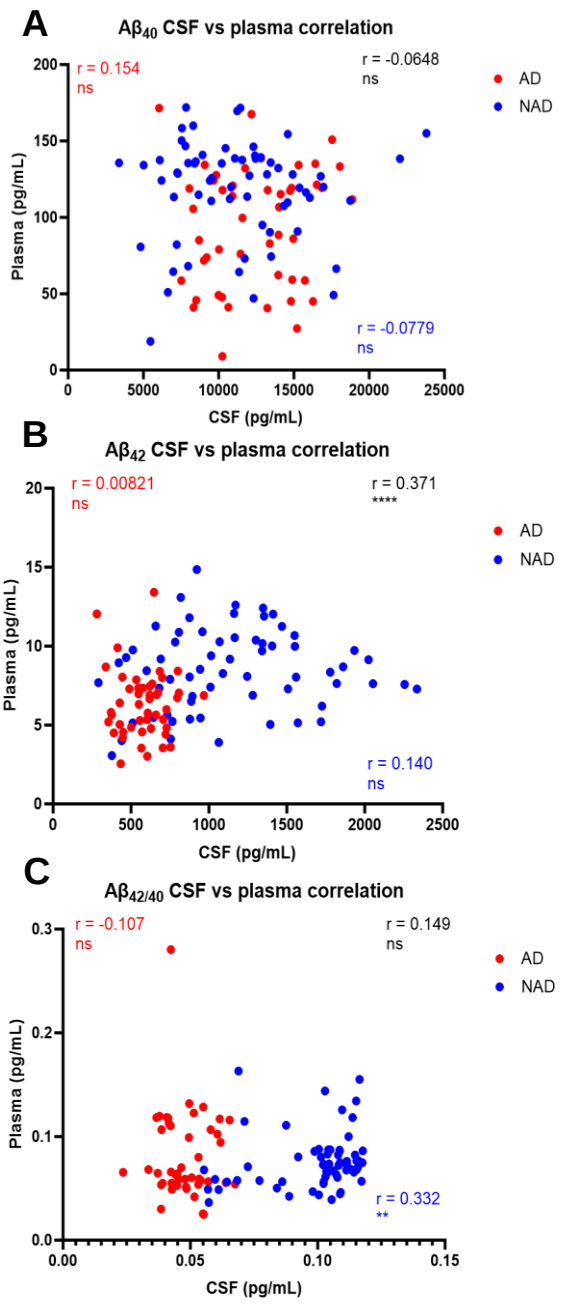

Figure 2.2 - Aβ CSF and plasma correlation plots

Spearman correlation plots of measured cerebrospinal fluid (CSF) and plasma amyloid-β (Aβ) concentrations. ***A:*** *$Aβ_{40}$ shows poor correlation between plasma and CSF (r = -0.0648, 95% CI -0.253-0.129, p = 0.500), nor is there correlation in these biofluids when looking at Alzheimer's disease (AD; r = 0.154, 95% CI -0.148-0.430, p = 0.300) or non-AD (NAD; r = -0.0779, 95% CI -0.324-0.178, p = 0.541) measurements individually.* ***B:*** *$Aβ_{42}$ shows a weak but statistically significant correlation between plasma and CSF (r = 0.371, 95% CI 0.193-0.525, p = <0.0001****), but not when looking at AD (r = 0.000821, 95% CI -0.288-0.303, p = 0.956) and NAD (r = 0.140, 95% CI -0.117-0.379, p = 0.272) measurements individually.* ***C:*** *$Aβ_{42/40}$ shows poor correlation between plasma and CSF (r = 0.149, 95% CI -0.0446-0.331, p = 0.120), nor when looking at AD measurements individually (r = -0.107, 95% CI -0.389-0.195, p = 0.476). However, NAD measurements show a weak positive but statistically significant correlate (r = 0.332, 95% CI 0.0859-0.539, p = 0.0075**). 'ns' indicates non-significant findings (p>0.05); 'CI', confidence interval.*

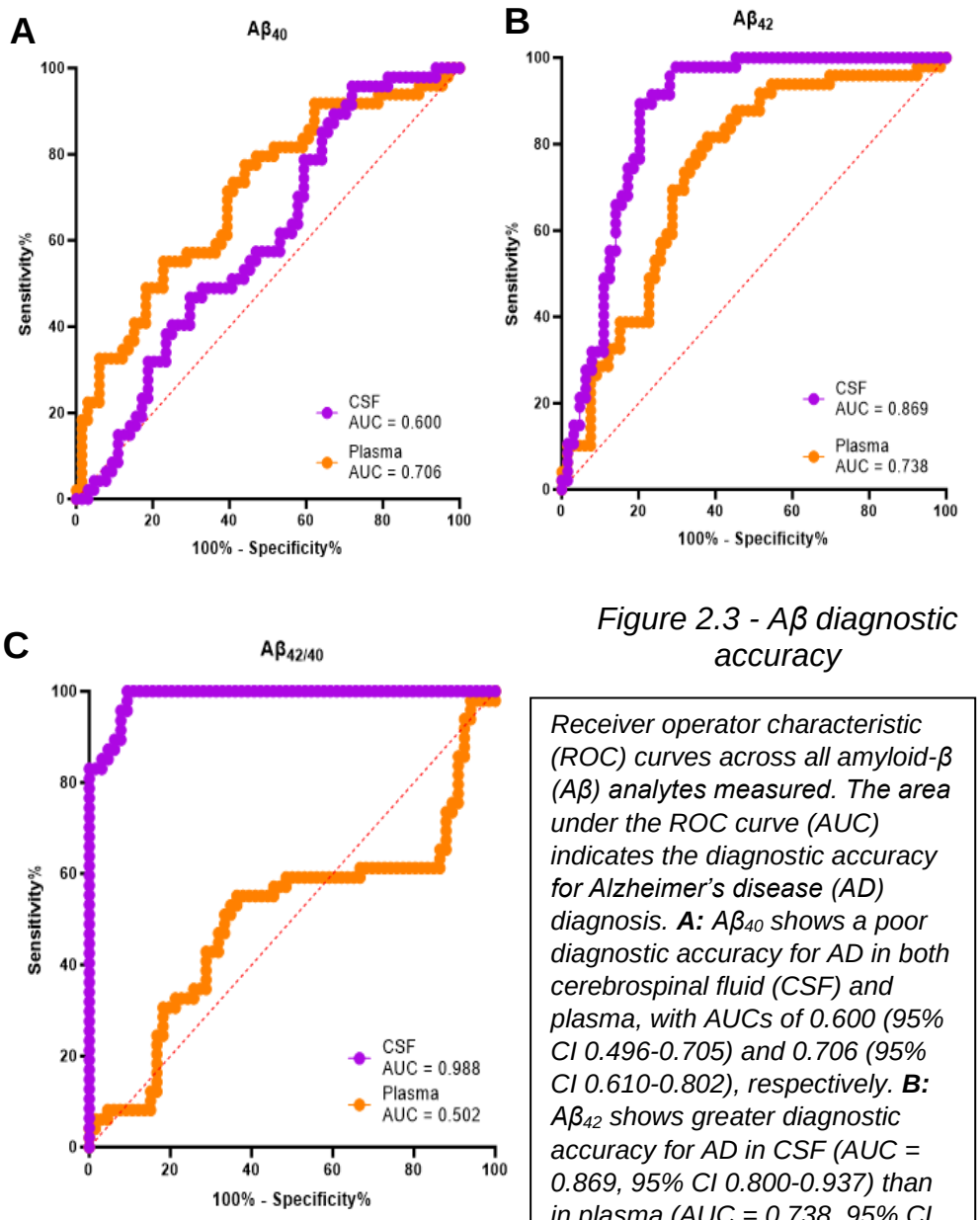

Figure 2.3 - Aβ diagnostic accuracy

Receiver operator characteristic (ROC) curves across all amyloid-β (Aβ) analytes measured. The area under the ROC curve (AUC) indicates the diagnostic accuracy for Alzheimer's disease (AD) diagnosis. ***A:*** *$Aβ_{40}$ shows a poor diagnostic accuracy for AD in both cerebrospinal fluid (CSF) and plasma, with AUCs of 0.600 (95% CI 0.496-0.705) and 0.706 (95% CI 0.610-0.802), respectively.* ***B:*** *$Aβ_{42}$ shows greater diagnostic accuracy for AD in CSF (AUC = 0.869, 95% CI 0.800-0.937) than in plasma (AUC = 0.738, 95% CI 0.646-0.830).* ***C:*** *$Aβ_{42/40}$ shows a high diagnostic accuracy for AD in CSF (AUC = 0.988, 95% CI 0.975-1.00), but poor diagnostic accuracy in plasma (AUC = 0.502, 95% CI 0.388-0.616). 'CI' indicates confidence interval.*

2.3.2 Phosphorylated tau results

2.3.2.1 Phosphorylated tau-181 and -217 are significantly increased in both plasma and CSF samples

Both p-tau$_{181}$ and p-tau$_{217}$ were measured to assess which of the two biomarkers better distinguished between AD and NAD diagnostic groups. Whilst the absolute concentrations of p-tau$_{181}$ were higher than those of p-tau$_{217}$ in both biofluids, the mean concentrations of both analytes in plasma and CSF were significantly higher in AD than in NAD individuals (Figure 2.4). For p-tau$_{181}$, mean plasma and CSF concentrations were 50.1 pg/mL (95% CI 45.1-55.1 pg/mL; p-value <0.0001) and 169 pg/mL (95% CI 150-187 pg/mL; p-value <0.0001), respectively in AD, whilst for NAD they were 37.0 pg/mL (95% CI 32.0-42.0 pg/mL) and 43.8 pg/mL (95% CI 39.9-47.6 pg/mL), respectively (Figure 2.4A&B). For p-tau$_{217}$, mean plasma and CSF concentrations were 1.54 pg/mL (95% CI 1.33-1.74 pg/mL; p-value <0.0001) and 97.1 pg/mL (95% CI 83.2-111 pg/mL; p-value <0.0001), respectively, for AD, whereas for NAD they were 0.487 pg/mL (95% CI 0.410-0.564 pg/mL) and 11.4 pg/mL (95% CI 9.20-13.5 pg/mL), respectively (Figure 2.4C&D).

2.3.2.2. Plasma phosphorylated tau-181 and -217 correlate with CSF measurements

Spearman correlation analysis revealed a statistically significant positive correlation between CSF and plasma p-tau$_{181}$, with an r-value of 0.520 (95% CI 0.365-0.648; p-value <0.0001; Figure 2.5A). Similarly, CSF and plasma p-tau$_{217}$ showed a strong positive correlation, with an r-value of 0.792 (95% CI 0.708-0.854; p-value <0.0001; Figure 2.5B). This is summarised in Figure 2.5, which also details individual r-values and statistical significance for AD and NAD with each p-tau biomarker measured.

2.3.2.3 Phosphorylated tau-217 correlates strongly with phosphorylated tau-181

Further Spearman correlation analysis revealed that in both plasma and CSF, p-tau$_{217}$ shows a strong positive, statistically significant correlation with p-tau$_{181}$, with r-values of 0.792 (95% CI 0.653-0.880;

p-value <0.0001; Figure 2.5C) and 0.920 (95% CI 0.857-0.955; p-value <0.0001; Figure 2.5D), respectively. However, the correlation is far stronger in CSF than in plasma. This is summarised in Figure 2.5, which also details individual r-values and statistical significance for AD and NAD with each p-tau biomarker measured.

2.3.2.4 Plasma phosphorylated tau-217 has higher diagnostic accuracy than plasma phosphorylated tau-181 for Alzheimer's disease

ROC curves and AUCs were assessed to consider the diagnostic accuracy of both p-tau biomarker. CSF p-tau$_{181}$ and p-tau$_{217}$ had very similar diagnostic accuracies, with AUCs of 0.998 (95% CI 0.995-1.00) and 0.996 (95% CI 0.990-1.00), respectively (Figure 2.6). However, plasma p-tau$_{217}$ had a far greater diagnostic accuracy than plasma p-tau$_{181}$, with AUCs of 0.945 (95% CI 0.908-0.981) and 0.760 (95% CI 0.673-0.847), respectively (Figure 2.6).

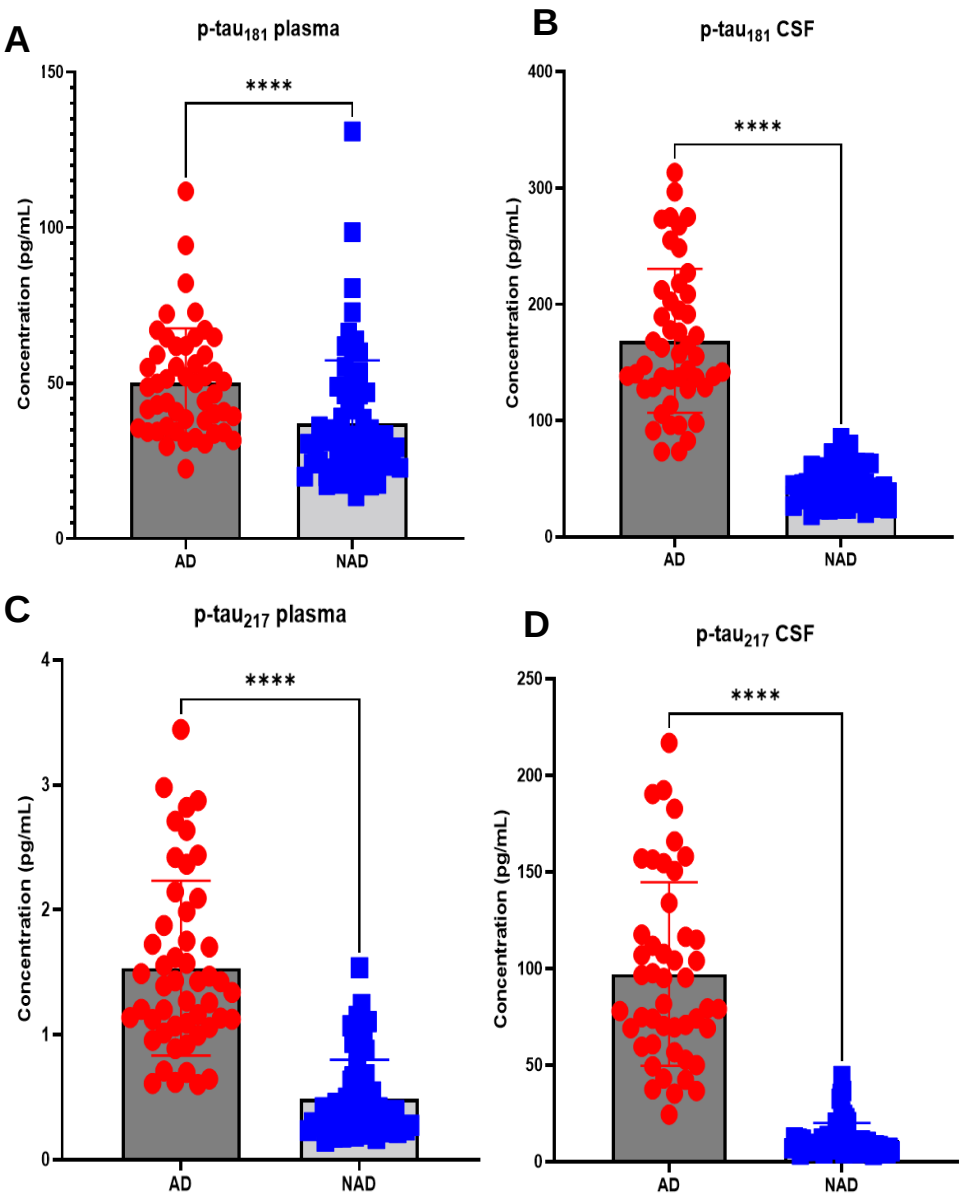

Figure 2.4 - Plasma and CSF p-tau concentrations

A&B**: Phosphorylated tau (p-tau)$_{181}$ is significantly increased in both plasma (p = <0.0001*) and cerebrospinal fluid (CSF; p = <0.0001****) Alzheimer's disease (AD) compared to non-AD (NAD). **C&D:** P-tau$_{217}$ is significantly increased in both plasma (p = <0.0001****) and CSF (p = <0.0001****).*

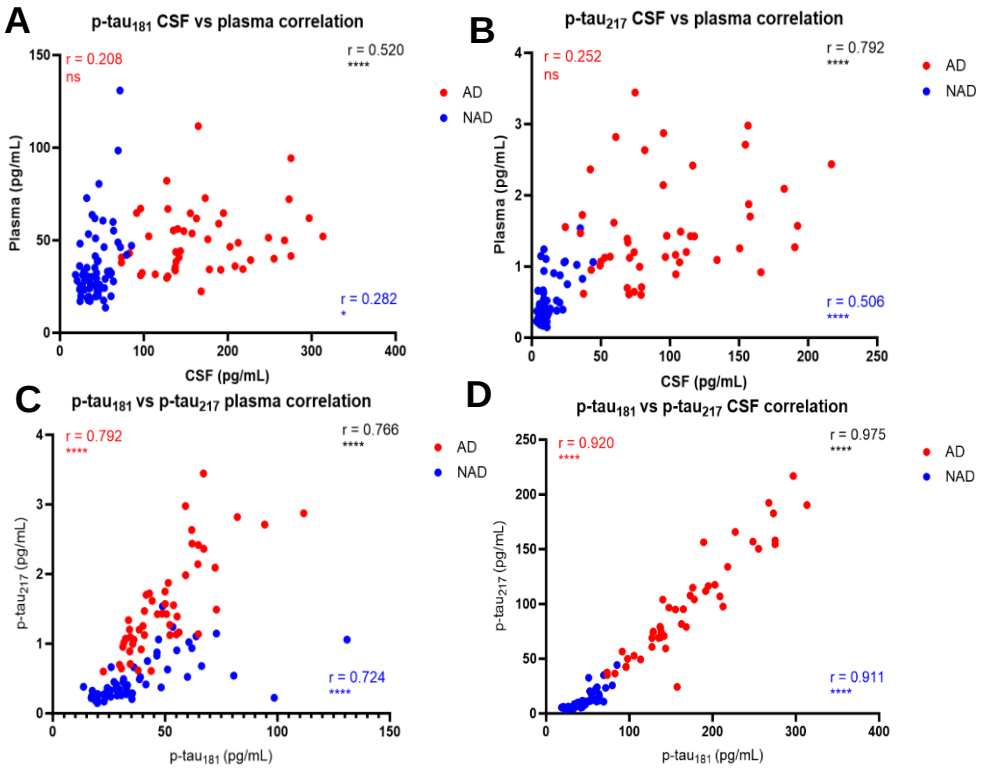

Figure 2.5 - P-tau CSF and plasma correlation plots

Spearman correlation plots of measured cerebrospinal fluid (CSF) and plasma phosphorylated tau (p-tau) concentrations. ***A:*** *p-tau$_{181}$ shows a positive statistically significant correlation between plasma and CSF (r = 0.520, 95% CI 0.365-0.648, p = <0.0001****), including significant correlation in these biofluids when looking at non-Alzheimer's disease (NAD; r = 0.282, 95% CI = 0.0313-0.499, p = 0.0241*) but not Alzheimer's disease (AD; r = 0.208, 95% CI = 0.0929-0.474, p = 0.161) measurements individually.* ***B:*** *p-tau$_{217}$ shows a strong positive correlation between plasma and CSF (r = 0.792, 95% CI 0.708-0.854, p = <0.0001****), including when looking at NAD (r = 0.506, 95% CI 0.506-0.291, p = <0.0001****) but not AD (r = 0.252, 95% CI -0.0467-0.509, p = 0.0875) measurements individually.* ***C:*** *Plasma measurements of p-tau$_{181}$ and p-tau$_{217}$ show a strong positive correlation with one another (r = 0.766, 95% CI 0.675-0.834, p = <0.0001****), including when looking AD (r = 0.792, 95% CI = 0.653-0.880, p = <0.0001****) and NAD (r = 0.724, 95% CI = 0.579-0.824, p = <0.0001****) measurements individually.* ***D:*** *CSF measurements of p-tau$_{181}$ and p-tau$_{217}$ show strong correlation with one another (r = 0.975, 95% CI 0.964-0.983, p = <0.0001****), including when looking AD (r = 0.920, 95% CI = 0.857-0.955, p = <0.0001****) and NAD (r = 0.911, 95% CI = 0.855-0.946, p = <0.0001****) measurements individually. 'ns' indicates non-significant findings (p>0.05); 'CI', confidence interval.*

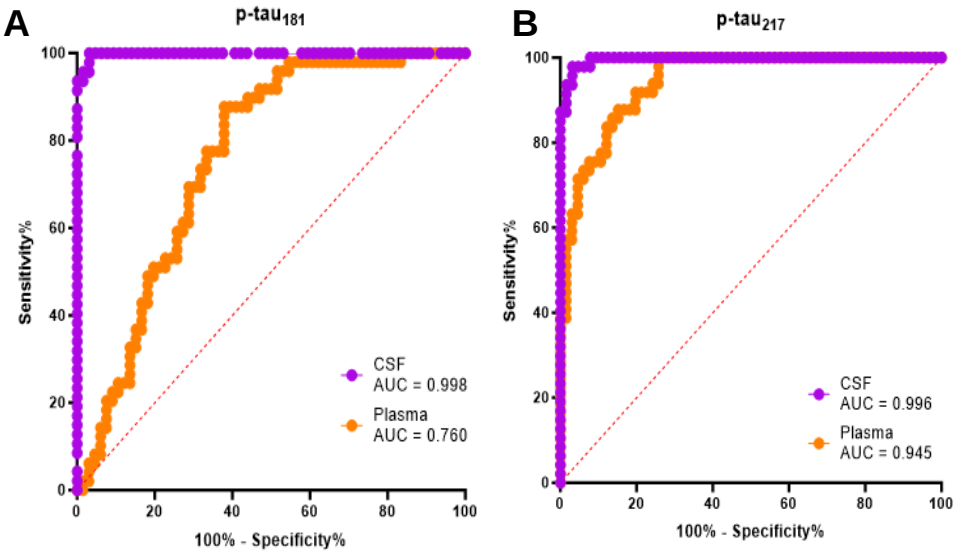

Figure 2.6 - p-tau diagnostic accuracy

Receiver operator characteristic (ROC) curves across phosphorylated tau (p-tau) analytes measured. The area under the ROC curve (AUC) indicates the diagnostic accuracy for Alzheimer's disease (AD) diagnosis. ***A:*** *p-tau$_{181}$ shows a stronger diagnostic accuracy for AD in cerebrospinal fluid (CSF) than in plasma, with AUCs of 0.998 (95% CI 0.995-1.00) and 0.760 (95% CI 0.673-0.847), respectively.* ***B:*** *p-tau$_{217}$ shows similarly strong diagnostic accuracy for AD in both CSF (AUC = 0.996, 95% CI 0.990-1.00) and plasma (AUC = 0.945, 95% CI 0.908-0.981). 'CI' indicates confidence interval.*

2.3.3 Glial fibrillary acidic protein results

2.3.3.1 Plasma glial fibrillary acidic protein is significantly increased in Alzheimer's disease with a good diagnostic accuracy

Whilst CSF measurements were not available for GFAP, given that plasma GFAP has been included in the ATXN criteria, assessing its concentrations in AD compared with NAD was still of benefit. Our results showed that plasma GFAP was significantly increased in AD compared with NAD, with mean concentrations of 220.2 pg/mL (95% CI 188-252 pg/mL; p-value <0.0001) and 137 pg/mL (95% CI 119-155 pg/mL), respectively (Figure 2.7A). However, large amounts of overlap existed between the individual concentrations seen in both diagnostic groups. Additionally, plasma GFAP was found to have an AUC of 0.766 (95% CI 0.692-0.850) for distinguishing between AD and NAD cases, indicating a reasonably good diagnostic accuracy (Figure 2.7B).

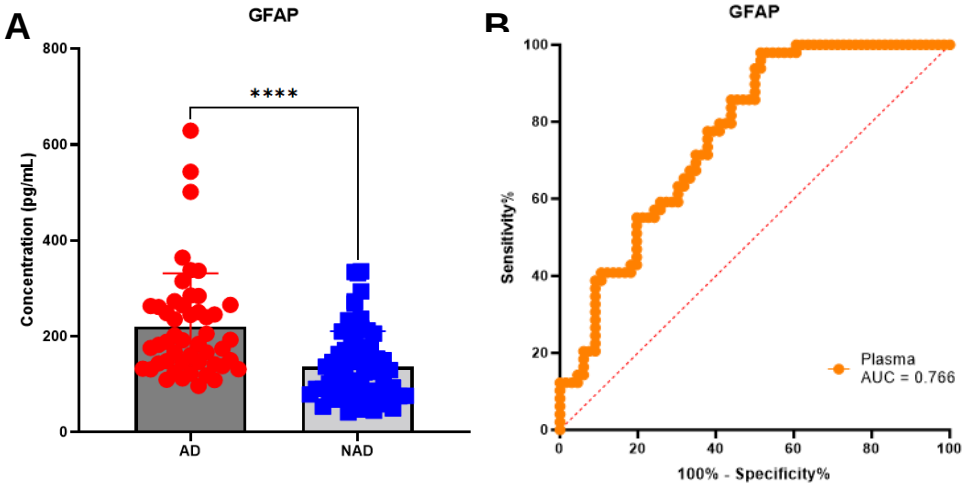

Figure 2.7 - GFAP plasma concentration and diagnostic accuracy

A: *Plasma glial fibrillary acidic protein (GFAP) was significantly increased in Alzheimer's disease (AD) compared to non-AD (NAD) individuals (p = <0.0001****).* ***B:*** *The area under the receiver operator characteristic curve (AUC) indicates the diagnostic accuracy for Alzheimer's disease (AD) diagnosis. Plasma GFAP showed a good diagnostic accuracy for AD, with an AUC of 0.766 (95% CI 0.682-0.850). 'CI' indicates confidence interval*

2.3.4 Neurofilament light chain results

2.3.4.1 Plasma neurofilament light chain shows no significant difference in Alzheimer's disease with a poor diagnostic accuracy

Similar to GFAP, CSF measurements were not available for NfL. However, given its continued inclusion in the ATXN criteria as a biomarker of neurodegeneration and neuronal injury, assessing its concentrations in AD compared with NAD was still of benefit. Our results showed that there is no significant difference between plasma NfL concentrations in AD compared with NAD individuals, with mean concentrations of 26.8 pg/mL (95% CI 23.3-30.4 pg/mL; p-value 0.618) and 32.7 pg/mL (95% CI 23.3-30.4 pg/mL), respectively (Figure 2.8A). However, given the nature of our NAD group, this is not unexpected. Additionally, NfL was found to have an AUC 0.528 (95% CI 0.422-0.633), indicating a poor diagnostic accuracy for AD (Figure 2.8B).

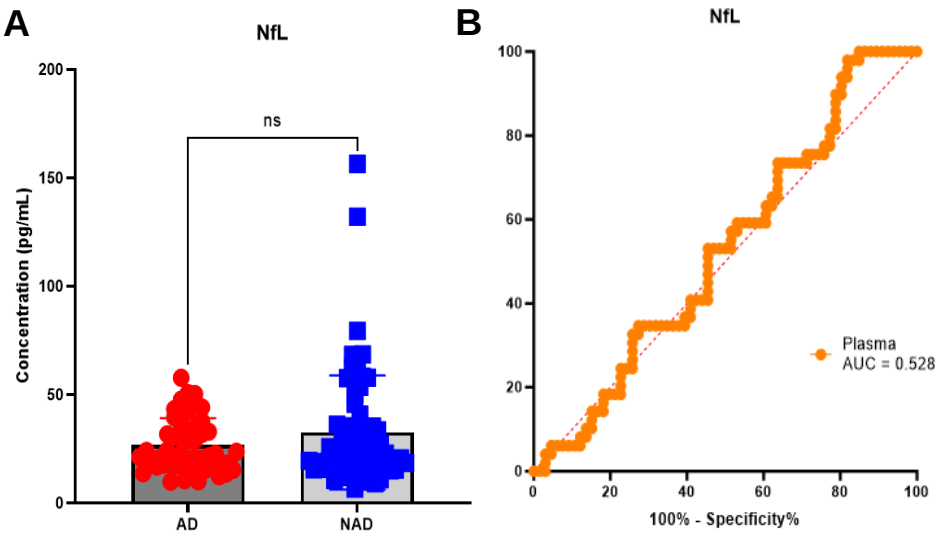

Figure 2.8 - NfL plasma concentration and diagnostic accuracy

A: *Plasma neurofilament light chain (NfL) showed no significant difference in Alzheimer's disease (AD) compared to non-AD (NAD) individuals (p = 0.618).* ***B:*** *The area under the receiver operator characteristic curve (AUC) indicates the diagnostic accuracy for Alzheimer's disease (AD) diagnosis. Plasma NfL showed a poor diagnostic accuracy for AD, with an AUC of 0.528 (95% CI 0.422-0.633). 'CI' indicates confidence interval.*

2.3.5 Results summary

In summary, our results showed a significant decrease in the $A\beta_{42/40}$ in AD compared with NAD in CSF, but not in plasma. Furthermore, there was extensive overlap between the diagnostic groups in plasma $A\beta_{42/40}$, nor does plasma $A\beta_{42/40}$ correlate with CSF $A\beta_{42/40}$ measurements. In contrast, CSF and plasma $A\beta_{42}$ correlated with one another, and $A\beta_{42}$ was significantly decreased in both biofluids. Additionally, plasma $A\beta_{42/40}$ showed the poorest diagnostic accuracy in comparison to CSF $A\beta_{42/40}$, $A\beta_{42}$, and $A\beta_{40}$, and plasma $A\beta_{40}$ and $A\beta_{42}$.

Both p-tau_{181} and p-tau_{217} were significantly increased in AD plasma and CSF compared with NAD, however p-tau_{217} showed a clearer distinction between the diagnostic groups. Both p-tau analytes showed a strong correlation between plasma and CSF measurements, as well as with one another. Although, whilst both analytes show a similarly strong diagnostic accuracy in CSF, p-tau_{217} showed a greater diagnostic accuracy in plasma than p-tau_{181}.

Plasma GFAP was significantly increased in AD compared with NAD, with a good diagnostic accuracy. Whereas NfL showed no significant difference between the diagnostic groups, with a poor diagnostic accuracy for AD.

2.4 Discussion

This study confirmed CSF $A\beta_{42}$, $A\beta_{42/40}$, p-tau_{181} and p-tau_{217} to be robust diagnostic biomarkers for AD, which is in line with previous literature (45, 195, 227). The high diagnostic accuracy seen in our study using the Lumipulse instrument for CSF measurements corroborates the results seen in a recent study by Gobom and colleagues (333), who observed AUCs of 0.784 (95% CI 0.749-0.820), 0.873 (95% CI 0.845-0.901) and 0.854 (95% CI 0.824-0.885) for $A\beta_{42}$, $A\beta_{42/40}$ and p-tau_{181}, respectively, in their study using 642 AD and 684 CTRL samples from three independent disease cohorts. This is compared with our observed AUCs of 0.869 (95% CI 0.800-0.937; Figure 2.3B), 0.988 (95% CI 0.9750-1.000; Figure 2.3C) and 0.998 (95% CI 0.995-1.00; Figure 2.6A) for $A\beta_{42}$, $A\beta_{42/40}$, and p-tau_{181}, respectively.

The distinction between AD and NAD cases with both CSF p-tau_{181} and p-tau_{217} was very similar (Figure 2.4B&D), which is in line with the observations of Karikari and colleagues (334). Whilst p-tau_{217} is a far less abundant analyte in plasma than p-tau_{181}, as indicated by their respective absolute concentrations (Figure 2.4A&C), plasma p-tau_{217} showed far less overlap between diagnostic groups, and its increase in AD compared with NAD was far more profound than that of plasma p-tau_{181}, although both were significantly increased (p-value <0.0001****). This highlights that plasma p-tau_{217} may serve as a more distinctive biomarker for AD pathology than p-tau_{181}, which is in line with recent literature (335-338).

Despite p-tau_{217} being measured on the Simoa instrument with one additional freeze-thaw cycle to the other CSF measurements, we observed an AUC of 0.996 (95% CI 0.990-1.00; Figure 2.6B), indicating CSF p-tau may in fact be resistant to at least one freeze-thaw cycle, particularly given the strong correlation of CSF p-tau_{217} with p-tau_{181} despite the additional freeze-thaw (Figure 2.4C&D). The stability of p-tau following freeze-thaws has had conflicting results, with one study finding a reduction in CSF p-tau concentration with

each freeze-thaw up to three cycles (339), and another finding CSF p-tau remains stable up to three freeze-thaw cycles (340). However, these studies measured p-tau$_{181}$, not p-tau$_{217}$, hence it is possible that different CSF p-tau epitopes display differing susceptibilities to degradation with freeze-thaw cycles. Additionally, we did not conduct p-tau$_{217}$ measurements prior to the additional freeze-thaw cycle, hence it is impossible to confirm or deny any significant effect of freeze-thaws on CSF p-tau concentrations.

Similar to CSF Aβ$_{42}$, we observed plasma Aβ$_{42}$ to be significantly decreased in AD compared with NAD in our cohort. As such, it is interesting that this biomarker has been removed from the recent update of the NIA-AA research framework[1]. However, given the improved diagnostic accuracy provided by looking at Aβ$_{42}$ in relation to Aβ$_{40}$ in the Aβ$_{42/40}$, this change to the diagnostic criteria for AD is understandable. Contrary to Hansson and colleagues (341), we observed a weak but statistically significant correlation between plasma and CSF Aβ$_{42}$ (r = 0.371 [95% CI 0.193-0.525]; p-value = <0.0001; Figure 2.2B). The differences in our results compared with that of Hansson and colleagues may be due to an increase in the sensitivity of immunoassay instruments since their study was conducted. Indeed, they observed plasma Aβ$_{42}$ concentrations in the range of 15-60 pg/mL, whereas we observed concentrations in the range of 2.55-14.9 pg/mL.

Interestingly, we observed plasma Aβ$_{42/40}$ to be a poor biomarker for AD, exhibiting a poor diagnostic performance (AUC 0.502; 95% CI 0.388-0.616; Figure 2.3C) and no significant difference in AD compared with NAD individuals (p-value 0.975; Figure 2.1E). In fact, we observed plasma Aβ$_{42}$ to out-perform plasma Aβ$_{42/40}$, with an AUC of 0.738 (95% CI 0.646-0.830; Figure 2.3B). Similar to the observations of Schindler and colleagues (206), who used MS for plasma measurements and Elecsys (ECL) for CSF measurements, we observed an extensive overlap between diagnostic groups in plasma Aβ$_{42/40}$ (Figure 2.1E). We did see an overlap in CSF Aβ$_{42/40}$

between diagnostic groups, however the overlap was to a far smaller degree (Figure 2.1F). Whist there was a visible outlier in the plasma $A\beta_{42/40}$ AD group in our data (Figure 2.1E), the use of non-parametric data analysis methods mitigates the effect of this individual on the statistical significance of the data. Furthermore, the removal of this individual from the data analysis had negligible effect on the mean $A\beta_{42/40}$, and the data remained of no statistical significance.

One possible reason for the poor plasma $A\beta_{42/40}$ in our cohort could be due to variability in pre-analytical handling factors. In their study looking at the effects of pre-analytical sample handling on AD blood biomarkers measured using MS, ELISA and Simoa, Verberk and colleagues (342) observed that blood collection tube type, delayed centrifugation and delayed storage (post-centrifugation and aliquoting) negatively impacted plasma $A\beta_{40}$ and $A\beta_{42}$ concentrations. Indeed, they observed a percentage recovery as low as 59% for $A\beta_{42}$ and 62% for $A\beta_{40}$ with samples held at room temperature for 24 hours prior to centrifugation. These percentage recoveries are in comparison to the standard sample handling conditions – EDTA plasma collection tubes centrifuged at 1800xg at room temperature after a standing time of 30 minutes at room temperature, immediately followed by aliquoting and -80°C storage. Whilst in some assays and conditions, the decrease in $A\beta_{40}$ and $A\beta_{42}$ concentrations caused by the variability in pre-analytical handling factors could be mitigated by assessing the plasma $A\beta_{42/40}$, this was not the case for all pre-analytical variables, including for some measurements conducted using Simoa (342). The observations of Verberk and colleagues have been further corroborated by Kurz and colleagues (343), who agree that $A\beta_{40}$ and $A\beta_{42}$ are the most sensitive plasma AD biomarkers to pre-analytical handling factors, with the negative effects only partially being rectified by the $A\beta_{42/40}$. It is possible, therefore, that in our cohort, plasma $A\beta_{40}$ concentrations were more greatly affected by pre-analytical factors than plasma $A\beta_{42}$, thus resulting in a higher $A\beta_{42/40}$ for each AD individual than expected, and hence closer values to that of the NAD group.

Although, this is unlikely given that the same sample handling protocol was used for all samples in our cohort.

Another possible reason for the non-significant differences in plasma $A\beta_{42/40}$ could be due to the peripheral production of Aβ, which may be interfering with the brain-derived Aβ crossing the BBB, thus making it more difficult to distinguish between AD and NAD individuals. As a result, specificity in the assays used is paramount to minimise the confounding effect of this additional Aβ. Evidence has shown that detection of full length Aβ (1-42 and 1-40) in plasma provides a clearer distinction between diagnostic groups than measuring their truncated counterparts (x-42 and x-40) (344). The Simoa N4PE assay has been developed to detect full length $A\beta_{42}$ and $A\beta_{40}$ (345), hence poor assay specificity is unlikely to be the cause of the results we observed.

Finally, the poor results observed for plasma $A\beta_{42/40}$ in our study could be due to matrix effects caused by plasma proteins (346), and the general robustness issues with the measurement of this biomarker in blood (347). These matrix effects can be minimised by diluting the samples prior to their measurements. However, when using the Quanterix Simoa N4PE assay to detect Aβ species, plasma has a recommended dilution of 4x, whereas CSF has a recommended dilution of 400x. Whilst this is due to the absolute concentrations of Aβ in plasma being lower than that seen in CSF, it is possible that a 4x dilution in plasma is not large enough to mitigate the matrix effects within this biofluid. Given that the limit of detection (LOD) and analytical lower limit of quantification (LLOQ) using Simoa are 0.384 pg/mL and 1.02 pg/mL for $A\beta_{40}$, respectively, and 0.136 pg/mL and 0.378 pg/mL for $A\beta_{42}$, respectively, and also that a dilution linearity of 112% for $A\beta_{40}$ and 93% for $A\beta_{42}$ was observed for these assays using an 8x dilution[3], a greater dilution of our samples may have produced more robust results. However, given how close this

[3] Values obtained from Quanterix Corporation Customer portal

would take the measured concentrations of these analytes to the analytical LLOQ, there is clearly a need for the development of instruments with an increased analytical sensitivity.

In addition, to the poor diagnostic accuracy and non-significant findings of plasma $A\beta_{42/40}$ for AD, we also observed a poor correlation in $A\beta_{42/40}$ (and $A\beta_{40}$) between CSF and plasma (Figure 2.2C). The use of two different instruments for each of these biofluids may have caused the poor correlation in our cohort. However, given this had minimal effect on p-tau_{181}, p-tau_{217}, and $A\beta_{42}$, all of which showed a significant correlation between CSF and plasma in our data, this is unlikely to be the case. Whilst several studies, including Schindler and colleagues (206), have observed a good correlation between plasma and CSF $A\beta_{42/40}$, $A\beta_{40}$ and $A\beta_{42}$, a recent study assessing Aβ in CAA measured using ELISA in plasma alongside ELISA and Lumipulse in CSF observed a correlation similar to that seen in our study (348). In fact, several studies in AD have shown a poor correlation between CSF and plasma $A\beta_{40}$, $A\beta_{42}$ and/or $A\beta_{42/40}$ (331, 349). It is possible that our study lacked the statistical power to show a correlation between CSF and plasma $A\beta_{42/40}$ and $A\beta_{40}$. However, it is also possible that plasma Aβ does not reflect its CSF counterpart, but rather its concentrations are predominantly influenced by peripheral processes in the case of $A\beta_{40,}$ and hence also the $A\beta_{42/40}$.

Unlike $A\beta_{42/40}$, plasma GFAP showed a significant distinction between diagnostic groups, with it being increased in AD compared with NAD individuals (p-value = <0.0001; Figure 2.7A), although there was a large extent of overlap between diagnostic groups. In addition, plasma GFAP showed a good diagnostic accuracy for AD (AUC = 0.766; 95% CI 0.692-0.850; Figure 2.7B). The observed results for plasma GFAP are in line with previous literature, which have shown plasma, but not CSF, GFAP is specific to AD, correlating strongly with cerebral Aβ pathology and functioning as a robust early AD screening tool (251, 350-352).

On the other hand, plasma NfL showed no significant difference between diagnostic groups (p-value = 0.618; Figure 2.8A), alongside a poor diagnostic accuracy for distinguishing AD from NAD in our cohort (Figure 2.8B). However, given the nature of the NAD group within our study, these results are not unexpected. NfL is a non-specific marker of neuronal injury and neurodegeneration, hence it is elevated in several neurodegenerative and non-neurodegenerative diseases with neuroaxonal injury.

In conclusion, whilst our CSF biomarker results have confirmed $A\beta_{42}$, $A\beta_{42/40}$, p-tau_{181} and p-tau_{217} to be robust biomarkers for distinguishing between AD and NAD, our plasma biomarker results have shown plasma $A\beta_{42/40}$ is a poor AD biomarker. Whilst plasma $A\beta_{42}$ performed well in our cohort, it was recently removed from the NIA-AA diagnostic criteria for AD. This highlights a need for more robust plasma biomarkers of Aβ pathology which not only better distinguish between diagnostic groups, but which also correlate well with CSF Aβ measures, and which show a good diagnostic accuracy for AD.

CHAPTER 3: SIMOA UPGRADE VALIDATION

3.1 Introduction and rationale

Preliminary investigations conducted on the SRx Pro, as well as the MOSAIC platform, have enabled the detection of molecules down to subattomolar concentrations (214, 303). On the SRx Pro, this was tested on several established Simoa assays, but the highest increase in sensitivity observed by Kan and colleagues (214) was seen on the Simoa interleukin 17A (IL17A) assay. This assay was chosen by Quanterix to be tested on the upgraded software predominantly due to it being one of their most sensitive assays to date on the standard 500 000 bead Simoa instruments. From the 50 plasma and 50 serum samples on which IL17A was measured by Kan and colleagues (214), they observed an improvement in quantification from 12% of plasma samples and 24% of serum samples using the standard platform, to 100% and 96% in plasma and serum, respectively, using the upgraded platform. However, alongside assessing whether the upgraded Simoa instrument is truly more sensitive than standard Simoa instruments, of additional interest to us is the role of IL17A in AD.

IL17A is a proinflammatory cytokine which plays a key role in the innate immune response to pathogens, and tissue inflammation (353, 354). Considering the neuroinflammatory nature of AD (see section 1.3.2.3 The neuroinflammatory hypothesis – Alzheimer's disease as a neuroinflammatory condition), some studies have shown that IL17A may be involved in AD pathogenesis. *In vivo* investigations have observed a significant increase in IL17A concentrations in the serum and CSF of rat and mouse models of AD, respectively, compared to CTRLs (355, 356). However, studies conducted in humans have shown mixed results. Whilst some have observed a significant increase in concentrations of IL17A in AD serum compared to CTRLs (357), others have observed a significant decrease in plasma (358), and still others no significant change at all in CSF (359). In fact,

some studies have suggested IL17A may be a more useful diagnostic biomarker for FTLD (360). However, Hu and colleagues (361) were unable to quantify CSF IL17A reliably using five distinct commercially available kits in AD and FTLD samples. Interestingly, a recent review proposed the idea that IL17A concentrations may vary with disease stage in AD (362), although they acknowledged that further investigations into the plausibility of this idea must be conducted. Nonetheless, it is clear that further investigations into the associations between IL17A and AD are needed.

Due to ongoing close working connections with Quanterix, our lab has been given access to the SRx Pro instrument prior to it becoming commercially available. Outside of Quanterix, our lab in London and our sister lab in Gothenburg are the only two labs globally with access to this instrument, which provides exclusive opportunities to independently verify the increased sensitivity of this instrument, as well as develop our own, supersensitive assays. In light of this, the primary aim of this project is to independently validate the results of Kan and colleagues (214) on IL17A, albeit with a refined protocol to that used in the original publication. Additionally, our secondary aim is to compare and contrast the performance of the SRx Pro instruments at UCL and at Quanterix Research and Development (RnD) department with the HDx instrument at UCL. Furthermore, given the inflammatory nature of AD, we will assess whether IL17A is raised in AD using matched AD and CTRL CSF and serum samples.

3.2 Materials and methods

3.2.1 Cohort and diagnostic criteria

A total of 32 paired serum and CSF samples (13 AD and 19 CTRLs) were obtained from University of Gothenburg clinical neurochemistry laboratory. Samples were divided into 300µL aliquots upon receipt. One aliquot of each serum and CSF sample was sent to Quanterix RnD department. The samples were grouped as AD and CTRL based on CSF AD biomarker results with the following cut-points used: t-tau>479ng/L, $A\beta_{42}$ <620ng/L and p-tau_{181} >60ng/L

3.2.2 Sample collection, processing and storage

Lumbar punctures were performed in the morning (non-fasted). Serum was collected in serum separator tubes (SSTs) whereas plasma was collected in EDTA blood tubes. Following collection, SSTs were inverted several times, and were left to coagulate for minimum 30 minutes. CSF and plasma samples were processed immediately following tube inversion. CSF, plasma and serum samples were all centrifuged at 2200xg and 20°C for 10 minutes. Samples were subsequently aliquoted into 0.5-1.0mL aliquots, labelled appropriately, and stored at -80°C.

3.2.3 IL17A Simoa HDx measurement

IL17A kits were purchased from Quanterix Corporation, and CSF and serum samples measured as per manufacturer's instructions except for sample dilutions. Instead, CSF samples were diluted 1:2 and plasma samples were diluted 1:10, in keeping with dilutions performed on SRx Pro instruments.

In brief, the assay was performed as follows. Sample diluent, calibrator diluent, calibrator concentrate stock and samples were left to equilibrate to room temperature, allowing minimum 30 minutes for refrigerated reagents and minimum 1 hour for frozen reagents. All other reagents for the assay (IL17A beads, detector, and SβG) remained refrigerated until the sample plate had been prepared. RGP vials were shaken in an orbital shaker (Quanterix Corporation) at 30°C and 800rpm for a minimum of 30 minutes and maximum of 4

hours. An eight-point calibration curve and CTRLs were made using IL17A calibrator stock to concentrations detailed on assay instructions. Samples were diluted, then 250µL of sample, CTRLs and calibrators were pipetted onto Simoa conical 96-well plate to be measured in duplicates (taken from the same well). Plate was sealed with Simoa perforated plate seal. Reagents were subsequently loaded onto Simoa HDx instrument, vortexing IL17A beads for minimum 30 seconds, and run was performed.

3.2.4 IL17A Simoa SRx Pro measurement

IL17A 488-dyed[4] superparamagnetic bead stock, sample diluent, detector, SβG and calibrator diluent were custom made by Quanterix RnD department. All serum and CSF samples were measured on three separate SRx Pro instruments – UCL SRx Pro, Quanterix SRx Pro plus unit[5], and Quanterix SRx Pro alpha unit[6] – across two days per instrument to measure the full sample cohort. Plus unit and alpha unit measurements were conducted at Quanterix Corporation.

In brief, the assay was performed as follows. Sample diluent, calibrator diluent, homebrew bead diluent, calibrator concentrate stock and samples were left to equilibrate to room temperature, allowing minimum of 30 minutes for refrigerated reagents and minimum of 1 hour for frozen reagents. Detector and SβG reagents remained refrigerated until a later stage in the assay protocol. A microclime lid (Beckman Coulter, USA) was filled with ultrapure water and left to equilibrate. IL17A custom bead stock was diluted 1:10, then 6.37µL of 1:10 bead stock was added to 3400µL of homebrew bead diluent and vortexed[7]. This volume of beads is enough for one 96-well plate. CSF samples were diluted 1:2 and plasma samples

[4] '488-dyed' refers to the beads carrying a molecule that emits light at 488nm
[5] 'plus unit' refers to a standard SRx Simoa instrument that has received a software upgrade to become an SRx Pro instrument. This is the same software upgrade performed on the UCL SRx instrument
[6] 'alpha unit' refers to a new SRx Pro Simoa instrument made uniquely to conduct ultrasensitive measurements
[7] IL17A beads were not washed, as is custom when using homebrew beads, to prevent bead loss due to lower bead number of SRx Pro compared to standard Simoa

were diluted 1:10. Eight-point calibration curve was made using IL17A calibrator stock to concentrations in Table 3.1. CTRLs were also made using IL17A calibrator stock. 100µL of samples, CTRLs and calibrators were pipetted onto 96-well plate with duplicates in adjacent wells. Prepared bead stock was vortexed for minimum of 30 seconds, then tipped into reagent reservoir. 25µL of IL17A beads per well was promptly added to each sample well using a multichannel pipette, changing tips each column. This step must be performed within 2 minutes of bead vortexing to prevent beads from settling in bottom of reagent reservoir. Excess water was tipped out of the microclime lid, then the plate was covered and incubated at 35°C and 800rpm for 4 hours.

After the 4-hour incubation, beads were washed using the BioTek ELISA plate washer (1 cycle of 3 washes taking 4 minutes) using a 96-well magnetic manifold to retain the beads during washing. One vial of RGP is shaken at 35°C and 800rpm for a minimum of 25 minutes and maximum of 2 hours. A second, 10-minute, incubation of the beads with 100µL of IL17A detector antibody, was conducted, followed by a further wash (1 cycle of 3 washes). Following this, the beads underwent a final 10-minute incubation with 100µL SβG, and were washed (1 cycle of 3 washes taking 4 minutes). The plate was left for a minimum of 10 minutes and maximum of 1 hour to allow the bead pellets on the 96-well plate to dry before the plate was analysed on the SRx Pro.

3.2.5 Statistical analysis

All statistical analysis was performed in GraphPad Prism 9.3.1. Kruskal-Wallis analysis was performed to assess the differences in concentrations measured across all four instruments in AD compared to CTRLs. Spearman rank correlation revealed the extent of correlation between both serum and CSF measurements, and inter-instrument measurements. 95% CI were reported, and a p-value <0.05 was considered statistically significant.

Calibrator	Concentration (pg/mL)
A	0
B	0.00274
C	0.00823
D	0.0247
E	0.0741
F	0.222
G	0.667
H	2

Table 3.1 - IL17A SRx Pro calibration curve concentrations

3.3 Results

3.3.1 Upgraded Simoa, but not standard Simoa, can measure interleukin 17A in both cerebrospinal fluid and serum

The standard Simoa (HDx) instrument was unable to quantify IL17A in any of the AD and CTRL CSF samples measured, whereas CSF IL17A concentrations were obtained for 100% of samples measured using all three upgraded Simoa (SRx Pro) instruments, regardless of the phenotype (Figure 3.1). However, of these measured CSF concentrations, 84.4% (27 samples) obtained on the UCL SRx Pro were above the functional LLOQ[8] for IL17A on this instrument (0.600 fg/mL in CSF). This is compared with 96.9% (31 samples) on both Quanterix SRx Pro plus and alpha units. In addition, serum IL17A concentrations were obtained for 100% of samples on the HDx and SRx Pro instruments (Figure 3.2). However, of these measured serum concentrations, only 37.5% (12 samples) obtained on the HDx were above the functional LLOQ[8] (0.210 pg/mL in serum). This is compared with 100% of serum IL17A concentrations obtained on all three SRx Pro instruments lying above the functional LLOQ for IL17A on the SRx Pro (0.003 pg/mL).

Kruskal-Wallis analysis revealed a significant difference in the CSF IL17A AD concentrations measured using the HDx compared with the Quanterix SRx Pro plus unit (p-value 0.0002 [Figure 3.1i]), alongside CTRL measurements using the HDx compared with the plus unit (p-value <0.0001 [Figure 3.1k]). There were also significant differences between the CSF AD HDx compared with alpha unit measurements (p-value <0.0001 [Figure 3.1f]) and CSF CTRL HDx compared with alpha unit measurements (p-value <0.0001 [Figure 3.1e]). Furthermore, there were significant differences between the CSF CTRL HDx compared with UCL SRx Pro measurements (p-value 0.0007 [Figure 3.1k]), but not the CSF AD HDx compared with UCL SRx Pro measurements (p-value 0.0649). There were no significant differences between intra-instrument AD compared with

[8] Functional LLOQ refers to the analytical LLOQ multiplied by thw dilution factor

CTRL measurements (e.g. UCL SRx Pro AD vs UCL SRx Pro CTRL). However, several inter-instrument AD compared with CTRL significant differences can be seen on Figure 3.1. Given that these inter-instrument differences compare the AD measurement of one instrument to the CTRL measurement of a different instrument (e.g. Figure 3.1a refers to a significant difference between CSF AD HDx and CTRL alpha unit measurements), we did not deem it to be appropriate to comment on them. However, they have been included in Figure 3.1 for the sake of completeness. There were no significant differences in the serum IL17A concentrations measured across all instruments (Figure 3.2).

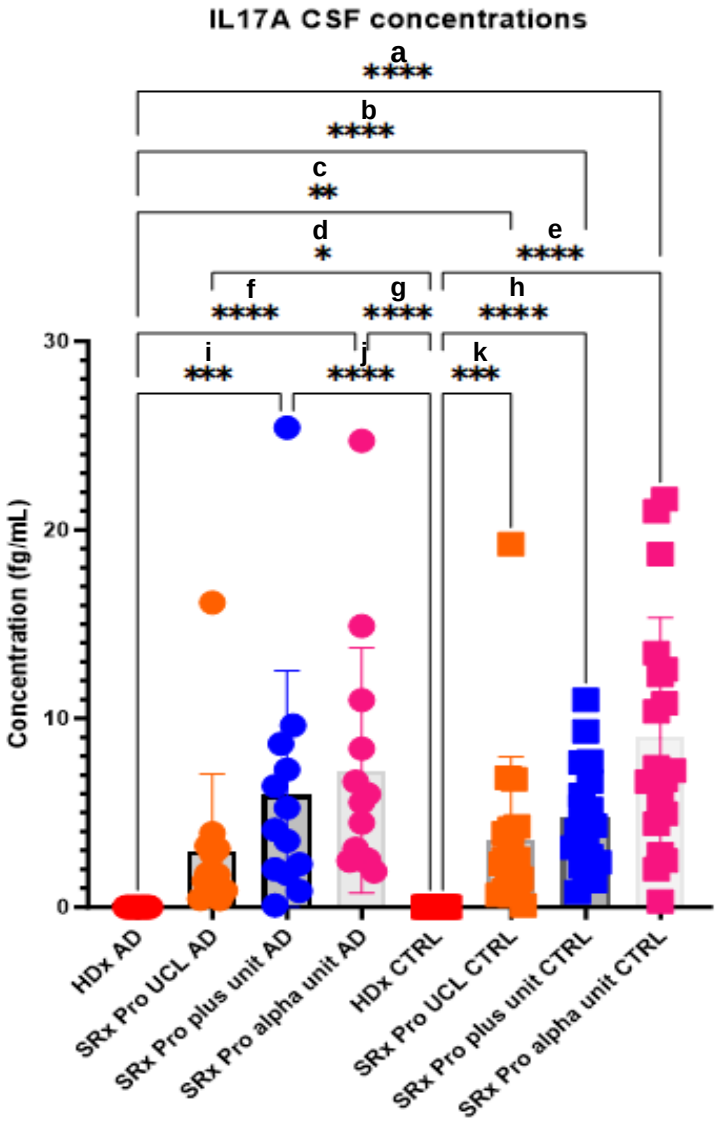

Figure 3.1 - CSF IL17A concentrations

*Alzheimer's disease (AD) and control (CTRL) interleukin 17A (IL17A) cerebrospinal fluid (CSF) concentrations across all Simoa platforms tested. CSF IL17A was unquantifiable using the HDx instrument but could be quantified in all three SRx Pro instruments. Compared to HDx, IL17A concentrations were significantly increased in SRx Pro plus unit (AD p-value = 0.0002*** [**i**]; CTRL p-value = <0.0001****[**h**]) and alpha unit (AD p-value = <0.0001**** [**f**]; CTRL p-value = <0.0001**** [**e**]). In contrast, only CTRL SRx Pro UCL IL17A concentrations were significantly increased compared with HDx (AD p-value = 0.0649; CTRL p-value = 0.0007*** [**k**]). There were no significant differences between intra-instrument AD compared with CTRL IL17A concentrations. However, inter-instrument significant differences existed between HDx AD and SRx Pro UCL CTRL (p-value = 0.0041** [**c**]), plus unit CTRL (p-value = <0.0001**** [**b**]) and alpha unit CTRL (p-value = <0.0001**** [**a**]), as well as between HDx CTRL and UCL SRx Pro AD (p-value = 0.0253* [**d**]), plus unit AD (p-value = <0.0001**** [**j**]) and alpha unit AD (p-value = <0.0001**** [**g**]).*

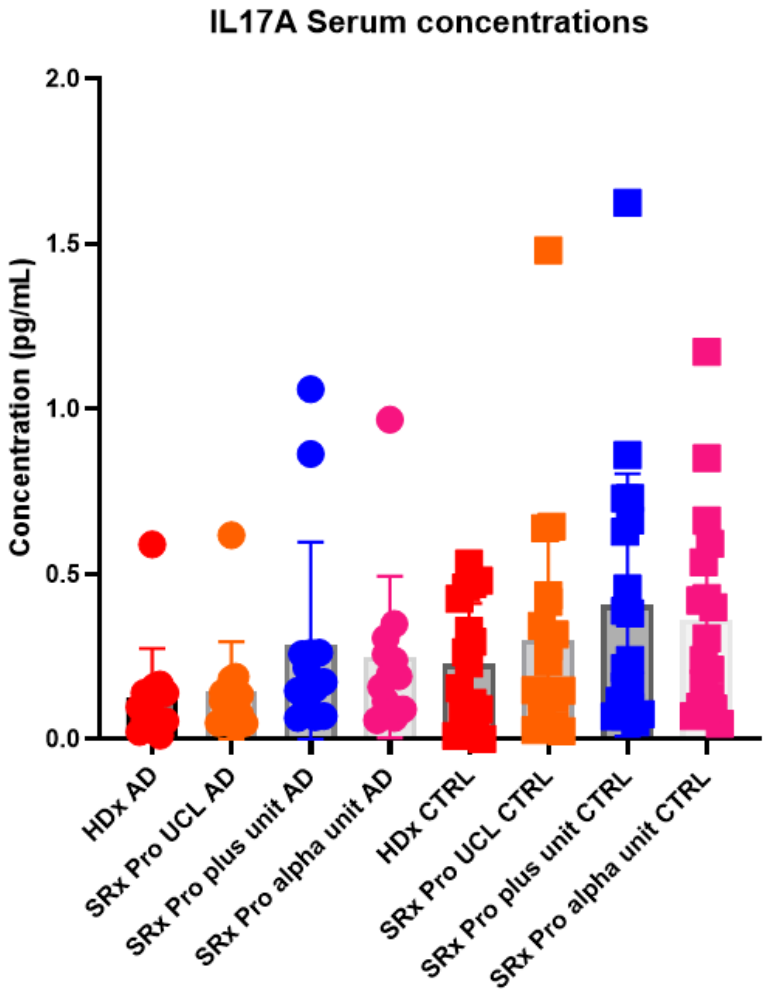

Figure 3.2 - Serum IL17A concentrations

Alzheimer's disease (AD) and control (CTRL) interleukin 17A (IL17A) serum concentrations across all Simoa platforms tested. Serum IL17A was obtained in all samples across all four Simoa platforms tested. However, only 37.5% of the measurements obtained on the HDx were above the functional lower limit of quantification. Additionally, there were no significant differences in inter- or intra- instrument comparisons of AD and CTRLs.

3.3.2 UCL SRx Pro correlates with Quanterix SRx Pro instruments

Spearman correlation analysis revealed that in CSF, there was a statistically significant positive correlation between the UCL SRx Pro and both the Quanterix SRx Pro plus unit (r-value 0.540; 95% CI 0.212-0.758; p-value 0.0021; Figure 3.3A) and alpha unit (r-value 0.446; 95% CI 0.0980-0.697; p-value 0.0119; Figure 3.3B). However, there was poor statistically non-significant correlation between the Quanterix SRx Pro plus unit and alpha unit (r-value 0.261; 95% CI -0.113-0.571; p-value 0.156; Figure 3.3C).

In contrast, a strong statistically significant correlation was observed in serum between the UCL SRx Pro and both the Quanterix SRx Pro plus unit (r-value 0.744; 95% CI 0.526-0.870; p-value <0.0001; Figure 3.4A) and alpha unit (r-value 0.940; 95% CI 0.875-0.972; p-value <0.0001; Figure 3.4B), between the Quanterix SRx Pro plus unit and alpha unit (r-value 0.941; 95% CI 0.877-0.973; p-value <0.0001; Figure 3.4C), and between the HDx and UCL SRx Pro (r-value 0.902; 95% CI 0.802-0.953; p-value <0.0001; Figure 3.5A), Quanterix SRx Pro plus unit (r-value 0.608; 95% CI 0.314-0.796; p-value 0.0003; Figure 3.5B) and alpha unit (r-value 0.911; 95% CI 0.814-0.959; p-value <0.0001; Figure 3.5C).

However, a poor statistically non-significant correlation was observed between CSF and serum measurements across all three SRx Pro instruments, with r-values of 0.269 (95% CI -0.105-0.576; p-value 0.144; Figure 3.6A), -0.0294 (95% CI -0.389-0.338; p-value 0.875; Figure 3.6B) and -0.00779 (95% CI -0.377-0.363; p-value 0.967; Figure 3.6C) for the UCL SRx Pro, Quanterix SRx Pro plus unit and alpha unit, respectively.

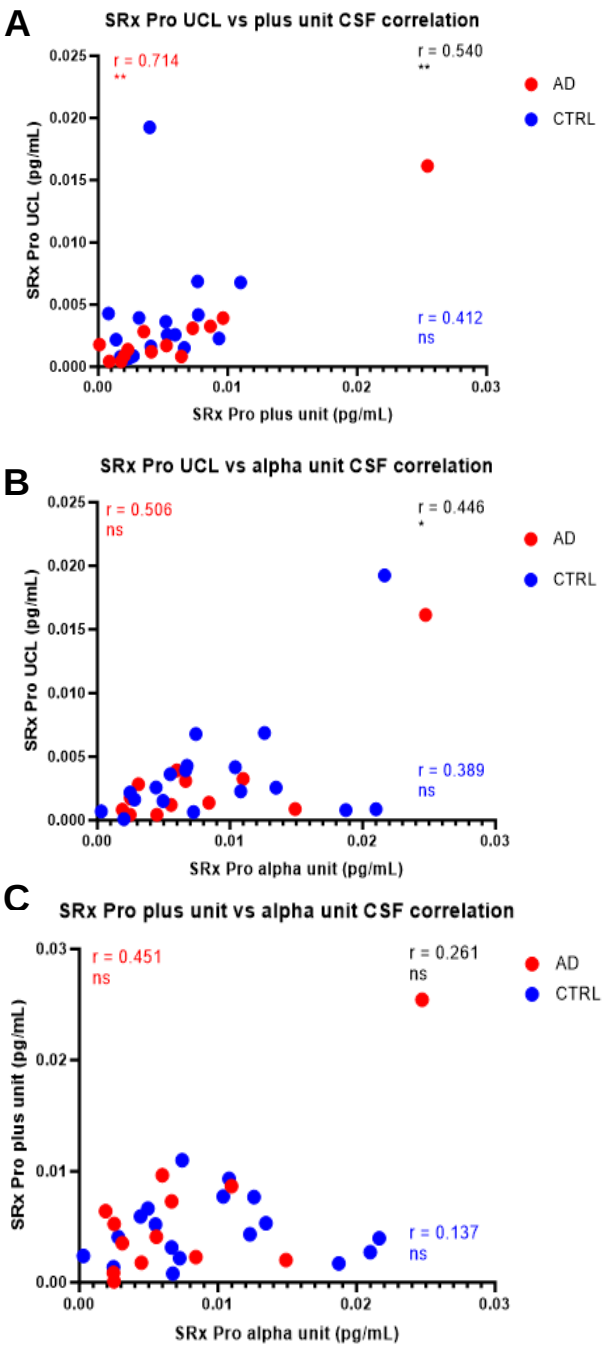

Figure 3.3 - CSF IL17A SRx Pro correlation plots

Alzheimer's disease (AD) and control (CTRL) interleukin 17A (IL17A) cerebrospinal fluid (CSF) correlation plots across all three SRx Pro platforms. ***A****: SRx Pro UCL showed positive statistically significant correlation with plus unit in CSF (r = 0.540, 95% CI 0.212-0.758, p-value = 0.0021**), with a stronger correlation when looking at AD samples alone (r = 0.714, 95% CI 0.252-0.911, p-value = 0.0079**), but a non-significant (ns) correlation when looking at CTRL samples alone (r = 0.412, 95% CI -0.101-0.752, p-value = 0.102).* ***B****: UCL SRx Pro showed a weak but statistically significant correlation with alpha unit in CSF (r = 0.446, 95% CI 0.0980-0.697, p-value = 0.0119*) but not when looking at either AD (r = 0.506, 95% CI -0.0813-0.832, p-value = 0.0812) or CTRL (r = 0.389, 95% CI -0.110-0.731, p-value = 0.111) samples alone.* ***C****: SRx Pro plus unit showed poor statistically ns correlation with alpha unit in CSF (r = 0.261, 95% CI -0.113-0.571, p-value = 0.156), nor when looking at AD (r = 0.451, 95% CI -0.152-0.809, p-value = 0.125) or CTRL (r = 0.137, 95% CI -0.365-0.578, p-value = 0.587) samples alone. 'ns' indicates non-significant findings (p>0.05); 'CI', confidence interval.*

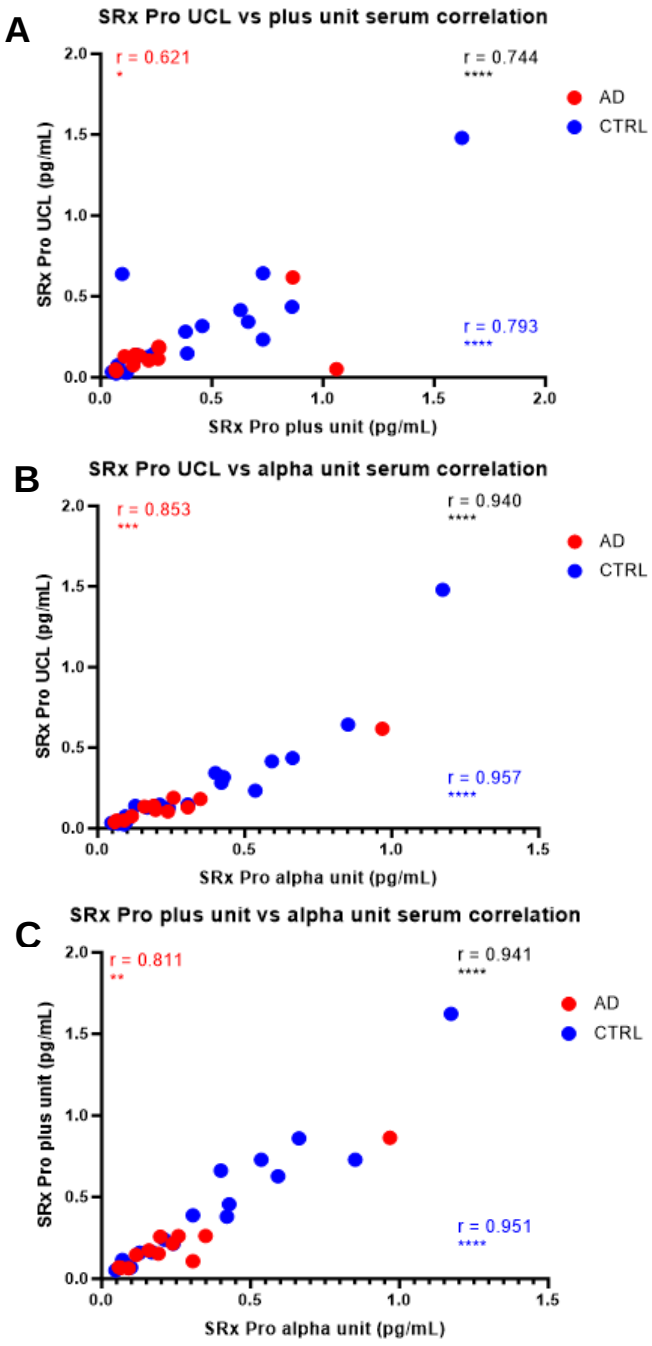

Figure 3.4 - Serum IL17A SRx Pro correlation plots

Alzheimer's disease (AD) and control (CTRL) interleukin 17A (IL17A) serum correlation plots across all three SRx Pro platforms. ***A****: UCL SRx Pro showed a strong positive, statistically significant correlation with plus unit in serum (r = 0.744, 95% CI 0.526-0.870, p-value = <0.0001****), with a strong positive statistically significant correlation also evident when looking at AD (r = 0.621, 95% CI = 0.0881-0.877, p-value = 0.0268*) and CTRL (r = 0.793, 95% CI = 0.519-0.919, p-value = <0.0001****) samples alone.* ***B****: SRx Pro UCL showed a strong positive statistically significant correlation with alpha unit in serum (r = 0.940, 95% CI 0.875-0.972, p-value = <0.0001****), including when looking at AD (r = 0.853, 95% CI 0.534-0.960, p-value = 0.0008***) and CTRL (r = 0.957, 95% CI 0.882-0.985, p-value = <0.0001****) samples alone.* ***C****: SRx Pro plus unit showed a strong positive statistically significant correlation with alpha unit in serum (r = 0.941, 95% CI 0.877-0.973, p-value = <0.0001****), including when looking at AD (r = 0.811, 95% CI = 0.428-0.947, p-value = 0.0022**) and CTRL (r = 0.951, 95% CI 0.866-0.982, p-value = <0.0001****) samples alone. 'CI' indicates confidence interval.*

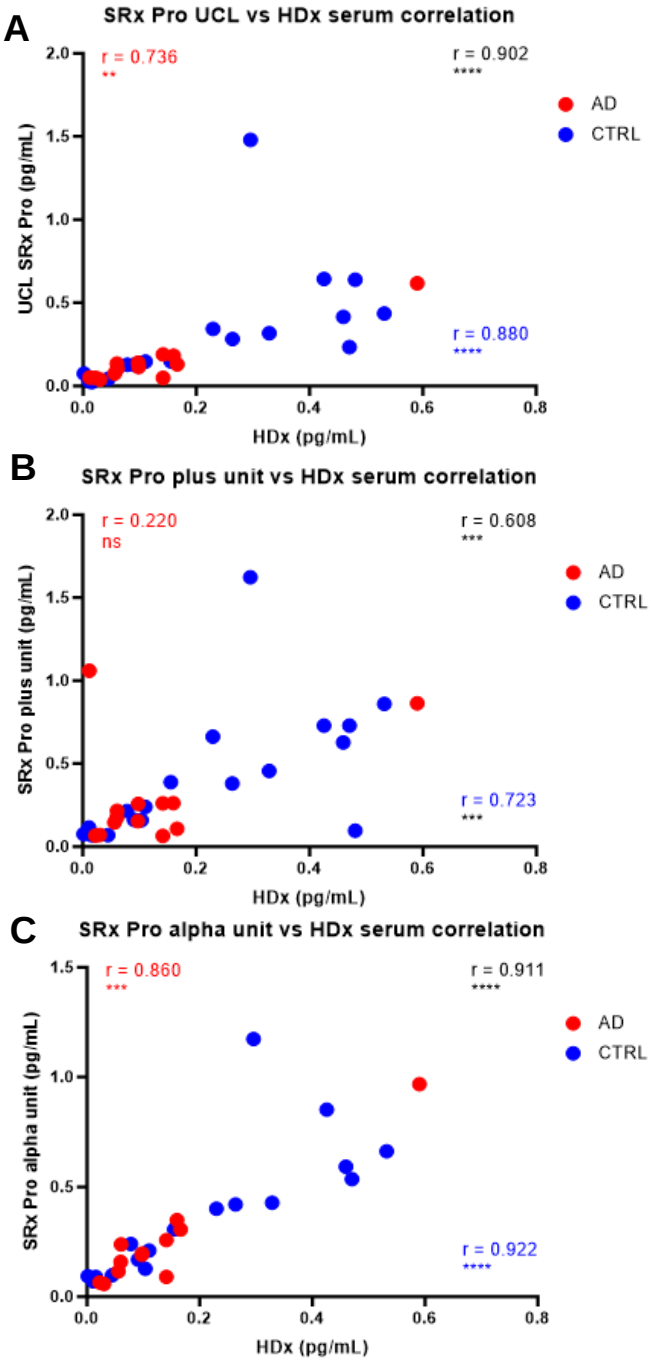

Figure 3.5 - Serum IL17A HDx vs SRx Pro correlation plots

Alzheimer's disease (AD) and control (CTRL) interleukin 17A (IL17A) serum correlation plots between HDx and all three SRx Pro platforms. ***A****: SRx Pro UCL showed a strong positive statistically significant correlation with HDx in serum (r = 0.902, 95% CI 0.802-0.953, p-value = <0.0001****), with a strong positively statistically significant correlation also evident when looking at AD (r = 0.736, 95% CI 0.295-0.919, p-value 0.0056**) and CTRL (r = 0.880, 95% CI 0.694-0.956, p-value <0.0001****) samples alone.* ***B****: SRx Pro plus unit showed a good statistically significant correlation with HDx in serum (r = 0.608, 95% CI 0.314-0.796, p-value = 0.0003***), with a poor non-significant correlation when looking at AD samples alone (r = 0.220, 95% CI -0.393-0.697, p-value = 0.470), but good correlation when looking at CTRL samples alone (r = 0.723, 95% CI 0.375-0.893, p-value = 0.0007***).* ***C****: SRx Pro alpha unit showed a strong positive statistically significant correlation with HDx in serum (r = 0.911, 95% CI 0.814-0.959, p-value = <0.0001****), including when looking at AD (r = 0.860, 95% CI 0.552-0.962, p-value = 0.0006***), and CTRL (r = 0.922, 95% CI = 0.786-0.973, p-value = <0.0001****) samples alone. 'ns' indicates non-significant findings (p>0.05); 'CI', confidence interval.*

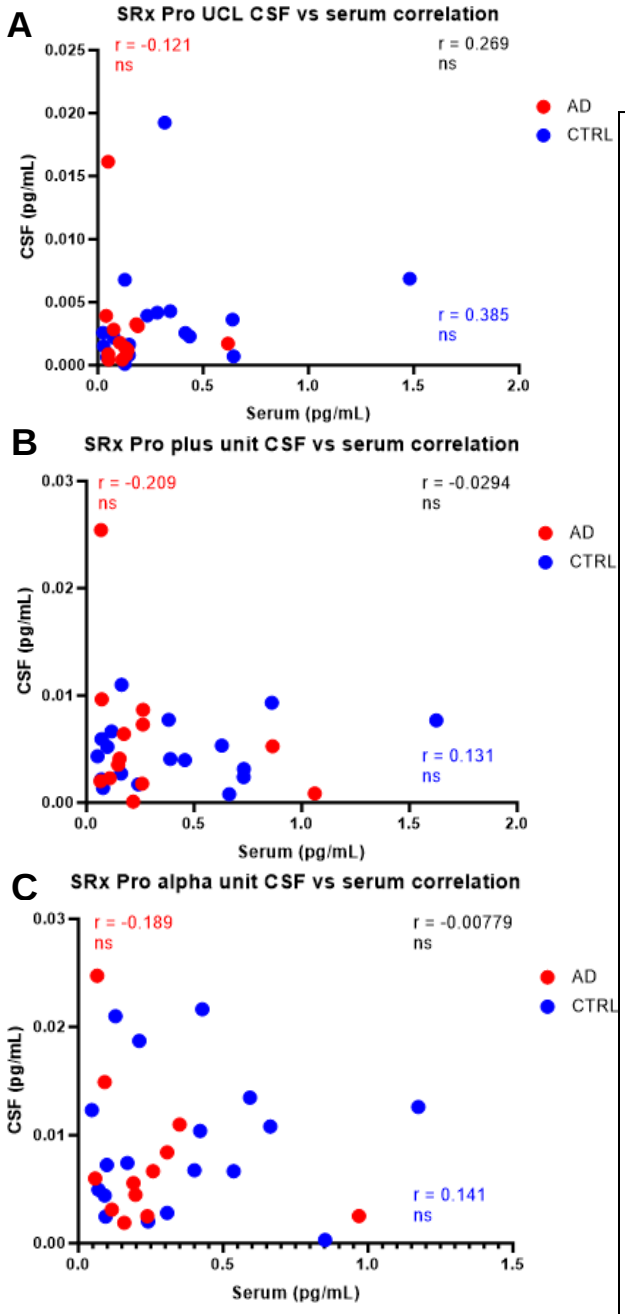

Figure 3.6 - SRx Pro CSF vs serum correlation plots

Alzheimer's disease (AD) and control (CTRL) interleukin 17A (IL17A) cerebrospinal fluid (CSF) compared to serum correlation plots across all three SRx Pro platforms. ***A****: SRx Pro UCL CSF ed a poor statistically non-significant correlation with serum (r = 0.269, 95% CI -0.105-0.576, p-value = 0.144), including when assessing AD (r = -0.121, 95% CI -0.641-0.475, p-value = 0.696) and CTRL (r = 0.385, 95% CI -0.115-0.729, p-value = 0.115) samples in isolation.* ***B****: SRx Pro plus unit CSF showed a poor statistically non-significant correlation with serum (r = -0.0294, 95% CI -0.389-0.338, p-value = 0.875), including when assessing AD (r = -0.209, 95% CI 0.691-0.402, p-value= 0.493) and CTRL (r = 0.131, 95% CI -0.371-0.574, p-value = 0.604) samples in isolation.* ***C****: SRx Pro alpha unit CSF showed a poor correlation with serum (r = -0.00779, 95% CI = -0.377-0.363, p-value = 0.967), including when assessing AD (r = -0.189, 95% CI -0.698-0.448, p-value = 0.5577) and CTRL (r = 0.141, 95% CI -0.362-0.581, p-value = 0.576) samples in isolation. 'ns' indicates non-significant findings (p>0.05); 'CI', confidence interval.*

3.3.3 Interleukin 17A is not significantly increased in Alzheimer's disease

Interestingly, whilst there were several inter-instrument significant differences between CSF AD and CTRL concentrations of IL17A, there were no such intra-instrument significant differences (Figure 3.1). The UCL SRx Pro measured a mean CSF IL17A concentration in AD of 2.92 fg/mL (95% CI 0.416-5.42 fg/mL) compared with 3.60 fg/mL (95% CI 1.42-5.77 fg/mL; p-value >0.9999) in CTRLs. This is in comparison to the Quanterix SRx Pro plus unit and alpha unit, which measured mean CSF AD concentrations of 5.95 fg/mL (95% CI 1.98-9.92 fg/mL) and 7.25 fg/mL (95% CI 3.32-11.2 fg/mL), respectively, and mean CSF CTRL concentrations of 4.75 fg/mL (95% CI 3.32-6.17 fg/mL; p-value >0.9999) and 9.02 fg/mL (95% CI 5.98-12.1 fg/mL; p-value >0.9999), respectively.

Similarly, there were no significant differences between serum AD and CTRL concentrations of IL17A (Figure 3.2). Mean serum AD concentrations were 0.126 pg/mL (95% CI 0.0355-0.216 pg/mL) on the HDx, 0.145 pg/mL (95% CI 0.0533-0.236 pg/mL) on the UCL SRx Pro, 0.285 pg/mL (95% CI 0.0969-0.473 pg/mL) on the Quanterix SRx Pro plus unit, and 0.249 pg/mL (95% CI 0.0940-0.405 pg/mL) on the Quanterix SRx Pro alpha unit. Whilst mean serum CTRL concentrations were 0.228 pg/mL (95% CI 0.136-0.319 pg/mL; p-value >0.9999) on the HDx, 0.300 pg/mL (95% CI 0.134-0.466 pg/mL; p-value >0.9999) on the UCL SRx Pro, 0.406 pg/mL (95% CI 0.215-0.598 pg/mL; p-value >0.9999) on the Quanterix SRx Pro plus unit, and 0.362 pg/mL (95% CI 0.209-0.515 pg/mL; p-value >0.9999) on Quanterix SRx Pro alpha unit.

However, whilst the differences may not be significant, the results suggest that in both CSF and serum, IL17A is of a marginally lower concentration in AD than in CTRLs within our cohort.

3.3.4 Results summary

In summary, whilst the HDx was able to quantify IL17A in only a small subset of serum samples, the SRx Pro instruments successfully quantified IL17A in all serum samples and the majority of CSF samples. Furthermore, there was a stronger correlation between all four instruments in serum than in CSF, with the Quanterix SRx Pro plus unit and alpha unit surprisingly showing poor correlation with one another in CSF. Finally, in our cohort, there was no significant difference in IL17A measurements in AD compared with CTRLs.

3.4 Discussion

This study confirms that the SRx Pro upgraded Simoa platform has a greater sensitivity than the HDx standard Simoa platform, as shown by its ability to measure IL17A in both serum and CSF (Figure 3.1 and Figure 3.2). This is in comparison to the HDx instrument only quantifying IL17A in 37.5% of our serum samples, with the remainder of serum samples falling below the functional LLOQ, and all CSF samples generating AEBs similar to or below that of the blank calibrator. Despite only 37.5% of serum samples measured using the HDx lying above the functional LLOQ, serum measurements from all three SRx Pro instruments showed a strong correlation with the HDx – the strongest correlation being observed with the SRx Pro alpha unit ($r = 0.911$; 95% CI 0.814-0.959; p-value = <0.0001; Figure 3.5C). This emphasises the validity of the SRx Pro for measuring this analyte in serum.

An important observation to note is that only 84.4% of the CSF IL17A sample concentrations measured using the UCL SRx Pro were above the functional LLOQ in comparison to 96.9% of samples on both Quanterix SRx Pro plus unit and alpha unit. Whilst the exact cause of this difference is not clear, it is possible that the environmental temperature had an impact on the calibration curves and extrapolated IL17A concentrations, particularly given that ambient temperature is known within Quanterix Corporation to affect the SRx (and by proxy, the SRx Pro) instrument. Indeed, the samples on all three SRx instruments were not measured at the same time of year, with the samples on the UCL SRx Pro being measured two months prior to the Quanterix SRx Pro instruments, when the ambient temperature was far lower. This theory is further supported by all concentrations obtained on the UCL SRx Pro being visibly lower than those obtained on the Quanterix SRx Pro plus and alpha units.

Whilst all three SRx Pro instruments displayed a strong correlation with one another in serum (Figure 3.4), this correlation was far

weaker in CSF (Figure 3.3). In fact, the SRx Pro plus unit and alpha unit showed no correlation in CSF at all (Figure 3.3C). Reasons for this disparity, particularly given the strong inter-instrument correlations observed in serum, remain unclear. However, they are likely to fall with the biofluid, rather than the instruments themselves. It is possible that the low absolute concentration of IL17A in CSF compared with serum, particularly given that it was unmeasurable by the HDx instrument, may be contributing to the poor inter-instrument correlations.

Whilst all SRx Pro instruments successfully measured IL17A in CSF, a poor correlation was observed between CSF and serum measurements across all instruments (Figure 3.6). This is consistent with the observations of Schofield and colleagues (363), as well as Pastuszczak and colleagues (364), although neither of these studies were conducted in AD individuals. Furthermore, similarly poor correlations have been observed with other CSF-peripheral cytokine comparisons (365). This consistently poor correlation between CSF and serum IL17A, and other cytokines, across several diseases suggests CSF IL17A concentrations are more greatly influenced by its production from CNS-derived cells, such as astrocytes, rather than by peripherally produced IL17A crossing the BBB. This suggests that peripheral IL17A may be a poor indicator of CNS inflammatory processes, but it may still provide key information relating to the inflammatory profile of the individual.

Interestingly, we observed no significant difference in IL17A concentrations between AD and CTRLs in either biofluid, which seemed somewhat surprising given the neuroinflammatory nature of AD. One reason for this may be due to the small sample cohort used in our study. However, *in vivo* investigations conducted by Zimmerman and colleagues (366) suggest that IL17A does not play a direct role in inducing and exacerbating neuroinflammation or neurodegeneration, but rather it does activate glial cells and alter CNS inflammatory responses. It may also be that the inflammatory

component of AD is dominated by the innate immune system, where IL17A may play a limited role. However, further investigations will need to be conducted to verify this theory.

In conclusion, we have successfully validated the results of Kan and colleagues (214), confirming that the SRx Pro does indeed provide additional sensitivity in comparison to the HDx Simoa platform, and allowing the quantification of IL17A in CSF. Alongside this, we observed no significant differences in IL17A concentration in AD compared with CTRL individuals in neither CSF nor serum.

CHAPTER 4: NOVEL ASSAY DEVELOPMENT

4.1 Introduction and rationale

Following the poor diagnostic accuracy of plasma $A\beta_{42/40}$ for AD observed in our cohort, along with the extensive overlap between AD and NAD diagnostic groups, and the poor correlation with CSF $A\beta_{42/40}$, it is clear that novel biomarkers for Aβ pathology in plasma are needed to provide a more definitive and robust diagnosis for AD. Whilst there may be some benefit to investigating markers of tissue responses to Aβ as surrogate biomarkers of Aβ pathology – a topic recently reviewed by myself and colleagues (225) – it would be of more benefit to consider alternative isoforms of Aβ. This is because several of the biomarkers relating to tissue responses to Aβ already serve a function in other aspects of the AD diagnostic criteria[1]. As highlighted in Figure 1.2, the sequential cleavage of Aβ by γ-secretase produces Aβ peptides of varying amino acid chain lengths, hence it may be of benefit to consider detecting Aβ peptides further up the cleavage sequence, such as $A\beta_{43}$. Additionally, given that the vast majority of Aβ present within the brains of AD patients is either modified or truncated at the N-terminus (63), investigating such an isoform of Aβ, such as $A\beta_{pE}$, could also confer greater specificity to AD, and hence a clearer demarcation between diagnostic groups, particularly in plasma.

CSF $A\beta_{43}$ has been successfully measured in FAD individuals using ELISA, with a significantly reduced concentration being observed in AD compared with CTRLs, alongside a reduction in the $A\beta_{43/40}$ (40) – results which were recently replicated by De Kort and colleagues (367). However, to our knowledge, $A\beta_{43}$ has not been successfully quantified in plasma. Furthermore, given that the concentration of CSF $A\beta_{43}$ for AD patients in these studies ranged from approximately 5-35 pg/mL ($1.84x10^{-11}$ to $1.28x10^{-10}$ M), we anticipate plasma $A\beta_{43}$ concentrations to reach the attomolar (10^{-18} M) to femtomolar (10^{-15} M) range. Detecting such low concentrations would require increased levels of sensitivity than is currently supported by the available

instruments. Similarly, $A\beta_{pE}$ has yet to be measured in human samples of either biofluid, which is highly likely to be a consequence of limited instrument sensitivity. Given that $A\beta_{pE}$ is a plaque-specific form of Aβ (74), which we hypothesise is secreted from plaques in small quantities in the presence of AD-related Aβ pathology, its concentrations are expected to be so low that greater sensitivity is required for its measurement. Given the recent clinical trial successes observed with the phase III clinical trial of Donanemab, a monoclonal antibody against $A\beta_{pE}$, being able to quantify this peptide may provide an opportunity to further monitor the efficacy of this drug. In light of this, we aim to develop novel assays for $A\beta_{43}$ and $A\beta_{pE3\text{-}40}$ for use in CSF and/or plasma using the upgraded Simoa technology based on the hypotheses that the $A\beta_{43/40}$ will decrease more than and/or earlier than the $A\beta_{42/40}$, and that $A\beta_{pE}$ is secreted in small quantities in the presence of plaque pathology from within the plaque into the CSF, and hence increases with greater plaque burden.

4.2 Considerations for developing novel Simoa assays

When developing novel assays on any immunoassay platform, but particularly on Simoa, there are several key components that must be considered, both with regards to the analyte of interest, as well as the materials required to develop the assay. Namely, already established assays for detecting the analyte, the material to be used for the calibration curve, the specificity and binding affinity of selected antibodies to the target analyte, and finally the matrix within which the analyte will be measured.

4.2.1 Existing assays to measure analyte

Identifying any existing assays to measure the analyte of interest is key as this will provide insight into whether the analyte has successfully been measured *in vitro* or *in vivo*, and hence the estimated concentration range of the analyte in healthy and diseased states. Whilst any immunoassay platform would be beneficial, of particular interest in relation to Simoa is an established conventional ELISA test. Given that Simoa is a digitalised version of conventional ELISA, an established ELISA test would offer the greatest information on translation to Simoa.

We identified five existing conventional sandwich ELISAs for the measurement of $A\beta_{43}$, and one for the measurement of $A\beta_{pE3}$ (Table 4.1). Of those specified on the manufacturer website, the $A\beta_{43}$ assays had a calibration curve range of 2.34-150 pg/mL, with a sensitivity of 1.28 pg/mL. The $A\beta_{pE3}$ assay, whilst not being specific to $A\beta_{pE3\text{-}40,}$ had a calibration curve range of 7.75-496 pg/mL.

Manufacturer	Specificity	Cross-reactivity	Calibration curve range (pg/mL)	Sensitivity (pg/mL)	Website links
American Research Products	$A\beta_{43}$	Unknown	Unknown	Unknown	https://www.arp1.com/amyloid-beta-1-43-fl-human-elisa-kit-27710.html
IBL international	$A\beta_{43}$	Unknown	2.34-150	Unknown	https://ibl-international.com/en/amyloid-beta-1-43-fl
FIVEphoton biochemicals	$A\beta_{43}$	<1% $A\beta_{42}$ <0.1% $A\beta_{45}$	2.34-150	1.28	https://fivephoton.com/index.php?route=product/product&product_id=363
Demeditec	$A\beta_{43}$	Unknown	2.34-150	Unknown	https://www.demeditec.com/en/products/amyloid-beta-1-43-fl-human-elisa-jp27710
Cell Signalling technology	$A\beta_{43}$	Extensively with $A\beta_{42}$	Unknown	Unknown	https://www.cellsignal.com/products/elisa-kits/b-amyloid-1-43-sandwich-elisa-kit/43825?Ns=product.displayName%7C0&N=102262+1634459133+4294956287&Nrpp=30&No=%7Boffset%7D&fromPage=plp
IBL America	$A\beta_{pE3}$	Unknown	7.75-496	1.94	https://www.ibl-america.com/amyloid-beta-n3pe-a/

Table 4.1 – Existing ELISA assays for the detection of $A\beta_{43}$ and $A\beta_{pE3}$

4.2.2 Calibration curve component

Assays of any kind require a calibration curve of known concentrations against which signals detected in samples can be compared in order to extrapolate analyte concentrations within the samples. Calibration curves are generated using a serial dilution of either a recombinant or a synthetic version of the protein of interest.

Recombinant proteins are synthesised by transforming a cell – most commonly the *Escherichia coli* bacterium due to its fast growth rate and high product yield (368) – with a plasmid carrying the gene encoding the protein of interest. Alternatively, peptides can be synthesised synthetically via a chemical process. One benefit of using recombinant proteins over synthetic peptides is that the product more closely replicates the endogenous structure and behaviour of the protein. However, this does not come without significant financial implications. In contrast, as well as being comparatively cheaper, synthetic peptides are less time-consuming to generate. Furthermore, of particular use to us is the ability to modify the amino acid sequence of synthetic peptides, whilst keeping specific epitopes unchanged.

4.2.3 Antibody specificity and binding affinity to target analyte

The antibody binding affinity refers to the strength with which an antibody binds to its antigen. The binding affinity is measured quantitatively using the inverse of the equilibrium dissociation constant (K_D). In essence, the smaller the value of K_D, the higher the affinity of the antibody to its antigen, and hence a smaller concentration of the antibody is required for antigen detection (369). Similarly, the specificity of the antibody to the target, with minimal cross-reactivity with similar analytes, will greatly impact the efficacy of the assay developed.

4.2.4 Target matrix

The target matrix the analyte will be measured in will offer unique challenges that must be considered. Whilst the main component of plasma is water, it also contains coagulants (mainly fibrinogen), plasma proteins (*e.g.* albumin, globulin), electrolytes (*e.g.* potassium, bicarbonate, chloride, calcium) and immunoglobulins (370). Serum and plasma have very a similar composition to one another, except serum no longer contains coagulants. Similarly, CSF is predominantly composed of water, but it also contains proteins, vitamins, and electrolytes. Indeed, CSF and plasma mainly differ only in concentrations of proteins and electrolytes (371). Each of these components may interact, interfere, and compete with the target analyte binding to the epitope of the antibody.

4.2.5 Optimal characteristics of a Simoa assay[9]

As with the development of any immunoassay, optimal characteristics of a novel Simoa assay include: 1) low background signal (i.e. low AEB at blank calibrator); 2) high signal:background noise ratio (S/N); 3) suitable dynamic range for target analyte.

On the standard Simoa platforms (SRx and HDx), an AEB of between 0.005-0.02 at the blank calibrator (i.e. calibrator A) is desirable. This equates to an f_{on} of <0.02. On the upgraded Simoa platform (SRx Pro), an AEB at calibrator A of no less than 0.01 is optimal due to the lower number of beads used.

With regards to calibrator B, whilst there is no specific target AEB, an S/N of between 2-4 is most optimal. In contrast, with regards to the top calibrator (calibrator F of a six-point curve; calibrator H of an eight-point curve), a target AEB no greater than 16 is optimal, as values above this saturate the optics used to capture images of the beads during analysis on the Simoa instrument. However, as with all

[9] Summarised from Quanterix Homebrew assay development guide, available on Quanterix Customer Portal

assays, the concentration of the highest calibrator will be dependent on the dynamic range required for the assay. As such, in some instances, it may be of greater benefit to prioritise sensitivity, sacrificing a wider dynamic range of both the calibration curve and the resultant AEBs.

4.3 Materials and methods

4.3.1 Materials

Homebrew assay development starter kit was purchased from Quanterix Corporation (101351), alongside generic Simoa instrument consumables (*e.g.* wash buffers, pipette tips etc). Antibodies against the N- and C-termini of $A\beta_{43}$ and $A\beta_{pE3\text{-}40}$ were all purchased from BioLegend, as detailed in Figure 4.1. Synthetic peptides for $A\beta_{43}$ and $A\beta_{pE3\text{-}40}$ were purchased from rPeptide (A-1005-1) and Anaspec (AS-29906-1), respectively, as detailed in Figure 4.1. Beckman Coulter MicroClime lids for SRx Pro were purchased from Fisher Scientific (NC1732006).

4.3.2 MSD antibody test

The Meso Scale Discovery (MSD) instrument, which utilises ECL detection, was used to determine whether the antibodies purchased for development of the $A\beta_{43}$ assay can detect $A\beta_{43}$.

Wash buffer (1x phosphate buffer saline + 0.1% Tween-20 [PBST]), block buffer (50mL PBST + 250mg bovine serum albumin [BSA]), sample diluent (1:2 dilution of block buffer with PBST) and 1xphosphate buffer saline (PBS) were made as described. $A\beta_{43}$ peptide was diluted using sample diluent to concentrations of 0.1, 0.25, 0.5 and 1µg/mL. A 96-well standard MSD plate was coated with 50µL per well of $A\beta_{43}$ or $A\beta_{pE3\text{-}40}$ peptide at the concentrations described, with duplicate measurements being placed in separate wells. Sides of plate were tapped gently to ensure well was completely covered by antibody solution, before being covered with plastic plate seal, wrapped in foil, and incubated at 2-8°C overnight to coat plate with peptide.

Following the overnight incubation, all reagents (block buffer, sample diluent and plate) were left to equilibrate to room temperature for 30 minutes. For 6E10 and anti-$A\beta_{43}$ antibodies were diluted in sample diluent to both 1:1000 and 1:2000. Liquid on plate was discarded,

and plate was tapped onto tissue to remove any remaining peptide not bound to plate. 25µL of each antibody was pipetted into appropriate wells, and plate was incubated for 1 hour at 500rpm and room temperature. Shortly before incubation was finished, goat-anti-mouse sulfo-tag antibody (MSD; R32AC-1) was diluted 1:2000 in block buffer. Following incubation, plate was washed three times with 200µL of wash buffer, tapping plate thoroughly onto tissue after third wash to remove excess wash buffer. 25µL of sulfo-tag antibody was pipetted onto each well using multichannel pipette, and plate was incubated for a further 1 hour at 500rpm and room temperature. Following incubation, plate was washed three times with 200µL of wash buffer, and two times with PBS only, tapping plate onto tissue thoroughly after final wash to remove excess PBS. 150µL of MSD read buffer T (4X; R92TC-3) was pipetted into each well using multichannel pipette, before placing plate on MSD reader to be analysed.

4.3.3 Simoa assay development

The assay development process on the Simoa involves 7 key stages: 1) antibody screening and calibrator selection; 2) capture antibody bead conjugation and detector antibody biotinylation; 3) 2-step and 3-step assay comparison; 4) assay optimisation; 5) dilution linearity; 6) spike recovery; 7) trials on clinical samples. Beyond these baseline stages of assay development, Andreasson and colleagues (372) describe a far more extensive series of validation assessments to be performed for any novel immunoassays.

Assay development for both the $A\beta_{43}$ and $A\beta_{pE3\text{-}40}$ assays were initially completed on the SRx, then were transferred onto the HDx, prior to development on the SRx Pro. A six-point calibration curve was used throughout stages 1-4 of the assay development process primarily for reagent preservation purposes. However, upon returning to the HDx instrument to finalise our assays, we expanded our calibration curve to an eight-point curve, as is standard for

immunoassays, particularly when entering stages 5) to 7) of the assay development process.

4.3.3.1 Antibody screening and calibrator selection

Antibody manufacturer websites were searched for antibodies of interest, and the epitope targeted was labelled on an amino acid diagram of the Aβ peptide of interest, as depicted in Figure 4.1. Antibodies were selected based on their epitope specificity (C-terminus, N-terminus or non-specific), and cross-reactivity with similar analytes. Monoclonal antibodies were favoured over polyclonal antibodies due to their specificity and batch-to-batch stability. Furthermore, antibodies previously used for ELISA-based experiments were also favoured. Selected antibodies for the $A\beta_{43}$ assay were anti-$A\beta_{1\text{-}16}$ (6E10; BioLegend; 803003) and anti-$A\beta_{43}$ (specific to the C-terminus; BioLegend; 805601), and for the $A\beta_{pE3\text{-}40}$ assay were anti-$A\beta_{pE3\text{-}16}$ (BioLegend; 822301) and anti-$A\beta_{40}$ (specific to the C-terminus; BioLegend; 805403). The calibrators used during assay development were the synthetic peptide for the assay being developed, already detailed in section 4.3.1 Materials. However, experiments conducted on the standard SRx revealed extensive oligomerisation was occurring within the $A\beta_{43}$ calibrator (see section 4.4.2.1.1 $A\beta_{43}$ assay). As such, we generated amino acid sequences for four $A\beta_{43}$ custom peptides (CP) using the GenScript peptide analysing tool[10] to reduce the hydrophobicity of the $A\beta_{43}$ peptide, and hence decrease the extent of oligomerisation. This involved either replacing the amino acid glycine (hydrophobic) with the amino acid glutamate (hydrophilic) or removing several amino acids in the centre of the peptide and replacing them with a glutamate linking chain. These four CPs, alongside the original $A\beta_{43}$ amino acid sequence can be seen in Figure 4.2. The CP amino acid sequences were sent to rPeptide, who manufactured the synthetic peptides. All peptides

[10] https://www.genscript.com/tools/peptide-analyzing-tool

used in this PhD were reconstituted in ammonium hydroxide, aliquoted and stored at -20°C until use.

4.3.3.2 Capture antibody bead conjugation

The standard bead conjugation protocol uses 1-ethyl-3-(3-dimethylaminopropyl)carbodiimide hydrochloride (EDC) to conjugate the antibody to 488-dyed[4] superparamagnetic beads. 2mL and 0.5mL Protein LoBind tubes (Eppendorf; EP0030108132 and EP0030108094, respectively) were used to reduce antibody lost during preparation. The protocol was obtained from Quanterix Customer portal and followed as instructed, starting with 100µg of antibody.

In brief, capture antibodies did not undergo buffer exchange as they were already dissolved in PBS and were both azide- and BSA-free. However, should the antibodies have required buffer exchange into the Quanterix bead conjugation buffer (BCB), this process would be conducted using Amicon Ultra-0.5 50kDa centrifugal filters (Merck; UFC505096), diluting the final buffer exchanged antibody in BCB to a desired concentration of 0.2mg/mL and volume of 300µL. $1.4x10^9$ beads/mL of 488-dyed[4] superparamagnetic beads (Quanterix; 104006) were prepared and washed with bead wash buffer (BWB), activated with EDC (30 minute incubation using Hula Mixer at 2-8°C), then bead-EDC solution was incubated with buffer exchanged antibody for 2 hours at 2-8°C to conjugate. Following this, conjugated beads were washed and blocked with bead blocking buffer for 45 minutes at room temperature using the Hula Mixer. Beads were then washed once with BWB, and twice with bead diluent before being pelleted and stored at 4°C until use.

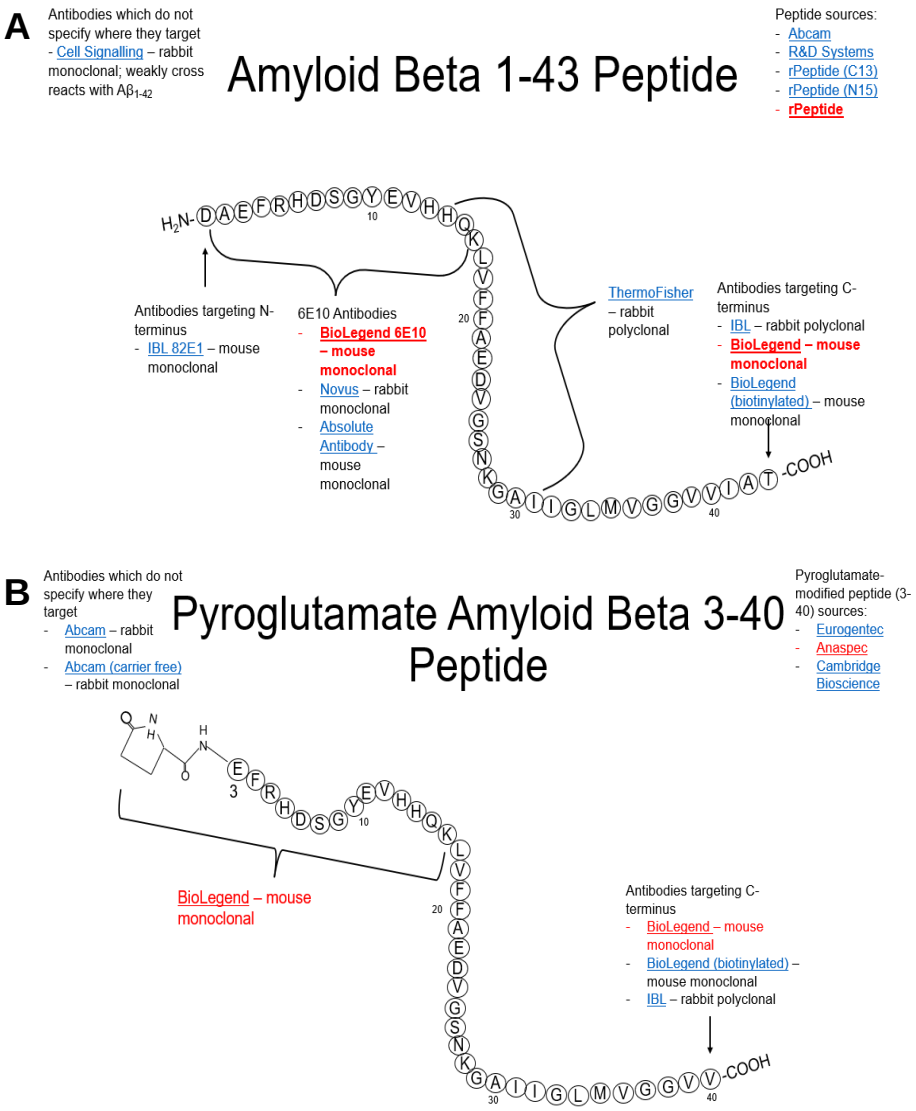

Figure 4.1 - Aβ antibody screen and calibrator selection

A: *Amyloid-β 1-43 ($Aβ_{43}$) peptide diagram labelled with antibodies according to epitope targeted. Peptide used for calibrator, alongside antibodies selected for assay development, are labelled in red.* ***B:*** *Pyroglutamate-modified Aβ 3-40 ($Aβ_{pE3-40}$) peptide diagram labelled with antibodies according to epitope targeted. Peptide used for calibrator, alongside antibodies selected for assay development, are labelled in red.*

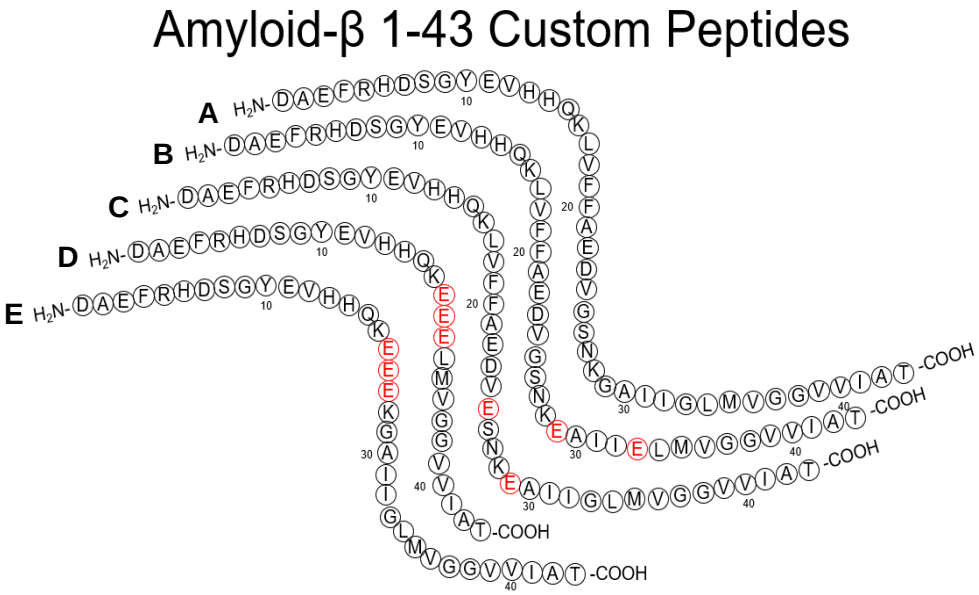

Figure 4.2 - Aβ$_{43}$ custom peptides

*Amyloid-β 1-43 (Aβ$_{43}$) custom peptide diagrams (**B-E**). Altered amino acids are labelled in red against original Aβ$_{43}$ amino acid chain (**A**). Amino acids 1-16 and 34-43 were left unaltered to not interfere with epitopes targeted by selected antibodies for assay development.*

4.3.3.3 Detector antibody biotinylation

The protocol for biotinylation of the detector antibodies was obtained from Quanterix Customer portal and followed as instructed.

In brief, the detector antibodies did not undergo buffer exchange as they were already dissolved in PBS, and were both azide- and BSA-free. However, should the antibodies have required buffer exchange into the Quanterix biotinylation reaction buffer (BRB), this process would have been conducted using Amicon Ultra-0.5 50kDa centrifugal filters (Merck; UFC505096), adjusting the final buffer exchanged antibody to a desired concentration of 1mg/mL. 8.9mM NHS-PEG4-biotin (Thermo Fisher Scientific; A3959) was added to the antibody at a standard challenge ratio of 40x, vortexed briefly and incubated for 30 minutes at room temperature. Excess biotin, along with unlabelled surplus antibody were removed through a series of several Amicon filter buffer exchanges. Concentration of resultant

biotinylated dectector antibody was determined using a NanoDrop One microvolume Spectrophotometer (ThermoFisher Scientific).

4.3.3.4 2-step and 3-step assay protocol – SRx and HDx

All diluents were left to equilibrate to room temperature, alongside samples if they were being used, leaving 30 minutes for refrigerated reagents, and 1 hour for frozen reagents.

Bead stock was vortexed for 30 seconds to resuspend, then the required volume was pipetted into an Eppendorf tube and placed in a magnetic rack for 30-60 seconds to separate the beads from the diluent. Supernatant was discarded, and the beads were resuspended in 300 µL bead diluent, vortexed, briefly spun and placed back into the magnetic rack. This sequence was repeated 2-3 times, then beads were resuspended in the required volume of bead diluent for the experiment. Detector antibody reagent was then prepared, diluting the detector stock in the same diluent as the calibrators and samples, and inverting several times to mix. SβG reagent was prepared to the required concentration, using SβG concentrate diluted in SβG diluent, and inverting several times to mix. Finally, the calibration curve was prepared, diluting the synthetic peptide in the same diluent as the detector and samples, and vortexing well between each calibrator. RGP reagent was placed on Simoa microplate shaker for minimum 30 minutes (maximum 4 hours) at 30°C and 800rpm. If using the HDx, beads, detector and SβG were stored on ice until they were loaded onto the instrument.

4.3.3.4.1 SRx

For the SRx, 100µL per well of each calibrator/samples/CTRLs was pipetted into adjacent wells for duplicate measurements. For the 2-step assay protocol, detector reagent was gently inverted to mix, tipped into reagent reservoir and 20µL of detector was pipetted into each well using a multi-channel pipette. Prepared beads were

vortexed for minimum 30 seconds to resuspend beads, solution was then tipped into reagent reservoir and 25µL of beads were pipetted into each well using multi-channel pipette, aspirating several times to ensure beads were well mixed with sample and detector. Pipette tips were changed each time. Plate was covered with Quanterix plate lid and incubated on the Simoa microplate shaker for 30 minutes at 30°C and 800rpm. For the 3-step assay protocol, prepared beads were vortexed for minimum 30 seconds to resuspend, tipped into reagent reservoir then 25µL of beads was pipetted into each well using multi-channel pipette, aspirating several times to ensure beads were well mixed with sample. Pipette tips were changed each time. Plate was covered with Quanterix plate lid and incubated on Simoa microplate shaker for 30 minutes at 30°C and 800rpm.

During incubation, the BioTek washer protocol was begun. When instructed, and upon completion of 30-minute incubation, plate was placed on BioTek washer and washer protocol was continued. Upon completion of washes (3 washes with wash buffer A; 4 minutes), for the 2-step assay protocol, SβG reagent was gently inverted, 100µL was pipetted into each well and plate was incubated on Simoa microplate shaker for a further 10 minutes at 30°C and 800rpm. For 3-step assay protocol, detector reagent was gently inverted, 100µL was pipetted into each well, then plate was incubated on the Simoa microplate shaker for a further 10 minutes at 30°C and 800rpm.

Upon completion of second incubation, plate was placed back on the BioTek washer and washer protocol was continued. For 2-step assay, plate was left for 10 minutes for beads to dry prior to loading onto the SRx instrument for plate analysis. For the 3-step protocol, SβG reagent was gently inverted, 100µL was pipetted into each well, and the plate was incubated on Simoa microplate shaker for a further 10 minutes at 30°C and 800rpm. Upon completion of final incubation, plate was returned to the BioTek washer for a final wash (wash buffer B), left for 10 minutes for the beads to dry, and loaded onto the SRx.

4.3.3.4.2 HDx

For the HDx, 250µL per well of each calibrator/sample/CTRL was pipetted onto the plate (duplicates are taken from the same well by the HDx instrument), then the plate was covered with Quanterix perforated plate seal. Reagents (beads, detector, SβG, RGP, plate) were loaded onto HDx, the appropriate assay settings to differentiate between 2-step and 3-step protocol were applied, and the run was begun.

The key differences between the 2-step and 3-step assay protocols are summarised below in Table 4.2.

Reagent	**2-step assay protocol (µL)**	**3-step assay protocol (µL)**	**Default final concentration (prior to optimisation)**
Beads	25	25	$2x10^7$ beads/mL
Detector	20	100	1.0µg/mL (2-step) 0.3µg/mL (3-step)
SβG	100	100	150pM
Calibrator, sample and CTRLs	100[11]	100[11]	N/A

Table 4.2 – Summary of differences between 2-step and 3-step assay protocols

4.3.3.5 2-step and 3-step assay protocol – SRx Pro

All diluents were left to equilibrate to room temperature, alongside samples if they were being used, leaving 30 minutes for refrigerated reagents, and 1 hour for frozen reagents.

MicroClime lid was prepared. Bead stock was vortexed for 30 seconds to resuspend, then diluted 10x to account for the lower bead

[11] Although 250µL is pipetted for HDx, the instrument only takes 100µL when conducting the assay protocol

concentration used with the SRx Pro. Required volume of beads was resuspended in the required volume of bead diluent. Beads were not washed to minimise bead loss considering lower bead number, and were left at room temperature. Finally, calibration curve was prepared, diluting the synthetic peptide in the same diluent as the detector and sample, and vortexing well between each calibrator.

100µL per well of each calibrator/samples/CTRLs was pipetted into adjacent wells for duplicate measurements. Prepared beads were vortexed for minimum 30 seconds to resuspend beads, solution was then tipped into a reagent reservoir and 25µL of beads was pipetted into each well using a multi-channel pipette, aspirating several times to ensure beads were well mixed with sample and detector. Pipette tips were changed each time. Excess water within MicroClime lid was discarded, then plate was covered with MicroClime lid and incubated on Simoa microplate shaker for 4 hours at 35°C and 800rpm.

In the final hour of the 4-hour incubation, detector antibody reagent was prepared, diluting detector stock in the same diluent as the calibrators and samples, and inverting several times to mix. SβG reagent was also prepared to the required concentration, using SβG concentrate diluted in SβG diluent, and inverting several times to mix. Finally, BioTek washer protocol was begun. For the 2-step assay protocol, 25µL of detector reagent was spiked into final 30 minutes of the 4-hour incubation.

Following incubation, plate was placed on the BioTek washer and washer protocol was continued, placing RGP reagent on shaker at 35°C and 800rpm for minimum 25 minutes (maximum 2 hours). After the washes, for the 2-step protocol, 100µL of SβG reagent was pipetted into each well, plate was covered with MicroClime lid and incubated for a further 10 minutes. For 3-step assay protocol, detector reagent was gently inverted and 100µL was pipetted into

each well, plate was covered with MicroClime lid and incubated for a further 10 minutes at 35°C and 800rpm.

Upon completion of the second incubation, plate was placed back on the BioTek washer and washer protocol was continued. For the 2-step assay, plate was left for 10 minutes for the beads to dry prior to loading onto the SRx instrument for plate analysis. For the 3-step protocol, SβG reagent was gently inverted, 100µL was pipetted into each well, and plate was incubated on Simoa microplate shaker for a further 10 minutes at 35°C and 800rpm. Upon completion of final incubation, plate was returned to the BioTek washer for final wash (wash buffer A), left for 10 minutes for beads to dry, and loaded onto the SRx Pro.

A summary of the differences between the SRx and SRx Pro can be seen in Table 4.3.

Assay aspect	**SRx**	**SRx Pro**
Capture beads	500 000 beads/well	5000 beads/well
2-step protocol sample incubations	30 mins beads and detector + 10 mins SβG	4 hours beads (detector is spiked in during final 30 mins) + 10 mins SβG
3-step protocol sample incubations	30 mins beads + 10 mins detector + 10 mins SβG	4 hours beads + 10 mins detector + 10 mins SβG
BioTek Washer protocol	Wash buffer A and B	Wash buffer A only

Table 4.3 - Summary of differences between SRx and SRx Pro

4.3.3.5 Assay optimisation

There are four key aspects of the assay that require optimisation on the HDx and SRx – detector and SβG concentrations, sample diluent, and use of helper beads. The SRx Pro does not require use of helper beads due to the lower bead number. Table 4.4 shows the optimisation comparisons that can be carried out for each assay

aspect. Table 4.5 details the differing compositions of the standard homebrew (HB) diluent in comparison to diluents A-E.

Assay aspect	Default concentration/reagent		Suggested optimisation comparisons	
	2-step	3-step	2-step	3-step
Detector concentration (µg/mL)	1.0	0.3	0.6, 0.8, 1.2, 1.4	0.1, 0.6, 0.8, 1.0
SβG (pM)	150		50, 300	
Sample diluent	HB diluent		Diluents A-E	
Assay bead:helper bead ratio	100:0		70:30, 50:50, 30:70	

Table 4.4 - Suggested assay optimisation comparisons

Diluent	Contents
HB	PBS, BSA, EDTA, low tween, heterophilic blocker
A	PBS, BSA, low tween, heterophilic blocker
B	PBS, BSA, high tween, heterophilic blocker
C	Low molarity PBS, low BSA, low tween, heterophilic blocker
D	PBS, newborn calf serum, low tween, heterophilic blocker
E	Tris buffer, high pH, BSA, low tween heterophilic blocker

Table 4.5 - Compositions of sample diluents

4.3.3.6 Dilution linearity and spike recovery

Dilution linearity was performed to demonstrate that a sample with a high spiked concentration can be diluted and still provide a reliable result. 400 pg/mL of calibrator material (synthetic peptide) was spiked into three CTRL CSF samples and diluted 1:2 up to seven times. Undiluted samples were measured alongside all dilutions, and a graph of observed compared with expected concentrations was plotted to assess the linearity of dilutions and recovery of spiked material. A recovery within 80-120% of the expected concentration was deemed acceptable.

4.3.4 CSF samples

A total of 10 CSF samples (2 AD, 5 mixed phenotype [MP] and 3 CTRL) were obtained from University of Gothenburg clinical neurochemistry laboratory. Samples were divided into 500µL aliquots upon receipt. The samples were grouped as AD or CTRL based on CSF AD biomarker results with the same cut-points already described in section 3.2.1 Cohort and diagnostic criteria. MP samples were defined as samples with abnormal Aβ measurements but normal tau measurements.

The three CTRL samples used for dilution linearity and spike recovery were as already described in section 3.2.1 Cohort and diagnostic criteria.

4.3.4 Results analysis and statistical analysis

S/N was calculated for all results by dividing mean AEB at each calibrator/sample/CTRL with the mean AEB at calibrator A (blank). All statistical analysis was performed in GraphPad Prism 9.3.1. Spearman correlation coefficient was used for dilution linearity. 95% CI were reported, and a p-value <0.05 was considered statistically significant. All numerical values are displayed to three significant figures, or to the nearest whole number where more appropriate.

4.4 Results and discussion

4.4.1 MSD $A\beta_{43}$ antibody specificity test

The $A\beta_{43}$ antibody specificity test revealed a sufficient signal produced by both 6E10 and anti-$A\beta_{43}$ antibodies diluted 1:1000 and 1:2000 at all peptide concentrations investigated (0.1, 0.25, 0.5 and 1µg/mL), as depicted in Figure 4.3. Both antibodies showed an increase in mean $A\beta_{43}$ signal with increasing peptide concentration. 6E10 produced the highest signals at both dilutions compared to anti-$A\beta_{43}$ antibody. This is due to us not accounting for the lower concentration of the anti-$A\beta_{43}$ antibody compared with the 6E10 antibody in the dilutions. Given that the anti-$A\beta_{43}$ antibody had a stock concentration of 0.5mg/mL, we should have diluted it 1:500 and 1:1000, respectively, in order to make it more comparable to the 6E10 antibody, which had a stock concentration of 1mg/mL. Interestingly, the anti-$A\beta_{43}$ antibody produced higher signals at 1:2000 dilution compared to 1:1000 dilution across all peptide concentrations. However, the reasons for this remain unclear.

To further confirm the specificity of the anti-$A\beta_{43}$ antibody for $A\beta_{43}$, given that details of specificity tests were not available on the manufacturer website, it would have been beneficial to concurrently assess its ability to detect other isoforms of Aβ, namely $A\beta_{40}$ and $A\beta_{42}$. Given that the 6E10 antibody is not specific to $A\beta_{43}$, but rather to amino acids 1-16 of Aβ, we would expect the signals for $A\beta_{40}$ and $A\beta_{42}$ to be equally as strong with this antibody as what we saw with $A\beta_{43}$. However, given the reputability of the manufacturer, along with the added expense of sourcing $A\beta_{40}$ and $A\beta_{42}$ peptides, we deemed it unnecessary at this stage of the assay development process.

This test was conducted on the antibodies purchased for development of the $A\beta_{43}$ assay only because the cost of sourcing additionally MSD materials outweighed the necessity of this specificity test. As such, given that the antibodies purchased for the

$A\beta_{pE3\text{-}40}$ assay were from the same company, we assumed specificity to our target analyte.

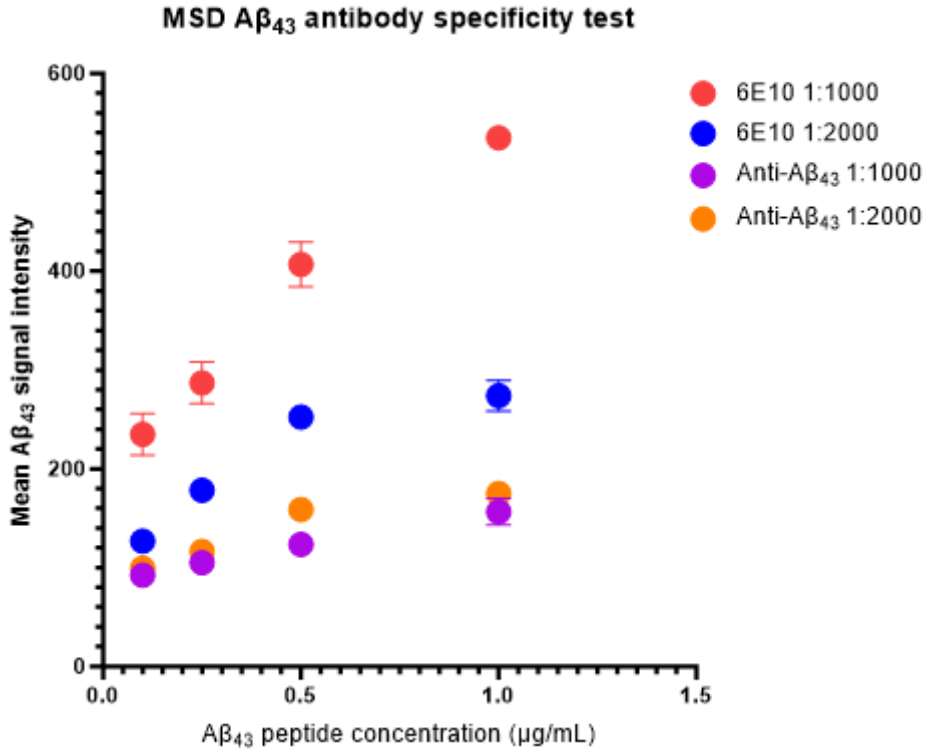

Figure 4.3 - MSD $A\beta_{43}$ antibody specificity test

$A\beta_{43}$ antibody specificity test conducted on MSD instrument revealed both 6E10 and anti-$A\beta_{43}$ antibodies were able to detect $A\beta_{43}$ peptide at all four concentrations investigated (0.1, 0.25, 0.5 and 1µg/mL), with an increase in mean signal intensity with increasing peptide concentration.

4.4.2 SRx assay development

Prior to the upgrade of our standard SRx instrument to the SRx Pro, assay development for both the $A\beta_{43}$ and $A\beta_{pE3\text{-}40}$ assays were begun on the SRx instrument. For the $A\beta_{43}$ assay, the standard $A\beta_{43}$ peptide with no modifications was used as our calibrator. It should also be noted that throughout this assay development process, we prioritised S/N over absolute AEB values, as directed by our contact at Quanterix. However, we later realised this was not the most optimal approach. Whilst the S/N is easier to comprehend and compare between the parameters being tested in any given run, particularly when looking at the lower concentration calibration points, the absolute AEB values provide a more accurate indication of the assay performance. With this view in mind, there are one or two aspects of the assay development process on the SRx which we considered to be the correct choice upon initial analysis in 2021, but which we later realised was not. However, we have opted to still include this section as it lays a necessary foundation for the further development of our assays conducted on the HDx, and subsequently on the SRx Pro.

4.4.2.1 Antibody combinations and assay protocol comparison

Two homogeneous and two heterogeneous combinations of antibodies were analysed and compared on the SRx instrument for both the $A\beta_{43}$ (Table 4.6) and $A\beta_{pE3\text{-}40}$ (Table 4.7) assays to ascertain which combination produced the most optimal AEBs and S/N in relation to calibrator A (blank). Given that the synthetic peptides used as our calibrators should theoretically remain in their monomeric form, we expected a negligible increase in the AEBs with increasing peptide concentration with the homogeneous combinations since the target binding site for the detector antibody would already be taken by the capture bead, thus preventing the formation of an immunocomplex. Furthermore, the use of the same antibody on both the capture beads and the biotinylated detector would risk

competitive binding interactions as they would be binding to the same epitope (373).

Capture bead antibody	Detector antibody	Combination number
6E10	6E10	1
	Anti-$A\beta_{43}$	2
Anti-$A\beta_{43}$	6E10	3
	Anti-$A\beta_{43}$	4

Table 4.6 - $A\beta_{43}$ antibody combinations

Capture bead antibody	Detector antibody	Combination number
Anti-$A\beta_{pE3-16}$	Anti-$A\beta_{pE3-16}$	1
	Anti-$A\beta_{40}$	2
Anti-$A\beta_{40}$	Anti-$A\beta_{pE3-16}$	3
	Anti-$A\beta_{40}$	4

Table 4.7 - $A\beta_{pE3-40}$ antibody combinations

4.4.2.1.1 $A\beta_{43}$ assay

We assessed all four antibody combinations detailed in Table 4.6 with both the 2-step and 3-step assay protocols in order to ascertain which protocol performed the most optimally for this assay using a calibration curve range of 4 to 40 000 pg/mL. Across all antibody combinations, the 2-step assay protocol produced the highest AEBs and S/N at calibrator F (Table 4.8). The two heterogeneous combinations (2 and 3) saturated at calibrator F, excluding the 3-step assay for combination 3, indicating that the AEB at this concentration was too high for the SRx to quantify, and hence suggesting that these combinations had the highest sensitivity for $A\beta_{43}$. However,

given that combination 2 (6E10 beads and anti-$A\beta_{43}$ detector) had an AEB at calibrator E of 12.5 (S/N 1146) for the 2-step assay protocol compared with 6.70 (S/N 673) for the 3-step protocol, whereas combination 3 had an AEB at calibrator E of 6.86 (S/N 711) for the 2-step protocol, we opted to proceed with antibody combination 2.

Interestingly, we noticed a very high AEB and S/N at calibrator F with homogeneous antibody combination 1, indicating possible oligomerisation occurring within our calibrator (Table 4.8). This suspected oligomerisation is further supported by homogenous antibody combination 4 having extremely low AEBs, suggesting that the C-terminus of the $A\beta_{43}$ epitope was hidden within the oligomer. Aβ peptides, particularly longer peptides, are known to be extremely sticky and prone to aggregation (60, 374). This is because Aβ is amphiphatic in nature, with a hydrophilic N-terminus and hydrophobic C-terminus (37). This hydrophobicity results in an increased propensity to aggregation, particularly at the C-terminus, and is likely the cause of the oligomerisation we identified within our calibrators. To combat this issue, as alluded to in section 4.3.3.2 Capture antibody bead conjugation and Figure 4.2, we developed four $A\beta_{43}$ CPs as previously described. Whilst we continued the assay development process on the SRx using the full-length (FL) $A\beta_{43}$ peptide, we tested these CPs on the HDx instrument upon continuing the assay development process on that platform (section 4.4.3.1 $A\beta_{43}$ custom peptide comparison) to investigate whether any of these CPs showed a decreased level of oligomerisation compared to the FL $A\beta_{43}$ peptide. Alternatively, it is possible that this oligomerisation occurred solely due to the high concentrations used within our calibration curve – concentrations which realistically would not be seen endogenously. However, given that the suspected oligomerisation is still visible at calibrators B, C and D of antibody combination 1 (Table 4.8), this is unlikely to be the cause.

4.4.2.1.2 $A\beta_{pE3\text{-}40}$ assay

We conducted an equivalent investigation for the $A\beta_{pE3\text{-}40}$ assay, using a calibration curve range of 0.8 to 8000 pg/mL. Similar to the $A\beta_{43}$ assay, the 2-step protocol produced the highest AEBs and S/N compared with the 3-step protocol at each antibody combination (Table 4.9). Whilst both heterogeneous combinations produced higher AEBs than both homogeneous combinations, combination 3 (anti-$A\beta_{40}$ beads with anti-$A\beta_{pE3\text{-}16}$ detector) produced higher AEBs than combination 2 (anti-$A\beta_{pE3\text{-}16}$ beads with anti-$A\beta_{40}$ detector). The 2-step protocol of combination 3 saturated at calibrator F, indicating that it had a higher sensitivity, hence this is the combination we opted to carry forward for further development.

Unlike the $A\beta_{43}$ assay, the low signals at both homogeneous combinations (1 and 4) highlight that we were not experiencing the same issues of oligomerisation within this calibrator. This is particularly interesting, given that $A\beta_{pE\text{-}40}$ is a plaque-specific form of Aβ, and the addition of the pyroglutamate ring has been shown to increase the hydrophobicity of the peptide (375, 376). However, Aβ peptides ending in amino acid 40 are known to be less prone to aggregation than Aβ peptides ending in either amino acid 42 or 43 (60, 377), hence it is possible that the hydrophobicity of the C-terminus has a greater effect on the formation of oligomers.

$A\beta_{43}$		**Mean AEB (S/N)**							
Bead and detector combination number		1		2		3		4	
Calibrator	Concentration (pg/mL)	2-step	3-step	2-step	3-step	2-step	3-step	2-step	3-step
A	0	0.0113	0.00866	0.0109	0.00996	0.00965	0.0111	0.00991	0.00799
B	4	0.0136 (1.20)	0.0117 (1.35)	0.0166 (1.53)	0.0147 (1.48)	0.0126 (1.31)	0.0110 (0.990)	0.0106 (1.06)	0.00808 (1.01)
C	40	0.0320 (2.82)	0.0117 (2.17)	0.0751 (6.91)	0.0623 (6.25)	0.0419 (4.34)	0.0294 (2.65)	0.0120 (1.21)	0.00752 (0.941)
D	400	0.210 (18.5)	0.0188 (8.26)	0.548 (50.5)	0.404 (40.6)	0.306 (31.7)	0.0451 (4.07)	0.00972 (0.981)	0.00787 (0.984)
E	4000	2.10 (186)	0.0716 (70.1)	12.5 (1146)	6.70 (673)	6.86 (711)	0.354 (31.9)	0.0181 (1.82)	0.0117 (1.46)
F	40 000	13.8 (1219)	6.58 (760)	*SAT*	*SAT*	*SAT*	4.73 (427)	0.0820 (8.27)	0.0342 (4.28)

Table 4.8 – SRx $A\beta_{43}$ antibody combinations and assay protocol comparison

Amyloid-β 1-43 ($A\beta_{43}$) antibody combinations and assay protocol comparison on SRx. Signal:noise ratio (S/N) for each mean average number of enzymes per bead (AEB) value is indicated in brackets. 'SAT' indicates saturation of AEB signal at that calibrator point.

$A\beta_{pE3-40}$		**Mean AEB (S/N)**							
Bead and detector combination number		1		2		3		4	
Calibrator	Concentration (pg/mL)	2-step	3-step	2-step	3-step	2-step	3-step	2-step	3-step
A	0	0.0101	0.0117	0.00926	0.0168	0.00998	0.0125	0.0214	0.0584
B	0.8	0.00888 (0.883)	0.0115 (0.986)	0.00993 (1.07)	0.0156 (0.932)	0.0103 (1.03)	0.0121 (0.97)	0.0219 (1.02)	0.0530 (0.909)
C	8	0.00845 (0.840)	0.0124 (1.06)	0.00718 (0.775)	0.0128 (0.764)	0.0218 (2.18)	0.0152 (1.22)	0.0226 (1.05)	0.0581 (0.995)
D	80	0.00883 (0.878)	0.0135 (1.16)	0.00909 (0.982)	0.0146 (0.872)	0.332 (33.3)	0.0427 (3.42)	0.0233 (1.09)	0.0586 (1.00)
E	800	0.0147 (1.46)	0.0152 (1.30)	0.0572 (6.17)	0.0537 (3.20)	10.6 (1065)	0.436 (35.0)	0.0225 (1.05)	0.0544 (0.932)
F	8000	0.0731 (7.26)	0.0440 (3.78)	4.20 (453)	3.24 (193)	*SAT*	12.9 (1031)	0.0211 (0.983)	0.0561 (0.961)

Table 4.9 – SRx $A\beta_{pE3-40}$ antibody combinations and assay protocol comparison

Pyroglutamate-modified amyloid-β 3-40 ($A\beta_{pE3-40}$) antibody combinations and assay protocol comparison on SRx. Signal:noise ratio (S/N) for each mean average number of enzymes per bead (AEB) value is indicated in brackets. 'SAT' indicates saturation of AEB signal at that calibrator point.

4.4.2.2 Detector concentration titration

We next examined which concentration of detector produced the most optimal signals for our assays using the same calibration curve as that used for the antibody combinations and assay protocol comparisons in section 4.4.2.1 Antibody combinations and assay protocol comparison (see Table 4.8 and Table 4.9). Given that the standard detector concentration for a 2-step assay is 1.0µg/mL, we tested two concentrations above (1.2 and 1.4µg/mL) and two concentrations below (0.6 and 0.8µg/mL).

4.4.2.2.1 $A\beta_{43}$ assay

Carrying forward the 2-step assay protocol with 6E10 beads and anti-$A\beta_{43}$ detector, at all detector concentrations investigated, the AEB at calibrator F saturated (Table 4.10), which is consistent with our observations in Table 4.8. As such, we compared the AEBs at calibrator E across all concentrations. Whilst the 1.0µg/mL detector concentration at calibrator E produced the highest AEB of 12.9 (S/N 1486), with the 1.2µg/mL detector producing the second highest AEB of 12.2 (S/N 1287), we opted to proceed with the 0.8µg/mL detector to reduce risk of saturation as we continued to optimise other components of the assay.

Detector concentration (µg/mL)		**0.6**	**0.8**	**1.0**	**1.2**	**1.4**
Mean AEB (S/N) at calibrator	A	0.0102	0.00794	0.00865	0.00949	0.0104
	B	0.0146 (1.43)	0.0129 (1.63)	0.0131 (1.52)	0.0156 (1.64)	0.0143 (1.38)
	C	0.0400 (3.88)	0.0480 (6.04)	0.0505 (5.84)	0.0554 (5.84)	0.0578 (5.58)
	D	0.334 (32.6)	0.387 (48.7)	0.426 (49.2)	0.5154 (54.3)	0.485 (45.8)
	E	8.69 (849)	9.73 (1226)	12.9 (1486)	12.2 (1287)	11.9 (1146)
	F	*SAT*	*SAT*	*SAT*	*SAT*	*SAT*

Table 4.10 - SRx $Aβ_{43}$ detector concentration titration

Amyloid-β 1-43 ($Aβ_{43}$) detector concentration titration on SRx. Signal:noise ratio (S/N) for each mean average number of enzymes per bead (AEB) value is indicated in brackets. 'SAT' indicates saturation of AEB signal at that calibrator point.

4.4.2.2.2 $Aβ_{pE3-40}$ assay

Carrying forward the 2-step assay protocol with the anti-$Aβ_{40}$ beads with anti-$Aβ_{pE3-16}$ detector, similar to the $Aβ_{43}$ assay, at all detector concentrations investigated, the AEB at calibrator F saturated (Table 4.11), so we compared the AEBs at calibrator E across all concentrations. The 0.8µg/mL detector produced the highest AEB at both calibrators B (0.0133; S/N 1.12) and F (7.72; S/N 645; Table 4.11). Whilst AEB at calibrator F of the 1.4µg/mL detector was similar, with a value of 7.15 (S/N 588), it is better to use the lowest concentration at which an optimal AEB is obtained, partly to maximise reagent stocks. As such, we opted to proceed with the 0.8µg/mL detector.

Detector concentration (µg/mL)		0.6	0.8	1.0	1.2	1.4
Mean AEB (S/N) at calibrator	A	0.00827	0.0120	0.0125	0.00972	0.0121
	B	0.0103 (1.24)	0.0133 (1.12)	0.0104 (0.834)	0.00968 (0.997)	0.00939 (0.773)
	C	0.0134 (1.62)	0.0155 (1.30)	0.0234 (1.87)	0.0158 (1.63)	0.0173 (1.42)
	D	0.0908 (11.0)	0.164 (13.7)	0.135 (10.8)	0.149 (15.3)	0.170 (14.0)
	E	4.14 (500)	7.72 (645)	5.41 (434)	6.44 (663)	7.15 (588)
	F	*SAT*	*SAT*	*SAT*	*SAT*	*SAT*

Table 4.11 - SRx $Aβ_{pE3-40}$ detector concentration titration

Pyroglutamate-modified amyloid-β 3-40 ($Aβ_{pE3-40}$) detector concentration titration on SRx. Signal:noise ratio (S/N) for each mean average number of enzymes per bead (AEB) value is indicated in brackets. 'SAT' indicates

4.4.2.3 SβG concentration titration

We next titrated the concentration of SβG to consider whether using a lower or higher concentration than the standard SβG concentration of 150pM enhanced the AEB. Therefore, we compared 50pM, 150pM and 300pM in both of our assays, continuing with the same calibration curves as in Table 4.8 and Table 4.9.

4.4.2.3.1 $Aβ_{43}$ assay

Continuing with the 2-step assay protocol alongside the 6E10 beads and anti-$Aβ_{43}$ detector at a concentration of 0.8µg/mL, we observed that the 300pM SβG concentration produced the highest AEBs at both calibrators B (0.0381; S/N 2.69) and E (14.2; S/N 1008; Table 4.12). Upon initial analysis, we did not consider the increase in AEB compared with the 150pM concentration to be substantial enough to warrant making a change. Furthermore, the additional optimisation stages still to be completed meant there would be an increased risk of AEB saturation. However, given that we had yet to optimise our calibration curve, and also that the increase in AEB at the blank

calibrator (A) was negligible with the doubling of the SβG concentration from 150pM to 300pM, in hindsight, there was scope to increasing the concentration to 300pM. Nonetheless, we opted to continue with the 150pM SβG concentration given that this SβG concentration still produced high AEBs.

SβG concentration (pM)		**50**	**150**	**300**
Mean AEB (S/N) at calibrator	A	0.00366	0.0107	0.0141
	B	0.0178 (4.87)	0.0294 (2.75)	0.0381 (2.69)
	C	0.119 (32.6)	0.206 (19.2)	0.226 (16.0)
	D	0.352 (96.2)	0.530 (49.5)	0.619 (43.8)
	E	9.20 (2511)	12.0 (1116)	14.2 (1008)
	F	*SAT*	*SAT*	*SAT*

Table 4.12 – SRx $Aβ_{43}$ SβG concentration titration

Amyloid-β 1-43 ($Aβ_{43}$) streptavidin–β-galactosidase (SβG) concentration titration on SRx. Signal:noise ratio (S/N) for each mean average number of enzymes per bead (AEB) value is indicated in brackets. 'SAT' indicates saturation of AEB signal at that calibrator point.

4.4.2.3.2 $Aβ_{pE3-40}$ assay

Continuing with the 2-step assay protocol alongside the anti-$Aβ_{40}$ beads with anti-$Aβ_{pE3-16}$ detector at a concentration of 0.8µg/mL, we observed that similar to the $Aβ_{43}$ assay, the 300pM SβG concentration produced the highest AEB at both calibrators B (0.0288; S/N 1.55) and F (8.49; S/N 457; Table 4.13). At the time of conducting this experiment, given that the S/N of 457 at calibrator E was vastly lower than that of the 150pM concentration, which saw a S/N of 645 (AEB 5.99), we opted to proceed with an SβG

concentration of 150pM. However, similar to the $A\beta_{43}$ assay, had we looked at the absolute AEB values it may have been more appropriate to proceed with the 300pM SβG concentration in this instance. Nonetheless, given that the assay development on the SRx was the first stage of what would turn out to be a three-instrument assay development process in which each optimisation step would be repeated on each instrument, there would still be several opportunities to ensure we picked the correct assay parameters. Therefore, we continued with the 150pM SβG concentration.

Interestingly, for the first time in this assay, we observed an AEB at calibrator F of 24.6 (S/N 1862) with the 50pM SβG concentration. This AEB is extremely high, highlighting the need to further optimise the calibration curve.

SβG concentration (pM)		**50**	**150**	**300**
Mean AEB (S/N) at calibrator	A	0.0132	0.00929	0.0186
	B	0.0106 (0.804)	0.0204 (2.19)	0.0288 (1.55)
	C	0.00799 (0.604)	0.0159 (1.71)	0.0279 (1.50)
	D	0.0981 (7.42)	0.177 (19.0)	0.325 (17.5)
	E	3.33 (252)	5.99 (645)	8.49 (457)
	F	24.6 (1862)	*SAT*	*SAT*

Table 4.13 - SRx $A\beta_{pE3\text{-}40}$ SβG concentration titration

Pyroglutamate-modified amyloid-β 3-40 ($A\beta_{pE3\text{-}40}$) streptavidin–β-galactosidase (SβG) concentration titration on SRx. Signal:noise ratio (S/N) for each mean average number of enzymes per bead (AEB) value is indicated in brackets. 'SAT' indicates saturation of AEB signal at that calibrator point.

4.4.2.4 Diluent screen

We next compared the HB diluent, which we had been using up until this point, against the five sample diluents, named A to E, available from Quanterix to ascertain which sample diluent provided the greatest enhancement in AEB values. Each diluent differs in the type of buffer used (PBS or tris buffer solution), concentration of tween-20, and additional protein added (BSA or neonatal calf serum), as depicted in Table 4.5. We continued with the same calibration curves as in Table 4.8 and Table 4.9.

4.4.2.4.1 $A\beta_{43}$ assay

Continuing with the 2-step assay protocol alongside the 6E10 beads and anti-$A\beta_{43}$ detector at a concentration of 0.8µg/mL, and SβG at a concentration of 150pM, we observed diluent C to produce the highest S/N at both calibrators B (1.71; AEB 0.00695) and E (1594; AEB 6.47; Table 4.14). As a result, we opted to proceed with this diluent. However, looking at the absolute AEB values, the HB diluent produced the highest AEB at calibrator E of 9.75 (S/N 1113). In fact, diluents B and A also produced AEBs higher than that of diluent C, with values of 8.71 (S/N 408) and 7.52 (S/N 763), respectively. However, whilst the AEBs at the blank calibrators of these diluents are still within the acceptable range of 0.005 to 0.02 (see section 4.2.5 Optimal characteristics of a Simoa assay), they are far higher than that of calibrator C. Although diluent A produced a higher AEB at calibrator E compared with diluent C, the production of an AEB at calibrator F rather than saturation of the signal indicated that it was not as sensitive at higher $A\beta_{43}$ concentrations than the other diluents. Furthermore, diluents HB and A interestingly showed a decrease in AEB at calibrator B compared to the blank calibrator. As such, whilst diluent C did not have the highest absolute AEB value, it was clearly the most optimal diluent to proceed with in this case and at this phase of the assay development process.

Diluent		HB	A	B	C	D	E
Mean AEB (S/N) at calibrator	A	0.00876	0.00985	0.0213	0.00406	0.00476	0.00222
	B	0.00539 (0.615)	0.00460 (0.467)	0.0247 (1.16)	0.00695 (1.71)	0.00441 (0.927)	0.00358 (1.61)
	C	0.0389 (4.44)	0.0263 (2.67)	0.0263 (1.23)	0.0153 (3.76)	0.0116 (2.44)	0.0132 (5.93)
	D	0.368 (42.0)	0.225 (22.8)	0.212 (9.95)	0.163 (40.1)	0.113 (23.8)	0.104 (46.7)
	E	9.75 (1113)	7.52 (763)	8.71 (408)	6.47 (1594)	5.34 (1121)	4.68 (2110)
	F	*SAT*	30.0 (3042)	*SAT*	*SAT*	*SAT*	*SAT*

Table 4.14 - SRx $A\beta_{43}$ diluent screen

Amyloid-β 1-43 ($A\beta_{43}$) diluent screen on SRx. Signal:noise ratio (S/N) for each mean average number of enzymes per bead (AEB) value is indicated in brackets. 'SAT' indicates saturation of AEB signal at that calibrator point.

4.4.2.4.2 $A\beta_{pE3-40}$ assay

Continuing with the 2-step assay protocol alongside the anti-$A\beta_{40}$ beads with anti-$A\beta_{pE3-16}$ detector at a concentration of 0.8µg/mL, and SβG at a concentration of 150pM, we observed diluent C produced the highest AEB and S/N at calibrator E, with values of 3.88 and 371, respectively (Table 4.15). Although there was a slight decrease in AEB between calibrators A and B, this decrease was also seen with diluents HB, B and E. In fact, the only two diluents which did not show a decrease in AEB between calibrators A and B also produced AEBs at calibrator F, highlighting that they were not as sensitive at higher $A\beta_{pE3-40}$ concentrations. It is worth also acknowledging that diluent B showed a decrease in AEB between calibrators C and D, which was not seen with the other diluents. The cause of this decrease is not clear, but given that we were satisfied with the performance of diluent C, we did not investigate this further.

Diluent		HB	A	B	C	D	E
	A	0.0104	0.0109	0.0124	0.0105	0.0128	0.0103

Mean AEB (S/N) at calibrator	B	0.0102 (0.990)	0.0111 (1.03)	0.00971 (0.782)	0.0104 (0.992)	0.0133 (1.04)	0.0102 (0.990)
	C	0.0120 (1.16)	0.0126 (1.16)	0.122 (9.82)	0.0164 (1.57)	0.0130 (1.02)	0.0116 (1.12)
	D	0.0496 (4.79)	0.0589 (5.42)	0.0445 (3.58)	0.0853 (8.15)	0.0345 (2.69)	0.0274 (2.65)
	E	2.64 (255)	2.93 (270)	1.90 (153)	3.88 (371)	1.08 (84.1)	0.785 (76.0)
	F	*SAT*	25.8 (2376)	*SAT*	*SAT*	27.0 (2106)	25.4 (2458)

Table 4.15 - SRx $A\beta_{pE3-40}$ diluent screen

Pyroglutamate-modified amyloid-β 3-40 ($A\beta_{pE3-40}$) diluent screen on SRx. Signal:noise ratio (S/N) for each mean average number of enzymes per bead (AEB) value is indicated in brackets. 'SAT' indicates saturation of AEB signal at

4.4.2.5 Calibration curve optimisation

Prior to conducting the helper bead comparison, we performed a small calibration curve optimisation, with the main aim being to identify a calibrator F concentration that consistently produced AEBs for both of our assays.

4.4.2.5.1 $A\beta_{43}$ assay

Given that we consistently obtained an AEB with a calibrator E concentration of 4000 pg/mL, we lowered our calibrator F to 8000 pg/mL. On two separate occasions, this calibrator F produced AEBs, and hence was the curve we carried forward (Table 4.16). Whilst these AEBs were still higher than is optimal for a Simoa assay (see section 4.2.5 Optimal characteristics of a Simoa assay), they were a good starting point with which to proceed to the helper bead comparison, and subsequently to the HDx instrument. However, given the consistency of the 4000 pg/mL calibrator E in producing AEBs, and also that an AEB of around 10-12 is optimal for calibrator F, it may have been more beneficial to lower our calibrator F concentration to 4000 pg/mL.

Calibrator	**Concentration (pg/mL)**	**Mean AEB (S/N)**	
		Run 1	Run 2

A	0	0.00297	0.00336
B	0.8	0.00414 (1.40)	0.00433 (1.29)
C	8	0.00828 (2.79)	0.00907 (2.70)
D	80	0.0527 (17.7)	0.0425 (12.7)
E	800	0.538 (181)	0.599 (178)
F	8000	17.9 (6037)	20.4 (6082)

Table 4.16 - SRx $A\beta_{43}$ calibration curve optimisation

4.4.2.5.2 $A\beta_{pE3\text{-}40}$ assay

We first halved the concentration of calibrator F to 4000 pg/mL, keeping the concentration of calibrator E the same (800 pg/mL; run 1 in Table 4.17). Whilst we obtained an AEB of 31.3 (S/N 2866), this AEB was far too high to proceed with. As such, we lowered the calibrator F concentration to 2000 pg/mL (run 2 in Table 4.17), which produced an AEB of 20.3 (S/N 2756). To confirm that the AEBs obtained with this calibration curve were replicable, we repeated this same experiment on a separate day (run 3 in Table 4.17). However, on repetition, we obtained AEBs far higher than those obtained in run 2, with an AEB at calibrator F of 31.2 (S/N 1841). Whilst the reasons for this vast difference remain unclear, we were unable to explore a lower concentration calibrator F at this stage as our SRx instrument was due to be upgraded. As such, we opted to proceed with the helper bead comparison with the same curve, with the view of further optimising the curve on the HDx instrument.

Calibrator	**Run 1**	**Run 2**	**Run 3**

	Concentration (pg/mL)	Mean AEB (S/N)	Concentration (pg/mL)	Mean AEB (S/N)	Concentration (pg/mL)	Mean AEB (S/N)
A	0	0.0109	0	0.00738	0	0.0169
B	6.4	0.0133 (1.22)	7.81	0.0169 (2.30)	7.81	0.0308 (1.82)
C	32	0.0394 (3.61)	31.3	0.0399 (5.41)	31.3	0.106 (6.24)
D	160	0.440 (40.2)	125	0.267 (36.1)	125	0.874 (51.6)
E	800	4.79 (438)	500	2.95 (399)	500	8.83 (521)
F	4000	31.3 (2866)	2000	20.3 (2756)	2000	31.2 (1841)

Table 4.17 - SRx $A\beta_{pE3\text{-}40}$ calibration curve optimisation

4.4.2.6 Helper bead comparison

The final stage of our assay development process on the SRx was to evaluate whether the use of helper beads either maintained or enhanced the AEB values obtained with 100% assay beads, using the same calibration curves as optimised in section 4.4.2.5 Calibration curve optimisation (Table 4.16 and Table 4.17). We tested three assay bead to helper bead ratios against the standard 100% assay beads – 70% assay beads:30% helper beads, 50% assay beads:50% helper beads, and 30% assay beads:70% helper beads.

4.4.2.6.1 $A\beta_{43}$ assay

Both the 70:30 and 50:50 ratios of assay:helper beads enhanced the AEB at calibrator F, with values of 25.3 (S/N 3506) and 26.8 (S/N 3618; Table 4.18), respectively, compared with 24.1 (S/N 3775) using 100% assay beads. Whereas the 30:70 assay:helper bead ratio decreased the AEB at calibrator F to 20.5 (S/N 2341). However,

looking more closely at the AEBs across all other calibrators, the higher the ratio of helper beads used, the lower the AEB at each respective calibration point. Nonetheless, given the overall benefit of using helper beads, namely extending the duration of the bead stock, we opted to proceed with the 50:50 ratio of assay:helper beads.

Assay:helper bead ratio		**100:0**	**70:30**	**50:50**	**30:70**
Mean AEB (S/N) at calibrator	A	0.00638	0.00723	0.00740	0.00877
	B	0.0113 (1.78)	0.00944 (1.31)	0.0102 (1.37)	0.00810 (0.923)
	C	0.0324 (5.08)	0.0277 (3.83)	0.0263 (3.56)	0.0288 (3.29)
	D	0.0968 (15.2)	0.0981 (13.6)	0.0859 (11.6)	0.0839 (9.57)
	E	1.00 (157)	0.949 (131)	0.879 (119)	0.753 (85.8)
	F	24.1 (3775)	25.3 (3506)	26.8 (3618)	20.5 (2341)

Table 4.18 - SRx $A\beta_{43}$ helper bead comparison

4.4.2.6.2 $A\beta_{pE3-40}$ assay

In line with our observations in section 4.4.2.5.2 $A\beta_{pE3-40}$ assay, the calibrator F concentration of 2000 pg/mL was still too high for this assay, as highlighted by the AEB saturating at calibrator F for all assay:helper bead ratios except the 30:70 ratio (Table 4.19). Looking at calibrator E, the 50:50 ratio performed similar to the 100% assay beads, with AEBs of 8.65 (S/N 521) and 8.56 (S/N 540), respectively. Interestingly, the 70:30 and 30:70 ratios surpassed both the 100% and 50:50 ratio at calibrator E, with AEBs of 9.22 (S/N 543) and 9.05 (S/N 509), respectively. However, at all other calibrators, the 50:50 ratio produced higher AEBs than the 70:30 ratio. Therefore, we opted to proceed with the 50:50 ratio of assay:helper beads.

Assay:helper bead ratio		100:0	70:30	50:50	30:70
Mean AEB (S/N) at calibrator	A	0.0159	0.0170	0.0166	0.0178
	B	0.0308 (1.94)	0.0275 (1.62)	0.0365 (2.20)	0.0272 (1.53)
	C	0.104 (6.56)	0.114 (6.72)	0.115 (6.90)	0.122 (6.84)
	D	0.848 (53.5)	0.887 (52.3)	0.915 (55.1)	0.880 (49.5)
	E	8.56 (540)	9.22 (543)	8.65 (521)	9.05 (509)
	F	*SAT*	*SAT*	*SAT*	20.4 (1148)

Table 4.19 - SRx $A\beta_{pE3-40}$ helper bead comparison

Pyroglutamate-modified amyloid-β 3-40 ($A\beta_{pE3-40}$) helper bead comparison on SRx. Signal:noise ratio (S/N) for each mean average number of enzymes per bead (AEB) value is indicated in brackets. 'SAT' indicates saturation of the AEB signal at that calibrator point.

4.4.2.7 Summary of optimised assay parameters

To summarise, on the SRx, for the $A\beta_{43}$ assay, our optimised parameters were the 2-step assay protocol using the 6E10 beads at a ratio of 50:50 with helper beads, alongside the anti-$A\beta_{43}$ detector at a concentration of 0.8µg/mL, and SβG at a concentration of 150pM. Calibrators, samples and detectors would be diluted in diluent C with a calibration curve ranging from 0.8 to 8000 pg/mL, but which was still in need of optimisation.

Likewise, for the $A\beta_{pE3-40}$ assay, our optimised parameters were the 2-step assay protocol using the anti-$A\beta_{40}$ beads at a ratio of 50:50 with helper beads, alongside the anti-$A\beta_{pE3-16}$ detector at a concentration of 0.8µg/mL, and SβG at a concentration of 150pM. Calibrators, samples and detectors would be diluted in diluent C with a calibration curve ranging from 7.81 to 2000 pg/mL, but which was still in need of optimisation.

The optimised parameters for both assays can be seen in Table 4.20.

Assay component	**$A\beta_{43}$ assay**	**$A\beta_{pE3-40}$ assay**
Beads	6E10	Anti-$A\beta_{40}$
Detector	Anti-$A\beta_{43}$	Anti-$A\beta_{3-16}$
Detector concentration (µg/mL)	0.8	0.8
SβG concentration (pM)	150	150
Diluent	C	C
Assay:helper bead ratio	50:50	50:50

Table 4.20 - Summary of optimised SRx $A\beta_{43}$ and $A\beta_{pE3-40}$ assay parameters

4.4.3 HDx assay development

Following on from the assay development on the SRx, we opted to transfer our assays onto the HDx instrument primarily to ascertain the most optimal calibration curves for our assays. Whilst continuing this on the SRx would have been more convenient and more relevant to the SRx Pro, we were unable to do so as our SRx had already been upgraded to the SRx Pro by this stage. As such, we began our validation of the SRx Pro, as described in CHAPTER 3: SIMOA UPGRADE VALIDATION, whilst simultaneously continuing with the assay development on the HDx. Rather than transferring the assays directly as optimised on the SRx instrument, we repeated the assay development process from the very beginning, including the antibody combinations comparison. However, we began by addressing the suspected oligomerisation issue within our $A\beta_{43}$ calibrator.

4.4.3.1 $A\beta_{43}$ custom peptide comparison

In light of our observations with the FL $A\beta_{43}$ peptide in section 4.4.2.1.1 $A\beta_{43}$ assay, namely the suspected oligomerisation occurring with this peptide, prior to conducting the antibody combinations comparison we compared each of the four CPs, alongside the FL $A\beta_{43}$ peptide, in the homogeneous antibody combination 1 orientation (6E10 beads with 6E10 detector; see Table 4.6). This combination alone was investigated as this is the combination that highlighted the possible oligomerisation to us. The peptide that produced the lowest AEBs across the calibration curve would be the peptide we carried forward for continued development of the assay.

CP3 produced AEBs at all calibration curve points far below those of the other peptides, with AEBs at calibrator B and F of 0.00571 (S/N 1.25) and 1.68 (S/N 370), respectively (Table 4.21). As such, this is the peptide we opted to carry forward. However, whilst CP1, 2, and 3 performed better than the FL peptide, namely that they produced lower AEBs with this homogeneous antibody combination than the FL peptide, they still produced AEBs far higher than we expected.

Whilst it is true that the calibration curve required further optimisation, the concentrations used for calibration points B to D were within the range of Aβ within CSF. As such, it is clear that the generation of the CPs did not completely eradicate the oligomerisation, although it did significantly reduce it. Given that the C-terminus of $Aβ_{43}$ was left unchanged in these CPs, this is not unsurprising.

Interestingly, we observed even higher AEBs with CP4 than with the FL peptide. Comparing the alterations made across all CPs (see Figure 4.2), whilst theoretically the addition of the glutamate linking chain should have reduced the extent of oligomerisation, it appears that the suspected oligomerisation occurring within $Aβ_{43}$ is exacerbated by the combination of removing some of the hydrophilic amino acids in the centre of the peptide, and leaving some of the hydrophobic amino acids from amino acid 28 to 33 intact.

Interestingly, with both the FL and CP4 peptides, we observed an increase in AEB up to calibrator E, with a decrease in AEB at calibrator F. This nature of curve is characteristic of a possible hook effect occurring within the assay. In essence, there were far too many analyte molecules present which bound separately to the beads and detector without forming immunocomplexes, simultaneously saturating both the beads and the detector, thus falsely lowering the AEB (378, 379). It is not entirely clear why this hook effect was visible on the HDx but not in our initial experiments on the SRx, particularly given that our initial calibration curve extended as high in concentration as 40 000 pg/mL (see section 4.4.2 SRx assay development). However, it is possible that there was a hook effect of some sorts occurring in the form of a false lowering of the AEB signals compared to the true value, but the lowering was not drastic enough to reduce the AEB below that of calibrator E throughout our development process. Alongside optimising the calibration curve, the use of the 3-step assay protocol should theoretically improve or eradicate the hook effect, given that the

beads and detector are incubated separately. However, given the drastic decrease in AEB observed in the 3-step compared with the 2-step assay protocol conducted on the SRx (see section 4.4.2.1 Antibody combinations and assay protocol comparison), and also that the hook effect was not seen with either of the heterogeneous antibody combinations, changing protocols may have negatively impacted the sensitivity of our assay. Regardless, we were not planning to proceed with assay development on either of these two peptides, hence this was unlikely to present itself again.

Finally, it is important to acknowledge that an unexpected instrument error occurred during the measurement of calibrator F of CP2, resulting in no AEB value generated for either replicate. However, the AEBs generated at calibrators B-E of CP2 were higher than those generated for both CP1 and CP3, hence we had enough information to rule out proceeding with this peptide.

$A\beta_{43}$ peptide		**Mean AEB (S/N) at calibrator**				
Calibrator	Concentration (pg/mL)	FL	CP1	CP2	CP3	CP4
A	0	0.00574	0.00459	0.00441	0.00455	0.00528
B	0.8	0.0693 (12.1)	0.0135 (2.95)	0.0131 (2.98)	0.00571 (1.25)	0.465 (88.1)
C	8	0.554 (96.7)	0.0935 (20.4)	0.0905 (20.5)	0.0256 (5.63)	4.37 (827)
D	80	4.18 (730)	0.950 (207)	0.962 (218)	0.329 (72.4)	15.4 (2925)
E	800	8.35 (1456)	2.35 (511)	3.24 (734)	0.100 (220)	18.5 (3508)
F	8000	4.66 (813)	3.13 (682)	*Instrument error*	1.68 (370)	7.02 (1329)

Table 4.21 - HDx $A\beta_{43}$ custom peptide comparison

Amyloid-β 1-43 ($A\beta_{43}$) custom peptide (CP) comparison on HDx. Signal:noise ratio (S/N) for each mean average number of enzymes per bead (AEB) value is indicated in brackets. 'Instrument error' refers to no AEB value being generated for that calibration point due to an unexpected instrument error. 'FL' indicates full-length

4.4.3.2 Antibody combinations

We assessed the same antibody combinations as those assessed on the SRx in section 4.4.2.1 Antibody combinations and assay protocol comparison on both the $A\beta_{43}$ and $A\beta_{pE3\text{-}40}$ assays, repeated below in Table 4.22 and Table 4.23 for ease of access. For both assays, we used a 2-step assay protocol, since this was the assay protocol optimised on the SRx.

Capture bead antibody	Detector antibody	Combination number
6E10	6E10	1
	Anti-$A\beta_{43}$	2
Anti-$A\beta_{43}$	6E10	3
	Anti-$A\beta_{43}$	4

Table 4.22 - $A\beta_{43}$ antibody combinations

Capture bead antibody	Detector antibody	Combination number
Anti-$A\beta_{pE3-16}$	Anti-$A\beta_{pE3-16}$	1
	Anti-$A\beta_{40}$	2
Anti-$A\beta_{40}$	Anti-$A\beta_{pE3-16}$	3
	Anti-$A\beta_{40}$	4

Table 4.23 – $A\beta_{pE3-40}$ antibody combinations

4.4.3.2.1 $A\beta_{43}$ assay

Using CP3 and a calibration curve ranging from 0 to 160 pg/mL, heterogeneous antibody combination 3 (Table 4.22) produced the most optimal AEBs at calibrators B (0.00268) and F (0.0172), with S/N of 1.49 and 9.52, respectively (Table 4.24). This differs from our observations on the SRx, where heterogeneous antibody combination 2 was carried forward for further assay development (see section 4.4.2.1.1 $A\beta_{43}$ assay). This change is most likely due to the change in calibrator from FL $A\beta_{43}$ to CP3. In this case, combination 2, despite also being heterogeneous produced only a marginally higher S/N at calibrator F than the homogenous combinations (Table 4.24). A greater distinction between combination 2 and the two homogeneous antibody combinations (combinations 1 and 4) may have been visible had a higher concentration of calibrator F been assessed. However, the increased S/N with combination 3

was large enough to warrant not investigating combination 2 any further.

Of particular interest to us with regards to the oligomerisation, homogeneous antibody combination 1 performed similar to homogeneous antibody combination 4, highlighting that at these concentrations, there was little to no oligomerisation occurring within our calibrator.

$A\beta_{43}$		**Mean AEB (S/N)**			
Calibrator	Concentration (pg/mL)	Bead and detector combination number			
		1	2	3	4
A	0	0.00341	0.00281	0.00180	0.00218
B	10	0.00329 (0.964)	0.00281 (1.00)	0.00268 (1.49)	0.00252 (1.16)
C	20	0.00396 (1.16)	0.00311 (1.11)	0.00286 (1.59)	0.00293 (1.34)
D	40	0.00406 (1.19)	0.00279 (0.100)	0.00486 (2.70)	0.00271 (1.24)
E	80	0.00328 (0.962)	0.00320 (1.14)	0.00870 (4.84)	0.00304 (1.40)
F	160	0.00412 (1.21)	0.00401 (1.43)	0.0172 (9.52)	0.00279 (1.28)

Table 4.24 - HDx $A\beta_{43}$ antibody combinations results

4.4.3.2.2 $A\beta_{pE3\text{-}40}$ assay

In line with our observations on the SRx but now using a calibration curve ranging from 0 to 1620 pg/mL, heterogeneous antibody combination 3 (Table 4.23) produced the most optimal AEBs at calibrators B (0.0158) and F (9.94), with S/N of 6.68 and 4192, respectively (Table 4.25). A far greater distinction between the heterogeneous antibody combinations (2 and 3) and the homogeneous antibody combinations (1 and 4) was visible, particularly at calibrator F, and in comparison to the difference seen in these four antibody combinations with the $A\beta_{43}$ assay (Table 4.24).

However, a far wider range of calibrator concentrations was used here. Given that combination 3 once again produced the highest AEBs and S/N, this is the combination that we carried forward into the next stage of assay development.

$A\beta_{pE3-40}$		**Mean AEB (S/N)**			
Calibrator	Concentration (pg/mL)	Bead and detector combination number			
		1	2	3	4
A	0	0.00220	0.00160	0.00237	0.00913
B	20	0.00250 (1.14)	0.00236 (1.47)	0.0158 (6.68)	0.0101 (1.10)
C	60	0.00424 (1.93)	0.00302 (1.88)	0.0832 (35.1)	0.0126 (1.38)
D	180	0.00284 (1.29)	0.00461 (2.88)	0.351 (148)	0.0161 (1.76)
E	540	0.00387 (1.76)	0.0163 (10.1)	1.64 (690)	0.0111 (1.21)
F	1620	0.00877 (3.99)	0.122 (75.8)	9.94 (4192)	0.0263 (2.89)

Table 4.25 - HDx $A\beta_{pE3-40}$ antibody combinations results

4.4.3.3 Assay protocol comparison

Unlike on the SRx, we performed the comparison of the 2-step and 3-step assay protocols separately to the antibody combinations comparison. As such, only heterogeneous antibody combination 3 was tested for both assays. Whilst neither the 2-step nor the 3-step assay protocol is superior to the other, it is important to test both to ascertain which is best for the analyte being measured.

Interestingly, the N4PE Simoa assay, which measures $A\beta_{40}$ and $A\beta_{42}$ (along with NfL and GFAP) is run with a 2-step protocol both on the HDx and on the SRx. Given that we observed the 2-step protocol to be superior to the 3-step protocol with both of our assays on the SRx,

it is possible that the increased time with which the detector antibody is incubated along with the analyte in a 2-step assay may increase the likelihood of immunocomplex formation, thus enhancing the signal with the analyte. Alternatively, the additional washing step conducted with the 3-step assay protocol may result in a greater loss of unbound analyte and hence a dampening of the signal.

4.4.3.3.1 $A\beta_{43}$ assay

Using a calibration curve ranging from 0 to 320 pg/mL, in line with our observations on the SRx, the 2-step assay protocol produced a higher AEB at all calibration curve points, with an AEB at calibrator F on the 2-step assay protocol of 0.0786 (S/N 26.8) compared with 0.0201 (S/N 5.32) on the 3-step assay protocol (Table 4.26). As such, we proceeded with the 2-step assay protocol.

$A\beta_{43}$		**Mean AEB (S/N) at calibrator**	
Calibrator	Concentration (pg/mL)	Assay protocol	
		2-step	3-step
A	0	0.00293	0.00379
B	20	0.00505 (1.72)	0.00457 (1.21)
C	40	0.00870 (2.97)	0.00572 (1.51)
D	80	0.0150 (5.13)	0.00861 (2.27)
E	160	0.0354 (12.1)	0.0129 (3.40)
F	320	0.0786 (26.8)	0.0201 (5.32)

Table 4.26 - HDx $A\beta_{43}$ assay protocol comparison

4.4.3.3.2 $A\beta_{pE3\text{-}40}$ assay

Using the same calibration curve as that used for the antibody combinations test (Table 4.25), we observed that the 2-step assay protocol produced the highest AEB at all calibration curve points, with

an AEB at calibrator F of 12.5 (S/N 5753) compared with 0.205 (S/N 102) on the 3-step assay protocol (Table 4.27). As such, we carried forward the 2-step assay protocol for further assay development.

Assay protocol		**2-step**	**3-step**
Mean AEB (S/N) at calibrator	A	0.00217	0.00200
	B	0.0104 (4.78)	0.00375 (1.88)
	C	0.0524 (24.2)	0.00589 (2.94)
	D	0.324 (150)	0.0177 (8.86)
	E	2.24 (1033)	0.0477 (23.9)
	F	12.5 (5753)	0.205 (102)

Table 4.27 - HDx $A\beta_{pE3\text{-}40}$ assay protocol comparison

4.4.3.4 Calibration curve optimisation

Whilst we conducted a small calibration curve optimisation on the SRx, we were unable to conduct an extensive optimisation prior to the upgrade of our SRx to the SRx Pro. As such, fine tuning the calibration curve was one of the main objectives for transferring the assays on the HDx instrument prior to developing them on the SRx Pro.

When optimising calibration curves, whilst the AEBs must be kept into consideration, particularly at calibrator A as this determines the S/N at each subsequent calibration point, comparing S/N, rather than AEB, enables the data to be interpreted with the most ease. A higher AEB at the blank will cause a seemingly lower S/N, even if the AEBs across the calibration curves being compared are similar. A S/N of between 2-4 is most optimal for calibrator B, with the most optimal S/N at calibrator F being dependent on the dynamic range required

for the assay, however ideally in the range of around 10-12 and no greater than 16 (see section 4.2.5 Optimal characteristics of a Simoa assay).

4.4.3.4.1 $A\beta_{43}$ assay

The AEB obtained from calibrator B at a concentration of 20 pg/mL during the assay protocol comparison (section 4.4.3.3.1 $A\beta_{43}$ assay) was acceptable at this stage of the assay development process (i.e. prior to reagent optimisation). As such, the main objective of this calibration curve optimisation process was to determine the most optimal concentration for calibrator F. Given that a calibrator F of 320 pg/mL did not produce a high enough AEB (and S/N), we investigated three serial dilutions – 1:3, 1:4, and 1:5 – maintaining a calibrator B concentration of 20 pg/mL across all three curves (Table 4.28). We observed that whilst a 1:3 serial dilution, starting at a calibrator F concentration of 1620 pg/mL, did not produce a high enough S/N (411), a 1:4 serial dilution, starting at a calibrator F concentration of 5120 pg/mL produced the most optimal S/N at this stage of the assay development process (2177). Whilst the S/N at calibrator B of this curve appeared seemingly low (1.73), this can be attributed to a slight increase in the AEB at calibrator A and a slight decrease in the AEB at calibrator B in comparison to the AEBs at calibrators A and B of the 1:3 and 1:5 serial dilution curves. Furthermore, this AEB would be enhanced as we progressed through the assay optimisation stages. Whilst the 1:5 serial dilution produced an impressively high S/N (7725) at calibrator F (12 500 pg/mL), an AEB of 20.4 is far too high, risking saturation as we progressed through the optimisation process. As such, we proceeded with the 1:4 serial dilution to the next stage of the assay development process.

Calibrator	1:3 serial dilution		1:4 serial dilution		1:5 serial dilution	
	Concentration (pg/mL)	Mean AEB (S/N)	Concentration (pg/mL)	Mean AEB (S/N)	Concentration (pg/mL)	Mean AEB (S/N)
A	0	0.00295	0	0.00325	0	0.00264
B	20	0.00608 (2.06)	20	0.00562 (1.73)	20	0.00639 (2.42)
C	60	0.0124 (4.21)	80	0.0149 (4.59)	100	0.0208 (7.89)
D	180	0.0411 (13.9)	320	0.0993 (30.5)	500	0.165 (62.5)
E	540	0.221 (74.8)	1280	0.690 (212)	2500	2.68 (1015)
F	1620	1.21 (411)	5120	7.08 (2177)	12 500	20.4 (7725)

Table 4.28 - HDx $A\beta_{43}$ calibration curve optimisation

4.4.3.4.2 $A\beta_{pE3-40}$ assay

Following the AEB saturation on the SRx with a calibrator F concentration of 2000 pg/mL (see section 4.4.2.6.2 $A\beta_{pE3-40}$ assay), the antibody combinations (section 4.4.3.2.2 $A\beta_{pE3-40}$ assay) and assay protocol comparison (section 4.4.3.3.2 $A\beta_{pE3-40}$ assay) performed thus far on the HDx have revealed that a calibrator F concentration of 1620 pg/mL consistently produced an AEB and S/N. As such, the main objective of this calibration curve optimisation process was to determine the most appropriate concentration for calibrator B. A serial dilution of 1:3 was used in the earlier stages of the assay development process, giving a calibrator B concentration of 20 pg/mL. On occasion, this would produce a S/N too high, as shown in Table 4.25 (combination 3). As such we investigated 1:4, 1:5 and 1:6 serial dilutions, but observed all three produced a calibrator B S/N too low – 1.50 for 1:4 serial dilution with a calibrator

B concentration of 6.32 pg/mL (Table 4.29; 1:5 and 1:6 results not shown). As such, we compared a 1:3.2 and 1:3.5 serial dilution. We observed that a 1:3.5 serial dilution, with a calibrator B concentration of 10.8 pg/mL, produced a S/N of 3.27, whereas the 1:3.2 serial dilution, with a calibrator B concentration of 15.4 pg/mL produced a S/N of 6.48. Hence, we carried forward the 1:3.5 serial dilution calibration curve.

Calibrator	**1:3.2 serial dilution**		**1:3.5 serial dilution**		**1:4 serial dilution**	
	Concentration (pg/mL)	Mean AEB (S/N)	Concentration (pg/mL)	Mean AEB (S/N)	Concentration (pg/mL)	Mean AEB (S/N)
A	0	0.00227	0	0.00271	0	0.00227
B	15.4	0.0147 (6.48)	10.8	0.00886 (3.27)	6.32	0.00341 (1.50)
C	49.4	0.0627 (27.6)	37.8	0.0345 (12.8)	25.3	0.0111 (4.89)
D	158.2	0.264 (117)	132.2	0.249 (91.9)	101.3	0.0868 (38.2)
E	506.3	1.88 (830)	462.9	1.55 (574)	405	0.950 (418)
F	1620	12.7 (5600)	1620	12.2 (4490)	1620	9.88 (4351)

Table 4.29 - HDx $A\beta_{pE3-40}$ calibration curve optimisation

4.4.3.2.3 Calibration curve discussion

This left us with a calibration curve range of 20-5120 pg/mL for $A\beta_{43}$, and 10.8-1620 pg/mL for $A\beta_{pE3-40}$. This is particularly wide, considering the calibration curve ranges for $A\beta_{40}$ and $A\beta_{42}$ used in the Quanterix N4PE assay are 1.13-84.3 pg/mL and 0.378-21.8 pg/mL, respectively[3]. Our ranges were selected primarily to obtain a wide range of AEBs across the calibration curve. However, upon

reassessing the likely concentration of our analytes, this range would be far too high for the analytes we were attempting to detect. Furthermore, looking more closely into the IBL $A\beta_{43}$ assay used by both Perrone and colleagues (40) and De Kort and colleagues (367), the calibration curve optimised by IBL ranged from 2.34-150 pg/mL. Whilst our priority during this phase of the assay development process was obtaining a wide AEB and calibration curve range, we later realised this had a negative impact on the sensitivity of our assay, leading to us later return to the HDx instrument to refine our assays (section 4.4.5). As such, whilst we continued with these curves for the remainder of this phase of the assay development process, we acknowledge that this was not the most suitable approach to take.

4.4.3.5 Diluent screen

Once again, we compared the standard HB diluent to the five sample diluents A-E using the calibration curves optimised in section 4.4.3.4 Calibration curve optimisation

4.4.3.5.1 $A\beta_{43}$ assay

For the $A\beta_{43}$ assay, it should be noted that this experiment was conducted before the optimisation of the calibration curve, hence a calibrator F concentration of 1620 pg/mL was used (1:3 serial dilution curve in Table 4.28), rather than the optimised concentration of 5120 pg/mL (1:4 serial dilution curve in Table 4.28). Diluent D showed the greatest enhancement in AEB at both calibrators B and F, with AEBs of 0.00622 (S/N 2.00) and 1.39 (S/N 447), respectively (Table 4.30). This is in comparison to diluent C, which showed the second highest enhancement in AEB at calibrators B (0.00544; S/N 1.57) and F (0.820; S/N 237). However, due to unforeseen circumstances we were unable to source enough diluent D for the remainder of the assay development process on the HDx instrument. In light of this, whilst diluent C would have been the next best diluent to proceed with, diluent HB was the most accessible at the time. Since the enhancement in signal between diluents C and HB was minimal, we

proceeded with diluent HB. We deemed this an acceptable compromise to make at this phase of our three-instrument assay development process, given that we intended to repeat every optimisation step when transferring the assays onto the SRx Pro.

Diluent		HB	A	B	C	D	E
Mean AEB (S/N) at calibrator	A	0.00298	0.00228	0.00302	0.00346	0.00311	0.00250
	B	0.00461 (1.55)	0.00366 (1.61)	0.00481 (1.60)	0.00544 (1.57)	0.00622 (2.00)	0.00301 (1.20)
	C	0.00803 (2.70)	0.00705 (3.09)	0.00922 (3.05)	0.0119 (3.44)	0.0117 (3.77)	0.00431 (1.72)
	D	0.0253 (8.50)	0.0233 (10.2)	0.0223 (7.40)	0.0348 (10.1)	0.0423 (13.6)	0.0117 (4.69)
	E	0.127 (42.5)	0.0972 (42.6)	0.120 (39.8)	0.145 (41.9)	0.2016 (64.9)	0.0385 (15.4)
	F	0.804 (270)	0.594 (261)	0.738 (244)	0.820 (237)	1.39 (447)	0.188 (75.1)

Table 4.30 - HDx $A\beta_{43}$ diluent screen

4.4.3.5.2 $A\beta_{pE3\text{-}40}$ assay

Diluent C showed the greatest enhancement in AEB at calibrator F (11.3; S/N 5038) compared with 9.72 (S/N 3104) using diluent D and 9.55 (S/N 3841) using diluent B (Table 4.31). In contrast, diluent E showed the greatest enhancement in AEB at calibrator B, with an AEB of 0.00840 (S/N 4.78) compared with 0.00714 (S/N 3.17) using diluent C. Given that the absolute difference in AEB at calibrator B between these two diluents was minimal, and also given that at calibrator F, both diluents D and B outperformed diluent E, we opted to proceed with diluent C for the remainder of the assay development process.

Diluent		HB	A	B	C	D	E
Mean AEB (S/N) at calibrator	A	0.00245	0.00200	0.00249	0.00225	0.00313	0.00176
	B	0.00526 (2.15)	0.00506 (2.53)	0.00551 (2.22)	0.00714 (3.17)	0.00632 (2.02)	0.00840 (4.78)
	C	0.0233 (9.53)	0.0211 (10.5)	0.0235 (9.45)	0.0275 (12.2)	0.0287 (9.18)	0.0344 (19.5)
	D	0.104 (42.7)	0.122 (60.7)	0.160 (64.3)	0.197 (87.6)	0.171 (54.6)	0.214 (122)
	E	0.867 (355)	1.07 (534)	1.27 (510)	1.61 (713)	1.34 (429)	1.17 (663)
	F	7.16 (2927)	8.26 (4121)	9.55 (3841)	11.3 (5038)	9.72 (3104)	8.44 (4802)

Table 4.31 - HDx $A\beta_{pE3\text{-}40}$ diluent screen

4.4.3.6 Detector concentration titration

Up to this stage of the assay development process, the standard 2-step detector concentration of 1.0µg/mL was used. Therefore, for both of our assays, using the calibration curves optimised in section 4.4.3.4 Calibration curve optimisation, we tested the same four additional concentrations as was tested on the SRx – 0.6, 0.8, 1.2 and 1.4µg/mL – alongside the standard 1.0µg/mL to see whether increasing or decreasing the detector concentration enhanced the AEB at each calibration point.

4.4.3.6.1 $A\beta_{43}$ assay

The 1.4µg/mL detector produced the highest AEB at both calibrators B (0.00440; S/N 1.72) and F (11.6; S/N 4515; Table 4.32). However, given that the increase was only marginally higher than the 1.2µg/mL, we opted to carry forward both the 1.2 and 1.4µg/mL concentrations to the next stage of the assay development process, and compare them during the SβG concentration titration.

Detector concentration (µg/mL)		0.6	0.8	1.0	1.2	1.4
Mean AEB (S/N) at calibrator	A	0.00220	0.00204	0.00318	0.00240	0.00256
	B	0.00297 (1.35)	0.00355 (1.74)	0.00357 (1.12)	0.00365 (1.52)	0.00440 (1.72)
	C	0.00525 (2.39)	0.00611 (2.99)	0.00995 (3.13)	0.00946 (3.95)	0.00923 (3.60)
	D	0.0277 (12.6)	0.0431 (21.1)	0.0458 (14.4)	0.0540 (22.5)	0.0578 (22.6)
	E	0.387 (176)	0.504 (247)	0.633 (199)	0.761 (318)	0.827 (323)
	F	6.66 (3026)	6.84 (3348)	9.69 (3051)	10.7 (4471)	11.6 (4515)

Table 4.32 - HDx $A\beta_{43}$ detector concentration titration

4.4.3.6.2 $A\beta_{pE3\text{-}40}$ assay

Similar to the $A\beta_{43}$ assay, the 1.4µg/mL detector produced the highest AEB at both calibrators B and F (Table 4.33). However, the enhancement in AEB between the 1.2 and 1.4µg/mL detectors was even smaller than that seen with the $A\beta_{43}$ assay, with AEBs of 13.1 and 13.9, respectively. In light of our observations comparing the 1.2 and 1.4µg/mL detector concentrations during the $A\beta_{43}$ SβG concentration titration (see section 4.4.3.7.1 $A\beta_{43}$ assay), on this occasion we opted to only carry forward the 1.2µg/mL detector concentration to the next stage of the assay development process.

Detector concentration (µg/mL)		0.6	0.8	1.0	1.2	1.4
Mean AEB (S/N) at calibrator	A	0.00280	0.00218	0.00265	0.00315	0.00261
	B	0.00582 (2.08)	0.00649 (2.97)	0.00688 (2.60)	0.00947 (3.01)	0.0102 (3.90)
	C	0.0177 (6.35)	0.0283 (13.0)	0.0286 (10.8)	0.0330 (10.5)	0.106 (40.7)
	D	0.122 (43.5)	0.153 (70.4)	0.190 (71.6)	0.231 (73.3)	0.288 (110)
	E	1.03 (368)	1.46 (669)	1.65 (622)	1.95 (620)	2.21 (844)
	F	7.17 (2564)	9.51 (4362)	10.8 (4097)	13.1 (4167)	13.9 (5323)

Table 4.33 - HDx $A\beta_{pE3\text{-}40}$ detector concentration titration

4.4.3.7 SβG concentration titration

As was conducted on the SRx, we next titrated the concentration of SβG, comparing 50, 150 and 300pM concentrations, using the same calibration curve as optimised in section 4.4.3.4 Calibration curve optimisation.

4.4.3.7.1 $A\beta_{43}$ assay

We compared the 1.2 and 1.4µg/mL at all three SβG concentrations, and observed that the 1.2µg/mL detector produced the highest AEBs at calibrator F across all SβG concentrations (Table 4.34). Whilst the highest AEB was obtained with an SβG concentration of 300pM (14.5; S/N 2441) we opted to carry forward the 1.2µg/mL detector with the 150pM SβG concentration as the AEBs obtained with this combination were sufficiently high enough for our assay.

SβG concentration (pM)		**50**		**150**		**300**	
Detector concentration (µg/mL)		1.2	1.4	1.2	1.4	1.2	1.4
Mean AEB (S/N) at calibrator	A	0.00153	0.00208	0.00318	0.00387	0.00594	0.00524
	B	0.00450 (2.94)	0.00362 (1.74)	0.00671 (2.11)	0.00704 (1.82)	0.00947 (1.59)	0.0101 (1.92)
	C	0.00873 (5.70)	0.00980 (4.71)	0.0181 (5.71)	0.0209 (5.40)	0.0270 (4.53)	0.0262 (5.01)
	D	0.0568 (37.1)	0.0572 (27.5)	0.105 (33.0)	0.149 (38.4)	0.153 (25.7)	0.174 (33.2)
	E	0.498 (325)	0.565 (272)	1.02 (320)	1.08 (280)	1.59 (267)	1.48 (284)
	F	5.83 (3803)	5.78 (2779)	10.8 (3392)	9.68 (2502)	14.5 (2441)	12.6 (2411)

Table 4.34 - HDx $A\beta_{43}$ SβG concentration titration

4.4.3.7.2 $A\beta_{pE3\text{-}40}$ assay

Whilst the 300pM SβG produced the highest AEBs at both calibrators B and F, with values of 0.0133 (S/N 1.79) and 13.3 (S/N 1788; Table 4.35) respectively, we opted to carry forward the 150pM SβG concentration as the AEBs obtained were sufficient.

SβG concentration (pM)		**50**	**150**	**300**
Mean AEB (S/N) at calibrator	A	0.00300	0.00606	0.00742
	B	0.00597 (1.99)	0.00863 (1.42)	0.0133 (1.79)
	C	0.0185 (6.17)	0.0283 (4.66)	0.0490 (6.61)
	D	0.106 (35.5)	0.153 (25.2)	0.265 (35.8)
	E	0.914 (305)	1.33 (219)	1.91 (258)
	F	6.81 (2271)	9.87 (1627)	13.3 (1788)

Table 4.35 - HDx $A\beta_{pE3\text{-}40}$ SβG concentration titration

4.4.3.8 Helper bead comparison

Finally, we evaluated whether the use of helper beads either maintained or enhanced the AEB values obtained with 100% assay beads, using the same calibration curves as optimised in section 4.4.3.4 Calibration curve optimisation. As with the SRx, we tested three assay bead to helper bead ratios against the standard 100% assay beads – 70% assay beads:30% helper beads, 50% assay beads:50% helper beads, and 30% assay beads:70% helper beads.

4.4.3.8.1 $A\beta_{43}$

All assay:helper bead ratios enhanced the AEBs at every calibration point compared with the 100% assay beads (Table 4.36). The 30:70 ratio of assay:helper beads produced the highest AEB at calibrator F (12.1; S/N 2906), whereas the 50:50 ratio produced the highest AEB at calibrator B (0.00735; S/N 2.13; Table 4.36). We opted to proceed with the 50:50 ratio as this produced a sufficient improvement in our AEBs. Whilst the 30:70 ratio similarly improved our AEBs, we did not believe it was necessary to decrease the assay bead usage by such a large percentage.

Assay:helper bead ratio		**100:0**	**70:30**	**50:50**	**30:70**
Mean AEB (S/N) at calibrator	A	0.00314	0.00429	0.00345	0.00415
	B	0.00547 (1.74)	0.00674 (1.57)	0.00735 (2.13)	0.00725 (1.75)
	C	0.0190 (6.07)	0.0213 (4.97)	0.0276 (7.99)	0.0240 (5.79)
	D	0.131 (41.6)	0.124 (28.9)	0.136 (39.5)	0.141 (33.9)
	E	1.10 (351)	1.27 (296)	1.33 (385)	1.33 (320)
	F	10.7 (3423)	11.1 (2597)	11.7 (3396)	12.1 (2906)

Table 4.36 - HDx $A\beta_{43}$ helper bead comparison

4.4.3.8.2 $A\beta_{pE3-40}$

Both the 70:30 and 50:50 ratios increased the AEBs at calibrator F, with values of 14.1 (S/N 2582) and 14.4 (S/N 2467), respectively, in comparison to the 100% assay beads (AEB 13.7; S/N 2466; Table 4.37). The 30:70 ratio produced higher AEBs at calibrators B and C in comparison to the 50:50 ratio, but lagged behind at calibrators D, E and F. As such, we opted to carry forward the 50:50 ratio.

Assay:helper bead ratio		**100:0**	**70:30**	**50:50**	**30:70**
Mean AEB (S/N) at calibrator	A	0.00557	0.00546	0.00582	0.00436
	B	0.0108 (1.94)	0.00957 (1.75)	0.0114 (1.96)	0.0126 (2.90)
	C	0.0383 (6.87)	0.0375 (6.87)	0.0400 (6.88)	0.0432 (9.92)
	D	0.232 (41.6)	0.238 (43.5)	0.257 (44.2)	0.256 (58.7)
	E	2.13 (382)	2.19 (401)	2.37 (407)	1.97 (452)
	F	13.7 (2466)	14.1 (2582)	14.4 (2467)	12.8 (2936)

Table 4.37 - HDx $A\beta_{pE3-40}$ helper bead comparison

4.4.3.9 Summary of optimised $A\beta_{43}$ or $A\beta_{pE3-40}$ assays

To summarise, on the HDx, for the $A\beta_{43}$ assay, our optimised parameters were the 2-step assay protocol using the anti-$A\beta_{43}$ beads at a ratio of 50:50 with helper beads alongside the 6E10 detector at a concentration of 1.2µg/mL, and SβG at a concentration of 150pM. Calibrators, samples and detectors would be diluted in diluent HB with a calibration curve ranging from 20 to 5120 pg/mL using CP3 as the calibrator.

Likewise, for the $A\beta_{pE3-40}$ assay, our optimised parameters were the 2-step assay protocol using the anti-$A\beta_{40}$ beads at a ratio of 50:50 with helper beads, alongside the anti-$A\beta_{pE3-16}$ detector at a

concentration of 1.2µg/mL, and SβG at a concentration of 150pM. Calibrators, samples and detectors would be diluted in diluent C with a calibration curve ranging from 10.8 to 1620 pg/mL.

The optimised parameters for both assays can be seen in Table 4.38.

Assay component	**$Aβ_{43}$ assay**	**$Aβ_{pE3-40}$ assay**
Beads	Anti-$Aβ_{43}$	Anti-$Aβ_{40}$
Detector	6E10	Anti-$Aβ_{3-16}$
Detector concentration (µg/mL)	1.2	1.2
SβG concentration (pM)	150	150
Diluent	HB	C
Assay:helper bead ratio	50:50	50:50

Table 4.38 - Summary of optimised HDx $Aβ_{43}$ and $Aβ_{pE3-40}$ assay parameters

4.4.3.10 HDx pilot CSF $Aβ_{43}$ and $Aβ_{pE3-40}$ measurements

To ascertain whether the HDx had the required sensitivity to measure our analytes of interest in clinical samples, we performed a small pilot study using 8 CSF samples – 1 AD, 3 MP, and 4 CTRL – measured at four levels of dilution – neat (undiluted), 1:2 (2x), 1:4 (4x) and 1:8 (8x). Given that we expected the analytes to be of a higher concentration in CSF than in plasma, we opted to only measure CSF samples at this stage of our assay development process.

4.4.3.10.1 $Aβ_{43}$

For $Aβ_{43}$, we obtained concentrations for 19 data points (59.4%; Table 4.39), 17 of which fell below the concentration of calibrator B (20 pg/mL) prior to accounting for the dilution factor (Figure 4.4). The

highest concentrations were obtained for the neat and 2x dilution measurements of MP1, measuring 103 pg/mL and 25.7 pg/mL (47.4 pg/mL after accounting for dilution factor – see Table 4.46), respectively (Table 4.39). Three samples were measurable neat but unmeasurable upon dilution (MP3, CTRL2 and CTRL4), and two samples were measurable across all dilution levels (MP1 and CTRL1). After accounting for the dilution factor, the concentrations of these two samples appeared to vary greatly at each dilution level (see 'A' measurements for MP1 and CTRL1 in Table 4.46), seen graphically in Figure 4.5B&C. Investigating the dilution linearity in these two samples more closely, CTRL1 showed a poor linearity, with an r-value of -0.246 (95% CI -0.976-0.937; p-value 0.754; Figure 4.5A). In contrast, MP1 showed a strong positive dilution linearity that was marginally statistically significant, with an r-value of 0.970 (95% CI 0.126-0.999; p-value 0.0303*; Figure 4.5A).

4.4.3.10.2 Aβ$_{pE3-40}$

In comparison, we obtained concentrations for Aβ$_{pE3-40}$ for 10 data points (31.3%; Table 4.39), 6 of which fell below the concentration of calibrator B (10.8 pg/mL; Figure 4.6). The highest concentrations were obtained for the neat measurements of MP1, AD1 and CTRL3, measuring 41.5 pg/mL, 27.2 pg/mL and 24.6 pg/mL, respectively (Table 4.39). Four samples were measurable neat but unmeasurable upon dilution (MP3, CTRL2, CTRL3 and CTRL4), although two of these samples (MP3 and CTRL4) were not measured at the 8x dilution level due to an instrument error. One sample was unmeasurable at all four dilution levels (MP2). No samples were measurable at all four dilution levels, although one sample (MP1) was measurable at three of the four dilution levels. After accounting for the dilution factor in this sample, there was again a large variation in concentration at each dilution level (see 'A' measurements for MP1 in Table 4.46), seen graphically in Figure 4.7B. Investigating the dilution linearity in MP1 more closely, we observed a strong but

statistically non-significant linearity, with an r-value of 0.903 (95%CI -0.439-0.998; p-value 0.0968; Figure 4.7A).

4.4.3.10.3 Summary

Whilst we were able to obtain concentration values for some of our samples, there still remained a large proportion of samples in which the HDx was not sensitive enough to detect our analytes, particularly $A\beta_{pE3\text{-}40}$. Furthermore, the poor dilution linearity observed may highlight that at the neat measurements, there was some interference from matrix effects, or that our chosen sample diluents do not mimic the normal biological matrix. In light of these results, we concluded that the HDx instrument lacks the required sensitivity to measure $A\beta_{43}$ and/or $A\beta_{pE3\text{-}40}$ in CSF, highlighting a need for the additional sensitivity offered by the SRx Pro.

Sample phenotype	$A\beta_{43}$ concentration (pg/mL)				$A\beta_{pE3-40}$ concentration (pg/mL)			
	Neat	2x	4x	8x	Neat	2x	4x	8x
AD1	8.84	-	-	10.8	27.2	-	-	4.15
MP1	103	25.7	7.56	7.93	41.5	0.0408	-	1.68
MP2	7.60	9.33	-	12.7	-	-	-	-
MP3	10.0	-	-	-	5.68	-	-	Instrument error
CTRL1	6.36	6.02	2.52	12.0	-	-	2.37	-
CTRL2	15.4	-	-	-	12.5	-	-	-
CTRL3	13.9	11.7	4.98	-	24.6	-	-	-
CTRL4	15.9	-	-	-	8.15	-	-	Instrument error

Table 4.39 - HDx pilot CSF $A\beta_{43}$ and $A\beta_{pE3-40}$ concentrations (unadjusted)

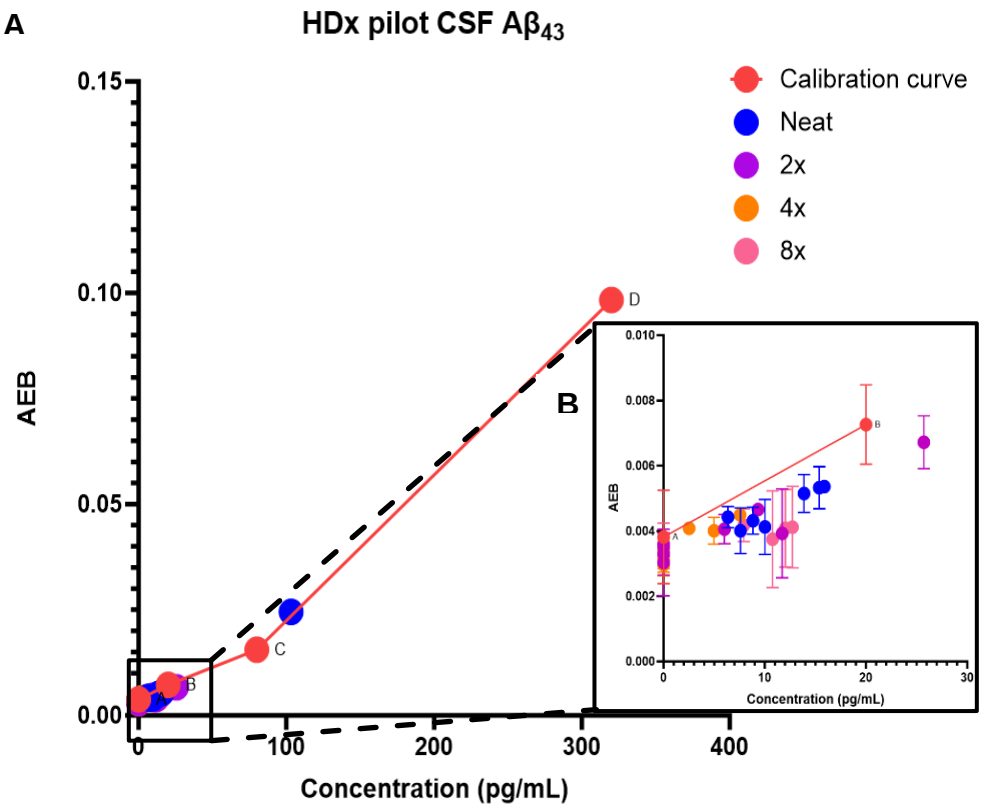

Figure 4.4 - HDx pilot CSF $A\beta_{43}$ concentrations

***A**: Amyloid-β 1-43 ($A\beta_{43}$) cerebrospinal fluid (CSF) concentrations in eight pilot cohort samples undiluted (neat) and diluted 1:2 (2x), 1:4 (4x) and 1:8 (8x) in relation to average number of enzyme complexes per bead (AEB) calculated by HDx instrument. Six-point calibration curve was used but only calibration points A to D were included in graph. **B**: Zoom in of sample concentrations around calibration points A and B.*

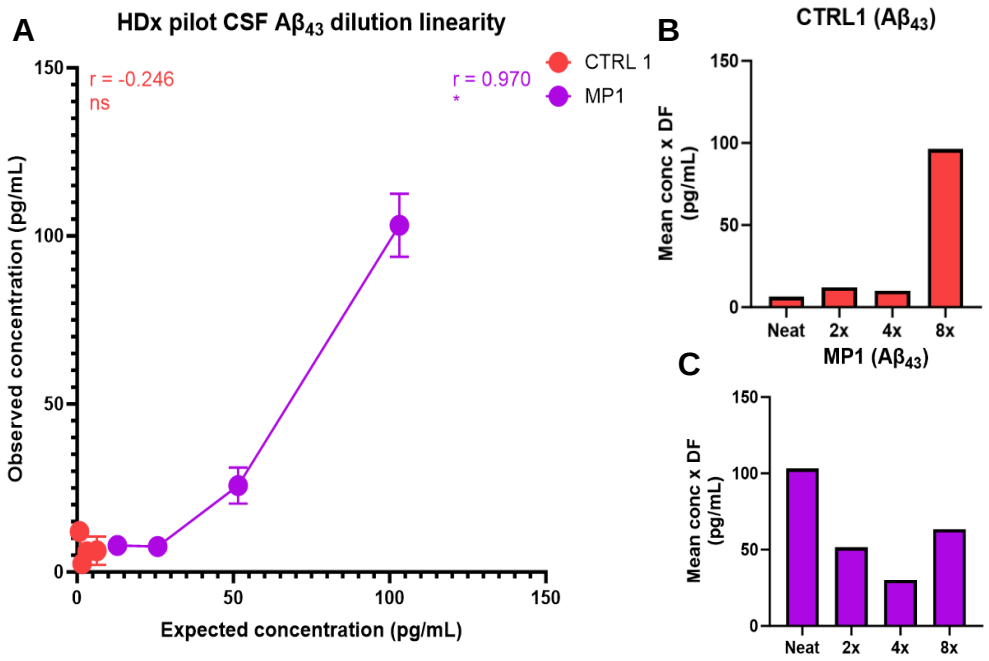

Figure 4.5 - HDx pilot CSF Aβ$_{43}$ dilution linearity

***A**: Amyloid-β 1-43 (Aβ$_{43}$) cerebrospinal fluid (CSF) control (CTRL) 1 and mixed phenotype (MP) 1 observed concentration compared with expected concentration dilution linearity. Correlation coefficient (r-value) is stated for each sample. CTRL1 showed a weak negative dilution linearity, with an r-value of -0.246 (95% CI -0.976-0.937) and p-value of 0.754. MP1 showed a strong statistically significant positive dilution linearity with an r-value of 0.970 (95% CI 0.126-0.999) and a p-value of 0.0303*: **B**: CTRL1 Aβ$_{43}$ concentrations after adjusting for extent of dilution; **C**: MP1 Aβ$_{43}$ concentrations after adjusting for extent of dilution. 'ns' indicates non-significant; 'DF', dilution factor*

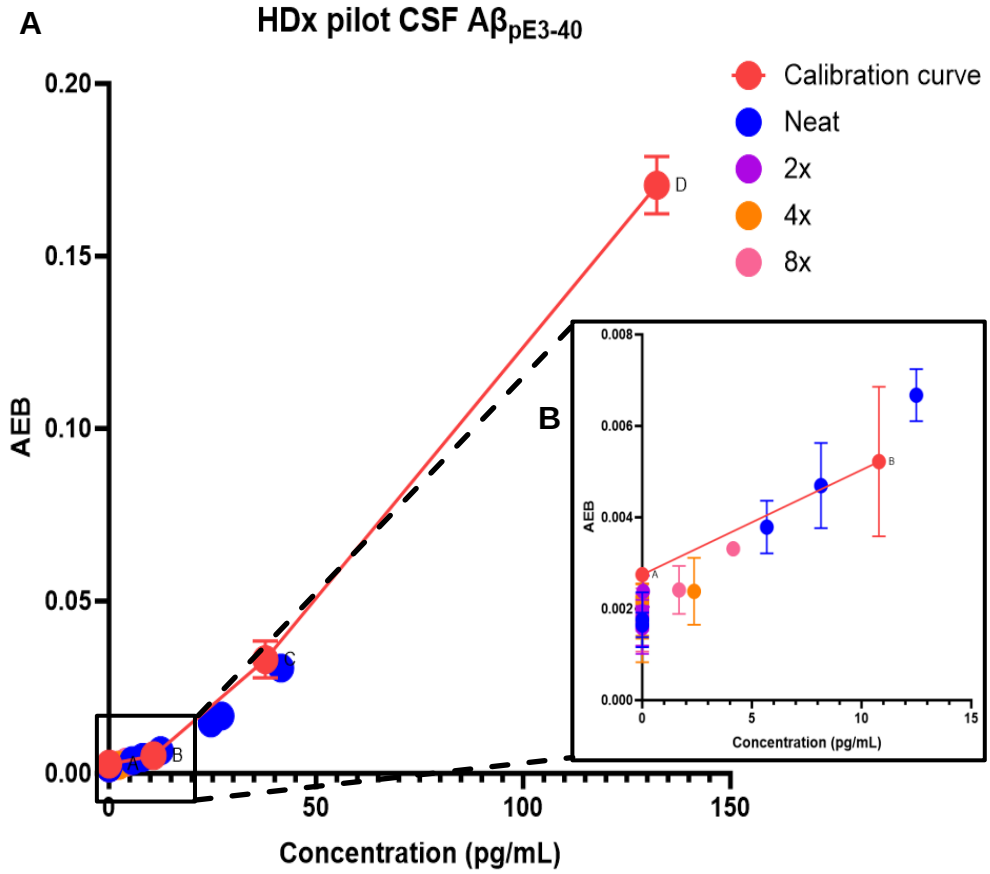

Figure 4.6 - HDx pilot CSF $A\beta_{pE3\text{-}40}$ concentrations

***A**: Pyroglutamate amyloid-β 3-40 ($A\beta_{pE3\text{-}40}$) cerebrospinal fluid (CSF) concentrations in eight pilot cohort samples undiluted (neat) and diluted 1:2 (2x), 1:4 (4x) and 1:8 (8x) in relation to average number of enzyme complexes per bead (AEB) calculated by HDx instrument. Six-point calibration curve was used but only calibration points A to D were included in graph. **B**: Zoom in of sample concentrations around calibration points A and B.*

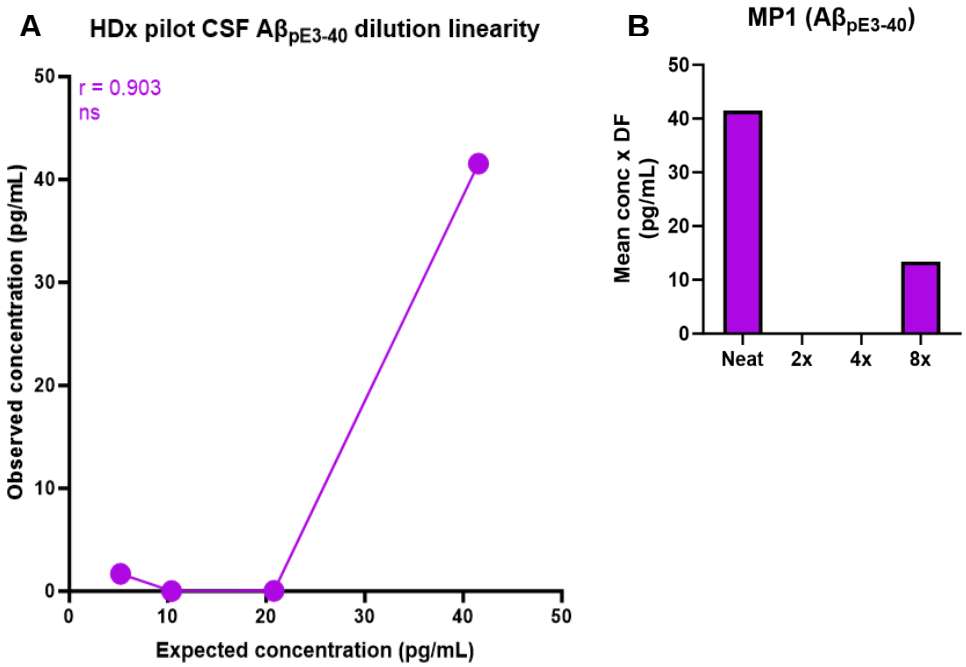

Figure 4.7 - HDx pilot CSF Aβ$_{pE3-40}$ dilution linearity

***A**: Pyroglutamate amyloid-β 3-40 (Aβ$_{pE3-40}$) cerebrospinal fluid (CSF) mixed phenotype (MP) 1 observed concentration compared with expected concentration dilution linearity. MP1 showed a strong positive by non-significant (ns) dilution linearity, with an r-value of 0.903 (95%CI -0.439-0.998) and a p-value 0.0968; **B**: MP1 Aβ$_{pE3-40}$ concentrations after adjusting for extent of dilution; 'ns' indicates non-significant; 'DF', dilution factor*

4.4.4 SRx Pro assay development

The results of the pilot CSF analysis highlighted the need for the increased sensitivity provided by the SRx Pro instrument for our two assays. As the SRx Pro is up to 189-fold more sensitive than the HDx (214) we approached the assay development process in a slightly different manner to the way we approached the development process on the HDx. Rather than re-starting the development process from scratch, we assumed the orientation of the antibodies conjugated onto the beads and biotinylated as the detector would remain the same. Furthermore, we used the 2-step assay protocol with the same optimised diluent and concentrations of detector and SβG to begin with, although we intended to repeat these optimisation stages as we moved through assay development on this platform. The only aspect not carried forward was the use of helper beads. This is because the lower bead number used by the SRx Pro of 5000 beads already serves the purpose of increasing the ratio of assay beads to target analyte. As such, decreasing the number of assay beads any further through the use of helper beads would negatively impact the sensitivity of the assays. With regards to AEBs at the blank calibrator, whereas with the HDx instrument an AEB between 0.005 and 0.02 is optimal (see section 4.2.5 Optimal characteristics of a Simoa assay), with the SRx Pro, a value of no lower than 0.01 is optimal. This is because given the lower number of beads used, an AEB below 0.01 indicates an f_{on} less than 1% (50 beads), which can't accurately be quantified by the Simoa instruments.

4.4.4.1 Calibration curve optimisation and 2-step vs 3-step assay protocol comparison

We first attempted to re-optimise the calibration curve to suite the increased sensitivity provided by the SRx Pro, using the calibration curve optimised on the HDx as a starting point. We tested three curves for both of our assays – curve 1) 10x lower than the HDx curve; curve 2) calibrator F was equal to calibrator D of HDx curve; and curve 3) 100x lower than the HDx curve – first on the 2-step

protocol and subsequently on the 3-step assay protocol. However, due to several unexpected challenges on both assays, we spent the final portion of this PhD troubleshooting these challenges, and hence did not progress as far as we had hoped in their development on the SRx Pro instrument.

4.4.4.1.1 Challenge 1: "Low intensity single precision" error

The first challenge we faced was the sporadic generation of AEBs, and a frequent "low intensity single precision" error. Whilst obtaining this error on Simoa instruments usually indicates that the concentration of calibrator B is not low enough for the instrument to be sure of I_{single}[12] and hence is unable to calculate AEBs, upon decreasing calibrator B to as low as 0.000416 pg/mL for $A\beta_{pE3\text{-}40}$, it became clear that in our case the reason for this error did not lie with the concentration of calibrator B. We explored the possibility of this error being due to issues with the instrument, rather than with our analytes, particularly given the SRx Pro is a prototype that is not yet available commercially. However, given that we did not encounter this during the validation of the SRx Pro with IL17A (see CHAPTER 3: SIMOA UPGRADE VALIDATION), this was unlikely to be the case.

Although the reason for this recurrent error remained unclear, we soon discovered that whilst the instrument was not calculating the AEBs automatically, it was generating the required information to enable the manual calculation of the AEBs offline. Simoa technology assumes a Poisson distribution of molecules over the beads, which refers to the probability of an event occurring if the average number of events is known (380). This information is outputted in the form of AEBs, calculated on the instrument using one of two equations, depending on whether the f_{on} is above or below 0.7 (i.e. 70%):

[12] I_{single} = mean fluorescence intensity of a single enzyme immunocomplex on a bead

1) $AEB_{digital} = -\ln(1 - f_{on})$ is used when $f_{on} \leq 0.7$

2) $AEB_{analog} = \frac{f_{on} \times I_{bead}}{I_{single}}$ is used when $f_{on} > 0.7$

Together, these two equations are referred to as the 'piecewise' method for calculating AEB (i.e. $AEB_{piecewise}$). When the assay being measured is Poisson consistent, for any given data point, regardless of f_{on}, $AEB_{digital} = AEB_{analog}$. In this way, we realised that we now had a wealth of data that we previously did not have. We also came to discover that expanding the calibration curve to an eight-point curve eradicated this error. Regardless, upon manually calculating the AEBs for all of our experiments on the SRx Pro up to that point, we ran into our second challenge.

4.4.4.1.2 Challenge 2: "Up-down" nature of calibration curves

The second challenge we faced was that our calibration curves did not increase linearly, but rather exhibited an "up-down" nature, as depicted in Table 4.40. A variation in AEB between calibration curves is expected, particularly between curves run on separate occasions, as seen throughout the assay development process on the HDx. Comparing S/N mitigates for these differences, enabling both intra-run and inter-run comparisons to be made. However, these inconsistencies were unique in that they appeared to be independent of the concentrations at each calibration point (i.e. were of an irregular nature, making them particularly difficult to troubleshoot). Furthermore, they seemed to be more evident at the lower concentration calibration points.

One possible cause may have been the high propensity of our analytes to aggregate. Indeed, whilst the concentrations used were low, such that aggregation should not have been evident, the

additional vortexing of our calibrators required to get to these lower concentrations may have caused unintentional aggregation and/or oligomerisation. Given that for the $A\beta_{43}$ assay, we were using CP3, which theoretically should have eradicated any oligomerisation due to its decreased hydrophobicity compared to the FL $A\beta_{43}$ peptide, the use of CP3 only limited the oligomerisation in $A\beta_{43}$, rather than eradicating it, as highlighted in Table 4.21. Furthermore, the addition of the pyroglutamate ring in $A\beta_{pE3-40}$, coupled with the loss of the first two amino acids, is known to increase this peptide's propensity to aggregate (75). Whilst it may have been beneficial to explore alternative methods for mixing our calibration material sufficiently to create the calibration curves without compromising on CVs, such as through the use of a sonicator, we discovered that vortexing very briefly on a low speed improved the nature of our calibration curves, whilst maintaining CVs within acceptable limits. Therefore, we re-tested the same three calibration curves mentioned in section 4.4.4.1 Calibration curve optimisation and 2-step vs 3-step assay protocol comparison, now using an eight-point calibration curve on both the 2-step and 3-step assay protocols.

	$A\beta_{43}$		**$A\beta_{pE3-40}$**	
Calibrator	Concentration (pg/mL)	Mean AEB (S/N)	Concentration (pg/mL)	Mean AEB (S/N)
A	0	0.00750	0	0.00385
B	1.25	0.00920 (1.23)	0.0123	0.0545 (14.2)
C	5	0.0577 (7.70)	0.0741	0.713 (185)
D	20	0.0351 (4.69)	0.444	0.0311 (8.08)
E	80	0.245 (32.7)	2.67	2.11 (547)
F	320	0.154 (20.5)	16	0.437 (114)

Table 4.40 – Example of SRx Pro non-linear calibration curves

4.4.4.1.3 $A\beta_{43}$ assay

Across all three curves, the 3-step assay appeared to be more sensitive, producing higher AEBs than the 2-step assay protocol (Table 4.41). The exceptions to this were calibrator H of curve 1, which produced an AEB of 5.19 (S/N 477) with the 2-step compared with 3.93 (S/N 241) with the 3-step assay protocol, and calibrator H of curve 2, which produced an AEB of 2.79 (S/N 348) with the 2-step compared with 2.46 (S/N 175) with the 3-step assay protocol. Given that the 2-step assay protocol produced higher AEBs than the 3-step throughout our development process on the SRx and HDx instruments, this highlights that for $A\beta_{43}$, the 2-step assay protocol is more sensitive when measuring higher concentrations of our analyte. Whereas a change to the 3-step protocol is necessary to aid the additional sensitivity required.

The AEBs obtained at calibrator H of curves 1 and 2 (3.93 and 2.46, respectively), are far more optimal than that obtained at calibrator H of curve 3 (0.548). As such, it would be interesting to explore a calibrator H concentration between 50 and 320 pg/mL, particularly given that there would still be opportunities to further enhance the AEBs as we moved through the assay optimisation process.

It is important to also comment on the slight curve irregularities still visible between calibrator B, C and D in curves 1 and 3 (Table 4.41). These irregularities are of a far smaller magnitude than we were experiencing before, depicted in Table 4.40, hence they may merely highlight that we were reaching the limit of sensitivity for this assay on the SRx Pro for this analyte. In section 4.4.4.2 Poisson inconsistency unlikely to be the cause of SRx Pro assay development challenges, we discuss further theories for the causes of these irregularities, and potential solutions. Nonetheless, it would be interesting to explore a calibrator B concentration between 0.0488 and 0.125 pg/mL.

4.4.4.1.4 $A\beta_{pE3-40}$ assay

Similar to the $A\beta_{43}$ assay, across all three curves, the 3-step produced higher AEBs than the 2-step assay protocol (Table 4.42), further supporting our theory that the 2-step assay protocol is more sensitive when measuring higher concentrations of our analytes, whereas a change to the 3-step protocol is necessary to aid the additional sensitivity required when measuring lower concentrations.

The AEBs obtained at calibrator H of curves 1 and 2 (3.14 and 2.76, respectively), were far more optimal than that obtained at calibrator H of curve 3 (0.364). Therefore, it would be interesting to explore a calibrator H concentration between 16 and 132 pg/mL.

We did experience one curve irregularity in the 3-step protocol at calibrators D, E and F of curve 3 (Table 4.42). However, similar to what we observed with $A\beta_{43}$, this irregularity is of a far smaller magnitude to what we experienced earlier in the optimisation process on this instrument, depicted in Table 4.40. Whilst the AEBs generally require enhancement, the S/N obtained at calibrator B of curve 3 (1.56; AEB 0.00831) appeared sufficient to carry forward for further optimisation. However, keeping curve 2 in consideration, exploring a calibrator B concentration between 0.0305 and 0.0718 pg/mL may also be of benefit.

$A\beta_{43}$ calibrator	**Curve 1**			**Curve 2**			**Curve 3**		
	Concentration (pg/mL)	Mean AEB (S/N)	Mean AEB (S/N)	Concentration (pg/mL)	Mean AEB (S/N)	Mean AEB (S/N)	Concentration (pg/mL)	Mean AEB (S/N)	Mean AEB (S/N)
		2-step	3-step		2-step	3-step		2-step	3-step
A	**0**	0.0109	0.0163	**0**	0.00801	0.0141	**0**	0.00823	0.00975
B	**0.125**	0.00722 (0.663)	0.0231 (1.41)	**0.0781**	0.00822 (1.03)	0.0147 (1.04)	**0.0122**	0.00707 (0.860)	0.0136 (1.40)
C	**0.5**	0.0129 (1.19)	0.0216 (1.33)	**0.313**	0.0127 (1.59)	0.0147 (1.05)	**0.0488**	0.00768 (0.934)	0.0103 (1.06)
D	**2**	0.0160 (1.47)	0.0351 (2.15)	**1.25**	0.0114 (1.42)	0.0199 (1.41)	**0.195**	0.00670 (0.814)	0.0155 (1.59)
E	**8**	0.0298 (2.74)	0.0925 (5.67)	**5**	0.0206 (2.57)	0.0580 (4.12)	**0.781**	0.0118 (1.44)	0.0254 (2.60)
F	**32**	0.129 (11.9)	0.351 (21.5)	**20**	0.0849 (10.6)	0.176 (12.5)	**3.13**	0.00942 (1.14)	0.0532 (5.46)
G	**128**	0.714 (65.6)	0.982 (60.2)	**80**	0.359 (44.8)	0.557 (39.6)	**12.5**	0.0608 (7.39)	0.142 (14.5)
H	**512**	5.19 (477)	3.93 (241)	**320**	2.79 (348)	2.46 (175)	**50**	0.280 (34.1)	0.548 (56.2)
Relation to HDx curve	10x lower			Cal H = cal D of HDx			100x lower		

Table 4.41 - SRx Pro $A\beta_{43}$ calibration curve optimisation

$A\beta_{pE3-40}$ calibrator	**Curve 1**			**Curve 2**			**Curve 3**		
	Concentration (pg/mL)	Mean AEB (S/N)	Mean AEB (S/N)	Concentration (pg/mL)	Mean AEB (S/N)	Mean AEB (S/N)	Concentration (pg/mL)	Mean AEB (S/N)	Mean AEB (S/N)
		2-step	3-step		2-step	3-step		2-step	3-step
A	**0**	0.00131	0.00548	**0**	0.00339	0.00500	**0**	0.00380	0.00531
B	**0.0881**	0.00292 (2.22)	0.00838 (1.53)	**0.0718**	0.00475 (1.40)	0.0111 (2.21)	**0.00870**	0.00462 (1.21)	0.00831 (1.56)
C	**0.308**	0.00427 (3.26)	0.0135 (2.46)	**0.251**	0.00405 (1.19)	0.0190 (3.80)	**0.0305**	0.00271 (0.714)	0.0110 (2.07)
D	**1.08**	0.0110 (8.37)	0.0284 (5.18)	**0.880**	0.0110 (3.24)	0.0227 (4.54)	**0.107**	0.00445 (1.17)	0.0277 (5.22)
E	**3.78**	0.0331 (25.2)	0.0926 (16.9)	**3.08**	0.0267 (7.87)	0.0695 (13.9)	**0.373**	0.00710 (1.87)	0.0165 (3.10)
F	**13.2**	0.117 (89.5)	0.267 (48.7)	**10.8**	0.0828 (24.4)	0.218 (43.6)	**1.31**	0.0115 (3.03)	0.0365 (6.86)
G	**46.3**	0.376 (286)	0.779 (142)	**37.7**	0.342 (101)	0.746 (149)	**4.57**	0.0396 (10.4)	0.116 (21.8)
H	**162**	2.12 (1614)	3.14 (574)	**132**	1.81 (534)	2.76 (551)	**16**	0.172 (45.3)	0.364 (68.6)
Relation to HDx curve	10x lower			Cal H = cal D of HDx			100x lower		

Table 4.42 - SRx Pro $A\beta_{pE3-40}$ calibration curve optimisation

4.4.4.2 Poisson inconsistency unlikely to be the cause of SRx Pro assay development challenges

In section 4.4.4.1.1 Challenge 1: "Low intensity single precision" error, we discussed the reliance of Simoa on Poisson statistics to calculate AEBs using the $AEB_{piecewise}$ equations, which assume the target analyte is Poisson consistent (i.e. follows a Poisson distribution of molecules over the beads). However, in May 2023, Zhang and colleagues (381) published a paper exploring the issues with the $AEB_{piecewise}$ calculation method, namely when $AEB_{digital} \neq AEB_{analog}$, which occurs when the analyte is not Poisson consistent. An analyte being Poisson inconsistent results in I_{single} no longer being representative of a single enzyme binding event on the beads, thus resulting in inaccurate/imprecise AEB values, along with a discontinuity in AEB values around the 0.7 threshold differentiating between the use of the $AEB_{piecewise}$ equations (381). This is of importance for our assays as Zhang and colleagues discovered the $A\beta_{40}$ analyte in the N4PE assay to be Poisson inconsistent, most likely due to its aggregative nature. Given that our assays also measure Aβ analytes that are prone to aggregation, it is possible that they too exhibited Poisson inconsistency, which may explain the cause of the "poor intensity single precision errors", and the "up-down" nature of our calibration curves, both of which significantly impacted our ability to develop and optimise our assays on the SRx Pro instrument.

Zhang and colleagues (381) describe two methods for identifying Poisson inconsistency within an assay – 1) graphically, by plotting a graph of f_{on} against I_{bead}[13]/I_{single}; or 2) numerically using the equation:

$$n = \left(\frac{f_{on} \times I_{bead}}{-\ln(1 - f_{on}) \times I_{single}} \right)_{when\ 0.55 < f_{on} < 0.85}$$

[13] I_{bead} = mean fluorescence intensity of active beads in an array

Where n = 1 indicates a perfect Poisson distribution of enzyme complexes on the beads, and hence a perfectly Poisson consistent analyte. This equation should be applied only to data points where f_{on} is between 0.55 and 0.85 because before and after the threshold of 0.7 is where deviations from the Poisson distribution will have the greatest effect on accurate AEB measurements (381). Upon applying this to the three calibration curves investigated on the SRx Pro using the 3-step assay protocol (Table 4.41and Table 4.42), we observed a poor yield of data points with an f_{on} between 0.55 and 0.85 across most curves, with only two data points from curve 1 of $A\beta_{43}$ and one data point from curve 2 of $A\beta_{pE3\text{-}40}$ within the f_{on} threshold for calculating n. Regardless, curve 1 of $A\beta_{43}$ displayed an n value of 1.02, and curve 2 of $A\beta_{pE3\text{-}40}$ an n value of 1.00, seen graphically in Figure 4.8. This highlights a strong Poisson consistency in our assays, much to our surprise. To confirm whether this has always been the case for our assays, we calculated n for all of our experiments on the SRx Pro, and the CSF analysis experiment on the HDx, and discovered a consistent $n \approx 1$ throughout (data not shown).

Whilst our analytes were not Poisson inconsistent, some of the principles discussed by Zhang and colleagues (381) may still apply. It is possible that our challenges with developing our assays on the SRx Pro may have been due to a suboptimal antibody binding efficiency on the beads, the effects of which may have been enhanced by the additional sensitivity and lower analyte concentrations used on the SRx Pro. Therefore, exploring alternative bead conjugation protocols to enhance the efficiency and strength of antibody binding may prove beneficial. One way to do this would be through the use of a sulfo-N-hydroxysulfosuccinimide (S-NHS) and EDC bead conjugation method. The addition of S-NHS, rather than using EDC alone as was used for our beads, produces a stronger link

between the beads and antigen, offering up to 80-90% antibody binding efficiency (382).

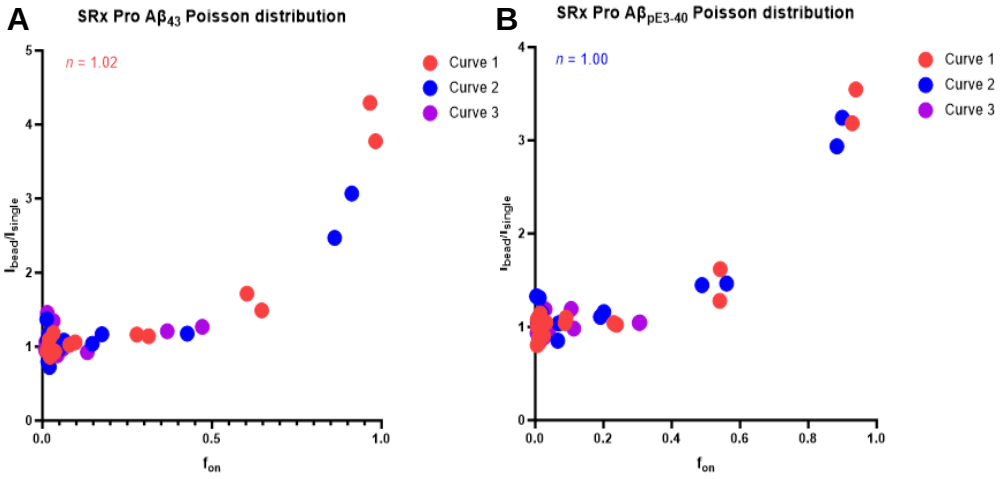

Figure 4.8 - SRx Pro Aβ$_{43}$ and Aβ$_{pE3-40}$ Poisson distribution

*Amyloid-β 1-43 (Aβ$_{43}$) and pyroglutamate amyloid-β 3-40 (Aβ$_{pE3-40}$) Poisson distribution graph plots for calibration curves 1 to 3 tested on the SRx Pro (see Table 4.41 and Table 4.42). **A**: Aβ$_{43}$ showed an n-value of 1.02 for curve 1. n-values could not be calculated for curves 2 and 3; **B**: Aβ$_{pE3-40}$ showed an n-value of 1.00 for curve 2. n-values could not be calculated for curves 1 and 3; 'f$_{on}$' indicates fraction of enzyme-associated (on) beads; 'I$_{bead}$', mean fluorescence intensity of active beads in an array; 'I$_{single}$', mean fluorescence intensity of a single enzyme complex on a bead*

4.4.4.3 SRx Pro assay development summary

To summarise, the development of our assays on the SRx Pro was greatly hindered by two key challenges – 1) a frequent "low intensity single precision" error, resulting in sporadic AEB output from the instrument; and 2) the unconventional nature of our calibration curves. Working through these challenges, we managed to produce data on the SRx Pro to highlight an increase in sensitivity for the Aβ$_{43}$ assay from a calibrator B concentration of 9.94 pg/mL on the HDx (see section 4.4.5 Refining HDx assays) to between 0.0488 and 0.125 pg/mL, equating to a sensitivity increase of between 79.5- and 204-fold, and for the Aβ$_{pE3-40}$ assay from a calibrator B concentration of 3.75 pg/mL on the HDx (see section 4.4.5 Refining HDx assays) to between 0.0305 and 0.0718 pg/mL, equating to a sensitivity increase of between 52.2- and 123-fold. Whilst these assays require further optimisation and validation on this instrument, these results are promising.

4.4.5 Refining HDx assays

In light of the challenges faced in developing our assays on the SRx Pro instrument, we decided it would be of benefit to refine our HDx assays – namely: 1) extend the calibration curves from six-points to eight-points with a lower concentration calibrator H to better fit with the dynamic range of the analytes and existing ELISA assays; 2) investigate the dilution linearity and spike recovery using a spiked known concentration of analyte; and 3) remeasure CSF samples from section 4.4.3.10 HDx pilot CSF $A\beta_{43}$ and $A\beta_{pE3\text{-}40}$ measurements with the refined calibration curve. Although we could not detect $A\beta_{43}$ or $A\beta_{pE3\text{-}40}$ in all samples during our pilot experiments in CSF, to our knowledge, these are the first $A\beta_{43}$ and $A\beta_{pE3\text{-}40}$ assays to ever be developed on the Simoa instrument. As such, we wanted to make them as robust as possible.

4.4.5.1 Calibration curve re-optimisation

Using the calibration curves of the established ELISA assays for our two analytes as a starting point (see Table 4.1), we tested six different eight-point calibration curves. The primary aim of this re-optimisation was to see how low we could take calibrators B and H whilst still being able to obtain an acceptable range of AEBs and S/Ns across the calibration curve.

4.4.5.1.1 $A\beta_{43}$ assay

All six curves produced AEBs at all calibration points (Table 4.43). However, curves 5 and 6, which both had a calibrator H concentration of 100 pg/mL, had too narrow a range of AEBs to consider carrying them forward. We initially proceeded with Curve 4 (0.614 to 150 pg/mL), mainly in an attempt to obtain increased sensitivity beyond that of the IBL ELISA assay. However, further testing highlighted that calibrator B of both curves 3 and 4 did not produce high enough AEBs consistently, even after increasing the concentration of SβG (data not shown). As such, we opted to proceed with Curve 2 (9.94 to 240 pg/mL). Looking at the AEB of

calibrator H at 240 pg/mL (Curves 1 and 2), it was clear that we would not obtain values as high as is optimal for Simoa assays (see section 4.2.5 Optimal characteristics of a Simoa assay). However, upon increasing the concentration of SβG from 150pM to 300pM, our AEBs increased sufficiently to warrant continuing with this curve (data not shown).

4.4.5.1.2 $A\beta_{pE3\text{-}40}$ assay

All six curves produced an acceptable range of AEBs across the calibration curve (Table 4.44), highlighting that the HDx offers an increased level of sensitivity for this analyte compared to the ELISA assay for $A\beta_{pE3}$, which uses a calibration curve range of 7.75 to 496 pg/mL (Curve 2; see also Table 4.1). We opted to proceed with Curve 4 (3.75 to 240 pg/mL) as the AEB obtained for calibrator H was sufficiently high enough, given the lower dynamic range of our refined assay. Similar to the $A\beta_{43}$ assay, increasing the concentration of SβG to 300pM enhanced the AEBs, further supporting the selection of this curve.

Calibrator	Curve 1		Curve 2		Curve 3		Curve 4		Curve 5		Curve 6	
	Concentration (pg/mL)	Mean AEB (S/N)	Concentration (pg/mL)	Mean AEB (S/N)	Concentration (pg/mL)	Mean AEB (S/N)	Concentration (pg/mL)	Mean AEB (S/N)	Concentration (pg/mL)	Mean AEB (S/N)	Concentration (pg/mL)	Mean AEB (S/N)
A	0	0.00891	0	0.00846	0	0.00895	0	0.00738	0	0.00947	0	0.0119
B	21.1	0.0234 (2.62)	9.94	0.0169 (2.00)	2.34	0.00972 (1.08)	0.614	0.0112 (1.51)	0.512	0.0134 (1.42)	0.410	0.0109 (0.914)
C	31.6	0.0287 (3.22)	16.9	0.0209 (2.47)	4.69	0.0134 (1.49)	1.54	0.0118 (1.60)	1.28	0.0138 (1.45)	1.02	0.0132 (1.11)
D	47.4	0.0412 (4.62)	28.7	0.0280 (3.31)	9.38	0.0182 (2.03)	3.84	0.0132 (1.79)	3.20	0.0136 (1.44)	2.56	0.0125 (1.05)
E	71.1	0.0670 (7.52)	48.8	0.0455 (5.38)	18.8	0.0220 (2.46)	9.60	0.0155 (2.10)	8.00	0.0175 (1.85)	6.40	0.0155 (1.30)
F	107	0.103 (11.6)	83.0	0.0820 (9.69)	37.5	0.0349 (3.90)	24..0	0.0257 (3.48)	20.0	0.0261 (2.75)	16.0	0.0210 (1.76)
G	160	0.173 (19.5)	141	0.159 (18.8)	75.0	0.0725 (8.10)	60.0	0.0572 (7.74)	50.0	0.0444 (4.69)	40.0	0.0357 (3.00)
H	240	0.328 (36.7)	240	0.350 (41.4)	150	0.193 (21.6)	150	0.174 (23.6)	100	0.0965 (10.2)	100	0.0981 (8.24)

Table 4.43 – HDx $A\beta_{43}$ calibration curve re-optimisation

Calibrator	Curve 1		Curve 2		Curve 3		Curve 4		Curve 5		Curve 6	
	Concentration (pg/mL)	Mean AEB (S/N)	Concentration (pg/mL)	Mean AEB (S/N)	Concentration (pg/mL)	Mean AEB (S/N)	Concentration (pg/mL)	Mean AEB (S/N)	Concentration (pg/mL)	Mean AEB (S/N)	Concentration (pg/mL)	Mean AEB (S/N)
A	0	0.00870	0	0.0112	0	0.0119	0	0.00988	0	0.0102	0	0.00876
B	10.5	0.0347 (4.00)	7.75	0.0261 (2.34)	5.10	0.0202 (1.71)	3.75	0.0170 (1.72)	1.88	0.0152 (1.49)	0.492	0.0106 (1.21)
C	20.0	0.0464 (5.33)	15.5	0.0402 (3.60)	9.69	0.0275 (2.32)	7.50	0.0219 (2.21)	3.75	0.0231 (2.26)	1.23	0.0168 (1.92)
D	38.1	0.101 (11.7)	31.0	0.0837 (7.50)	18.4	ERROR	15	0.0345 (3.52)	7.5	0.0241 (2.35)	3.07	0.0185 (2.12)
E	72.3	0.237 (27.3)	62.0	0.194 (17.4)	35.0	0.0993 (8.37)	30.0	0.0718 (7.26)	15.0	0.0394 (3.85)	7.68	0.0238 (2.72)
F	137	0.614 (70.7)	124	0.518 (46.4)	66.5	0.221 (18.7)	60.0	0.160 (16.2)	30.0	0.0790 (7.72)	19.2	0.0442 (5.05)
G	261	1.77 (204)	248	1.55 (139)	126	0.579 (48.8)	120	0.462 (46.7)	60.0	0.195 (19.0)	48.0	0.130 (14.8)
H	496	4.85 (558)	496	5.13 (460)	240	1.55 (131)	240	1.37 (138)	120	0.532 (52.0)	120	0.464 (53.0)

Table 4.44 - HDx $A\beta_{pE3\text{-}40}$ calibration curve re-optimisation

4.4.5.2 Repeated measurement of pilot CSF samples

To ascertain whether the re-optimisation of the calibration curves improved the ability of the HDx to measure our analytes of interest in clinical samples, we repeated the pilot study performed in section 4.4.3.10 HDx pilot CSF $A\beta_{43}$ and $A\beta_{pE3\text{-}40}$ measurements. However, two of the samples previously used (AD1 and MP3; Table 4.39) did not have a sufficient volume available to be retested. As such, we used two new samples of the same phenotype – AD2 and MP4. All samples were measured at the same four levels of dilution as was previously investigated – neat, 2x, 4x and 8x.

4.4.5.2.1 $A\beta_{43}$ assay

For $A\beta_{43}$, we obtained concentrations for 22 data points (68.8%; Table 4.45), 16 of which fell below the concentration of calibrator B (9.94 pg/mL) prior to accounting for the dilution factor (Figure 4.9). The highest concentrations were obtained for the neat dilution measurements of MP1 and MP4, measuring 47.4 pg/mL and 26.6 pg/mL, respectively (Table 4.45). One sample was measurable neat but unmeasurable upon dilution (CTRL2), whereas one sample was only measurable at the 8x dilution level (AD2). Three samples were measurable across all dilution levels (MP1, CTRL1 and CTRL 3). After accounting for the dilution factor, the concentrations of these three samples appeared to vary largely across each dilution level (see 'B' measurements for MP1, CTRL1 and CTRL 3 in Table 4.46), seen graphically in Figure 4.10B-D, although the variation does not appear to be as large for CTRL1 and MP1 as was seen previously (Figure 4.5B&C). Investigating the dilution linearity in these three samples more closely, they all displayed the same hook-shaped trend of an increase in observed concentration at the 8x dilution point in comparison to the expected concentration (Figure 4.10A). All three showed a strong but statistically non-significant dilution linearity, with r-values of 0.931 (95%CI -0.284-0.999; p-value 0.0687), 0.818 (95%CI -0.668-0.996; p-value 0.182) and 0.937 (95% CI -0.240-0.999) for CTRL1, CTRL3 and MP1, respectively.

4.4.5.2.2 $A\beta_{pE3-40}$ assay

In comparison, we obtained concentrations for $A\beta_{pE3-40}$ for 30 data points (93.8%; Table 4.45), 29 of which fell below the concentration of calibrator B (3.75 pg/mL) prior to accounting for the dilution factor (Figure 4.11). The highest concentrations were obtained for the 4x dilution measurement of MP4 and CTRL1, measuring 4.00 pg/mL and 3.26 pg/mL, (16.0 pg/mL and 13.0 pg/mL, respectively, after accounting for dilution factor – see Table 4.46), respectively, and the 8x measurements of AD2 and MP2, measuring 3.45 pg/mL and 3.38 pg/mL (27.6 pg/mL and 27.1 pg/mL, respectively, after accounting for dilution factor – see Table 4.46), respectively (Table 4.44). Six samples (AD2, MP1, MP2, MP4, CTRL1 and CTRL3) were measurable at all four dilution levels, with CTRL2 being unmeasurable at 4x dilution, and CTRL4 being unmeasurable at 8x dilution. After accounting for the dilution factor in these six samples, as we have seen throughout, the concentrations in these samples vary at each dilution level (see 'B' measurements for AD2, MP1, MP2, MP4, CTRL1 and CTRL3 in Table 4.46), seen graphically in Figure 4.12B-G. Investigating the dilution linearity in these six samples more closely (Figure 4.12A), CTRL3 showed a strong but statistically non-significant dilution linearity, with an r-value of 0.905 (95% CI -0.429-0.998; p-value 0.0947). In contrast, the five remaining samples showed a poor dilution linearity, with r-values of -0.582 (95% CI -0.90-0.860; p-value 0.418) and -0.0351 (95% CI -0.964-0.958; p-value 0.965) for AD2 and CTRL1, respectively, and r-values of 0.367 (95% CI -0.918-0.982; p-value 0.633), -0.315 (95% IC -0.980-0.927; p-value 0.686) and 0.131 (95% CI -0.950-0.970; p-value 0.869) for MP1, MP2 and MP4, respectively.

4.4.5.2.3 Correlation between HDx measurements

Given that six of the samples measured in this assessment had also been measured previously in section 4.4.3.10 HDx pilot CSF $A\beta_{43}$ and $A\beta_{pE3-40}$ measurements, we compared the correlation between

concentrations obtained for each dilution measurement available on both instruments. This amalgamated to seventeen comparisons in the $A\beta_{43}$ assay, but only seven in the $A\beta_{pE3\text{-}40}$ assay. For $A\beta_{43}$, we observed a statistically significant strong positive correlation, with an r-value of 0.953 (95% CI 0.870-0.983; p-value <0.0001****; Figure 4.13A). In contrast, for $A\beta_{pE3\text{-}40}$, we observed a non-significant weakly positive correlation, with an r-value of 0.368 (95% CI -0.532-0.878; p-value 0.416; Figure 4.13B). It is possible that having more data points for the $A\beta_{pE3\text{-}40}$ comparisons may have produced a stronger correlation. However, the concentrations obtained upon remeasuring the samples (measurement B) were ≥10-fold lower in concentration compared with the concentrations originally obtained in some cases (Figure 4.13B). Such a large degree of change was not seen with the $A\beta_{43}$ measurements, suggesting that this may be unique to $A\beta_{pE3\text{-}40}$. One theory is that $A\beta_{pE3\text{-}40}$ is susceptible to degradation with increasing time following sample collection. However, further investigations would need to be performed to verify this hypothesis.

4.4.5.2.4 Summary

In light of these refined results, it is clear that the sensitivity of the HDx in measuring these analytes was improved by re-optimising the calibration curves, allowing a greater proportion of samples to be measurable with both assays in comparison to the initial measurement of these samples in section 4.4.3.10 HDx pilot CSF $A\beta_{43}$ and $A\beta_{pE3\text{-}40}$ measurements. However, there are still several samples which remain unmeasurable, particularly with regards to $A\beta_{43}$. The dilution linearity remains poor in our samples, which may reflect the sensitivity limitations of this instrument for measuring our analytes. Therefore, we concluded that the HDx instrument still lacks the required sensitivity to measure $A\beta_{43}$ and/or $A\beta_{pE3\text{-}40}$ in CSF, further highlighting the need for the additional sensitivity offered by the SRx Pro.

Sample phenotype	$A\beta_{43}$ observed concentration (pg/mL)				$A\beta_{pE3-40}$ observed concentration (pg/mL)			
	Neat	2x	4x	8x	Neat	2x	4x	8x
AD2	-	-	-	3.56	2.04	1.67	2.17	3.45
MP1	47.4	13.2	8.08	10.9	2.93	2.02	3.28	1.70
MP2	8.91	6.01	-	4.02	2.34	1.55	1.91	3.38
MP4	26.6	7.85	-	0.835	2.79	2.67	4.00	1.56
CTRL1	10.8	3.17	2.22	2.84	1.30	1.31	3.26	0.201
CTRL2	9.39	-	-	-	1.71	1.89	-	0.752
CTRL3	6.96	2.36	2.46	3.44	2.37	1.12	1.40	0.825
CTRL4	11.3	-	-	2.92	2.20	1.64	2.68	-

Table 4.45 - HDx remeasured pilot CSF $A\beta_{43}$ and $A\beta_{pE3-40}$ concentrations (unadjusted)

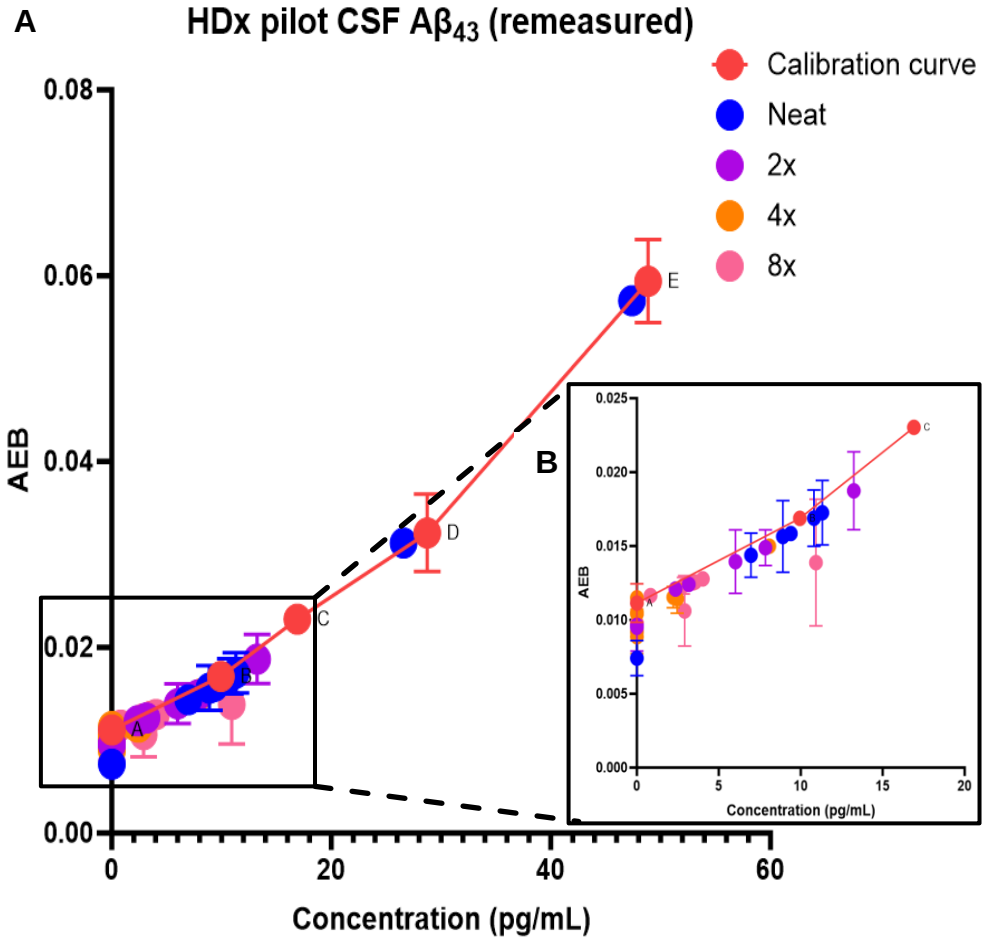

Figure 4.9 - HDx remeasured pilot CSF $A\beta_{43}$ concentrations

***A**: Amyloid-β 1-43 ($A\beta_{43}$) cerebrospinal fluid (CSF) concentrations in eight pilot cohort samples undiluted (neat) and diluted 1:2 (2x), 1:4 (4x) and 1:8 (8x) in relation to average number of enzyme complexes per bead (AEB) calculated by HDx instrument. Eight-point calibration curve was used but only calibration points A to E were included in graph. **B**: Zoom in of sample concentrations around calibration points A, B and C*

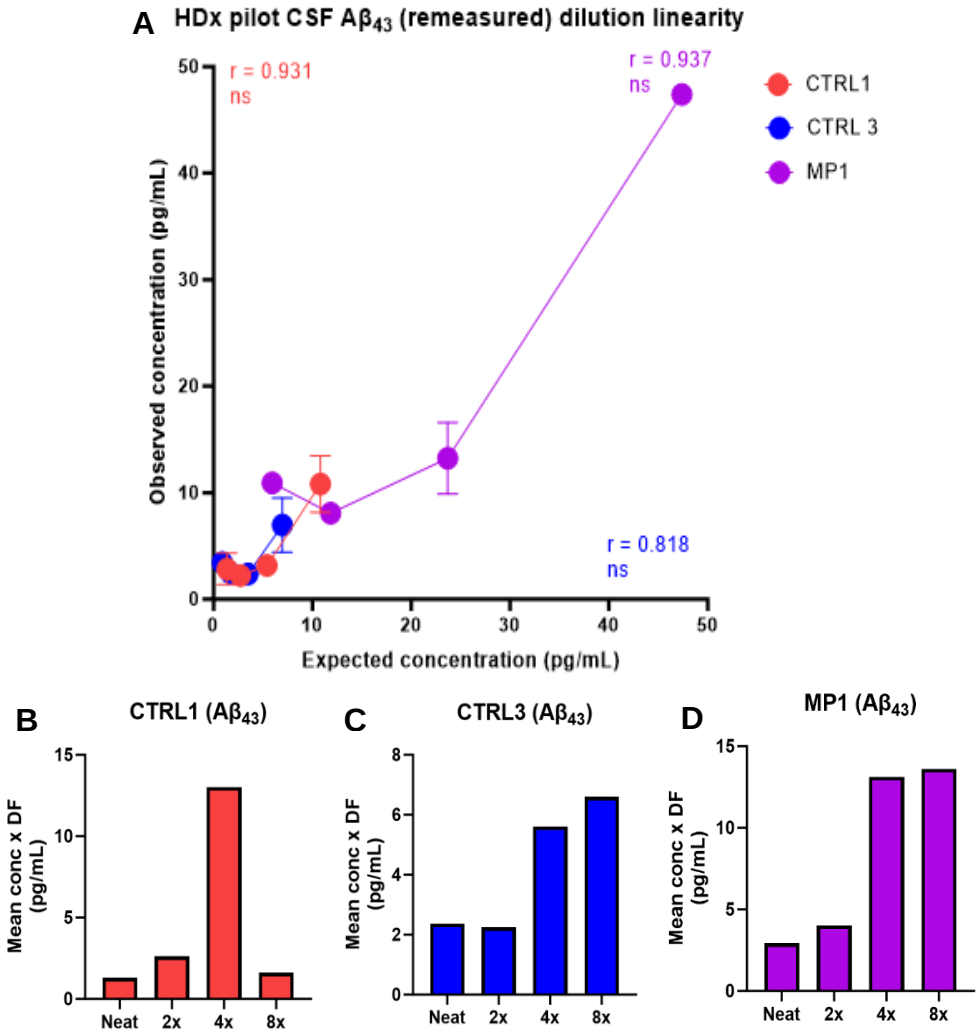

Figure 4.10 - HDx remeasured pilot CSF Aβ43 dilution linearity

***A**: Amyloid-β 1-43 (Aβ43) cerebrospinal fluid (CSF) control (CTRL) 1, CTRL3 and mixed phenotype (MP) 1 observed concentration compared with expected concentration dilution linearity. All three samples showed a strong positive but non-significant (ns) dilution linearity, with r-values of 0.931 (95%CI -0.284-0.999; p-value 0.0687), 0.818 (95%CI -0.668-0.996; p-value 0.182) and 0.937 (95% CI -0.240-0.999) for CTRL1, CTRL3 and MP1, respectively. **B**: CTRL1 Aβ43 concentrations after adjusting for extent of dilution; **C**: CTRL1 Aβ43 concentrations after adjusting for extent of dilution; **D**: MP1 Aβ43 concentrations after adjusting for extent of dilution; 'DF' indicates dilution factor*

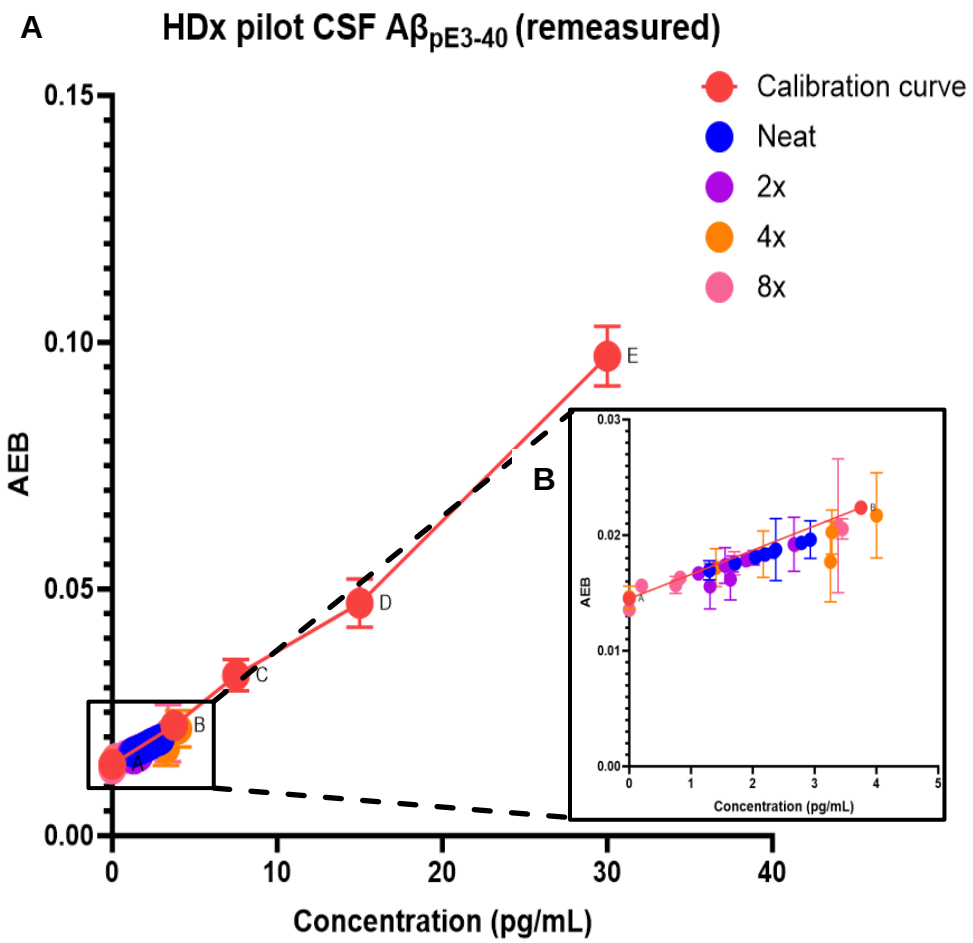

Figure 4.11 - HDx remeasured pilot CSF $A\beta_{pE3\text{-}40}$ concentrations

***A**: Pyroglutamate amyloid-β 3-40 ($A\beta_{pE3\text{-}40}$) cerebrospinal fluid (CSF) concentrations in eight pilot cohort samples undiluted (neat) and diluted 1:2 (2x), 1:4 (4x) and 1:8 (8x) in relation to average number of enzyme complexes per bead (AEB) calculated by HDx instrument. Eight-point calibration curve was used but only calibration points A to E were included in graph. **B**: Zoom in of sample concentrations around calibration points A and B.*

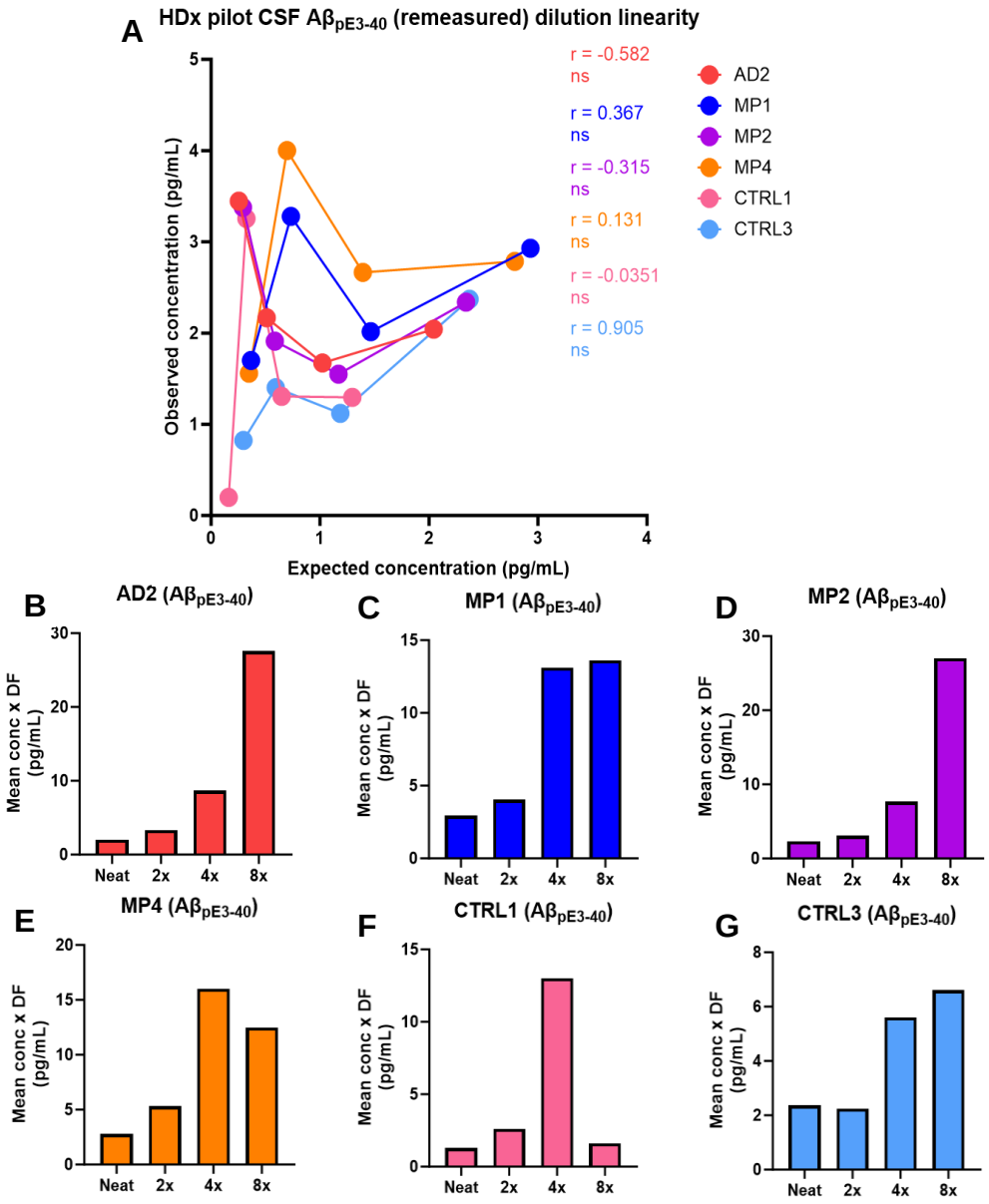

Figure 4.12 - HDx remeasured pilot CSF Aβ$_{pE3-40}$ dilution linearity

***A**: Pyroglutamate amyloid-β 3-40 (Aβ$_{pE3-40}$) cerebrospinal fluid (CSF) Alzheimer's disease (AD) 2, mixed phenotype (MP) 1, MP2, MP4, control (CTRL) 1 and CTRL3 observed concentration compared with expected concentration dilution linearity. CTRL3 showed a strong but statistically non-significant linearity, with an r-value of 0.905 (95% CI -0.429-0.998; p-value 0.0947). The five remaining samples showed a poor linearity, with r-values of -0.582 (95% CI -0.90-0.860; p-value 0.418) and -0.0351 (95% CI -0.964-0.958; p-value 0.965) for AD2 and CTRL1, respectively, and r-values of 0.367 (95% CI -0.918-0.982; p-value 0.633), -0.315 (95% IC -0.980-0.927; p-value 0.686) and 0.131 (95% CI -0.950-0.970; p-value 0.869) for MP1, MP2 and MP4, respectively. **B**: AD2 Aβ$_{pE3-40}$ concentrations after adjusting for extent of dilution; **C**: MP1 Aβ$_{pE3-40}$ concentrations after adjusting for extent of dilution; **D**: MP2 Aβ$_{pE3-40}$ concentrations after adjusting for extent of dilution; **E**: MP4 Aβ$_{pE3-40}$ concentrations after adjusting for extent of dilution; **F**: CTRL1 Aβ$_{pE3-40}$ concentrations after adjusting for extent of dilution; **G**: CTRL3 Aβ$_{pE3-40}$ concentrations after adjusting for extent of dilution; 'DF' indicates dilution factor*

Sample phenotype	$A\beta_{43}$ observed concentration x dilution factor (pg/mL)								$A\beta_{pE3-40}$ observed concentration x dilution factor (pg/mL)							
	Neat		**2x**		**4x**		**8x**		**Neat**		**2x**		**4x**		**8x**	
	A	**B**	**A**	**B**	**A**	**B**	**A**	**B**	**A**	**B**	**A**	**B**	**A**	**B**	**A**	**B**
AD1	8.84		-		-		86.1		27.2		-		-		33.2	
AD2		-		-		-		28.5		2.04		3.34		8.67		27.6
MP1	103	47.4	51.4	26.5	30.2	32.3	63.4	87.4	41.5	2.93	0.0816	4.03	-	13.1	13.4	13.6
MP2	7.60	8.91	18.7	12.0	-	-	102	32.2	-	2.34	-	3.10	-	7.65	-	27.1
MP3	10.0		-		-		-		5.68		-		-		Instrument error	
MP4		26.6		15.7		-		6.68		2.79		5.33		16.0		12.5
CTRL1	6.36	10.8	12.0	6.35	10.1	8.89	96.3	22.7	-	1.30	-	2.62	9.47	13.0	-	1.61
CTRL2	15.4	9.39	-	-	-	-	-	-	12.5	1.71	-	3.78	-	-	-	6.01
CTRL3	13.9	6.96	23.4	4.72	19.9	9.83	-	27.5	24.6	2.37	-	2.24	-	5.61	-	6.60
CTRL4	15.9	11.3	-	-	-	-	-	23.3	8.15	2.20	-	3.27	-	10.7	Instrument error	-

HDx pilot CSF $A\beta_{43}$ and $A\beta_{pE3-40}$ concentrations adjusted for dilution factor. 'A' refers to measurements conducted in section 4.4.3.10 HDx pilot CSF Aβ43 and AβpE3-40 measurements. 'B' refers to measurements conducted in section 4.4.5.2 Repeated measurement of pilot CSF samples. 'Instrument error' refers to measurements not obtained due to an unexpected instrument error.

Table 4.46 - HDx all pilot CSF $A\beta_{43}$ and $A\beta_{pE3-40}$ concentrations (adjusted)

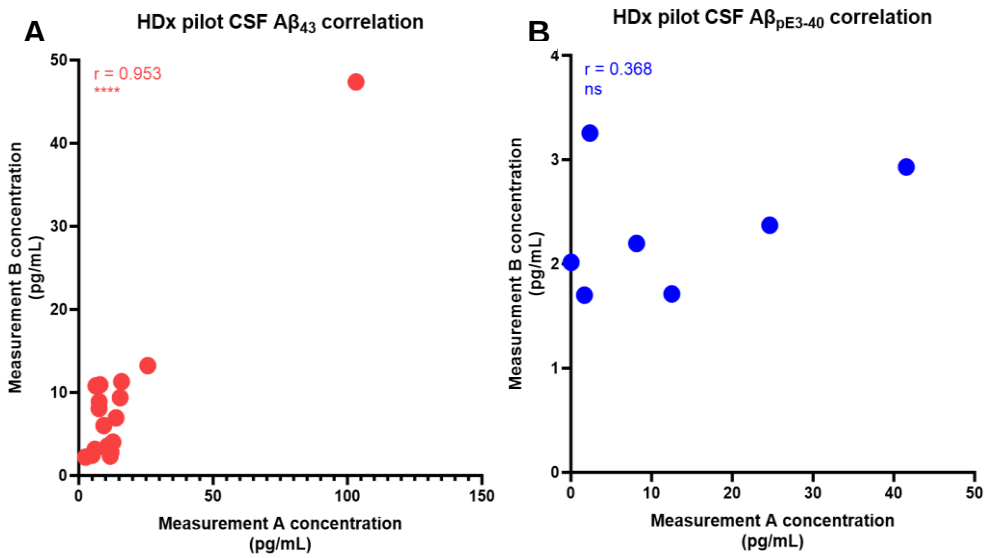

Figure 4.13 - HDx pilot CSF $A\beta_{43}$ and $A\beta_{pE3-40}$ correlation

Correlation of pilot cerebrospinal fluid (CSF) amyloid-β 1-43 ($A\beta_{43}$) and pyroglutamate amyloid-β 3-40 ($A\beta_{pE3-40}$) measurements conducted in section 4.4.3.10 HDx pilot CSF Aβ43 and AβpE3-40 measurements (measurement A) and section 4.4.5.2 Repeated measurement of pilot CSF samples (measurement B). ***A****: $A\beta_{43}$ showed a statistically significant strong positive correlation between measurements A and B, with an r-value of 0.953 (95% CI 0.870-0.983; p-value <0.0001****). **B**: $A\beta_{pE3-40}$ showed a non-significant (ns) weakly positive correlation, with an r-value of 0.368 (95% CI -0.532-0.878; p-value 0.416).*

4.4.5.3 Dilution linearity and spike recovery

Given that there appeared to be poor dilution linearity in our CSF samples measured first in section 4.4.3.10 HDx pilot CSF $A\beta_{43}$ and $A\beta_{pE3\text{-}40}$ measurements, and again in section 4.4.5.2 Repeated measurement of pilot CSF samples using a refined calibration curve, we decided to further investigate the dilution linearity using three additional CTRL CSF samples. We spiked each sample with 400 pg/mL of calibrator material and performed a 1:2 serial dilution six times for $A\beta_{43}$ and seven times for $A\beta_{pE3\text{-}40}$ (due to the lower calibrator B concentration for the $A\beta_{pE3\text{-}40}$ assay). Alongside assessing the dilution linearity, we also assessed the recovery of the spiked peptide in comparison to the concentration measured by the HDx for the undiluted (neat) sample. Whilst a conventional spike recovery assessment includes the measurement of the samples without calibration material spiked into it (372), the sensitivity challenges of our assays on the HDx meant we opted to measure only spiked dilutions of our samples. A recovery within 80-120% of the expected concentration was deemed acceptable.

4.4.5.4.1 $A\beta_{43}$ assay

Of the 400 pg/mL of calibration material spiked into the neat samples, we obtained concentrations of 227 pg/mL, 208 pg/mL and 234 pg/mL for CSF samples 1, 2 and 3, respectively, indicating a % recovery of the spiked peptide of 56.8%, 52.0% and 58.5%, respectively (Table 4.47). Using the expected concentration as a fraction of the observed neat sample concentration, across all dilution levels within our three samples, the percentage of peptide recovered was within acceptable limits 0/18 times, with most samples recovering >120% of the peptide, and a mean spike recovery across all dilution levels of 128%, 167% and 148% for CSF samples 1, 2 and 3, respectively. Given that the samples tested were CTRLs, it is possible that there was endogenous $A\beta_{43}$ present alongside the spiked synthetic peptide, thus resulting in a greater recovery. However, when we calculated the percentage of peptide recovered

as a fraction of the spiked peptide concentration, the recovery was within acceptable limits 11/21 times, with most samples recovering <90% of the peptide, and a mean spike recovery across all dilution levels of 70.5%, 82.0% and 82.3% for CSF samples 1, 2 and 3, respectively. This suggests, rather, that the CSF matrix may be suppressing and interfering with the detection of our analyte.

Looking more closely at the linear relationship between observed and expected $A\beta_{43}$ concentration in each sample upon increasing dilution, we obtained a strong statistically significant linearity, with r-values of 0.979 (95% CI 0.860-0.997; p-value 0.0001***), 0.969 (95% CI 0.797-0.996; p-value 0.0003***) and 0.977 (95% CI 0.848-0.997; p-value 0.0001***) for CSF 1, 2 and 3, respectively (Figure 4.14A). After accounting for the dilution factor, the concentrations for each spiked CSF remain relatively stable (Figure 4.14B-D).

4.4.5.4.2 $A\beta_{pE3-40}$ assay

Of the 400 pg/mL of calibration material spiked into the neat samples, we obtained concentrations of 226 pg/mL, 227 pg/mL and 256 pg/mL for CSF samples 1, 2 and 3, respectively, indicating a % recovery of the spiked peptide of 56.5%, 56.8% and 64.0%, respectively (Table 4.48). Using the expected concentration as a fraction of the observed neat sample concentration, across all dilution levels within our three samples, the percentage of peptide recovered was within acceptable limits 10/21 times, with most samples recovering >110% of the peptide, and mean spike recovery across all dilution levels of 126%, 125% and 116% for CSF samples 1, 2 and 3, respectively. However, when we calculated the percentage of peptide recovered as a fraction of the spiked peptide concentration, the recovery was within acceptable limits 3/24 times, with most samples recovering <80% of the peptide, and a mean spike recovery across all dilution levels of 69.7%, 69.3% and 73.3 for CSF samples 1, 2 and 3, respectively. This decrease in the number of recoveries within acceptable limits further supports that the CSF matrix may be

suppressing and interfering with the detection of $A\beta_{pE3-40}$, and to a greater extent than that seen with $A\beta_{43}$.

Looking more closely at the linear relationship between observed and expected $A\beta_{pE3-40}$ concentration in each sample upon increasing dilution, we obtained a strong statistically significant linearity, with *r*-values of 0.993 (95% CI 0.961-0.999; p-value<0.0001****), 0.989 (95% CI 0.937-0.998; p-value <0.0001****) and 0.995 (95% CI 0.974-0.999; p-value <0.0001****) for CSF 1, 2 and 3, respectively (Figure 4.15A). After accounting for the dilution factor, the concentrations for each spiked CSF remain relatively stable (Figure 4.15B-D).

CSF sample	Dilution factor	Observed concentration (pg/mL)	Expected concentration of neat sample (pg/mL)	Peptide recovery of neat (%)	Expected concentration of spiked $A\beta_{43}$ (pg/mL)	Peptide recovery of spiked (%)
1	Neat	227	-	-	400	56.8
	2x	156	114	137	200	78.0
	4x	91.2	56.8	161	100	91.2
	8x	37.4	28.4	132	50	74.8
	16x	18.9	14.2	133	25	75.6
	32x	9.68	7.10	136	12.5	77.4
	64x	2.50	3.55	70.4	6.25	40.0
2	Neat	208	-	-	400	52.0
	2x	157	104	151	200	78.5
	4x	85.2	52.0	164	100	85.2
	8x	44.9	26.0	173	50	89.8
	16x	20.8	13.0	160	25	83.2
	32x	11.1	6.50	170	12.5	88.8
	64x	6.05	3.25	186	6.25	96.8
3	Neat	234	-	-	400	58.5
	2x	169	117	145	200	84.5
	4x	86.1	58.5	147	100	86.1
	8x	38.0	29.3	130	50	76.0
	16x	20.4	14.6	140	25	81.6
	32x	10.8	7.31	147	12.5	86.4
	64x	6.45	3.66	176	6.25	103

Table 4.47 - HDx $A\beta_{43}$ dilution linearity and spike recovery

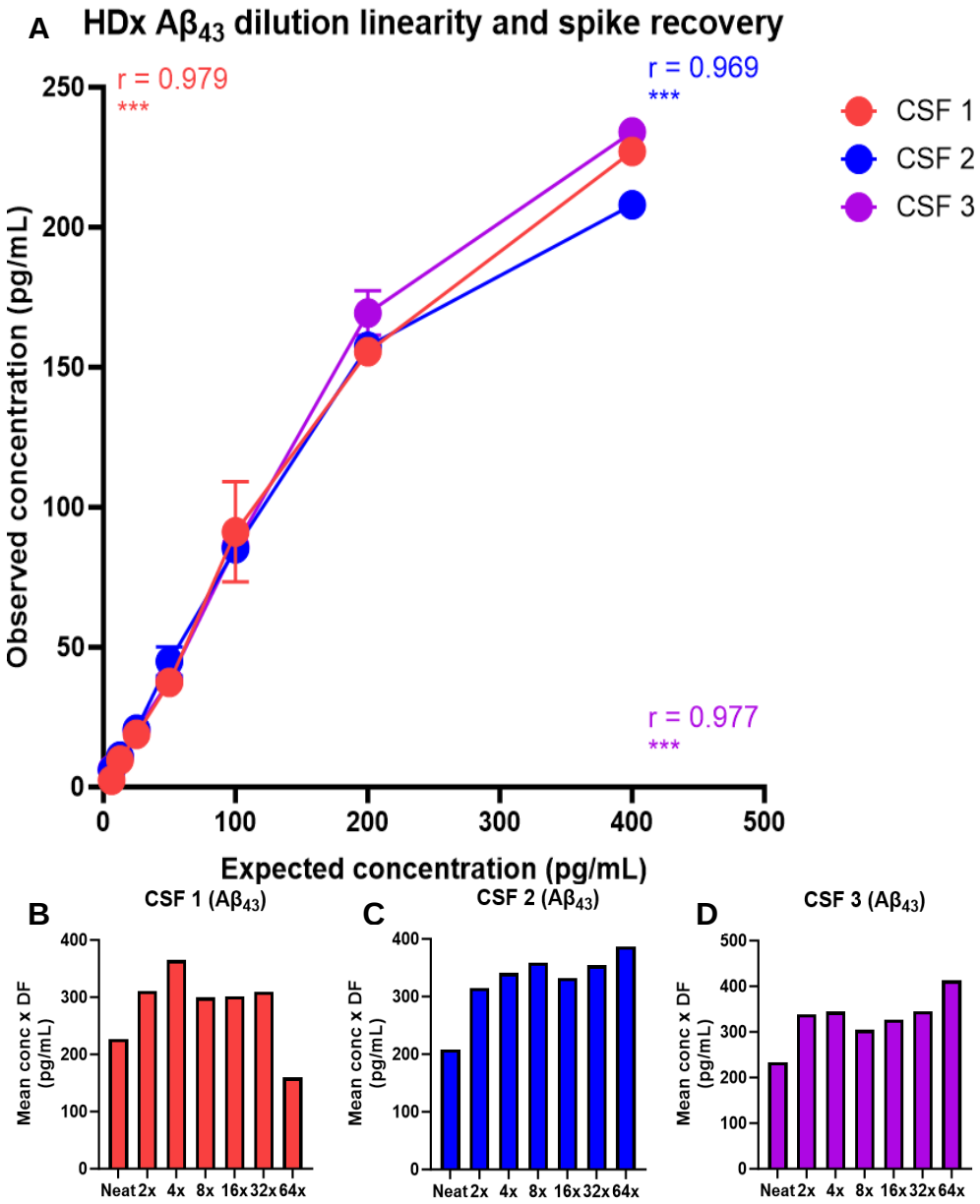

Figure 4.14 - HDx Aβ43 dilution linearity and spike recovery

A**: Amyloid-β 1-43 (Aβ43) dilution linearity and spike recovery in three control cerebrospinal fluid (CSF) samples spiked with Aβ43 custom peptide 3. All three CSF samples showed a strong statistically significant dilution linearity, with r-values of 0.979 (95% CI 0.860-0.997; p-value 0.0001), 0.969 (95% CI 0.797-0.996; p-value 0.0003***) and 0.977 (95% CI 0.848-0.997; p-value 0.0001***) for CSF 1, 2 and 3, respectively. **B**: Concentrations (conc) obtained at each dilution level for CSF 1, adjusted for dilution factor (DF). **C**: Conc obtained at each dilution level for CSF 2, adjusted for DF. **D**: Conc obtained at each dilution level for CSF 3, adjusted for DF.*

CSF sample	Dilution factor	Observed concentration (pg/mL)	Expected concentration of neat (pg/mL)	Peptide recovery of neat (%)	Expected concentration of spiked (pg/mL)	Peptide recovery of spiked (%)
1	Neat	226	-	-	400	56.5
	2x	141	113	125	200	70.5
	4x	69.2	56.6	122	100	69.2
	8x	31.2	28.3	110	50	62.4
	16x	16.2	14.2	115	25	64.8
	32x	7.89	7.08	111	12.5	63.1
	64x	5.18	3.54	146	6.25	82.9
	128x	2.76	1.77	156	3.125	88.3
2	Neat	227	-	-	400	56.8
	2x	150	113	132	200	75.0
	4x	72.4	56.7	128	100	72.4
	8x	33.2	28.4	117	50	66.4
	16x	17.3	14.2	122	25	69.2
	32x	9.15	7.09	129	12.5	73.2
	64x	4.12	3.55	116	6.25	65.9
	128x	2.35	1.77	132	3.125	75.2
3	Neat	256	-	-	400	64.0
	2x	154	128	121	200	77.0
	4x	73.5	64.0	115	100	73.5
	8x	34.1	32.0	106	50	68.2
	16x	17.1	16.0	107	25	68.4
	32x	9.16	8.00	115	12.5	73.3
	64x	4.35	4.00	109	6.25	69.6
	128x	2.87	2.00	144	3.125	91.8

Table 4.48 - HDx $A\beta_{pE3\text{-}40}$ dilution linearity and spike recovery

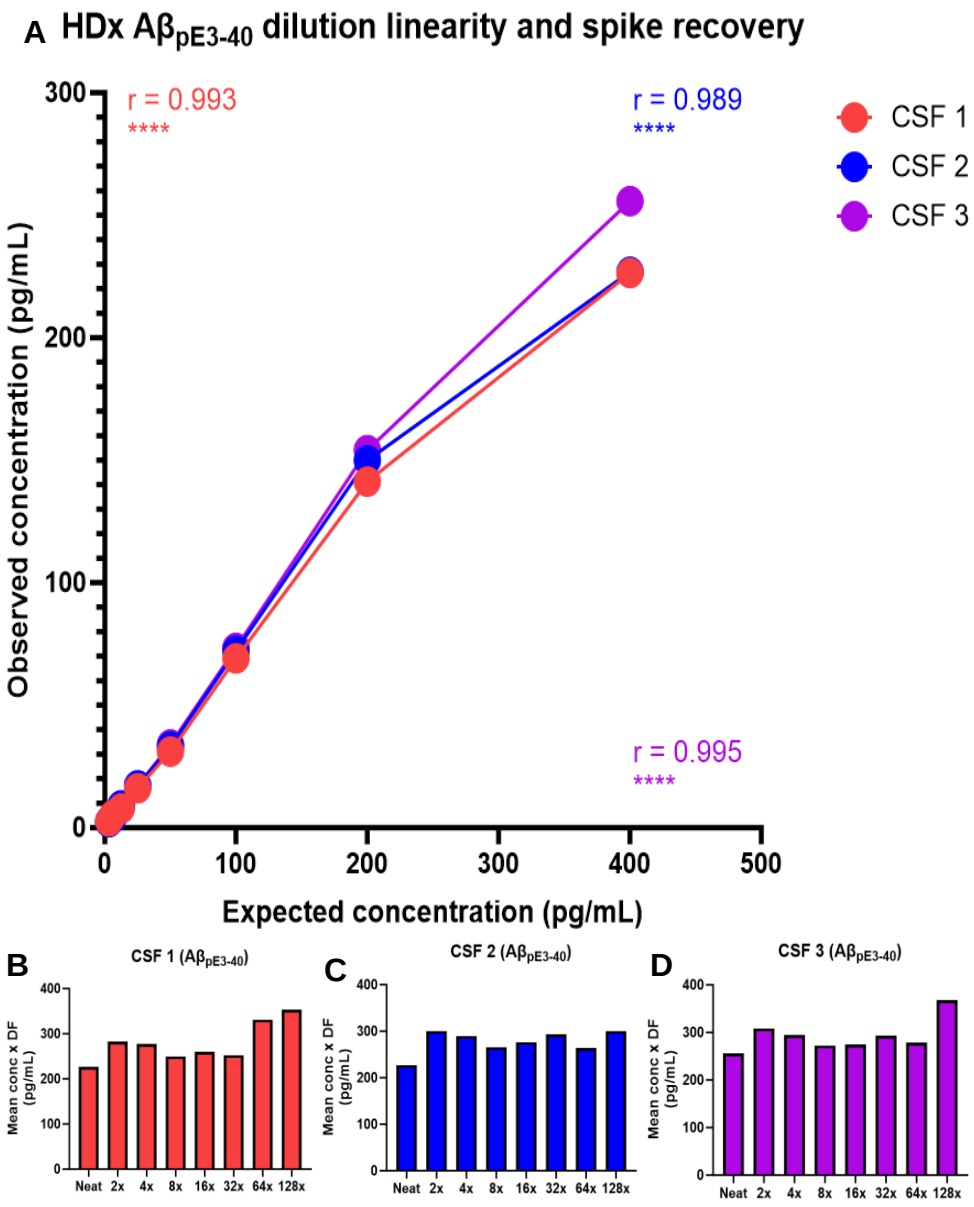

Figure 4.15 - HDx Aβ$_{pE3-40}$ dilution linearity and spike recovery

A: Pyroglutamate amyloid-β 3-40 (Aβ$_{pE3-40}$) dilution linearity and spike recovery in three control cerebrospinal fluid (CSF) samples spiked with Aβ$_{pE3-40}$ peptide. All three CSF samples showed a strong statistically significant dilution linearity, with r-values of 0.993 (95% CI 0.961-0.999; p-value<0.0001****), 0.989 (95% CI 0.937-0.998; p-value <0.0001****) and 0.995 (95% CI 0.974-0.999; p-value <0.0001****) for CSF 1, 2 and 3, respectively. **B**: Concentrations (conc) obtained at each dilution level for CSF 1, adjusted for dilution factor (DF). **B**: Conc obtained at each dilution level for CSF 2, adjusted for DF. **B**: Conc obtained at each dilution level for CSF 3, adjusted for DF.

4.5 General Discussion

In this chapter, we have gone through the process of developing novel $A\beta_{43}$ and $A\beta_{pE3\text{-}40}$ Simoa assays, beginning on the standard SRx, moving onto the HDx and SRx Pro, then returning to the HDx to finalise our assays. On the HDx and SRx, we followed stages 1 to 4 of the seven stages of assay development outlined in section 4.3, delving briefly into stages 5 to 7 on the HDx instrument. Andreasson and colleagues (372) describe further validation assessments that should be performed during the development of novel immunoassays. Given the challenges faced during the development of our assays on the SRx Pro, we were unable to further validate our assays using the protocols described in their paper, particularly given that the HDx did not perform sufficiently to warrant conducting these additional validation tests. However, given the promising initial results on the SRx Pro, highlighting the potential for increased sensitivity for our assays on this instrument, it would be of benefit to perform these validation tests at a future date.

4.5.1 Assay sensitivity

Comparing the calibration curves we initially optimised on the HDx to the curves we re-optimised following the challenges we faced on the SRx Pro, it is clear that prioritising optimal AEB values hindered the sensitivity of our assays, particularly given that our target concentration range for both analytes lies below 20 pg/mL. This is further highlighted by the increase in the number of CSF measurements obtained using the re-optimised calibration curves, with an increase from 19 to 22 measurements for $A\beta_{43}$ and from 10 to 30 for $A\beta_{pE3\text{-}40}$ (Table 4.46). Had we prioritised the target analyte range from the beginning, we would have had the opportunity to explore additional methods for enhancing the AEB, such as altering: 1) antibody and EDC concentrations for bead preparation; 2) molar excess of biotin for detector biotinylation; or 3) the time length of incubations with the beads/detector/SβG.

With the $A\beta_{pE3-40}$ assay, we were able to obtain a small increase in the level of sensitivity using the HDx compared with the IBL ELISA $A\beta_{pE3}$ assay, with calibration curves ranging from 3.75 to 240 pg/mL and 7.75 to 496 pg/mL, respectively. In contrast, the opposite is true with the $A\beta_{43}$ assay, with calibration curves ranging from 9.94 to 240 pg/mL on the HDx compared with 2.34 to 150 pg/mL on the IBL ELISA assay. One possible reason for the lower sensitivity may be the antibodies purchased to develop our assays. Whilst there were limited antibodies available to purchase for the development of the $A\beta_{pE3-40}$ assay, as highlighted in Figure 4.1B, there were other antibodies available for the $A\beta_{43}$ assay, namely the 82E1 IBL mouse monoclonal antibody against the N-terminus of Aβ (Figure 4.1A). Perhaps we should have considered purchasing this antibody and including it in our antibody combination comparison experiments alongside the BioLegend antibodies to ascertain the most sensitive antibody combination for our assay more robustly.

Despite the challenges faced on the SRx Pro, we were able to show that this instrument offers an even greater increase in sensitivity compared with both the HDx and ELISA assay equivalents for both of our analytes. Whilst further development is required, this is particularly promising given that the SRx Pro is not yet commercially available, and also given that these analytes have yet to be successfully measured in CSF, blood or both biofluids.

4.5.2 Assay specificity

We hypothesised that the $A\beta_{43/40}$ would decrease more than and/or earlier than the $A\beta_{42/40}$ in AD. Given that to our knowledge, the pilot CSF samples in which we measured $A\beta_{43}$ did not have $A\beta_{40}$ measurements available, we were unable to verify whether our hypothesis of a greater decrease in $A\beta_{43/40}$ compared with $A\beta_{42/40}$ could be accepted or rejected. Whilst it may have been possible for us to conduct our own measurements of $A\beta_{40}$ on these samples, we did not intend for this to be our final clinical cohort on which this assay was tested. Rather we intended to test our assays on the same clinical cohort used in

 – samples in which $A\beta_{40}$ was measured. In order to confirm whether the $A\beta_{43/40}$ decreases earlier than the $A\beta_{42/40}$, we would need to perform either a longitudinal study, or a cross-sectional study similar to that performed by Palmqvist and colleagues (92). However, prior to reaching that stage, we would need to verify the specificity of our assay more robustly for $A\beta_{43}$.

We hypothesised that $A\beta_{pE}$ is secreted in small quantities in the presence of plaque pathology from within the plaque into the CSF, and hence it should increase with greater plaque burden. In essence, we did not expect to be able to detect $A\beta_{pE3\text{-}40}$ in either the MP or CTRL samples, given that $A\beta_{pE}$ is thought to be a plaque specific form of Aβ (74). Having only one AD sample to measure this analyte in within our pilot cohort made it particularly challenging to comment fully on whether $A\beta_{pE}$ is exclusive to AD. However, we cannot overlook that we were able to measure what we presumed to be $A\beta_{pE3\text{-}40}$ in all samples and at all dilution levels for most samples in section 4.4.5.2 Repeated measurement of pilot CSF samples. Given that we did not perform any specificity tests on this analyte, including the MSD antibody specificity test conducted on the antibodies used for the $A\beta_{43}$ assay, it is unclear whether $A\beta_{pE}$ is in fact not specific to AD, or whether our assay was not as specific to $A\beta_{pE3\text{-}40}$ as we anticipated.

In order to verify that our assays are specific to the target analytes, and are not measuring additional proteins within our target matrices, we would need to perform specificity assessments, such as immunodepleting our samples using specific antibodies, followed by remeasuring them with our respective assays.

4.5.3 Matrix effects, dilution linearity and spike recovery

Whilst information on the neat concentrations of our samples is useful to have, the measurement of Aβ in CSF is known to be

impacted by matrix effects (383). Indeed, matrix effects have been shown to either enhance or suppress measurements obtained for analytes (384). As such, dilution of samples is paramount to minimise this in biological matrices. However, the linearity of these dilutions should simultaneously be assessed to ensure a reliable and accurate concentration can still be obtained upon dilution.

Few of our samples were measurable at all four dilution levels with both of our assays (assessed in sections 4.4.3.10 HDx pilot CSF $A\beta_{43}$ and $A\beta_{pE3\text{-}40}$ measurements and 4.4.5.2 Repeated measurement of pilot CSF samples). In our initial measurements (section 4.4.3.10 HDx pilot CSF Aβ43 and AβpE3-40 measurements), MP1 showed a strong dilution linearity in both assays, with only its $A\beta_{43}$ measurements being statistically significant (Figure 4.5 and Figure 4.7). However, upon remeasuring this sample (section 4.4.5.2 Repeated measurement of pilot CSF samples), MP1 showed a strong but statistically non-significant dilution linearity with $A\beta_{43}$ (Figure 4.10), and a poor linearity with $A\beta_{pE3\text{-}40}$ (Figure 4.12). Similarly, in our initial measurements (section 4.4.3.10 HDx pilot CSF $A\beta_{43}$ and $A\beta_{pE3\text{-}40}$ measurements), CTRL1 showed a poor linearity in its $A\beta_{43}$ measurements (Figure 4.7), but was only measurable at a 4x dilution with $A\beta_{pE3\text{-}40}$ (Table 4.39). Upon remeasuring this sample (section 4.4.5.2 Repeated measurement of pilot CSF samples), CTRL1 showed a strong but statistically non-significant dilution linearity with $A\beta_{43}$ (Figure 4.10), and a poor linearity with $A\beta_{pE3\text{-}40}$ (Figure 4.12). The change with CTRL1 from a poor linearity in its initial $A\beta_{43}$ measurements to a strong linearity upon repeating the measurements can be attributed to refining the calibration curve. Given that our spiked CSF samples showed a strong linearity upon dilution, the poor linearity, particularly with regards to $A\beta_{pE3\text{-}40}$ may be due to reaching the sensitivity limits of the HDx instrument, further highlighted by the “hook-like” shape of the $A\beta_{43}$ measurements in Figure 4.10 comparing expected and observed concentrations.

400 pg/mL of calibration material was spiked into our samples. However, when measured neat, we obtained concentrations in the range of 208-256 pg/mL (Table 4.47 and Table 4.48), giving a % recovery for our neat samples of 52-64% compared to the concentration spiked in. As a fraction of the peptide concentration spiked into our samples, for $A\beta_{43}$ there were 11/21 instances in which the recovery was within the acceptable range of 80-120%, whereas for $A\beta_{pE3-40}$, this number was reduced to 3/24. The increased recovery for $A\beta_{43}$ could possibly be attributed to the use of CP3, a less hydrophobic version of the FL $A\beta_{43}$ peptide. Nonetheless, the poor spike recovery for both analytes may be indicative of interference from the CSF matrix, which literature has shown suppresses the quantification of $A\beta_{42}$ (383). However, the poor recovery may also indicate that the optimised sample diluents may not match the sample matrix as closely as is optimal, particularly in the case of $A\beta_{pE3-40}$. Investigating alternative sample diluents may improve the peptide recovery, perhaps through the use of artificial CSF (385), or the addition of various proteins and electrolytes to better mimic the composition of CSF. Alternatively, it would be interesting to investigate greater levels of CSF dilutions, and assess the impact this has on the recovery of our analytes, particularly given that the recommended CSF dilution for the Quanterix N4PE assay is 400x. However, the low concentration of our analytes *in vivo* may impact the extent of dilution possible in clinical samples.

4.5.4 Conclusion

In conclusion, we have successfully developed novel assays for the measurement of $A\beta_{43}$ and $A\beta_{pE3-40}$ initially on the standard SRx, and subsequently on the HDx Simoa instrument. However, sensitivity limitations in pilot experiments on CSF highlight the need for the increased sensitivity offered by the SRx Pro. Upon transferring our assays onto the SRx Pro, we were faced with several challenges which impacted our ability to obtain interpretable results, and hence to fully develop our assays on this novel prototype instrument.

However, following these challenges, we have preliminarily shown that the SRx Pro does indeed offer an increased level of sensitivity for both of our assays.

CHAPTER 5: DISCUSSION

5.1 Thesis synopsis

The overarching purpose of this project was to examine the performance of blood biomarkers for AD diagnosis, particularly focussing on the ability of plasma Aβ to differentiate between diagnostic groups. On the basis of those results, we aimed to develop novel Aβ Simoa assays for the quantification of $Aβ_{43}$ and $Aβ_{pE3-40}$. This final chapter summarises the outcomes of our research, highlights key limitations, and proposes future directions for the continuation of this work.

5.1.1 The need for novel plasma amyloid-β tests for Alzheimer's disease

The existence of AD on a continuum beginning up to 20 years before symptom onset has led to major changes in the methodology used for its diagnosis. Whilst for decades AD diagnoses were largely based on symptoms and symptom severity, there has been a shift to a biomarker-based diagnostic criteria, which is used in tandem with patient history and neurocognitive assessments (36). Both fluid and neuroimaging biomarkers play a key role in aiding a diagnosis of AD, as highlighted by the ATXN criteria (see section 1.4.1 The ATXN criteria). Together, biomarkers of Aβ and tau pathology make up the core AD biomarkers, with GFAP and NfL being included as non-specific biomarkers of tissue reactions involved in AD pathophysiology (Table 1.1).

Whilst previously, AD 'fluid biomarkers' only included CSF biomarkers, the recent update to the ATXN criteria[1] has seen the addition of several blood biomarkers, mainly due to blood being far more accessible and less invasive to obtain than CSF, and technological advancements making it possible to measure these low-abundant biomarkers in the complex plasma matrix. Of the core AD biomarkers, studies in recent years have shown that plasma p-tau_{181} and p-tau_{217} perform as well as their CSF counterparts in

differentiating between AD and NAD or CTRL individuals (92, 230, 231, 334) – a finding corroborated by us in section 2.3.2 Phosphorylated tau results. We observed that both p-tau biomarkers were significantly increased in AD compared with NAD in both plasma and CSF (Figure 2.4), with positive statistically significant correlations observed when comparing CSF with plasma concentrations obtained for each individual (Figure 2.5A&B).

In contrast to p-tau, plasma $A\beta_{42/40}$ has been shown to not perform as well as CSF $A\beta_{42/40}$, with extensive overlap between diagnostic groups (206). Not only did we observe this same extensive overlap between diagnostic groups with plasma $A\beta_{42/40}$ (Figure 2.1E), but we also observed no significant difference in plasma $A\beta_{42/40}$ between AD and NAD individuals, along with a poor correlation between CSF and plasma (Figure 2.2C) and a poor diagnostic accuracy for AD (Figure 2.3C). Whilst in the past, the poor correlation could be attributed to a limitation in the analytical sensitivity of instruments available, this is no longer the case given the technological advances in recent years (212, 213, 215), already discussed in section 1.4.2.1 Amyloid-β biomarkers. Rather, the peripheral production of Aβ is making it more difficult to distinguish between AD and NAD phenotypes. What is particularly interesting is that in our cohort, plasma $A\beta_{42}$ not only showed a significant decrease in AD compared to NAD, albeit with a slight overlap between diagnostic groups (Figure 2.1C), but it also showed a statistically significant correlation with CSF $A\beta_{42}$, along with a good diagnostic accuracy for AD (Figure 2.3B). This is worth noting given that both CSF and plasma $A\beta_{42}$ were recently removed from the updated NIA-AA diagnostic criteria for AD[1].

In essence, these results highlight plasma $A\beta_{42/40}$ performs poorly as a diagnostic biomarker for AD, emphasising the need to identify alternative plasma biomarkers of Aβ pathology. We therefore explored the possibility of $A\beta_{43}$ and $A\beta_{pE3\text{-}40}$ as offering robust solutions to this dilemma. Post-mortem immunohistochemical

analysis has revealed that $A\beta_{43}$ is a more frequent constituent of plaques than $A\beta_{42}$ (59). As such, its absolute concentrations in both CSF and plasma will likely be less than that of $A\beta_{42}$ in these biofluids. Should this be the case, it is possible that the $A\beta_{43/40}$ will decrease more than and/or earlier than the $A\beta_{42/40}$ in AD, particularly in plasma when comparing AD to NAD/CTRL individuals. Whilst $A\beta_{43}$ has been successfully measured in CSF (40, 367), it has yet to be detected in plasma, most likely due to limitations in the sensitivity of the instruments currently available. Similarly, the specificity of $A\beta_{pE}$ to plaque pathology (74) suggests that in plasma, it may not be as affected by the peripheral production of Aβ as other isoforms. In light of our hypothesis that $A\beta_{pE}$ is secreted in small quantities from within the plaque into the CSF in the presence of established AD neuropathology, we expect its concentrations in CSF to be extremely low, and even lower in plasma. However, $A\beta_{pE}$ has not yet been successfully measured in human biofluids. Given the success of Donanemab in clinical trials, which has already been discussed in section 1.6.4 Donanemab, it is clear that $A\beta_{pE}$ forms a major constituent of plaques. Therefore, the lack of success with attempts to measure it further highlighting the need for increased instrument sensitivity, should our hypothesis be true.

5.1.2 Ultrasensitive Single molecule array technology as a solution

In light of the sensitivity limitations currently plaguing the scientific world, the development of upgraded Simoa technology by Quanterix Corporation, in the form of the SRx Pro, provides the opportunity to detect proteins down to sub-attomolar (10^{-18} M) concentrations, increasing sensitivity up to 189-fold in the case of IL17A (214). To validate the increase in sensitivity provided by the SRx Pro in comparison to the standard Simoa HDx instrument, we measured IL17A in 32 paired serum and CSF AD and CTRL samples (CHAPTER 3: SIMOA UPGRADE VALIDATION). We observed that the HDx quantified IL17A in 37.5% of our serum samples (see

section 3.3.1 Upgraded Simoa, but not standard Simoa, can measure interleukin 17A in both cerebrospinal fluid and serum), and 0% of our CSF samples (Figure 3.1). This is compared with the SRx Pro quantifying IL17A in 100% of our serum samples and up to 96.9% of our CSF samples (see Figure 3.1 and Figure 3.2). Whilst we observed a poor correlation between CSF and serum IL17A concentrations across all three SRx Pro instruments tested (Figure 3.6), this is in line with previous literature (363, 364). Therefore, this poor correlation is unlikely to be due to a fault in the SRx Pro instruments used, but rather may reflect that CSF IL17A is uninfluenced by peripheral IL17A concentrations. To our surprise, we observed no significant difference in IL17A concentrations in AD compared with CTRLs, albeit in a relatively small cohort. Regardless, our observations validate the results of Kan and colleagues (214), proving the SRx Pro does indeed provide increased sensitivity above the HDx, and therefore opening the door to detect and quantify previously unmeasurable analytes.

5.1.3 Novel amyloid-β biomarkers are detectable in cerebrospinal fluid

Having successfully validated the increased sensitivity provided by the SRx Pro, the final portion of this project was to develop novel Simoa assays for the detection of $A\beta_{43}$ and $A\beta_{pE3\text{-}40}$. Whilst these assays were primarily intended for use on the SRx Pro, we initially developed them on the established Simoa instruments (SRx and HDx), with the aim of transferring them onto the SRx Pro. This three-phase assay development process would enable us to compare the differences in sensitivity offered by the SRx Pro in comparison to standard Simoa instruments for our analytes specifically. This is of benefit because although the SRx Pro can offer up to a 189-fold increase in sensitivity in some cases, in other cases Kan and colleagues observed only a 2-fold increase in sensitivity, and still others a decrease in sensitivity was observed (214).

In sections 4.4.2 SRx assay development, 4.4.3 HDx assay development and 4.4.5 Refining HDx assays, we showed the successful development of novel assays measuring $A\beta_{43}$ and $A\beta_{pE3\text{-}40}$ on the standard Simoa instruments. Our final optimised calibration curves on the HDx, ranging from 9.94 to 240 pg/mL for $A\beta_{43,}$ and 3.75 to 240 pg/mL for $A\beta_{pE3\text{-}40}$, showed that Simoa offers an increased sensitivity for $A\beta_{pE3\text{-}40}$ but not for $A\beta_{43}$ when compared with the calibration curves of their equivalent conventional ELISA assays (see Table 4.1). Preliminary investigations on a small cohort of CSF samples (2 AD, 5 MP and 3 CTRL) measured at four dilution levels (neat, 2x, 4x and 8x) highlighted the importance of prioritising assay sensitivity over obtaining optimal AEBs. Indeed, using a calibration curve ranging from 20 to 5120 pg/mL, we obtained 19 $A\beta_{43}$ measurements, compared with 22 using the final optimised curve above, out of a possible 32 measurements. Similarly, using a calibration curve ranging from 10.8 to 1620 pg/mL, we obtained 10 $A\beta_{pE3\text{-}40}$ measurements compared with 30 using the final optimised curve above (Table 4.39, Table 4.45 and Table 4.46). We observed a poor linearity across the dilutions of the few samples that were measurable at all dilution levels tested (Figure 4.10 and Figure 4.12), most likely indicating that we were reaching the sensitivity limits of the HDx instrument for these analytes. Additionally, this pilot study highlighted a possible specificity limitation within our assays, particularly in relation to $A\beta_{pE3\text{-}40}$ given that it was detectable in all phenotypes assessed. Nonetheless, to our knowledge, we have successfully detected what we believe to be $A\beta_{pE3\text{-}40}$ in human CSF for the first time.

Given that our primary aim was for these assays to be used in blood as novel biomarkers of Aβ pathology, the successful and seamless transfer onto the SRx Pro was a paramount next step. Section 4.4.4 SRx Pro assay development highlights our attempt to transfer our assays onto the SRx Pro platform. However, we faced unexpected challenges which limited our progress in optimising our assays on

this instrument – the first being a frequent error which prevented the automatic generation of AEBs by the instrument (section 4.4.4.1.1 Challenge 1: “Low intensity single precision” error), and the second being non-linear calibration curves (section 4.4.4.1.2 Challenge 2: “Up-down” nature of calibration curves). Nonetheless, upon troubleshooting these challenges we showed that comparing the optimised HDx calibration curves to our initial calibration curves on the SRx Pro, this platform does offer some level of increased sensitivity. For the $A\beta_{43}$ assay, we were able to decrease our calibrator B from 9.94 pg/mL on the HDx to between 0.0488 and 0.125 pg/mL on the SRx Pro (Table 4.41), which equates to a sensitivity increase of between 79.5- and 204-fold. Similarly, for the $A\beta_{pE3\text{-}40}$ assay, we were able to decrease our calibrator B from 3.75 pg/mL on the HDx to between 0.0305 and 0.0718 pg/mL on the SRx Pro (Table 4.42), equating to a sensitivity increase of between 52.2- and 123-fold. Whilst further optimisation and validation of both assays on this instrument is still required, these are promising results to have obtained.

5.2 Implications for the Alzheimer's disease diagnostic field

Prior to addressing the limitations and future directions for our work, it is important to put our findings into the context of the rapidly changing AD diagnostic field, particularly in relation to fluid biomarkers.

Our observations that p-tau$_{217}$ exhibits a greater distinction between AD compared with NAD in both CSF and plasma in comparison to p-tau$_{181}$ corroborates recent findings that highlight p-tau$_{217}$ to be a top-performing AD biomarker, especially in plasma (386). This is particularly fascinating given that up until recently, p-tau$_{181}$ was the dominating tau phosphorylation site measured in relation to AD, a topic reviewed by myself and colleagues (46). The diagnostic benefit of p-tau$_{217}$ is emphasised by its recent addition to the ATXN criteria (see Table 1.1 and Table 1.2), which previously only recognised p-tau$_{181}$ as a biomarker of tau pathology (44). Whilst increasing evidence is coming to light revealing p-tau to be a reflection of Aβ-induced tau pathology, with some questioning whether it may better serve as an indirect marker of Aβ pathology – a concept briefly discussed in section 1.4.1 The ATXN criteria, and recently reviewed by myself and colleagues (225) – we remain of the view that p-tau best serves as a biomarker of tau pathology.

Whilst CSF Aβ$_{42/40}$ is undoubtedly a robust biomarker, there remains a gap in the plasma biomarkers identifying Aβ pathology, given the poor performance of plasma Aβ$_{42/40}$. Based on our findings, we believe it is imperative to find a direct Aβ plasma biomarker to fulfil this role, whether that be Aβ$_{43}$, Aβ$_{pE3-40}$, or another isoform of Aβ, and the dawn of the SRx Pro and MOSAIC platforms (see section 1.5.4 The need for increased sensitivity, upgraded Simoa, and MOSAIC technology) mean that in the coming years, we will see the detection of novel analytes, particularly in plasma, further advancing and transforming the field. Regardless of whether Aβ$_{pE3-40}$ can be used as a replacement biomarker for plasma Aβ$_{42/40}$, the success of

Donanemab in clinical trials highlights that there will be immense benefit to being able to detect this analyte, whether that be in CSF, blood or both. Nonetheless, this is a particularly exciting time for this scientific field, hence only time will tell what will come of the increased analytical sensitivity now available to us, and the implications this will have on the direct biomarkers of Aβ pathology.

5.3 Limitations

5.3.1 Existing biomarkers of Alzheimer's disease study

In relation to our study measuring existing biomarkers of AD pathology (CHAPTER 2), the first limitation to consider is that we measured the CSF and plasma biomarkers on two separate instruments for $A\beta_{40}$, $A\beta_{42}$ and p-tau_{181}, which may have contributed to the poor correlation between the CSF and plasma measurements for $A\beta_{40}$ and $A\beta_{42/40}$. However, given that $A\beta_{42}$ and p-tau_{181} both showed a statistically significant correlation between their CSF and plasma measurements, this is unlikely to be the case. Rather, it is possible that a greater proportion of peripherally produced Aβ is $A\beta_{40}$, therefore, by proxy the correlation between CSF and plasma $A\beta_{40}$ and $A\beta_{42/40}$ will be negatively affected.

The second limitation is that the diagnoses of the individuals within our cohort were made partly on information from CSF biomarker measurements, which inevitably favoured the diagnostic performance of the examined CSF tests over their blood biomarker counterparts. Nonetheless, this limitation would not alter our conclusions given that the primary aim of our study was to evaluate the performance of the blood biomarkers.

The third limitation is that CSF measurements were not available for GFAP and NfL, hence we could not assess correlations and comparisons between CSF and plasma concentrations of these biomarkers. Given that neither of these analytes are core AD biomarkers[1] (Table 1.1), we did not deem it paramount to ensure their measurements were available for our study. Rather, it would have been beneficial to have them for the sake of completeness. The Lumipulse instrument was chosen because it is the gold standard platform for CSF measurements at the UCL Hospital neuroimmunology laboratory, where the CSF $A\beta_{40}$, $A\beta_{42}$ and p-tau_{181} measurements were conducted. Whilst there does not appear to be a CSF GFAP assay available on the manufacturer website for the

Lumipulse instrument, there is a CSF NfL assay. Given that a recent study investigating CSF and serum NfL in multiple sclerosis patients showed a strong correlation in both biofluids between measurements conducted using Simoa compared with Lumipulse (387), it would have been interesting to validate whether the same could be seen within our cohort of AD and CTRL individuals.

Fourthly, our cohort size was relatively small, comprising of only 66 NAD and 49 AD individuals. Using this cohort of individuals, 115 samples was the maximum number available at our disposal, and was deemed sufficient for what we were investigating.

Finally, there was no genetic information, specifically *APOE* status, available for our cohort. This is because genetic information is not routinely collected from patients at the UCL DRC. Whilst knowledge of the genetic status would not have had any major implications on our findings, particularly given that the focus of this PhD has not been on AD genetics, additional information of this type would be interesting to have for identifying which individuals within our cohort developed AD due to genetic causes.

5.3.2 Simoa upgrade validation study

One key limitation of our SRx Pro validation study (CHAPTER 3: SIMOA UPGRADE VALIDATION) is that we were only able to compare the SRx Pro to the HDx, rather than the standard SRx platform. A comparison between the SRx Pro and SRx would have been more beneficial, as the sample preparation and washing protocols for these two instruments are similar, both occurring manually, whereas the automated nature of the HDx may have introduced key differences that are difficult to account for. However, it was not feasible at the time for us to purchase a replacement SRx instrument to conduct this comparison.

Another limitation is that we were unable to follow the exact same protocol used by Kan and colleagues, since they conducted their investigations when the SRx Pro was in its early stages of development. As such, there had been key adjustments to the operation protocol. This difference was unavoidable, given the novelty of the instrument. In line with this, it may have been beneficial for us to conduct an 8x dilution of our serum samples, given that this is the extent of dilution Kan and colleagues conducted on their serum samples. However, we opted to conduct a 10x dilution to push the sensitivity limits of the HDx instrument. Despite this, the HDx was still able to accurately quantify IL17A in 37.5% of our samples compared with 24% in Kan and colleagues (214). However, this is a poor yield in comparison to the 100% of serum samples quantified by the SRx Pro instruments.

The final limitation was that the sample cohort used within our study only comprised of 32 samples. However, again, given that this study was aimed to supplement this PhD project, we deemed 32 samples sufficient for our intended purpose.

5.3.3 Novel assay development

Key limitations of the development of our novel Simoa assays (CHAPTER 4) include that we did not perform extensive specificity assessments for our analytes in the target biofluids, leaving our assays open to interference from other analytes present within the matrices.

Secondly, we were unable to fully develop and optimise our assays on the SRx Pro, hence they are not yet at the sensitivity level required for their robust measurement within our target biofluids. This is largely because we did not anticipate encountering the challenges we faced upon transferring our assays onto this platform. However, given the novel nature of both our assays and the SRx Pro instrument itself, delays and setbacks were inevitable.

Another limitation is that we only tested our assays on a very small cohort of CSF samples, which only included one AD sample, and we did not reach the stage where we could test them in plasma due to the sensitivity limitations of the HDx instrument for our analytes. The assays were not yet at a stage where we could test them in a full cohort of samples, hence we chose a very small subset of samples to investigate the functionality of our assays, rather than for the purpose inter-phenotype comparisons of our analytes.

Beyond the limitations of our study, it is also important to note the time-consuming nature of developing novel assays on Simoa instruments of any kind, with unpredictable instrument errors disrupting the flow of development. However, this would be the case with any novel assays, and even more so when developing these assays on a prototype instrument. Furthermore, the changes made to the assay protocol on the SRx Pro compared with the SRx to achieve the desired increase in sensitivity makes the SRx Pro a particularly time-consuming instrument to operate in comparison to standard Simoa instruments. Nonetheless, the sensitivity possibilities made available through the SRx Pro make the additional operation time a worthwhile compromise.

5.4 Future directions

The first consideration for future work would be to validate the results of our existing AD biomarker analysis in another, similar, validation cohort of samples, namely containing an NAD group with a similar variety of both neurodegenerative and non-neurodegenerative diseases. It would also be important to consider using a larger sample size within this validation cohort, along with using samples within which genetic information is available.

Secondly, in relation to our Simoa validation study, a direct comparison between the SRx and SRx Pro would be beneficial. However, this would not be essential given that the HDx and SRx have the same level of sensitivity. Rather, it would merely ensure similar assay protocol conditions were used on both the SRx Pro and standard Simoa instrument.

Thirdly, it would be beneficial to continue with the assay development process on the SRx Pro, completing all immunoassay validation tests described by Andreasson and colleagues (372). Furthermore, exploring the S-NHS-EDC bead conjugation method, and comparing this to the standard EDC bead conjugation method to assess whether the suspected enhancement in antibody binding efficiency positively improves our assays, including further enhancing their sensitivity.

To verify that our assays detect $A\beta_{43}$ and $A\beta_{pE3\text{-}40}$ alone, carrying out sample immunodepletion experiments would also be beneficial, prior to measuring these analytes in clinical cohorts. This would formally and robustly verify the specificity of our assays for their target analytes.

Given the spike recovery limitations observed for both $A\beta_{43}$ and $A\beta_{pE3\text{-}40}$ on the HDx (Table 4.47 and Table 4.48), exploring alternative sample diluents which better mimic the sample matrix

would enhance the reliability of analyte measurements obtained. Alternatively, assessing greater levels of sample dilutions may provide the same benefit, although given the low concentrations of our analytes *in vivo*, this may not be feasible. Furthermore, establishing the LLOQ and LOD for our finalised assays on the HDx would further clarify whether our assays were truly limited by the analytical sensitivity of this instrument.

Finally, in light of the decreases in $A\beta_{pE3\text{-}40}$ concentration between the initial and repeat CSF measurements on the HDx (Table 4.46), investigating the susceptibility of $A\beta_{pE3\text{-}40}$ to degradation with increasing time following sample collection and storage would provide useful information on the stability of this analyte in storage.

5.5 Final conclusion

In conclusion, we have corroborated the need for novel blood biomarkers for Aβ which better distinguish between AD and NAD cases, and have validated the additional sensitivity provided by the Simoa SRx Pro, combatting the analytical sensitivity issues plaguing the scientific world and opening the door to a plethora of previously undetectable analytes. Whilst our assays require further optimisation to reach the sensitivity required, this PhD has developed novel Simoa assays for the detection of $A\beta_{43}$ and $A\beta_{pE3\text{-}40}$, successfully measuring $A\beta_{pE3\text{-}40}$ in any human biofluid for the first time.

REFERENCES

1. Gale SA, Acar D, Daffner KR. Dementia. The American journal of medicine. 2018;131(10):1161-9.
2. Scheltens P, De Strooper B, Kivipelto M, Holstege H, Chételat G, Teunissen CE, et al. Alzheimer's disease. The Lancet. 2021;397(10284):1577-90.
3. DeKosky ST. Epidemiology and pathophysiology of Alzheimer's disease. Clinical cornerstone. 2001;3(4):15-26.
4. Winner B, Kohl Z, Gage FH. Neurodegenerative disease and adult neurogenesis. European Journal of Neuroscience. 2011;33(6):1139-51.
5. Stelzmann RA, Norman Schnitzlein H, Reed Murtagh F. An english translation of alzheimer's 1907 paper, “über eine eigenartige erkankung der hirnrinde”. Clinical anatomy (New York, NY). 1995;8(6):429-31.
6. Villemagne VL, Doré V, Burnham SC, Masters CL, Rowe CC. Imaging tau and amyloid-? proteinopathies in Alzheimer disease and other conditions. Nature reviews Neurology. 2018;14(4):225-36.
7. Willumsen N, Poole T, Nicholas JM, Fox NC, Ryan NS, Lashley T. Variability in the type and layer distribution of cortical Aβ pathology in familial Alzheimer’s disease. Brain Pathology. 2022;32(3):e13009.
8. Julia TCW, Goate AM. Genetics of β-amyloid precursor protein in alzheimer’s disease. Cold Spring Harbor perspectives in medicine. 2017;7(6):a024539.
9. Scheuner D, Eckman C, Jensen M, Song X, Citron M, Suzuki N, et al. Secreted amyloid beta-protein similar to that in the senile plaques of Alzheimer's disease is increased in vivo by the presenilin 1 and 2 and APP mutations linked to familial Alzheimer's disease. Nat Med. 1996;2(8):864-70.
10. Wiseman FK, Al-Janabi T, Hardy J, Karmiloff-Smith A, Nizetic D, Tybulewicz VLJ, et al. A genetic cause of Alzheimer disease: Mechanistic insights from Down syndrome. Nature reviews Neuroscience. 2015;16(9):564-74.
11. Burger PC, Vogel FS. The development of the pathologic changes of Alzheimer's disease and senile dementia in patients with Down's syndrome. Am J Pathol. 1973;73(2):457-76.
12. Oyama F, Cairns NJ, Shimada H, Oyama R, Titani K, Ihara Y. Down's syndrome: up-regulation of beta-amyloid protein precursor and tau mRNAs and their defective coordination. J Neurochem. 1994;62(3):1062-6.
13. Wisniewski KE, Wisniewski HM, Wen GY. Occurrence of neuropathological changes and dementia of Alzheimer's disease in Down's syndrome. Ann Neurol. 1985;17(3):278-82.
14. Mann DM, Esiri MM. The pattern of acquisition of plaques and tangles in the brains of patients under 50 years of age with Down's syndrome. J Neurol Sci. 1989;89(2-3):169-79.
15. Zigman WB. Atypical aging in Down syndrome. Dev Disabil Res Rev. 2013;18(1):51-67.

16. Zigman WB, Schupf N, Urv T, Zigman A, Silverman W. Incidence and temporal patterns of adaptive behavior change in adults with mental retardation. Am J Ment Retard. 2002;107(3):161-74.
17. Tomita T, Iwatsubo T, Takasugi N, Hayashi I, Tsuruoka M, Niimura M, et al. The role of presenilin cofactors in the γ-secretase complex. Nature (London). 2003;422(6930):438-41.
18. Ryan NSD, Nicholas JMP, Weston PSJM, Liang YM, Lashley TP, Guerreiro RP, et al. Clinical phenotype and genetic associations in autosomal dominant familial Alzheimer's disease: a case series. Lancet Neurol. 2016;15(13):1326-35.
19. Ryman DC, Acosta-Baena N, Aisen PS, Bird T, Danek A, Fox NC, et al. Symptom onset in autosomal dominant Alzheimer disease: A systematic review and meta-analysis. Neurology. 2014;83(3):253-60.
20. Strittmatter WJ, Saunders AM, Schmechel D, Pericak-Vance M, Enghild J, Salvesen GS, Roses AD. Apolipoprotein E: high-avidity binding to beta-amyloid and increased frequency of type 4 allele in late-onset familial Alzheimer disease. Proc Natl Acad Sci U S A. 1993;90(5):1977-81.
21. Poirier J, Davignon J, Bouthillier D, Kogan S, Bertrand P, Gauthier S. Apolipoprotein E polymorphism and Alzheimer's disease. Lancet. 1993;342(8873):697-9.
22. Janssen JC, Beck JA, Campbell TA, Dickinson A, Fox NC, Harvey RJ, et al. Early onset familial Alzheimer's disease: Mutation frequency in 31 families. Neurology. 2003;60(2):235-9.
23. Liu C-C, Kanekiyo T, Xu H, Bu G. Apolipoprotein e and Alzheimer disease: Risk, mechanisms and therapy. Nature reviews Neurology. 2013;9(2):106-18.
24. Wolfe CM, Fitz NF, Nam KN, Lefterov I, Koldamova R. The role of APOE and TREM2 in Alzheimer s disease—Current understanding and perspectives. Int J Mol Sci. 2018;20(1):81.
25. Corder EH, Saunders AM, Strittmatter WJ, Schmechel DE, Gaskell PC, Small GW, et al. Gene dose of apolipoprotein E type 4 allele and the risk of Alzheimer's disease in late onset families. Science. 1993;261(5123):921-3.
26. Corder EH, Saunders AM, Risch NJ, Strittmatter WJ, Schmechel DE, Gaskell PC, et al. Protective effect of apolipoprotein E type 2 allele for late onset Alzheimer disease. Nature genetics. 1994;7(2):180-4.
27. Guerreiro R, Wojtas A, Bras J, Carrasquillo M, Rogaeva E, Majounie E, et al. TREM2 Variants in Alzheimer's Disease. NEW ENGL J MED. 2013;368(2):117-27.
28. Jonsson T, Jonsson PV, Stefansson H, Stefansson K, Steinberg S, Jonsdottir I, et al. Variant of TREM2 Associated with the Risk of Alzheimer's Disease. NEW ENGL J MED. 2013;368(2):107-16.
29. Heneka MTP, Carson MJP, Khoury JEP, Landreth GEP, Brosseron FP, Feinstein DLP, et al. Neuroinflammation in Alzheimer's disease. Lancet Neurol. 2015;14(4):388-405.

30. Wang Y, Cella M, Mallinson K, Ulrich Jason D, Young Katherine L, Robinette Michelle L, et al. TREM2 Lipid Sensing Sustains the Microglial Response in an Alzheimer's Disease Model. CELL. 2015;160(6):1061-71.
31. Reiman EM, Quiroz YT, Fleisher AS, Chen K, Velez-Pardo C, Jimenez-Del-Rio M, et al. Brain imaging and fluid biomarker analysis in young adults at genetic risk for autosomal dominant Alzheimer's disease in the presenilin 1 E280A kindred: a case-control study. Lancet Neurol. 2012;11(12):1048-56.
32. Villemagne VL, Burnham S, Bourgeat P, Brown B, Ellis KA, Salvado O, et al. Amyloid β deposition, neurodegeneration, and cognitive decline in sporadic Alzheimer's disease: a prospective cohort study. Lancet Neurol. 2013;12(4):357-67.
33. Bateman RJ, Xiong C, Benzinger TLS, Fagan AM, Goate A, Fox NC, et al. Clinical and Biomarker Changes in Dominantly Inherited Alzheimer's Disease. The New England journal of medicine. 2012;367(9):795-804.
34. Fagan AM, Shaw LM, Xiong C, Vanderstichele H, Mintun MA, Trojanowski JQ, et al. Comparison of Analytical Platforms for Cerebrospinal Fluid Measures of β-Amyloid 1-42, Total tau, and P-tau181 for Identifying Alzheimer Disease Amyloid Plaque Pathology. Archives of neurology (Chicago). 2011;68(9):1137-44.
35. Zetterberg H, Bendlin BB. Biomarkers for Alzheimer's disease-preparing for a new era of disease-modifying therapies. Mol Psychiatry. 2021;26(1):296-308.
36. Delaby C, Teunissen CE, Blennow K, Alcolea D, Arisi I, Amar EB, et al. Clinical reporting following the quantification of cerebrospinal fluid biomarkers in Alzheimer's disease: An international overview. Alzheimer's & dementia. 2022;18(10):1868-79.
37. Finder VH, Glockshuber R. Amyloid-β Aggregation. Neurodegener Dis. 2007;4(1):13-27.
38. Brothers HM, Gosztyla ML, Robinson SR. The Physiological Roles of Amyloid-β Peptide Hint at New Ways to Treat Alzheimer's Disease. Front Aging Neurosci. 2018;10:118.
39. Cacace R, Sleegers K, Van Broeckhoven C. Molecular genetics of early-onset Alzheimer's disease revisited. Alzheimer's & dementia. 2016;12(6):733-48.
40. Perrone F, Bjerke M, Hens E, Sieben A, Timmers M, De Roeck A, et al. Amyloid-β1–43 cerebrospinal fluid levels and the interpretation of APP, PSEN1 and PSEN2 mutations. Alzheimer's Research & Therapy. 2020;12(1).
41. Chen G-F, Xu T-H, Yan Y, Zhou Y-R, Jiang Y, Melcher K, Xu HE. Amyloid beta： structure, biology and structure-based therapeutic development. ACTA PHARMACOL SIN. 2017;38(9):1205-35.
42. Struyfs H, Van Broeck B, Timmers M, Fransen E, Sleegers K, Van Broeckhoven C, et al. Diagnostic Accuracy of Cerebrospinal Fluid Amyloid-beta Isoforms for Early and Differential Dementia Diagnosis. Journal of Alzheimer's disease. 2015;45(3):813-22.

43. Jack CR, Bennett DA, Blennow K, Carrillo MC, Feldman HH, Frisoni GB, et al. A/T/N: An unbiased descriptive classification scheme for Alzheimer disease biomarkers. Neurology. 2016;87(5):539-47.
44. Jack CR, Bennett DA, Blennow K, Carrillo MC, Dunn B, Haeberlein SB, et al. NIA-AA Research Framework: Toward a biological definition of Alzheimer's disease. Alzheimer's & Dementia. 2018;14(4):535-62.
45. Lewczuk P, Esselmann H, Otto M, Maler JM, Henkel AW, Henkel MK, et al. Neurochemical diagnosis of Alzheimer's dementia by CSF Abeta42, Abeta42/Abeta40 ratio and total tau. Neurobiol Aging. 2004;25(3):273-81.
46. Alawode DOT, Heslegrave AJ, Ashton NJ, Karikari TK, Simrén J, Montoliu-Gaya L, et al. Transitioning from cerebrospinal fluid to blood tests to facilitate diagnosis and disease monitoring in Alzheimer's disease. J Intern Med. 2021.
47. Hampel H, Hardy J, Blennow K, Chen C, Perry G, Kim SH, et al. The Amyloid-β Pathway in Alzheimer's Disease. Mol Psychiatr. 2021.
48. Koffie RM, Meyer-Luehmann M, Hashimoto T, Adams KW, Mielke ML, Garcia-Alloza M, et al. Oligomeric Amyloid β Associates with Postsynaptic Densities and Correlates with Excitatory Synapse Loss Near Senile Plaques. P NATL ACAD SCI USA. 2009;106(10):4012-7.
49. Kuchibhotla KV, Goldman ST, Lattarulo CR, Wu H-Y, Hyman BT, Bacskai BJ. Abeta plaques lead to aberrant regulation of calcium homeostasis in vivo resulting in structural and functional disruption of neuronal networks. Neuron (Cambridge, Mass). 2008;59(2):214-25.
50. Meyer-Luehmann M, Mielke M, Spires-Jones TL, Stoothoff W, Jones P, Bacskai BJ, Hyman BT. A Reporter of Local Dendritic Translocation Shows Plaque- Related Loss of Neural System Function in APP-Transgenic Mice. J NEUROSCI. 2009;29(40):12636-40.
51. Lesné S, Koh MT, Kotilinek L, Kayed R, Glabe CG, Yang A, et al. A specific amyloid-β protein assembly in the brain impairs memory. Nature. 2006;440(7082):352-7.
52. Ono K, Condron MM, Teplow DB. Structure–neurotoxicity relationships of amyloid β-protein oligomers. Proceedings of the National Academy of Sciences. 2009;106(35):14745-50.
53. Lorenzo A, Yankner BA. Beta-amyloid neurotoxicity requires fibril formation and is inhibited by congo red. Proceedings of the National Academy of Sciences. 1994;91(25):12243-7.
54. Chatani E, Yamamoto N. Recent progress on understanding the mechanisms of amyloid nucleation. Biophys Rev. 2018;10(2):527-34.
55. Pyun J-M, Kang MJ, Ryoo N, Suh J, Youn YC, Park YH, Kim S. Amyloid Metabolism and Amyloid-Targeting Blood-Based Biomarkers of Alzheimer's Disease. Journal of Alzheimer's disease. 2020;75(3):685-96.

56. Welander H, Frånberg J, Graff C, Sundström E, Winblad B, Tjernberg LO. Aβ43 is more frequent than Aβ40 in amyloid plaque cores from Alzheimer disease brains. J Neurochem. 2009;110(2):697-706.
57. Keller L, Welander H, Chiang H-H, Tjernberg LO, Nennesmo I, Wallin ÅK, Graff C. The PSEN1 I143T mutation in a Swedish family with Alzheimer's disease: Clinical report and quantification of AB in different brain regions. European journal of human genetics : EJHG. 2010;18(11):1202-8.
58. Hirayama A, Horikoshi Y, Maeda M, Ito M, Takashima S. Characteristic developmental expression of amyloid β40, 42 and 43 in patients with Down syndrome. Brain & development (Tokyo 1979). 2003;25(3):180-5.
59. Jäkel L, Boche D, Nicoll JAR, Verbeek MM. Aβ43 in human Alzheimer's disease: effects of active Aβ42 immunization. Acta neuropathologica communications. 2019;7(1):141-.
60. Saito T, Suemoto T, Brouwers N, Sleegers K, Funamoto S, Mihira N, et al. Potent amyloidogenicity and pathogenicity of Aβ43. Nature neuroscience. 2011;14(8):1023-32.
61. Colin LM, Gail S, Nicola AW, Gerd M, Brian LM, Konrad B. Amyloid Plaque Core Protein in Alzheimer Disease and Down Syndrome. Proceedings of the National Academy of Sciences - PNAS. 1985;82(12):4245-9.
62. Miller DL, Papayannopoulos IA, Styles J, Bobin SA, Lin YY, Biemann K, Iqbal K. Peptide Compositions of the Cerebrovascular and Senile Plaque Core Amyloid Deposits of Alzheimer′s Disease. Archives of biochemistry and biophysics. 1993;301(1):41-52.
63. Harigaya Y, Saido TC, Eckman CB, Prada C-M, Shoji M, Younkin SG. Amyloid β Protein Starting Pyroglutamate at Position 3 Is a Major Component of the Amyloid Deposits in the Alzheimer's Disease Brain. Biochem Bioph Res Co. 2000;276(2):422-7.
64. Portelius E, Bogdanovic N, Gustavsson MK, Volkmann I, Brinkmalm G, Zetterberg H, et al. Mass spectrometric characterization of brain amyloid beta isoform signatures in familial and sporadic Alzheimer’s disease. Acta Neuropathol. 2010;120(2):185-93.
65. Schilling S, Lauber T, Schaupp M, Manhart S, Scheel E, Böhm G, Demuth H-U. On the Seeding and Oligomerization of pGlu-Amyloid Peptides (in vitro). Biochemistry (Easton). 2006;45(41):12393-9.
66. Liu YD, Goetze AM, Bass RB, Flynn GC. N-terminal glutamate to pyroglutamate conversion in vivo for human IgG2 antibodies. The Journal of biological chemistry. 2011;286(13):11211-7.
67. Chelius D, Jing K, Lueras A, Rehder DS, Dillon TM, Vizel A, et al. Formation of Pyroglutamic Acid from N-Terminal Glutamic Acid in Immunoglobulin Gamma Antibodies. Analytical chemistry (Washington). 2006;78(7):2370-6.
68. Baglioni C. The role of pyrrolidone carboxylic acid in the initiation of immunoglobulin peptide chains. Biochem Bioph Res Co. 1970;38(2):212-9.

69. Twardzik DR, Peterkofsky A. Glutamic Acid as a Precursor to N-Terminal Pyroglutamic Acid in Mouse Plasmacytoma Protein. Proceedings of the National Academy of Sciences - PNAS. 1972;69(1):274-7.
70. Rehder DS, Dillon TM, Pipes GD, Bondarenko PV. Reversed-phase liquid chromatography/mass spectrometry analysis of reduced monoclonal antibodies in pharmaceutics. Journal of Chromatography A. 2006;1102(1):164-75.
71. Schilling S, Wasternack C, Demuth H-U. Glutaminyl cyclases from animals and plants: A case of functionally convergent protein evolution. Biological chemistry. 2008;389(8):983-91.
72. Vijayan DK, Zhang KYJ. Human glutaminyl cyclase: Structure, function, inhibitors and involvement in Alzheimer's disease. Pharmacological research. 2019;147:104342-.
73. Liu K, Solano I, Mann D, Lemere C, Mercken M, Trojanowski JQ, Lee VMY. Characterization of Abeta11-40/42 peptide deposition in Alzheimer's disease and young Down's syndrome brains: implication of N-terminally truncated Abeta species in the pathogenesis of Alzheimer's disease. Acta neuropathologica. 2006;112(2):163-74.
74. DeMattos Ronald B, Lu J, Tang Y, Racke Margaret M, DeLong Cindy A, Tzaferis John A, et al. A Plaque-Specific Antibody Clears Existing β-amyloid Plaques in Alzheimer's Disease Mice. Neuron (Cambridge, Mass). 2012;76(5):908-20.
75. Saido TC, Yamao-Harigaya W, Iwatsubo T, Kawashima S. Amino- and carboxyl-terminal heterogeneity of β-amyloid peptides deposited in human brain. Neurosci Lett. 1996;215(3):173-6.
76. Jawhar S, Wirths O, Bayer TA. Pyroglutamate amyloid-β (Aβ): A hatchet man in alzheimer disease. The Journal of biological chemistry. 2011;286(45):38825-32.
77. He W, Barrow CJ. The Aβ 3-Pyroglutamyl and 11-Pyroglutamyl Peptides Found in Senile Plaque Have Greater β-Sheet Forming and Aggregation Propensities in Vitro than Full-Length Aβ. Biochemistry (Easton). 1999;38(33):10871-7.
78. Saido TC. Alzheimer's Disease as Proteolytic Disorders: Anabolism and Catabolism of β-Amyloid. Neurobiol Aging. 1998;19(1):S69-S75.
79. Saido TC, Iwatsubo T, Mann DMA, Shimada H, Ihara Y, Kawashima S. Dominant and differential deposition of distinct β-amyloid peptide species, A βN3(pE), in senile plaques. Neuron (Cambridge, Mass). 1995;14(2):457-66.
80. Hosoda R, Saido TC, Otvos L, Arai T, Mann DMA, Lee VMY, et al. Quantification of Modified Amyloid β Peptides in Alzheimer Disease and Down Syndrome Brains. Journal of neuropathology and experimental neurology. 1998;57(11):1089-95.
81. Iwatsubo T, Saido TC, Mann DM, Lee VM, Trojanowski JQ. Full-length amyloid-beta (1-42(43)) and amino-terminally modified and truncated amyloid-beta 42(43) deposit in diffuse plaques. The American journal of pathology. 1996;149(6):1823-30.

82. Wirths O, Breyhan H, Cynis H, Schilling S, Demuth H-U, Bayer TA. Intraneuronal pyroglutamate-Abeta 3-42 triggers neurodegeneration and lethal neurological deficits in a transgenic mouse model. Acta neuropathologica. 2009;118(4):487-96.
83. Wittnam JL, Portelius E, Zetterberg H, Gustavsson MK, Schilling S, Koch B, et al. Pyroglutamate amyloid β(aβ) aggravates behavioral deficits in transgenic amyloid mouse model for Alzheimer disease. The Journal of biological chemistry. 2012;287(11):8154-62.
84. Güntert A, Döbeli H, Bohrmann B. High sensitivity analysis of amyloid-beta peptide composition in amyloid deposits from human and PS2APP mouse brain. Neuroscience. 2006;143(2):461-75.
85. Hardy J, Higgins G. Alzheimer's disease: the amyloid cascade hypothesis. Science (American Association for the Advancement of Science). 1992;256(5054):184-5.
86. Kepp KP, Robakis NK, Høilund-Carlsen PF, Sensi SL, Vissel B. The amyloid cascade hypothesis: an updated critical review. Brain. 2023.
87. Hardy J, Selkoe DJ. The Amyloid Hypothesis of Alzheimer's Disease: Progress and Problems on the Road to Therapeutics. Science (American Association for the Advancement of Science). 2002;297(5580):353-6.
88. Mawuenyega KG, Sigurdson W, Ovod V, Munsell L, Kasten T, Morris JC, et al. Decreased Clearance of CNS β-Amyloid in Alzheimer's Disease. SCIENCE. 2010;330(6012):1774-.
89. Haass C, Lemere CA, Capell A, Citron M, Seubert P, Schenk D, et al. The Swedish mutation causes early-onset Alzheimer's disease by beta-secretase cleavage within the secretory pathway. Nat Med. 1995;1(12):1291-6.
90. Jonsson T, Atwal JK, Steinberg S, Snaedal J, Jonsson PV, Bjornsson S, et al. A mutation in APP protects against Alzheimer's disease and age-related cognitive decline. NATURE. 2012;488(7409):96-9.
91. Maloney JA, Bainbridge T, Gustafson A, Zhang S, Kyauk R, Steiner P, et al. Molecular Mechanisms of Alzheimer Disease Protection by the A673T Allele of Amyloid Precursor Protein. J Biol Chem. 2014;289(45):30990-1000.
92. Palmqvist S, Insel PS, Stomrud E, Janelidze S, Zetterberg H, Brix B, et al. Cerebrospinal fluid and plasma biomarker trajectories with increasing amyloid deposition in Alzheimer's disease. Embo Mol Med. 2019;11(12):e11170.
93. Morris GP, Clark IA, Vissel B. Inconsistencies and controversies surrounding the amyloid hypothesis of Alzheimer's disease. Acta neuropathologica communications. 2014;2(1):135.
94. Salloway S, Sperling R, Fox NC, Blennow K, Klunk W, Raskind M, et al. Two Phase 3 Trials of Bapineuzumab in Mild-to-Moderate Alzheimer's Disease. The New England journal of medicine. 2014;370(4):322-33.
95. Bittner T, Duning T, Rabe C, Clayton D, Quartino A, Bohorquez SS, et al. P32 Phase III studies of crenezumab in early

(prodromal-to-mild) Alzheimers disease (CREAD/CREAD2): Biomarker results. Clinical neurophysiology. 2020;131(4):e194-e5.
96. Avgerinos KI, Ferrucci L, Kapogiannis D. Effects of monoclonal antibodies against amyloid-β on clinical and biomarker outcomes and adverse event risks: A systematic review and meta-analysis of phase III RCTs in Alzheimer's disease. Ageing research reviews. 2021;68:101339.
97. Doody RS, Thomas RG, Farlow M, Iwatsubo T, Vellas B, Joffe S, et al. Phase 3 Trials of Solanezumab for Mild-to-Moderate Alzheimer's Disease. NEW ENGL J MED. 2014;370(4):311-21.
98. Honig LS, Vellas B, Woodward M, Boada M, Bullock R, Borrie M, et al. Trial of Solanezumab for Mild Dementia Due to Alzheimer's Disease. The New England journal of medicine. 2018;378(4):321-30.
99. Salloway S, Farlow M, McDade E, Clifford DB, Wang G, Llibre-Guerra JJ, et al. A trial of gantenerumab or solanezumab in dominantly inherited Alzheimer's disease. Nat Med. 2021;27(7):1187-96.
100. Karran E, De Strooper B. The amyloid hypothesis in Alzheimer disease: new insights from new therapeutics. Nat Rev Drug Discov. 2022;21(4):306-18.
101. Rosenblum WI. Why Alzheimer trials fail: removing soluble oligomeric beta amyloid is essential, inconsistent, and difficult. Neurobiol Aging. 2014;35(5):969-74.
102. Selkoe DJ, Hardy J. The amyloid hypothesis of Alzheimer's disease at 25 years. Embo Mol Med. 2016;8(6):595-608.
103. Snowdon DA. Aging and Alzheimer's disease: lessons from the Nun Study. Gerontologist. 1997;37(2):150-6.
104. SantaCruz KS, Sonnen JA, Pezhouh MK, Desrosiers MF, Nelson PT, Tyas SL. Alzheimer disease pathology in subjects without dementia in 2 studies of aging: the Nun Study and the Adult Changes in Thought Study. J Neuropathol Exp Neurol. 2011;70(10):832-40.
105. Herrup K. The case for rejecting the amyloid cascade hypothesis. Nat Neurosci. 2015;18(6):794-9.
106. Neve RL, Robakis NK. Alzheimer's disease: a re-examination of the amyloid hypothesis. Trends Neurosci. 1998;21(1):15-9.
107. Stern Y. Cognitive reserve in ageing and Alzheimer's disease. Lancet Neurol. 2012;11(11):1006-12.
108. Long JM, Coble DW, Xiong C, Schindler SE, Perrin RJ, Gordon BA, et al. Preclinical Alzheimer's disease biomarkers accurately predict cognitive and neuropathological outcomes. Brain. 2022;145(12):4506-18.
109. Pera M, Montesinos J, Larrea D, Agrawal RR, Velasco KR, Stavrovskaya IG, et al. MAM and C99, key players in the pathogenesis of Alzheimer's disease. International Review of Neurobiology. 2020;154:235-78.
110. Moore BD, Martin J, de Mena L, Sanchez J, Cruz PE, Ceballos-Diaz C, et al. Short Aβ peptides attenuate Aβ42 toxicity in vivo. The Journal of experimental medicine. 2018;215(1):283-301.

111. Ittner LM, Götz J. Amyloid-β and tau — a toxic pas de deux in Alzheimer's disease. Nature reviews Neuroscience. 2011;12(2):65-72.
112. Alvarez A, Toro R, Cáceres A, Maccioni RB. Inhibition of tau phosphorylating protein kinase cdk5 prevents β-amyloid-induced neuronal death. FEBS letters. 1999;459(3):421-6.
113. Alvarez R, Alvarez V, Lahoz CH, Martínez C, Peña J, Sánchez JM, et al. Angiotensin converting enzyme and endothelial nitric oxide synthase DNA polymorphisms and late onset Alzheimer's disease. Journal of neurology, neurosurgery and psychiatry. 1999;67(6):733-6.
114. Guzman-Martinez L, Maccioni RB, Andrade V, Navarrete LP, Pastor MG, Ramos-Escobar N. Neuroinflammation as a common feature of neurodegenerative disorders. Frontiers in pharmacology. 2019;10:1008-.
115. Shen J, Kelleher RJ, III. Presenilin hypothesis of Alzheimer's disease: Evidence for a loss-of-function pathogenic mechanism. Proceedings of the National Academy of Sciences - PNAS. 2007;104(2):403-9.
116. Shen J. Function and Dysfunction of Presenilin. Neuro-degenerative diseases. 2014;13(2-3):61-3.
117. Saura CA, Choi S-Y, Beglopoulos V, Malkani S, Zhang D, Rao BSS, et al. Loss of Presenilin Function Causes Impairments of Memory and Synaptic Plasticity Followed by Age-Dependent Neurodegeneration. Neuron (Cambridge, Mass). 2004;42(1):23-36.
118. Shioi J, Georgakopoulos A, Mehta P, Kouchi Z, Litterst CM, Baki L, Robakis NK. FAD mutants unable to increase neurotoxic Aβ 42 suggest that mutation effects on neurodegeneration may be independent of effects on Aβ. J Neurochem. 2007;101(3):674-81.
119. Xia D, Kelleher RJ, 3rd, Shen J. Loss of Aβ43 Production Caused by Presenilin-1 Mutations in the Knockin Mouse Brain. Neuron. 2016;90(2):417-22.
120. Sun L, Zhou R, Yang G, Shi Y. Analysis of 138 pathogenic mutations in presenilin-1 on the in vitro production of Aβ42 and Aβ40 peptides by γ-secretase. Proc Natl Acad Sci U S A. 2017;114(4):E476-e85.
121. Veugelen S, Saito T, Saido TC, Chávez-Gutiérrez L, De Strooper B. Familial Alzheimer's Disease Mutations in Presenilin Generate Amyloidogenic Aβ Peptide Seeds. Neuron. 2016;90(2):410-6.
122. Mohandas E, Rajmohan V, Raghunath B. Neurobiology of Alzheimer's disease. Indian journal of psychiatry. 2009;51(1):55-61.
123. Kametani F, Hasegawa M. Reconsideration of Amyloid Hypothesis and Tau Hypothesis in Alzheimer's Disease. Front Neurosci. 2018;12:25.
124. Murphy DB, Johnson KA, Borisy GG. Role of tubulin-associated proteins in microtubule nucleation and elongation. J Mol Biol. 1977;117(1):33-52.
125. Trinczek B, Biernat J, Baumann K, Mandelkow EM, Mandelkow E. Domains of tau protein, differential phosphorylation,

and dynamic instability of microtubules. Mol Biol Cell. 1995;6(12):1887-902.
126. Barbier P, Zejneli O, Martinho M, Lasorsa A, Belle V, Smet-Nocca C, et al. Role of Tau as a Microtubule-Associated Protein: Structural and Functional Aspects. Front Aging Neurosci. 2019;11:204.
127. Barthélemy NR, Li Y, Joseph-Mathurin N, Gordon BA, Hassenstab J, Benzinger TLS, et al. A soluble phosphorylated tau signature links tau, amyloid and the evolution of stages of dominantly inherited Alzheimer's disease. Nat Med. 2020;26(3):398-407.
128. Vanmechelen E, Vanderstichele H, Davidsson P, Van Kerschaver E, Van Der Perre B, Sjögren M, et al. Quantification of tau phosphorylated at threonine 181 in human cerebrospinal fluid: a sandwich ELISA with a synthetic phosphopeptide for standardization. Neurosci Lett. 2000;285(1):49-52.
129. Buerger K, Zinkowski R, Teipel SJ, Tapiola T, Arai H, Blennow K, et al. Differential diagnosis of Alzheimer disease with cerebrospinal fluid levels of Tau protein phosphorylated at threonine 231.(Archives of Neurology). JAMA : the journal of the American Medical Association. 2002;288(18):2241.
130. Parnetti L, Lanari A, Amici S, Gallai V, Vanmechelen E, Hulstaert F. CSF phosphorylated tau is a possible marker for discriminating Alzheimer's disease from dementia with Lewy bodies. Neurol Sci. 2001;22(1):77-8.
131. Gómez-Isla T, Hollister R, West H, Mui S, Growdon JH, Petersen RC, et al. Neuronal loss correlates with but exceeds neurofibrillary tangles in Alzheimer's disease. Ann Neurol. 1997;41(1):17-24.
132. Metaxas A, Kempf SJ. Neurofibrillary tangles in Alzheimer's disease: Elucidation of the molecular mechanism by immunohistochemistry and tau protein phospho-proteomics. NEURAL REGEN RES. 2016;11(10):1579-81.
133. Braak H, Braak E. Neuropathological stageing of Alzheimer-related changes. Acta Neuropathol. 1991;82(4):239-59.
134. Braak H, Zetterberg H, Del Tredici K, Blennow K. Intraneuronal tau aggregation precedes diffuse plaque deposition, but amyloid-β changes occur before increases of tau in cerebrospinal fluid. Acta neuropathologica. 2013;126(5):631-41.
135. Arnsten AFT, Datta D, Del Tredici K, Braak H. Hypothesis: Tau pathology is an initiating factor in sporadic Alzheimer's disease. Alzheimers Dement. 2021;17(1):115-24.
136. Rapoport M, Dawson HN, Binder LI, Vitek MP, Ferreira A. Tau Is Essential to β-Amyloid-Induced Neurotoxicity. Proceedings of the National Academy of Sciences - PNAS. 2002;99(9):6364-9.
137. SantaCruz K, Lewis J, Spires T, Paulson J, Kotilinek L, Ingelsson M, et al. Tau Suppression in a Neurodegenerative Mouse Model Improves Memory Function. Science (American Association for the Advancement of Science). 2005;309(5733):476-81.
138. Roberson ED, Scearce-Levie K, Palop JJ, Yan F, Cheng IH, Wu T, et al. Reducing Endogenous Tau Ameliorates Amyloid ß-

Induced Deficits in an Alzheimer's Disease Mouse Model. Science (American Association for the Advancement of Science). 2007;316(5825):750-4.
139. Shipton OA, Leitz JR, Dworzak J, Acton CEJ, Tunbridge EM, Denk F, et al. Tau protein is required for amyloid β-induced impairment of hippocampal long-term potentiation. The Journal of neuroscience. 2011;31(5):1688-92.
140. Sato C, Barthélemy NR, Mawuenyega KG, Patterson BW, Gordon BA, Jockel-Balsarotti J, et al. Tau Kinetics in Neurons and the Human Central Nervous System. Neuron. 2018;98(4):861-4.
141. Maia LF, Kaeser SA, Reichwald J, Hruscha M, Martus P, Staufenbiel M, Jucker M. Changes in amyloid-β and tau in the cerebrospinal fluid of transgenic mice overexpressing amyloid precursor protein. Science translational medicine. 2013;5(194):194re2-re2.
142. Kanmert D, Cantlon A, Muratore CR, Jin M, O'Malley TT, Lee G, et al. C-terminally truncated forms of tau, but not full-length tau or its C-terminal fragments, are released from neurons independently of cell death. J NEUROSCI. 2015;35(30):10851-65.
143. Canevari L, Abramov AY, Duchen MR. Toxicity of Amyloid β Peptide: Tales of Calcium, Mitochondria, and Oxidative Stress. Neurochem Res. 2004;29(3):637-50.
144. Subramanian J, Savage JC, Tremblay M-È. Synaptic Loss in Alzheimer's Disease: Mechanistic Insights Provided by Two-Photon in vivo Imaging of Transgenic Mouse Models. Frontiers in cellular neuroscience. 2020;14:592607.
145. Bronzuoli MR, Iacomino A, Steardo L, Scuderi C. Targeting neuroinflammation in Alzheimer’s disease. Journal of inflammation research. 2016;9:199-208.
146. Perea G, Navarrete M, Araque A. Tripartite synapses: astrocytes process and control synaptic information. TRENDS NEUROSCI. 2009;32(8):421-31.
147. Morales I, Jiménez JM, Mancilla M, Maccioni RB. Tau oligomers and fibrils induce activation of microglial cells. J Alzheimers Dis. 2013;37(4):849-56.
148. Bamberger ME, Harris ME, McDonald DR, Husemann J, Landreth GE. A cell surface receptor complex for fibrillar beta-amyloid mediates microglial activation. J Neurosci. 2003;23(7):2665-74.
149. Ransohoff RM, Perry VH. Microglial physiology: Unique stimuli, specialized responses. Annual review of immunology. 2009;27(1):119-45.
150. Cameron B, Landreth GE. Inflammation, microglia, and alzheimer's disease. Neurobiol Dis. 2009;37(3):503-9.
151. Sanchez-Varo R, Trujillo-Estrada L, Sanchez-Mejias E, Torres M, Baglietto-Vargas D, Moreno-Gonzalez I, et al. Abnormal accumulation of autophagic vesicles correlates with axonal and synaptic pathology in young Alzheimer’s mice hippocampus. Acta Neuropathol. 2011;123(1):53-70.

152. Wang J, Tan L, Wang HF, Tan CC, Meng XF, Wang C, et al. Anti-inflammatory drugs and risk of Alzheimer's disease: an updated systematic review and meta-analysis. J Alzheimers Dis. 2015;44(2):385-96.
153. Jordan F, Quinn TJ, McGuinness B, Passmore P, Kelly JP, Tudur Smith C, et al. Aspirin and other non-steroidal anti-inflammatory drugs for the prevention of dementia. Cochrane Database Syst Rev. 2020;4(4):Cd011459.
154. Hirohata M, Ono K, Naiki H, Yamada M. Non-steroidal anti-inflammatory drugs have anti-amyloidogenic effects for Alzheimer's beta-amyloid fibrils in vitro. Neuropharmacology. 2005;49(7):1088-99.
155. Yan Q, Zhang J, Liu H, Babu-Khan S, Vassar R, Biere AL, et al. Anti-inflammatory drug therapy alters beta-amyloid processing and deposition in an animal model of Alzheimer's disease. J Neurosci. 2003;23(20):7504-9.
156. McGeer PL, McGeer EG. The amyloid cascade-inflammatory hypothesis of Alzheimer disease: implications for therapy. Acta Neuropathol. 2013;126(4):479-97.
157. Wyss-Coray T, Mucke L. Inflammation in Neurodegenerative Disease—A Double-Edged Sword. Neuron (Cambridge, Mass). 2002;35(3):419-32.
158. Hanisch U-K, Kettenmann H. Microglia: active sensor and versatile effector cells in the normal and pathologic brain. Nature neuroscience. 2007;10(11):1387-94.
159. Rogers J, Mastroeni D, Leonard B, Joyce J, Grover A. Neuroinflammation in Alzheimer's Disease and Parkinson's Disease: Are Microglia Pathogenic in Either Disorder? International Review of Neurobiology. 2007;82:235-46.
160. Ransohoff RM. A polarizing question: do M1 and M2 microglia exist? Nature neuroscience. 2016;19(8):987-91.
161. Ransohoff RM. How neuroinflammation contributes to neurodegeneration. Science (American Association for the Advancement of Science). 2016;353(6301):777-83.
162. Lyman M, Lloyd DG, Ji X, Vizcaychipi MP, Ma D. Neuroinflammation: the role and consequences. Neurosci Res. 2014;79:1-12.
163. Edwards FA. A Unifying Hypothesis for Alzheimer’s Disease: From Plaques to Neurodegeneration. Trends in neurosciences (Regular ed). 2019;42(5):310-22.
164. Katzman R, Terry R, DeTeresa R, Brown T, Davies P, Fuld P, et al. Clinical, pathological, and neurochemical changes in dementia: A subgroup with preserved mental status and numerous neocortical plaques. Ann Neurol. 1988;23(2):138-44.
165. Perea JR, Bolós M, Avila J. Microglia in Alzheimer's Disease in the Context of Tau Pathology. Biomolecules. 2020;10(10).
166. Leng F, Edison P. Neuroinflammation and microglial activation in Alzheimer disease: where do we go from here? Nat Rev Neurol. 2021;17(3):157-72.

167. Coart E, Barrado LG, Duits FH, Scheltens P, van der Flier WM, Teunissen CE, et al. Correcting for the Absence of a Gold Standard Improves Diagnostic Accuracy of Biomarkers in Alzheimer's Disease. Journal of Alzheimer's disease. 2015;46(4):889-99.
168. World Health O, International Programme on Chemical S. Biomarkers in risk assessment : validity and validation. Geneva: World Health Organization; 2001.
169. Atkinson AJ, Colburn WA, DeGruttola VG, DeMets DL, Downing GJ, Hoth DF, et al. Biomarkers and surrogate endpoints: Preferred definitions and conceptual framework. Clinical pharmacology and therapeutics. 2001;69(3):89-95.
170. Beach TG, Monsell SE, Phillips LE, Kukull W. Accuracy of the Clinical Diagnosis of Alzheimer Disease at National Institute on Aging Alzheimer Disease Centers, 2005–2010. Journal of neuropathology and experimental neurology. 2012;71(4):266-73.
171. Sabbagh MN, Lue L-F, Fayard D, Shi J. Increasing Precision of Clinical Diagnosis of Alzheimer's Disease Using a Combined Algorithm Incorporating Clinical and Novel Biomarker Data. Neurol Ther. 2017;6(S1):83-95.
172. Eikelboom WS, van Rooij JGJ, van den Berg E, Coesmans M, Jiskoot LC, Singleton E, et al. Neuropsychiatric Symptoms Complicating the Diagnosis of Alzheimer's Disease: A Case Report. Journal of Alzheimer's disease. 2018;66(4):1363-9.
173. Zetterberg H, Bähr M. Disease signatures: Biomarkers/indicators of neurodegeneration. Molecular and cellular neurosciences. 2019;97:1-2.
174. Hampel H, Cummings J, Blennow K, Gao P, Jack CR, Jr., Vergallo A. Developing the ATX(N) classification for use across the Alzheimer disease continuum. Nat Rev Neurol. 2021;17(9):580-9.
175. Molinuevo JL, Ayton S, Batrla R, Bednar MM, Bittner T, Cummings J, et al. Current state of Alzheimer's fluid biomarkers. Acta Neuropathologica. 2018;136(6):821-53.
176. Albani D, Marizzoni M, Ferrari C, Fusco F, Boeri L, Raimondi I, et al. Plasma A beta(42) as a Biomarker of Prodromal Alzheimer's Disease Progression in Patients with Amnestic Mild Cognitive Impairment: Evidence from the PharmaCog/E-ADNI Study. J Alzheimers Dis. 2019;69(1):37-48.
177. Shi L, Baird AL, Westwood S, Hye A, Dobson R, Thambisetty M, Lovestone S. A Decade of Blood Biomarkers for Alzheimer's Disease Research: An Evolving Field, Improving Study Designs, and the Challenge of Replication. Journal of Alzheimer's Disease , 62 (3) pp 1181-1198 (2018). 2018.
178. Janelidze S, Stomrud E, Palmqvist S, Zetterberg H, van Westen D, Jeromin A, et al. Plasma beta-amyloid in Alzheimer's disease and vascular disease. Sci Rep-Uk. 2016;6:26801.
179. Blennow K, Zetterberg H. Understanding Biomarkers of Neurodegeneration: Ultrasensitive detection techniques pave the way for mechanistic understanding. Nat Med. 2015;21(3):217-9.
180. Zetterberg H, Burnham SC. Blood-based molecular biomarkers for Alzheimer's disease. Mol Brain. 2019;12:26.

181. Hesse C, Rosengren L, Andreasen N, Davidsson P, Vanderstichele H, Vanmechelen E, Blennow K. Transient increase in total tau but not phospho-tau in human cerebrospinal fluid after acute stroke. Neurosci Lett. 2001;297(3):187-90.
182. Riemenschneider M, Wagenpfeil S, Vanderstichele H, Otto M, Wiltfang J, Kretzschmar H, et al. Phospho-tau total tau ratio in cerebrospinal fluid discriminates Creutzfeldt-Jakob disease from other dementias. Mol Psychiatr. 2003;8(3):343-7.
183. Kohnken R, Buerger K, Zinkowski R, Miller C, Kerkman D, Debernardis J, et al. Detection of tau phosphorylated at threonine 231 in cerebrospinal fluid of Alzheimer's disease patients. Neurosci Lett. 2000;287(3):187-90.
184. Verbeek MM, Kremer BP, Jansen RW, de Jong D. Tau protein phosphorylated at threonine 181 in cerebrospinal fluid as a possible biomarker for Alzheimer's disease. Neurobiol Aging. 2004;25:S364-S.
185. Welge V, Fiege O, Lewczuk P, Mollenhauer B, Esselmann H, Klafki HW, et al. Combined CSF tau, p-tau181 and amyloid-beta 38/40/42 for diagnosing Alzheimer's disease. J Neural Transm. 2009;116(2):203-12.
186. Shekhar S, Kumar R, Rai N, Kumar V, Singh K, Upadhyay AD, et al. Estimation of Tau and phosphorylated Tau181 in serum of Alzheimer's disease and mild cognitive impairment patients. Plos One. 2016;11(7):e0159099-e.
187. Tatebe H, Kasai T, Ohmichi T, Kishi Y, Kakeya T, Waragai M, et al. Quantification of plasma phosphorylated tau to use as a biomarker for brain Alzheimer pathology: pilot case-control studies including patients with Alzheimer's disease and down syndrome. Mol Neurodegener. 2017;12:63.
188. Janelidze S, Mattsson N, Palmqvist S, Smith R, Beach TG, Serrano GE, et al. Plasma P-tau181 in Alzheimer's disease: relationship to other biomarkers, differential diagnosis, neuropathology and longitudinal progression to Alzheimer's dementia. Nat Med. 2020;26(3):379-+.
189. Karikari TK, Pascoal TA, Ashton NJ, Janelidze S, Benedet AL, Rodriguez JL, et al. Blood phosphorylated tau 181 as a biomarker for Alzheimer's disease: a diagnostic performance and prediction modelling study using data from four prospective cohorts. Lancet Neurol. 2020;19(5):422-33.
190. Mattsson N, Smith R, Strandberg O, Palmqvist S, Schöll M, Insel PS, et al. Comparing (18)F-AV-1451 with CSF t-tau and p-tau for diagnosis of Alzheimer disease. Neurology. 2018;90(5):e388-e95.
191. Cassinelli Petersen G, Roytman M, Chiang GC, Li Y, Gordon ML, Franceschi AM. Overview of tau PET molecular imaging. Curr Opin Neurol. 2022;35(2):230-9.
192. Rowley PA, Samsonov AA, Betthauser TJ, Pirasteh A, Johnson SC, Eisenmenger LB. Amyloid and Tau PET Imaging of Alzheimer Disease and Other Neurodegenerative Conditions. Semin Ultrasound CT MR. 2020;41(6):572-83.

193. Wiltfang J, Esselmann H, Bibl M, Hüll M, Hampel H, Kessler H, et al. Amyloid beta peptide ratio 42/40 but not A beta 42 correlates with phospho-Tau in patients with low- and high-CSF A beta 40 load. J Neurochem. 2007;101(4):1053-9.
194. Hansson O, Lehmann S, Otto M, Zetterberg H, Lewczuk P. Advantages and disadvantages of the use of the CSF Amyloid β (Aβ) 42/40 ratio in the diagnosis of Alzheimer's Disease. Alzheimer's Research & Therapy. 2019;11(1):34.
195. Slaets S, Le Bastard N, Martin J-J, Sleegers K, Van Broeckhoven C, De Deyn PP, Engelborghs S. Cerebrospinal fluid Aβ1-40 improves differential dementia diagnosis in patients with intermediate P-tau181P levels. Journal of Alzheimer's disease. 2013;36(4):759-67.
196. Bousiges O, Cretin B, Lavaux T, Philippi N, Jung B, Hezard S, et al. Diagnostic Value of Cerebrospinal Fluid Biomarkers (Phospho-Tau(181), total-Tau, A beta(42), and A beta(40)) in Prodromal Stage of Alzheimer's Disease and Dementia with Lewy Bodies. J Alzheimers Dis. 2016;51(4):1069-83.
197. Janelidze S, Pannee J, Mikulskis A, Chiao P, Zetterberg H, Blennow K, Hansson O. Concordance Between Different Amyloid Immunoassays and Visual Amyloid Positron Emission Tomographic Assessment. Jama Neurol. 2017;74(12):1492-501.
198. Olsson B, Lautner R, Andreasson U, Ohrfelt A, Portelius E, Bjerke M, et al. CSF and blood biomarkers for the diagnosis of Alzheimer's disease: a systematic review and meta-analysis. The Lancet Neurology. 2016;15(7):673-84.
199. Lee JC, Kim SJ, Hong S, Kim Y. Diagnosis of Alzheimer's disease utilizing amyloid and tau as fluid biomarkers. Experimental & molecular medicine. 2019;51(5):1-10.
200. Sato C, Barthélemy NR, Mawuenyega KG, Patterson BW, Gordon BA, Jockel-Balsarotti J, et al. Tau Kinetics in Neurons and the Human Central Nervous System. Neuron (Cambridge, Mass). 2018;97(6):1284-98.e7.
201. Zetterberg H. Tauomics and Kinetics in Human Neurons and Biological Fluids. Neuron (Cambridge, Mass). 2018;97(6):1202-5.
202. Dage JL, Wennberg AMV, Airey DC, Hagen CE, Knopmand DS, Machulda MM, et al. Levels of tau protein in plasma are associated with neurodegeneration and cognitive function in a population-based elderly cohort. Alzheimers Dement. 2016;12(12):1226-34.
203. Zetterberg H, Wilson D, Andreasson U, Minthon L, Blennow K, Randall J, Hansson O. Plasma tau levels in Alzheimer's disease. Alzheimer's research & therapy. 2013;5(2):9-.
204. Chiu MJ, Chen YF, Chen TF, Yang SY, Yang FPG, Tseng TW, et al. Plasma tau as a window to the brain—negative associations with brain volume and memory function in mild cognitive impairment and early alzheimer's disease. Hum Brain Mapp. 2014;35(7):3132-42.

205. Mattsson N, Zetterberg H, Janelidze S, Insel PS, Andreasson U, Stomrud E, et al. Plasma tau in Alzheimer disease. Neurology. 2016;87(17):1827-35.
206. Schindler SE, Bollinger JG, Ovod V, Mawuenyega KG, Li Y, Gordon BA, et al. High-precision plasma β-amyloid 42/40 predicts current and future brain amyloidosis. Neurology. 2019;93(17):e1647-e59.
207. Mayeux R, Honig LS, Tang MX, Manly J, Stern Y, Schupf N, Mehta PD. Plasma Aβ40 and Aβ42 and Alzheimer's disease: Relation to age, mortality, and risk. Neurology. 2003;61(9):1185-90.
208. Pomara N, Willoughby LM, Sidtis JJ, Mehta PD. Selective Reductions in Plasma Aβ 1-42 in Healthy Elderly Subjects During Longitudinal Follow-Up: A Preliminary Report. The American journal of geriatric psychiatry. 2005;13(10):914-7.
209. van Oijen M, Hofman A, Soares HD, Koudstaal PJ, Breteler MMB. Plasma Aβ1-40 and Aβ1-42 and the risk of dementia: a prospective case-cohort study. Lancet Neurol. 2006;5(8):655-60.
210. Graff-Radford NR, Crook JE, Lucas J, Boeve BF, Knopman DS, Ivnik RJ, et al. Association of Low Plasma Aβ42/Aβ40 Ratios With Increased Imminent Risk for Mild Cognitive Impairment and Alzheimer Disease. Archives of neurology (Chicago). 2007;64(3):354-62.
211. Irizarry MC. Biomarkers of Alzheimer disease in plasma. Neurotherapeutics. 2004;1(2):226-34.
212. Li L, Chen Y, Zhu J-J. Recent Advances in Electrochemiluminescence Analysis. Analytical chemistry (Washington). 2017;89(1):358-71.
213. Cohen L, Walt DR. Highly Sensitive and Multiplexed Protein Measurements. Chemical reviews. 2019;119(1):293-321.
214. Kan CW, Tobos CI, Rissin DM, Wiener AD, Meyer RE, Svancara DM, et al. Digital enzyme-linked immunosorbent assays with sub-attomolar detection limits based on low numbers of capture beads combined with high efficiency bead analysis. Lab on a chip. 2020;20(12):2122-35.
215. Rissin DM, Kan CW, Campbell TG, Howes SC, Fournier DR, Song L, et al. Single-molecule enzyme-linked immunosorbent assay detects serum proteins at subfemtomolar concentrations. Nature biotechnology. 2010;28(6):595-9.
216. Nakamura A, Kaneko N, Villemagne VL, Kato T, Doecke J, Doré V, et al. High performance plasma amyloid-β biomarkers for Alzheimer's disease. Nature (London). 2018;554(7691):249-54.
217. Rembach A, Faux NG, Watt AD, Pertile KK, Rumble RL, Trounson BO, et al. Changes in plasma amyloid beta in a longitudinal study of aging and Alzheimer's disease. Alzheimer's & dementia. 2014;10(1):53-61.
218. Jessen F, Amariglio RE, van Boxtel M, Breteler M, Ceccaldi M, Chételat G, et al. A conceptual framework for research on subjective cognitive decline in preclinical Alzheimer's disease. Alzheimer's & dementia. 2014;10(6):844-52.

219. Pesaresi M, Lovati C, Bertora P, Mailland E, Galimberti D, Scarpini E, et al. Plasma levels of beta-amyloid (1–42) in Alzheimer's disease and mild cognitive impairment. Neurobiol Aging. 2006;27(6):904-5.
220. Vergallo A, Megret L, Lista S, Cavedo E, Zetterberg H, Blennow K, et al. Plasma amyloid beta 40/42 ratio predicts cerebral amyloidosis in cognitively normal individuals at risk for Alzheimer's disease. Alzheimers Dement. 2019;15(6):764-75.
221. Ovod V, Ramsey KN, Mawuenyega KG, Bollinger JG, Hicks T, Schneider T, et al. Amyloid β concentrations and stable isotope labeling kinetics of human plasma specific to central nervous system amyloidosis. Alzheimer's & dementia. 2017;13(8):841-9.
222. Roher AE, Esh CL, Kokjohn TA, Castaño EM, Van Vickle GD, Kalback WM, et al. Aβ peptides in human plasma and tissues and their significance for Alzheimer's disease. Alzheimer's & dementia. 2009;5(1):18-29.
223. Hansson O. Biomarkers for neurodegenerative diseases. Nat Med. 2021;27(6):954-63.
224. Teunissen CE, Verberk IMW, Thijssen EH, Vermunt L, Hansson O, Zetterberg H, et al. Blood-based biomarkers for Alzheimer's disease: towards clinical implementation. Lancet Neurol. 2022;21(1):66-77.
225. Alawode DOT, Fox NC, Zetterberg H, Heslegrave AJ. Alzheimer's Disease Biomarkers Revisited From the Amyloid Cascade Hypothesis Standpoint. Front Neurosci. 2022;16:837390.
226. Martin L, Latypova X, Terro F. Post-translational modifications of tau protein: Implications for Alzheimer's disease. Neurochem Int. 2011;58(4):458-71.
227. Suárez-Calvet M, Karikari TK, Ashton NJ, Lantero Rodríguez J, Milà-Alomà M, Gispert JD, et al. Novel tau biomarkers phosphorylated at T181, T217 or T231 rise in the initial stages of the preclinical Alzheimer's continuum when only subtle changes in Aβ pathology are detected. Embo Mol Med. 2020;12(12):e12921-n/a.
228. Nelson PT, Alafuzoff I, Bigio EH, Bouras C, Braak H, Cairns NJ, et al. Correlation of Alzheimer Disease Neuropathologic Changes With Cognitive Status: A Review of the Literature. J NEUROPATH EXP NEUR. 2012;71(5):362-81.
229. Bayoumy S, Verberk IMW, den Dulk B, Hussainali Z, Zwan M, van der Flier WM, et al. Clinical and analytical comparison of six Simoa assays for plasma P-tau isoforms P-tau181, P-tau217, and P-tau231. Alzheimer's research & therapy. 2021;13(1).
230. Mielke MM, Hagen CE, Xu J, Chai XY, Vemuri P, Lowe VJ, et al. Plasma phospho-tau181 increases with Alzheimer's disease clinical severity and is associated with tau- and amyloid-positron emission tomography. Alzheimers Dement. 2018;14(8):989-97.
231. Karikari TK, Benedet AL, Ashton NJ, Lantero Rodriguez J, Snellman A, Suárez-Calvet M, et al. Diagnostic performance and prediction of clinical progression of plasma phospho-tau181 in the Alzheimer's Disease Neuroimaging Initiative. Mol Psychiatr. 2020;26(2):429-42.

232. Funato H, Yoshimura M, Yamazaki T, Saido TC, Ito Y, Yokofujita J, et al. Astrocytes containing amyloid beta-protein (A beta)-positive granules are associated with AP40-positive diffuse plaques in the aged human brain. Am J Pathol. 1998;152(4):983-92.
233. Thal DR, Schultz C, Dehghani F, Yamaguchi H, Braak H, Braak E. Amyloid beta-protein (Abeta)-containing astrocytes are located preferentially near N-terminal-truncated Abeta deposits in the human entorhinal cortex. Acta neuropathologica. 2000;100(6):608-17.
234. Wyss-Coray T, Yan F, Brionne TC, Lu E, Husemann J, Loike JD, et al. Adult mouse astrocytes degrade amyloid-β in vitro and in situ. Nat Med. 2003;9(4):453-7.
235. Beach TG, McGeer EG. Lamina-specific arrangement of astrocytic gliosis and senile plaques in Alzheimer's disease visual cortex. Brain research. 1988;463(2):357-61.
236. Perez-Nievas BG, Serrano-Pozo A. Deciphering the astrocyte reaction in Alzheimer's disease. Front Aging Neurosci. 2018;10:114-.
237. Garwood CJ, Pooler AM, Atherton J, Hanger DP, Noble W. Astrocytes are important mediators of Aβ-induced neurotoxicity and tau phosphorylation in primary culture. CELL DEATH DIS. 2011;2(6):e167-e.
238. Söllvander S, Nikitidou E, Brolin R, Söderberg L, Sehlin D, Lannfelt L, Erlandsson A. Accumulation of amyloid-β by astrocytes result in enlarged endosomes and microvesicle-induced apoptosis of neurons. Mol Neurodegener. 2016;11(1):38-.
239. Pike CJ, Cummings BJ, Cotman CW. Early association of reactive astrocytes with senile plaques in Alzheimer's disease. EXP NEUROL. 1995;132(2):172-9.
240. Vehmas AK, Kawas CH, Stewart WF, Troncoso JC. Immune reactive cells in senile plaques and cognitive decline in Alzheimer’s disease. Neurobiol Aging. 2003;24(2):321-31.
241. Carter SF, Scholl M, Almkvist O, Wall A, Engler H, Langstrom B, Nordberg A. Evidence for Astrocytosis in Prodromal Alzheimer Disease Provided by C-11-Deuterium-L-Deprenyl: A Multitracer PET Paradigm Combining C-11-Pittsburgh Compound B and F-18-FDG. J NUCL MED. 2012;53(1):37-46.
242. Scholl M, Carter SF, Westman E, Rodriguez-Vieitez E, Almkvist O, Thordardottir S, et al. Early astrocytosis in autosomal dominant Alzheimer's disease measured in vivo by multi-tracer positron emission tomography. Sci Rep-Uk. 2015;5(1):16404-.
243. Rodriguez-Vieitez E, Saint-Aubert L, Carter SF, Almkvist O, Farid K, Schöll M, et al. Diverging longitudinal changes in astrocytosis and amyloid PET in autosomal dominant Alzheimer's disease. Brain. 2016;139(3):922-36.
244. Colangelo AM, Alberghina L, Papa M. Astrogliosis as a therapeutic target for neurodegenerative diseases. Neurosci Lett. 2014;565:59-64.
245. Ishiki A, Kamada M, Kawamura Y, Terao C, Shimoda F, Tomita N, et al. Glial fibrillar acidic protein in the cerebrospinal fluid of

Alzheimer's disease, dementia with Lewy bodies, and frontotemporal lobar degeneration. J Neurochem. 2016;136(2):258-61.
246. Milà-Alomà M, Salvadó G, Gispert JD, Vilor-Tejedor N, Grau-Rivera O, Sala-Vila A, et al. Amyloid beta, tau, synaptic, neurodegeneration, and glial biomarkers in the preclinical stage of the Alzheimer's continuum. Alzheimer's & dementia. 2020;16(10):1358-71.
247. Elahi FM, Casaletto KB, La Joie R, Walters SM, Harvey D, Wolf A, et al. Plasma biomarkers of astrocytic and neuronal dysfunction in early- and late-onset Alzheimer's disease. Alzheimer's & dementia. 2020;16(4):681-95.
248. Mayer CA, Brunkhorst R, Niessner M, Pfeilschifter W, Steinmetz H, Foerch C. Blood Levels of Glial Fibrillary Acidic Protein (GFAP) in Patients with Neurological Diseases. Plos One. 2013;8(4):e62101-e.
249. Heller C, Foiani MS, Moore K, Convery R, Bocchetta M, Neason M, et al. Plasma glial fibrillary acidic protein is raised in progranulin-associated frontotemporal dementia. Journal of neurology, neurosurgery and psychiatry. 2020;91(3):263-70.
250. van Ballegoij WJC, van de Stadt SIW, Huffnagel IC, Kemp S, Willemse EAJ, Teunissen CE, Engelen M. Plasma NfL and GFAP as biomarkers of spinal cord degeneration in adrenoleukodystrophy. Ann Clin Transl Neur. 2020;7(11):2127-36.
251. Verberk IMW, Thijssen E, Koelewijn J, Mauroo K, Vanbrabant J, de Wilde A, et al. Combination of plasma amyloid beta(1-42/1-40) and glial fibrillary acidic protein strongly associates with cerebral amyloid pathology. Alzheimer's research & therapy. 2020;12(1):1-118.
252. Asken BM, VandeVrede L, Rojas JC, Fonseca C, Staffaroni AM, Elahi FM, et al. Lower White Matter Volume and Worse Executive Functioning Reflected in Higher Levels of Plasma GFAP among Older Adults with and Without Cognitive Impairment. Journal of the International Neuropsychological Society. 2021:1-12.
253. Oeckl P, Halbgebauer S, Anderl-Straub S, Steinacker P, Huss AM, Neugebauer H, et al. Glial Fibrillary Acidic Protein in Serum is Increased in Alzheimer's Disease and Correlates with Cognitive Impairment. J Alzheimers Dis. 2019;67(2):481-8.
254. Rajan KB, Aggarwal NT, McAninch EA, Weuve J, Barnes LL, Wilson RS, et al. Remote Blood Biomarkers of Longitudinal Cognitive Outcomes in a Population Study. Ann Neurol. 2020;88(6):1065-76.
255. Chatterjee P, Peini S, Stoops E, Goozee K, Villemagne VL, Asih PR, et al. Plasma glial fibrillary acidic protein is elevated in cognitively normal older adults at risk of Alzheimer’s disease. Transl Psychiat. 2021;11(1):27-.
256. Cicognola C, Janelidze S, Hertze J, Zetterberg H, Blennow K, Mattsson-Carlgren N, Hansson O. Plasma glial fibrillary acidic protein detects Alzheimer pathology and predicts future conversion to Alzheimer dementia in patients with mild cognitive impairment. Alzheimer's research & therapy. 2021;13(1):68-.

257. Benedet AL, Milà-Alomà M, Vrillon A, Ashton NJ, Pascoal TA, Lussier F, et al. Differences Between Plasma and Cerebrospinal Fluid Glial Fibrillary Acidic Protein Levels Across the Alzheimer Disease Continuum. Jama Neurol. 2021.
258. Giannoni P, Badaut J, Dargazanli C, De Maudave AFH, Klement W, Costalat V, Marchi N. The pericyte-glia interface at the blood-brain barrier. Clinical science (1979). 2018;132(3):361-74.
259. Banks WA. Drug delivery to the brain in Alzheimer's disease: Consideration of the blood–brain barrier. Advanced drug delivery reviews. 2012;64(7):629-39.
260. Ashton NJ, Suárez-Calvet M, Karikari TK, Lantero-Rodriguez J, Snellman A, Sauer M, et al. Effects of pre-analytical procedures on blood biomarkers for Alzheimer's pathophysiology, glial activation, and neurodegeneration. Alzheimer's & dementia : diagnosis, assessment & disease monitoring. 2021;13(1):e12168-n/a.
261. Abdelhak A, Hottenrott T, Morenas-Rodríguez E, Suárez-Calvet M, Zettl UK, Haass C, et al. Glial Activation Markers in CSF and Serum From Patients With Primary Progressive Multiple Sclerosis: Potential of Serum GFAP as Disease Severity Marker? Front Neurol. 2019;10:280-.
262. Yuan A, Nixon RA. Neurofilament Proteins as Biomarkers to Monitor Neurological Diseases and the Efficacy of Therapies. Front Neurosci-Switz. 2021;15:689938-.
263. Schlaepfer WW, Lynch RG. Immunofluorescence Studies of Neurofilaments in the Rat and Human Peripheral and Central Nervous System. The Journal of cell biology. 1977;74(1):241-50.
264. Lista S, Toschi N, Baldacci F, Zetterberg H, Blennow K, Kilimann I, et al. Diagnostic accuracy of CSF neurofilament light chain protein in the biomarker-guided classification system for Alzheimer's disease. Neurochem Int. 2017;108:355-60.
265. Sjögren M, Blomberg M, Jonsson M, Wahlund LO, Edman Å, Lind K, et al. Neurofilament protein in cerebrospinal fluid: A marker of white matter changes. Journal of neuroscience research. 2001;66(3):510-6.
266. Zetterberg H, Skillbäck T, Mattsson N, Trojanowski JQ, Portelius E, Shaw LM, et al. Association of Cerebrospinal Fluid Neurofilament Light Concentration With Alzheimer Disease Progression. Jama Neurol. 2016;73(1):60-7.
267. Mattsson N, Insel PS, Palmqvist S, Portelius E, Zetterberg H, Weiner M, et al. Cerebrospinal fluid tau, neurogranin, and neurofilament light in Alzheimer's disease. EMBO Molecular Medicine , 8 (10) pp 1184-1196 (2016). 2016.
268. Petzold A, Keir G, Warren J, Fox N, Rossor MN. A systematic review and meta-analysis of CSF neurofilament protein levels as biomarkers in dementia. Neurodegener Dis. 2007;4(2-3):185-94.
269. Aschenbrenner AJ, Gordon BA, Fagan AM, Schindler SE, Balota DA, Morris JC, Hassenstab JJ. Neurofilament light predicts decline in attention but not episodic memory in preclinical Alzheimer disease. Journal of Alzheimer's disease. 2020;74(4):1119-29.

270. Jin M, Cao L, Dai Y-P. Role of Neurofilament Light Chain as a Potential Biomarker for Alzheimer's Disease: A Correlative Meta-Analysis. Front Aging Neurosci. 2019;11:254-.
271. Dhiman K, Gupta VB, Villemagne VL, Eratne D, Graham PL, Fowler C, et al. Cerebrospinal fluid neurofilament light concentration predicts brain atrophy and cognition in Alzheimer's disease. Alzheimer's & dementia : diagnosis, assessment & disease monitoring. 2020;12(1):e12005-n/a.
272. Mattsson N, Andreasson U, Zetterberg H, Blennow K, Neuroimaging AsD. Association of Plasma Neurofilament Light With Neurodegeneration in Patients With Alzheimer Disease. Jama Neurol. 2017;74(5):557-66.
273. Lewczuk P, Ermann N, Andreasson U, Schultheis C, Podhorna J, Spitzer P, et al. Plasma neurofilament light as a potential biomarker of neurodegeneration in Alzheimer's disease. Alzheimers Res Ther. 2018;10:71.
274. Lin YS, Lee WJ, Wang SJ, Fuh JL. Levels of plasma neurofilament light chain and cognitive function in patients with Alzheimer or Parkinson disease. Sci Rep-Uk. 2018;8(1):17368.
275. Sanchez-Valle R, Heslegrave A, Foiani MS, Bosch B, Antonell A, Balasa M, et al. Serum neurofilament light levels correlate with severity measures and neurodegeneration markers in autosomal dominant Alzheimer's disease. Alzheimers Res Ther. 2018;10(1):113.
276. Rohrer JD, Woollacott IOC, Dick KM, Brotherhood E, Gordon E, Fellows A, et al. Serum neurofilament light chain protein is a measure of disease intensity in frontotemporal dementia. Neurology. 2016;87(13):1329-36.
277. Weydt P, Oeckl P, Huss A, Müller K, Volk AE, Kuhle J, et al. Neurofilament levels as biomarkers in asymptomatic and symptomatic familial amyotrophic lateral sclerosis. Ann Neurol. 2016;79(1):152-8.
278. Rojas JC, Karydas A, Bang J, Tsai RM, Blennow K, Liman V, et al. Plasma neurofilament light chain predicts progression in progressive supranuclear palsy. Ann Clin Transl Neur. 2016;3(3):216-25.
279. Gisslén M, Price RW, Andreasson U, Norgren N, Nilsson S, Hagberg L, et al. Plasma Concentration of the Neurofilament Light Protein (NFL) is a Biomarker of CNS Injury in HIV Infection: A Cross-Sectional Study. EBIOMEDICINE. 2016;3(C):135-40.
280. Quiroz YT, Zetterberg H, Reiman EM, Chen Y, Su Y, Fox-Fuller JT, et al. Plasma neurofilament light chain in the presenilin 1 E280A autosomal dominant Alzheimer's disease kindred: a cross-sectional and longitudinal cohort study. Lancet Neurol. 2020;19(6):513-21.
281. Weston PSJ, Poole T, O'Connor A, Heslegrave A, Ryan NS, Liang Y, et al. Longitudinal measurement of serum neurofilament light in presymptomatic familial Alzheimer's disease. Alzheimers Res Ther. 2019;11(1):19-.

282. Preische O, Schultz SA, Apel A, Kuhle J, Kaeser SA, Barro C, et al. Serum neurofilament dynamics predicts neurodegeneration and clinical progression in presymptomatic Alzheimer's disease. Nat Med. 2019;25(2):277-83.
283. Engvall E, Perlmann P. Enzyme-linked immunosorbent assay (ELISA). Quantitative assay of immunoglobulin G. Immunochemistry. 1971;8(9):871-4.
284. Van Weemen BK, Schuurs AH. Immunoassay using antigen-enzyme conjugates. FEBS Lett. 1971;15(3):232-6.
285. Coons AH. The beginnings of immunofluorescence. J Immunol. 1961;87:499-503.
286. Oh ES, Mielke MM, Rosenberg PB, Jain A, Fedarko NS, Lyketsos CG, Mehta PD. Comparison of conventional ELISA with electrochemiluminescence technology for detection of amyloid-β in plasma. J Alzheimers Dis. 2010;21(3):769-73.
287. Brand AL, Lawler PE, Bollinger JG, Li Y, Schindler SE, Li M, et al. The performance of plasma amyloid beta measurements in identifying amyloid plaques in Alzheimer's disease: a literature review. Alzheimers Res Ther. 2022;14(1):195.
288. Galasko D. Biomarkers for Alzheimer's disease - Clinical needs and application. J Alzheimers Dis. 2005;8(4):339-46.
289. Jong Dd, Kremer HPH, Olde Rikkert MGM, Verbeek MM. Current state and future directions of neurochemical biomarkers for Alzheimer's disease. Clin Chem Lab Med. 2007;45(11):1421-34.
290. Glish GL, Vachet RW. The basics of mass spectrometry in the twenty-first century. Nat Rev Drug Discov. 2003;2(2):140-50.
291. van Andel E, Roosjen M, van der Zanden S, Lange SC, Weijers D, Smulders MMJ, et al. Highly Specific Protein Identification by Immunoprecipitation-Mass Spectrometry Using Antifouling Microbeads. ACS Appl Mater Interfaces. 2022;14(20):23102-16.
292. Crutchfield CA, Thomas SN, Sokoll LJ, Chan DW. Advances in mass spectrometry-based clinical biomarker discovery. Clinical proteomics. 2016;13(1):1-.
293. Oeckl P, Otto M. A Review on MS-Based Blood Biomarkers for Alzheimer's Disease. Neurol Ther. 2019;8(S2):113-27.
294. Pannee J, Törnqvist U, Westerlund A, Ingelsson M, Lannfelt L, Brinkmalm G, et al. The amyloid-β degradation pattern in plasma—A possible tool for clinical trials in Alzheimer's disease. Neurosci Lett. 2014;573:7-12.
295. Pitt JJ. Principles and applications of liquid chromatography-mass spectrometry in clinical biochemistry. Clin Biochem Rev. 2009;30(1):19-34.
296. Smith RW. Mass Spectrometry. Elsevier; 2013. p. 603-8.
297. Keshavan A, Pannee J, Karikari TK, Rodriguez JL, Ashton NJ, Nicholas JM, et al. Population-based blood screening for preclinical Alzheimer's disease in a British birth cohort at age 70. Brain (London, England : 1878). 2021;144(2):434-49.
298. Janelidze S, Teunissen CE, Zetterberg H, Allué JA, Sarasa L, Eichenlaub U, et al. Head-to-Head Comparison of 8 Plasma Amyloid-β 42/40 Assays in Alzheimer Disease. Jama Neurol. 2021.

299. Mandrekar JN. Receiver operating characteristic curve in diagnostic test assessment. J Thorac Oncol. 2010;5(9):1315-6.
300. Šimundić AM. Measures of Diagnostic Accuracy: Basic Definitions. Ejifcc. 2009;19(4):203-11.
301. O'Bryant SE, Gupta V, Henriksen K, Edwards M, Jeromin A, Lista S, et al. Guidelines for the standardization of preanalytic variables for blood-based biomarker studies in Alzheimer's disease research. Alzheimer's & dementia. 2015;11(5):549-60.
302. Song L, Zhao M, Duffy DC, Hansen J, Shields K, Wungjiranirun M, et al. Development and validation of digital enzyme-linked immunosorbent assays for ultrasensitive detection and quantification of clostridium difficile toxins in stool. J CLIN MICROBIOL. 2015;53(10):3204-12.
303. Wu C, Dougan TJ, Walt DR. High-Throughput, High-Multiplex Digital Protein Detection with Attomolar Sensitivity. ACS Nano. 2022;16(1):1025-35.
304. Cohen L, Cui N, Cai Y, Garden PM, Li X, Weitz DA, Walt DR. Single Molecule Protein Detection with Attomolar Sensitivity Using Droplet Digital Enzyme-Linked Immunosorbent Assay. ACS Nano. 2020;14(8):9491-501.
305. Wu C, Garden PM, Walt DR. Ultrasensitive Detection of Attomolar Protein Concentrations by Dropcast Single Molecule Assays. J Am Chem Soc. 2020;142(28):12314-23.
306. Maley AM, Garden PM, Walt DR. Simplified Digital Enzyme-Linked Immunosorbent Assay Using Tyramide Signal Amplification and Fibrin Hydrogels. ACS Sens. 2020;5(10):3037-42.
307. Cummings JL, Tong G, Ballard C. Treatment Combinations for Alzheimer's Disease: Current and Future Pharmacotherapy Options. J Alzheimers Dis. 2019;67(3):779-94.
308. Huang L-K, Chao S-P, Hu C-J. Clinical trials of new drugs for Alzheimer disease. Journal of biomedical science. 2020;27(1):18-.
309. Gilman S, Koller M, Black RS, Jenkins L, Griffith SG, Fox NC, et al. Clinical effects of Abeta immunization (AN1792) in patients with AD in an interrupted trial. Neurology. 2005;64(9):1553-62.
310. Yadollahikhales G, Rojas JC. Anti-Amyloid Immunotherapies for Alzheimer's Disease: A 2023 Clinical Update. Neurotherapeutics. 2023.
311. Tariot PN, Lopera F, Langbaum JB, Thomas RG, Hendrix S, Schneider LS, et al. The Alzheimer's Prevention Initiative Autosomal-Dominant Alzheimer's Disease Trial: A study of crenezumab versus placebo in preclinical PSEN1 E280A mutation carriers to evaluate efficacy and safety in the treatment of autosomal-dominant Alzheimer's disease, including a placebo-treated noncarrier cohort. Alzheimer's & dementia : translational research & clinical interventions. 2018;4(1):150-60.
312. Ostrowitzki S, Lasser RA, Dorflinger E, Scheltens P, Barkhof F, Nikolcheva T, et al. A phase III randomized trial of gantenerumab in prodromal Alzheimer's disease. Alzheimer's research & therapy. 2017;9(1):95-.

313. Arndt JW, Qian F, Smith BA, Quan C, Kilambi KP, Bush MW, et al. Structural and kinetic basis for the selectivity of aducanumab for aggregated forms of amyloid-β. Sci Rep-Uk. 2018;8(1):6412-16.
314. Lowe SL, Willis BA, Hawdon A, Natanegara F, Chua L, Foster J, et al. Donanemab (LY3002813) dose-escalation study in Alzheimer's disease. Alzheimer's & dementia : translational research & clinical interventions. 2021;7(1):e12112-e.
315. Tucker S, Möller C, Tegerstedt K, Lord A, Laudon H, Sjödahl J, et al. The murine Version of BAN2401 (mAb158) selectively reduces amyloid-β protofibrils in brain and cerebrospinal fluid of tg-ArcSwe Mice. J Alzheimers Dis. 2015;43(2):575-88.
316. Klein G, Delmar P, Kerchner GA, Hofmann C, Abi-Saab D, Davis A, et al. Thirty-Six-Month Amyloid Positron Emission Tomography Results Show Continued Reduction in Amyloid Burden with Subcutaneous Gantenerumab. The journal of prevention of Alzheimer's disease. 2021;8(1):3-6.
317. Mintun MA, Lo AC, Duggan Evans C, Wessels AM, Ardayfio PA, Andersen SW, et al. Donanemab in Early Alzheimer's Disease. The New England journal of medicine. 2021.
318. Sevigny J, Chiao P, Bussière T, Weinreb PH, Williams L, Maier M, et al. The antibody aducanumab reduces Aβ plaques in Alzheimer's disease. Nature (London). 2016;537(7618):50-6.
319. Swanson CJ, Zhang Y, Dhadda S, Wang J, Kaplow J, Lai RYK, et al. A randomized, double-blind, phase 2b proof-of-concept clinical trial in early Alzheimer's disease with lecanemab, an anti-Aβ protofibril antibody. Alzheimer's research & therapy. 2021;13(1):80-.
320. Ferrero J, Williams L, Stella H, Leitermann K, Mikulskis A, O'Gorman J, Sevigny J. First-in-human, double-blind, placebo-controlled, single-dose escalation study of aducanumab (BIIB037) in mild-to-moderate Alzheimer's disease. Alzheimer's & dementia : translational research & clinical interventions. 2016;2(3):169-76.
321. Budd Haeberlein S, Aisen PS, Barkhof F, Chalkias S, Chen T, Cohen S, et al. Two Randomized Phase 3 Studies of Aducanumab in Early Alzheimer's Disease. J Prev Alzheimers Dis. 2022;9(2):197-210.
322. Alexander GC, Emerson S, Kesselheim AS. Evaluation of Aducanumab for Alzheimer Disease: Scientific Evidence and Regulatory Review Involving Efficacy, Safety, and Futility. JAMA : the journal of the American Medical Association. 2021;325(17):1717-8.
323. Yang P, Sun F. Aducanumab: The first targeted Alzheimer's therapy. Drug discoveries & therapeutics. 2021;15(3):166-8.
324. Lalli G, Schott JM, Hardy J, De Strooper B. Aducanumab: a new phase in therapeutic development for Alzheimer's disease? EMBO Molecular Medicine , 13 , Article e14781 (2021). 2021.
325. Kueper JK, Speechley M, Montero-Odasso M. The Alzheimer's Disease Assessment Scale-Cognitive Subscale (ADAS-Cog): Modifications and Responsiveness in Pre-Dementia Populations. A Narrative Review. J Alzheimers Dis. 2018;63(2):423-44.

326. van Dyck CH, Swanson CJ, Aisen P, Bateman RJ, Chen C, Gee M, et al. Lecanemab in Early Alzheimer's Disease. The New England journal of medicine. 2023;388(1):9-21.
327. Sims JR, Zimmer JA, Evans CD, Lu M, Ardayfio P, Sparks J, et al. Donanemab in Early Symptomatic Alzheimer Disease: The TRAILBLAZER-ALZ 2 Randomized Clinical Trial. Jama. 2023;330(6):512-27.
328. Bechten A, Wattjes MP, Purcell DD, Aliaga ES, Daams M, Brashear HR, et al. Validation of an MRI Rating Scale for Amyloid-Related Imaging Abnormalities. Journal of neuroimaging. 2017;27(3):318-25.
329. Sperling RA, Jack CR, Black SE, Frosch MP, Greenberg SM, Hyman BT, et al. Amyloid-related imaging abnormalities in amyloid-modifying therapeutic trials: Recommendations from the Alzheimer's Association Research Roundtable Workgroup. Alzheimer's & dementia. 2011;7(4):367-85.
330. Wu G, Miller RA, Connolly B, Marcus J, Renger J, Savage MJ. Pyroglutamate-modified amyloid-β protein demonstrates similar properties in an Alzheimer's disease familial mutant knock-in mouse and Alzheimer's disease brain. Neurodegener Dis. 2014;14(2):53-66.
331. Zicha S, Bateman RJ, Shaw LM, Zetterberg H, Bannon AW, Horton WA, et al. Comparative analytical performance of multiple plasma Aβ42 and Aβ40 assays and their ability to predict positron emission tomography amyloid positivity. Alzheimers Dement. 2022.
332. Yilmaz A, Blennow K, Hagberg L, Nilsson S, Price RW, Schouten J, et al. Neurofilament light chain protein as a marker of neuronal injury: review of its use in HIV-1 infection and reference values for HIV-negative controls. Expert Rev Mol Diagn. 2017;17(8):761-70.
333. Gobom J, Parnetti L, Rosa-Neto P, Vyhnalek M, Gauthier S, Cataldi S, et al. Validation of the LUMIPULSE automated immunoassay for the measurement of core AD biomarkers in cerebrospinal fluid. Clin Chem Lab Med. 2022;60(2):207-19.
334. Karikari TK, Emeršič A, Vrillon A, Lantero-Rodriguez J, Ashton NJ, Kramberger MG, et al. Head-to-head comparison of clinical performance of CSF phospho-tau T181 and T217 biomarkers for Alzheimer's disease diagnosis. Alzheimer's & dementia. 2020:1-13.
335. Therriault J, Servaes S, Tissot C, Rahmouni N, Ashton NJ, Benedet AL, et al. Equivalence of plasma p-tau217 with cerebrospinal fluid in the diagnosis of Alzheimer's disease. Alzheimers Dement. 2023.
336. Palmqvist S, Janelidze S, Quiroz YT, Zetterberg H, Lopera F, Stomrud E, et al. Discriminative Accuracy of Plasma Phospho-tau217 for Alzheimer Disease vs Other Neurodegenerative Disorders. Jama-J Am Med Assoc. 2020;324(8):772-81.
337. Brickman AM, Manly JJ, Honig LS, Sanchez D, Reyes-Dumeyer D, Lantigua RA, et al. Plasma p-tau181, p-tau217, and other blood-based Alzheimer's disease biomarkers in a multi-ethnic, community study. Alzheimers Dement. 2021;17(8):1353-64.

338. Mielke MM, Frank RD, Dage JL, Jeromin A, Ashton NJ, Blennow K, et al. Comparison of Plasma Phosphorylated Tau Species With Amyloid and Tau Positron Emission Tomography, Neurodegeneration, Vascular Pathology, and Cognitive Outcomes. Jama Neurol. 2021;78(9):1108-17.
339. Simonsen AH, Bahl JM, Danborg PB, Lindstrom V, Larsen SO, Grubb A, et al. Pre-analytical factors influencing the stability of cerebrospinal fluid proteins. J Neurosci Methods. 2013;215(2):234-40.
340. Zimmermann R, Lelental N, Ganslandt O, Maler JM, Kornhuber J, Lewczuk P. Preanalytical sample handling and sample stability testing for the neurochemical dementia diagnostics. J Alzheimers Dis. 2011;25(4):739-45.
341. Hansson O, Zetterberg H, Vanmechelen E, Vanderstichele H, Andreasson U, Londos E, et al. Evaluation of plasma Abeta(40) and Abeta(42) as predictors of conversion to Alzheimer's disease in patients with mild cognitive impairment. Neurobiol Aging. 2010;31(3):357-67.
342. Verberk IMW, Misdorp EO, Koelewijn J, Ball AJ, Blennow K, Dage JL, et al. Characterization of pre-analytical sample handling effects on a panel of Alzheimer's disease-related blood-based biomarkers: Results from the Standardization of Alzheimer's Blood Biomarkers (SABB) working group. Alzheimers Dement. 2022;18(8):1484-97.
343. Kurz C, Stöckl L, Schrurs I, Suridjan I, Gürsel S, Bittner T, et al. Impact of pre-analytical sample handling factors on plasma biomarkers of Alzheimer's disease. J Neurochem. 2023;165(1):95-105.
344. Klafki HW, Morgado B, Wirths O, Jahn O, Bauer C, Esselmann H, et al. Is plasma amyloid-β 1-42/1-40 a better biomarker for Alzheimer's disease than AβX-42/X-40? Fluids Barriers Cns. 2022;19(1):96.
345. Thijssen EH, Verberk IMW, Vanbrabant J, Koelewijn A, Heijst H, Scheltens P, et al. Highly specific and ultrasensitive plasma test detects Abeta(1-42) and Abeta(1-40) in Alzheimer's disease. Sci Rep. 2021;11(1):9736.
346. Zetterberg H, Blennow K. From Cerebrospinal Fluid to Blood: The Third Wave of Fluid Biomarkers for Alzheimer's Disease. J Alzheimers Dis. 2018;64:S271-S9.
347. Rabe C, Bittner T, Jethwa A, Suridjan I, Manuilova E, Friesenhahn M, et al. Clinical performance and robustness evaluation of plasma amyloid-β(42/40) prescreening. Alzheimers Dement. 2023;19(4):1393-402.
348. de Kort AM, Kuiperij HB, Jäkel L, Kersten I, Rasing I, van Etten ES, et al. Plasma amyloid beta 42 is a biomarker for patients with hereditary, but not sporadic, cerebral amyloid angiopathy. Alzheimers Res Ther. 2023;15(1):102.
349. Pannee J, Shaw LM, Korecka M, Waligorska T, Teunissen CE, Stoops E, et al. The global Alzheimer's Association round robin

study on plasma amyloid β methods. Alzheimers Dement (Amst). 2021;13(1):e12242.
350. Álvarez-Sánchez L, Peña-Bautista C, Ferré-González L, Cubas L, Balaguer A, Casanova-Estruch B, et al. Early Alzheimer's Disease Screening Approach Using Plasma Biomarkers. Int J Mol Sci. 2023;24(18).
351. Thijssen EH, Verberk IMW, Kindermans J, Abramian A, Vanbrabant J, Ball AJ, et al. Differential diagnostic performance of a panel of plasma biomarkers for different types of dementia. Alzheimers Dement (Amst). 2022;14(1):e12285.
352. Chatterjee P, Pedrini S, Ashton NJ, Tegg M, Goozee K, Singh AK, et al. Diagnostic and prognostic plasma biomarkers for preclinical Alzheimer's disease. Alzheimers Dement. 2022;18(6):1141-54.
353. Zenobia C, Hajishengallis G. Basic biology and role of interleukin-17 in immunity and inflammation. Periodontol 2000. 2015;69(1):142-59.
354. Chen K, Kolls JK. Interluekin-17A (IL17A). Gene. 2017;614:8-14.
355. Zhang J, Ke KF, Liu Z, Qiu YH, Peng YP. Th17 cell-mediated neuroinflammation is involved in neurodegeneration of aβ1-42-induced Alzheimer's disease model rats. Plos One. 2013;8(10):e75786.
356. Jin JJ, Kim HD, Maxwell JA, Li L, Fukuchi K. Toll-like receptor 4-dependent upregulation of cytokines in a transgenic mouse model of Alzheimer's disease. J Neuroinflammation. 2008;5:23.
357. Chen JM, Jiang GX, Li QW, Zhou ZM, Cheng Q. Increased serum levels of interleukin-18, -23 and -17 in Chinese patients with Alzheimer's disease. Dement Geriatr Cogn Disord. 2014;38(5-6):321-9.
358. Doecke JD, Laws SM, Faux NG, Wilson W, Burnham SC, Lam CP, et al. Blood-based protein biomarkers for diagnosis of Alzheimer disease. Arch Neurol. 2012;69(10):1318-25.
359. Taipa R, das Neves SP, Sousa AL, Fernandes J, Pinto C, Correia AP, et al. Proinflammatory and anti-inflammatory cytokines in the CSF of patients with Alzheimer's disease and their correlation with cognitive decline. Neurobiol Aging. 2019;76:125-32.
360. Hu WT, Chen-Plotkin A, Grossman M, Arnold SE, Clark CM, Shaw LM, et al. Novel CSF biomarkers for frontotemporal lobar degenerations. Neurology. 2010;75(23):2079-86.
361. Hu WT, Watts K, Grossman M, Glass J, Lah JJ, Hales C, et al. Reduced CSF p-Tau181 to Tau ratio is a biomarker for FTLD-TDP. Neurology. 2013;81(22):1945-52.
362. Yan XZ, Lai L, Ao Q, Tian XH, Zhang YH. Interleukin-17A in Alzheimer's Disease: Recent Advances and Controversies. Curr Neuropharmacol. 2022;20(2):372-83.
363. Schofield C, Fischer SK, Townsend MJ, Mosesova S, Peng K, Setiadi AF, et al. Characterization of IL-17AA and IL-17FF in rheumatoid arthritis and multiple sclerosis. Bioanalysis. 2016;8(22):2317-27.

364. Pastuszczak M, Jakiela B, Wielowieyska-Szybinska D, Jaworek AK, Zeman J, Wojas-Pelc A. Elevated cerebrospinal fluid interleukin-17A and interferon-γ levels in early asymptomatic neurosyphilis. Sex Transm Dis. 2013;40(10):808-12.
365. Wijeyekoon RS, Moore SF, Farrell K, Breen DP, Barker RA, Williams-Gray CH. Cerebrospinal Fluid Cytokines and Neurodegeneration-Associated Proteins in Parkinson's Disease. Mov Disord. 2020;35(6):1062-6.
366. Zimmermann J, Krauthausen M, Hofer MJ, Heneka MT, Campbell IL, Müller M. CNS-targeted production of IL-17A induces glial activation, microvascular pathology and enhances the neuroinflammatory response to systemic endotoxemia. Plos One. 2013;8(2):e57307.
367. De Kort AM, Kuiperij HB, Marques TM, Jäkel L, van den Berg E, Kersten I, et al. Decreased Cerebrospinal Fluid Amyloid β 38, 40, 42, and 43 Levels in Sporadic and Hereditary Cerebral Amyloid Angiopathy. Ann Neurol. 2023;93(6):1173-86.
368. Tripathi NK, Shrivastava A. Recent Developments in Bioprocessing of Recombinant Proteins: Expression Hosts and Process Development. Front Bioeng Biotechnol. 2019;7:420.
369. Tajima N, Takai M, Ishihara K. Significance of antibody orientation unraveled: well-oriented antibodies recorded high binding affinity. Anal Chem. 2011;83(6):1969-76.
370. Mathew J, Sankar P, Varacallo M. Physiology, Blood Plasma: Treasure Island (FL): StatPearls; 2023 [Available from: https://www.ncbi.nlm.nih.gov/books/NBK531504/.
371. Czarniak N, Kamińska J, Matowicka-Karna J, Koper-Lenkiewicz OM. Cerebrospinal Fluid-Basic Concepts Review. Biomedicines. 2023;11(5).
372. Andreasson U, Perret-Liaudet A, van Waalwijk van Doorn LJC, Blennow K, Chiasserini D, Engelborghs S, et al. A Practical Guide to Immunoassay Method Validation. Front Neurol. 2015;6.
373. Crowther JR. The ELISA guidebook. Methods Mol Biol. 2000;149:Iii-iv, 1-413.
374. Jarrett JT, Berger EP, Lansbury PT. The carboxy terminus of the .beta. amyloid protein is critical for the seeding of amyloid formation: Implications for the pathogenesis of Alzheimer's disease. Biochemistry (Easton). 1993;32(18):4693-7.
375. Schlenzig D, Manhart S, Cinar Y, Kleinschmidt M, Hause G, Willbold D, et al. Pyroglutamate formation influences solubility and amyloidogenicity of amyloid peptides. Biochemistry. 2009;48(29):7072-8.
376. Piechotta A, Parthier C, Kleinschmidt M, Gnoth K, Pillot T, Lues I, et al. Structural and functional analyses of pyroglutamate-amyloid-β-specific antibodies as a basis for Alzheimer immunotherapy. J Biol Chem. 2017;292(30):12713-24.
377. Sgourakis NG, Yan Y, McCallum SA, Wang C, Garcia AE. The Alzheimer's peptides Abeta40 and 42 adopt distinct conformations in water: a combined MD / NMR study. J Mol Biol. 2007;368(5):1448-57.

378. Vashist SK, Luong JHT. Chapter 4 - Bioanalytical Requirements and Regulatory Guidelines for Immunoassays. In: Vashist SK, Luong JHT, editors. Handbook of Immunoassay Technologies: Academic Press; 2018. p. 81-95.
379. Davies C. Chapter 1.3 - Immunoassay Performance Measures11This chapter is from the first edition of The Immunoassay Handbook, with few changes, because of the high regard in which Chris Davies' original material is held. The theory still applies but some of the examples given are dated. In: Wild D, editor. The Immunoassay Handbook (Fourth Edition). Oxford: Elsevier; 2013. p. 11-26.
380. Rissin DM, Fournier DR, Piech T, Kan CW, Campbell TG, Song L, et al. Simultaneous detection of single molecules and singulated ensembles of molecules enables immunoassays with broad dynamic range. Anal Chem. 2011;83(6):2279-85.
381. Zhang J, Wiener AD, Meyer RE, Kan CW, Rissin DM, Kolluru B, et al. Improving the Accuracy, Robustness, and Dynamic Range of Digital Bead Assays. Anal Chem. 2023;95(22):8613-20.
382. Pei Z, Anderson H, Myrskog A, Dunér G, Ingemarsson B, Aastrup T. Optimizing immobilization on two-dimensional carboxyl surface: pH dependence of antibody orientation and antigen binding capacity. Anal Biochem. 2010;398(2):161-8.
383. Slemmon JR, Meredith J, Guss V, Andreasson U, Andreasen N, Zetterberg H, Blennow K. Measurement of Aβ1-42 in cerebrospinal fluid is influenced by matrix effects. J Neurochem. 2012;120(2):325-33.
384. Zhou W, Yang S, Wang PG. Matrix effects and application of matrix effect factor. Bioanalysis. 2017;9(23):1839-44.
385. Fogh JR, Jacobsen AM, Nguyen T, Rand KD, Olsen LR. Investigating surrogate cerebrospinal fluid matrix compositions for use in quantitative LC-MS analysis of therapeutic antibodies in the cerebrospinal fluid. Anal Bioanal Chem. 2020;412(7):1653-61.
386. Ashton NJ, Brum WS, Di Molfetta G, Benedet AL, Arslan B, Jonaitis E, et al. Diagnostic Accuracy of a Plasma Phosphorylated Tau 217 Immunoassay for Alzheimer Disease Pathology. Jama Neurol. 2024;81(3):255-63.
387. Vecchio D, Puricelli C, Malucchi S, Virgilio E, Martire S, Perga S, et al. Serum and cerebrospinal fluid neurofilament light chains measured by SIMOA™, Ella™, and Lumipulse™ in multiple sclerosis naïve patients. Mult Scler Relat Disord. 2024;82:105412.